Heinrich Heine Universität Düsseldorf

Development of a Thiol-Induced Controlled Radical Photopolymerization and Biomimetic Polymers to Modulate Bioadhesion

Inaugural Dissertation

for the attainment of the title of doctor

in the Faculty of Mathematics and Natural Sciences

at the Heinrich-Heine-University Düsseldorf

presented by

Lorand Bonda

from Cluj-Napoca

Düsseldorf, August 2024

From the Institute of Organic Chemistry and Macromolecular Chemistry at the Heinrich-Heine University Düsseldorf

Published by permission of the

Faculty of Mathematics and Natural Sciences

Heinrich-Heine-University Düsseldorf

Supervisor: Prof. Dr. Laura Hartmann

Co-supervisor: Priv.-Doz. Dr. Klaus Schaper

Date of oral examination: 05.12.2024

I hereby declare that the thesis submitted is my own work without making use of impermissible aids, considering the “Rules on the Principles for Safeguarding Good Scientific Practice at Heinrich-Heine-University Düsseldorf”. All direct or indirect sources used are acknowledged in the bibliography as references. I further declare that I have not submitted this nor a similar thesis at any other examination board in order to obtain a degree.

Date and Place Lorand Bonda

Table of Contents

Abstract

The development of free (FRP) and controlled radical polymerization (CRP) methods, especially their ease and high variability, have greatly impacted the modern way of life as we know it today. Both methods enabled the development of new adaptable materials, such as plastics or a wide range of different adhesives tailored to specific applications, which is essential for the production of many modern goods. However, these polymerization methods are often limited in their properties, like the controllability of the resulting polymers (FRP) or the variability of reactants (CRP). Due to the importance of polymer chemistry in terms of scientific and technical progress, the aim is to develop even more efficient and easier-to-handle polymerization methods that will drive progress forward.

Therefore, in its first part, this work presents the development of a new controlled radical polymerization method called TIRP – Thiol-Induced, Light-Activated Controlled Radical Polymerization. TIRP is a photopolymerization carried out under irradiation with 405 nm wavelength and a photoinitiator/photocatalyst system consisting of diphenyl-(2,4,6-trimethylbenzoyl)-phosphine oxide (TPO) and tris(2-phenylpyridine)iridium(III) ($Ir(ppy)_3$). A variety of molecules that contain at least one free thiol can be used as initiators. This is a major advantage of TIRP over other controlled radical polymerization methods, which often require specially synthesized initiators. To demonstrate the controlled nature of TIRP, a reactant mixture of tritylthiol as the thiol source and *N*-hydroxyethyl acrylamide (HEAA) or *tert*-butyl methacrylate as monomers were used. The optimized polymerization parameters are presented for both monomers. Polymers with targeted 20 as well as 100 repeating units were successfully synthesized and characterized. The number average molecular weights ($\overline{M}_n$) match with the theoretical ones and the determined dispersities (Đ), which are a value for the uniformity of the polymers, are in the range of CRPs (1.0-1.3). The controlled nature of TIRP was also demonstrated by kinetic ^{1}H NMR experiments demonstrating a linear relationship of monomer conversion to polymer chain length during the reaction. In addition, by repeatedly switching the light source on and off, it has been demonstrated that polymerization stagnates in the dark and reinitiates upon re-irradiation. The possibility of reinitiation was used to synthesize block copolymers, which is also a characteristic of CRPs. By specifically isolating and characterizing the products of the start reaction, a possible mechanism for TIRP has been postulated. In further experiments, limits of reaction control in TIRP were explored by changing polymerization parameters (TPO:thiol ratio, $Ir(ppy)_3$-concentration, irradiance intensity, and thiol species).

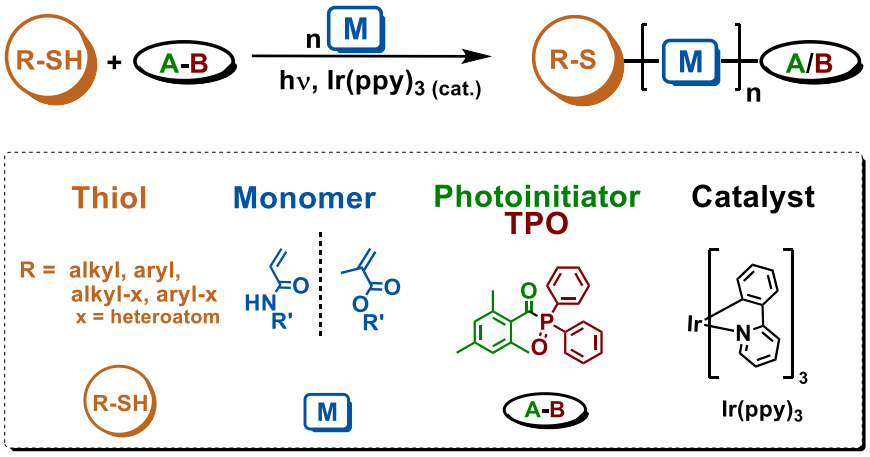

Figure 1. General TIRP scheme.[1]

In the second and third part of the thesis, both physiological bioadhesion and bioadhesion of living organisms with their environment were investigated. In the physiological field, for this work the bioadhesion of viruses to healthy cells is of great importance as this is often the very first step of the infection process. Understanding the process of viral infection in detail can lead to new methods of treating infections, which is highly topical and of great interest, not least since the Corona pandemic (2020-2023). Many viruses, including the pandemic causing corona virus SARS-CoV-2, start infection of healthy cells by adhering to them via special sugar receptors of the virus. Those bind to highly negatively charged, protein-bound sugar structures on the cell surface called glycosaminoglycans (GAGs). Prominent examples of GAGs are heparin (HP) and heparan sulfate (HS). Thus, one possible prevention against viral infections is to create artificial GAGs, to which the virus can adhere to, rather than to the natural GAGs of healthy cells. For this purpose, in this work, GAG mimetics were synthesized by free radical photopolymerization with the purpose to be tested against SARS-CoV-2. Two species of GAG mimetics were prepared. The first species as homopolymers from synthesized mannose monomers and the second as copolymers with HEAA as comonomer. To study the effect of inhibition of viral adhesion in relation to the polymer species and structure, homopolymers of different lengths and copolymers with various monomer ratios were prepared. All polymers were sulfated to create strongly negatively charged GAG mimetics. Initial results have shown that both, the length of the polymer chains and the density of the negative charge can influence the inhibition of viral adhesion.

The bioadhesion of living organisms with their environment and the synthesis of artificial adhesives inspired by them, was investigated using the example of the blue mussel. The mussel is able to adhere to organic and inorganic surfaces in an aqueous environment through a secretion that it produces. Responsible for this special adhesion are mussel foot proteins (mfps) that were found in the secretion, which largely contain catechols in the form of *L*-DOPA. Synergy with neighboring functional groups, such as charged amines and primary amides, further enhances the adhesion. Inspired by this, polymers

of four defined monomers were synthesized by free radical polymerization and their adhesive properties were investigated. The monomers used, are the catechol-containing dopamine acetonide acrylamide, the cationically charged dimethylaminopropyl acrylamide, *N*-acryloylglycinamide, which is containing a primary amide, and HEAA, that is known for only weak to no interactions. Eight final polymers with different compositions and monomer incorporations were synthesized and investigated for their ability to adsorb to glass in aqueous media using quartz crystal microbalance (QCM) and ellipsometry. Thus, it was shown that polymers with higher catechol contents exhibited the highest adsorption but also the enhanced adsorption through the synergistic effect of the catechols with primary amines and amides was determined.

Overall, this thesis demonstrates the successful development and investigation of the new controlled radical polymerization method called TIRP and presents both, the synthesis and characterization of GAG mimetics for the inhibition of viral adhesion to the cell surface, as well as studies concerning the adhesion of mussel-inspired polymers to glass in aqueous medium.

List of Publications

Publications included in this thesis

Bonda, L., Valles, D.J., Wigger, T.L., Meisner, J., Braunschweig, A.B., Hartmann, L., (2023). TIRP – Thiol-Induced, Light-Activated Controlled Radical Polymerization. *Macromolecules*.

Own Contribution:

Collaborative study design. Synthesis, isolation and characterization (NMR, SEC, MALDI-ToF) of all polymers and copolymers. Optimization of synthesis routes and development of optimal polymerization parameters. Performance of all kinetic studies and graphical and calculative analysis of the results. Mass spectrometric analysis of the products and collaborative establishment of a mechanistic proposal. Collaborative writing of the manuscript.

Bonda, L., Müller, J., Fischer, L., Löwe, M., Kedrov, A., Schmidt, S., Hartmann, L., (2023). Facile Synthesis of Catechol-Containing Polyacrylamide Copolymers: Synergistic Effects of Amine, Amide and Catechol Residues in Mussel-Inspired Adhesives. *Polymers*.

Own Contribution:

Synthesis, isolation and characterization (HPLC-MS, NMR, SEC) of all monomers, homopolymers and copolymers. Acetonide deprotection and characterization (^{1}H NMR) of the final polymers. Optimization of the synthesis routes and development of optimal polymerization parameters. Performance of ellipsometry measurements and graphical presentation of the results. Collaborative project development and writing of the manuscript.

Comment: parts of this publication were performed prior to this thesis. This includes: monomer/polymer synthesis and characterization; polymerization optimization. Part of this thesis are: DMAc-SEC measurements, acetonide deprotection and characterization; ellipsometry measurements of all polymers; quarz crystal microbalance measurements of all polymers; writing of manuscript.

Presentations at scientific conferences:

Poster: Bonda, L., Hoffmann, M., Blawitzki, L.-C., Groza, R., Ewers, H., Schelhaas, M., Snyder, N.L., Hartmann, L., Polymer Chemistry meets Virology – Sulfated Glycomacromolecules as GAG Mimetics. *Macromolecular Colloquium 2022, Freiburg.*

Poster: Bonda, L., Valles, D.J., Wigger, T.L., Meisner, J., Braunschweig, A.B., Hartmann, L., (2023). TIRP – Thiol-Induced, Light-Activated Controlled Radical Polymerization. *Macromolecular Colloquium 2023, Freiburg.*

Publications not included in this thesis

Merkt, F.M., Mazzone, F., Shaneh Sazzadeh, S., Bonda, L., Hinz, L.K.E., Gruber, I., Buchholz, K., Janiak, C., Pfeffer, K., Müller, T.J.J., (2021). Fluorescent Indolo[3,2-*a*]phenazines against *Toxoplasma gondii*: Concise Synthesis by Gold-Catalyzed Cycloisomerization with 1,2-Silyl Migration and *ipso*-Iodination Suzuki Sequence. *Chemistry – A European Journal*.

1. Introduction

1.1 General Introduction on Radical Polymerization Methods

The overall importance of polymer chemistry for industry as well as society could be seen in 1953 at the latest, when Hermann Staudinger was awarded the Nobel Prize for his pioneer work in that field.[2] His discovering, that synthetic polymers consist of many small molecules which are covalently bonded, led to the starting point of polymer chemistry research as we know it today and was followed by the development and advancement of many different polymerization techniques as well as synthetic polymeric materials that are part of our everyday life until today.[2] The first methods of macromolecular synthesis needed energy in form of thermal heat as an initiation trigger to build radicals and start polymerization. However, over the decades a lot of alternative activation options such as enzymatic,[3] redox-controlled,[4] voltage activated[5] and last but not least light-induced[6] polymerizations were developed.

1.1.1 Free and Controlled Radical Polymerizations

1.1.1.1 Free Radical Polymerization

The physical trigger of the reaction, however, is just one important aspect when performing a polymerization. Another one is the chemical trigger or in other words, the choice of the polymerization method used, that is a big criterion to create polymers with the attributes needed. One of the most used methods, both industrially and in academic research, is the free radical polymerization (FRP). While first FRPs were performed in the beginning of the 20th century[7], the mechanisms involved were studied and published in the 1930s[7-9] to 1940s.[10-11] For FRP an initiator is needed as a radical source, which gets cleaved homolytically by activation and builds two radical bearing fragments.[12] This step is called the radical generation, which is followed by the polymerization start reaction, where the initiator fragment reacts with a monomer, that often is an acrylic molecule (see Figure 2). Now this active species is able to react with more monomers and bond them covalently in the propagation step, followed by the termination. Here, the propagating polymer either reacts with another propagating molecule in a recombination reaction or one of the active chains abstracts a hydrogen from the other in a disproportionation reaction. The rate-determining step of a free radical polymerization is the initiator decomposition.[13] Furthermore, the rate of polymerization is influenced by the number of monomers that can attach. Thus, the growth rate in FRP is proportional to the monomer concentration and the square root of the initiator concentration.[13]

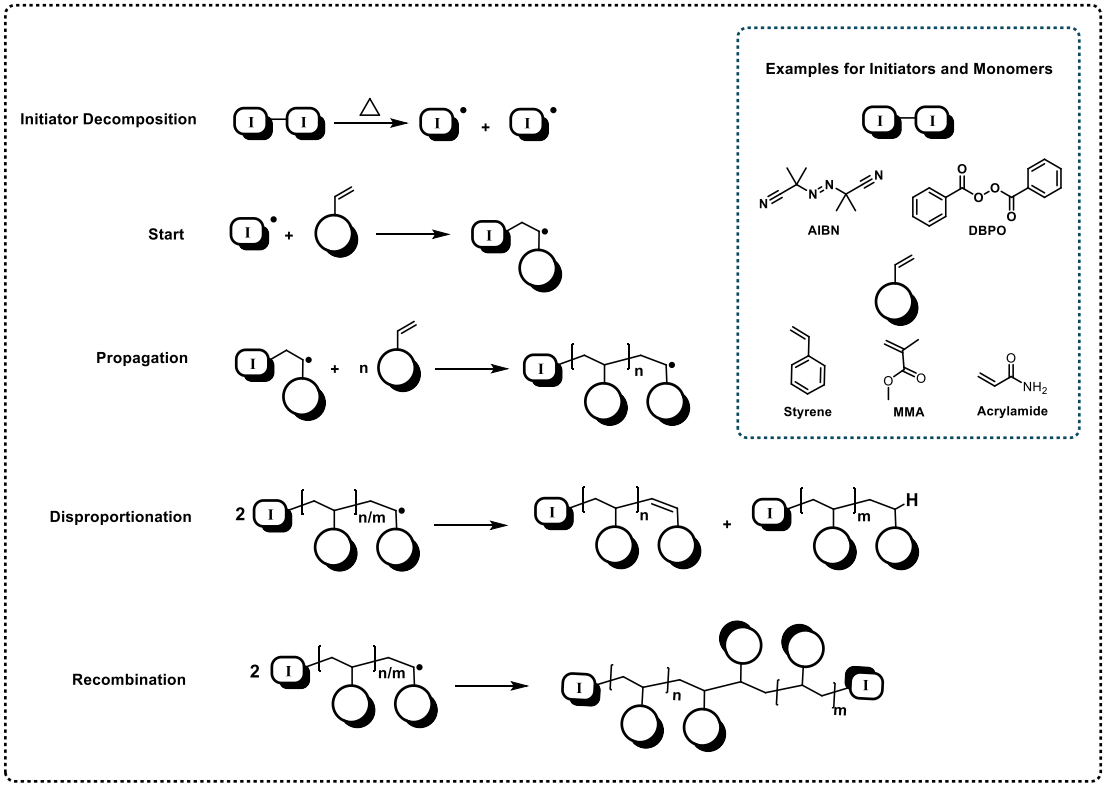

Figure 2. Schematic mechanism of a FRP with examples for common initiators and monomers.

In FRP commonly used initiators are azo and peroxy compounds like azobisisobutyronitrile (AIBN) or dibenzoyl peroxide (DBPO, see Figure 2). By thermal activation nitrogen (AIBN) or carbon dioxide (DBPO) is released and two identical radical bearing fragments are generated.[12] Monomers that are used in FRPs are often of vinylic, acrylic or methacrylic nature.[14-15]

Due to the fact that monomers accumulate in a fast and uncontrolled manner to the active chain ends and termination can randomly occur with polymer chains of completely different chain lengths, a broad molecular weight distribution of final polymers emerges. This distribution is calculated from the number-average molecular weight ($\bar{M}_n$), which is the molecular weight distribution of the synthesized polymers based on the amount of substance, and the weight-average molecular weight ($\bar{M}_w$), which is the distribution based on the weight of the respective polymer chains.[13]

$$\frac{\bar{M}w}{\bar{M}n} = Đ$$

Đ represents the dispersity and is a measure to describe the uniformity of the resulting polymers. For FRP reactions Đ is typically >1.5, which means that polymers synthesized via FRP are of different chain lengths due to their uncontrolled propagation behaviour.[16] However, researchers have made great effort to get more controlled and uniform polymers (Đ ≈ 1.0). Nature has set the example that it is possible to generate polymers of large molecular weights in a uniform way as can be seen, for example,

in the DNA and protein sequences.[17] In order to achieve this, different controlled radical polymerization methods have been developed, which will be presented in the following.

1.1.1.2 Reversible-Deactivation Radical Polymerization

Radical reactions that allow polymer synthesis with narrow molecular weight distributions (Đ < 1.5) are summed up as reversible-deactivation radical polymerizations (RDRPs) or controlled radical polymerizations (CRPs). All RDRPs have in common, that in comparison to FRPs the termination of growing polymer chains is reversible.[18] After reaction of the initiator with a monomer, an inactive dormant species is formed, that can be reactivated by energy transfer. This procedure is the speed limiting step in RDRPs. The equilibrium of this reaction is highly on the side of the dormant species, so that the concentration of propagating radicals stays low. Therefore, it can be assumed that the growing chains are predominantly present as dormant species and that upon activation all chains grow simultaneously, which leads to low dispersities (<1.3).[19-20] The most prominent CRPs are the nitroxide-mediated radical polymerization (NMP), the atom transfer radical polymerization (ATRP) and the reversible addition−fragmentation chain-transfer polymerization (RAFT).[21] Although industrially RDRPs are not as much used as FRPs, there are several commercial products synthesized by controlled radical polymerizations. For example, Daikin Industries made use of RDRPs to produce fluoroelastomers, while BYK-Chemie developed controlled polymerizations for their paint synthesis.[18]

NMP

Otsu *et al.* already described in 1982 the reversibility of the polymer termination step by using dithiocarbamate compounds as functional initiators that are able to react after polymerization.[22] This system was described as initiator-transfer agent-terminator, or short iniferter. However, it only addresses chain end modification after FRP, but does not influence polymer properties, like molecular weight distribution or dispersity during polymerization. While Solomon *et al.* first described a controlled polymerization using nitroxides in a patent from 1986[23], Georges *et al.* finally published the nitroxide-mediated radical polymerization in 1993, based on Solomon's work, that is not only reactivatable, but also leads to low dispersities.[24]

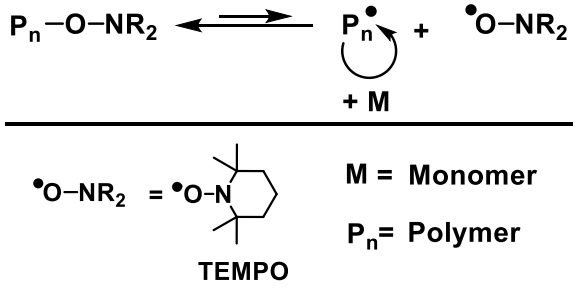

Figure 3. Generalized scheme for NMP mechanism.[18]

In NMP reactions (2,2,6,6-Tetramethylpiperidin-1-yl)oxyl (TEMPO) is commonly used as the nitroxide source. Due to the neighbored methyl groups the contained radical is stabilized, which is suited for NMP. Thus, while the polymer chain propagates, TEMPO does not significantly add monomers and is capable of terminating the propagating chain end, forming the dormant species.[25] While NMP was originally performed with a bimolecular initiation, by the use of an FRP initiator together with the nitroxide,[24] Hawker developed a unimolecular way of NMP.[26-27] Here the initiator and nitroxide belong to the same molecule and get cleaved once NMP is performed.

ATRP

The atom-transfer radical polymerization was developed by Krzysztof Matyjaszewski and Jin-Shan Wang in 1995 and is based on the concept that an active radical species is generated by a reversible redox process of a transition metal catalyst and an alkyl halide.[28] The metal catalyst, often a copper halogen complex, abstracts a halide from the alkyl halide initiator, which now is able to undergo polymer propagation. Via a reversed halogen abstraction to the polymer chain end the dormant species is built and can be reinitiated again to elongate the polymer or build block copolymers (see Figure 4).[29] The equilibrium of ATRP is highly on the side of the dormant species, allowing to activate most of the growing active species simultaneously. This leads to low dispersities of the final polymers (Đ < 1.5).[30] Termination reactions may also occur (mostly disproportionation or coupling of two active species), but only with a small amount of growing chains (<5%).[31-32]

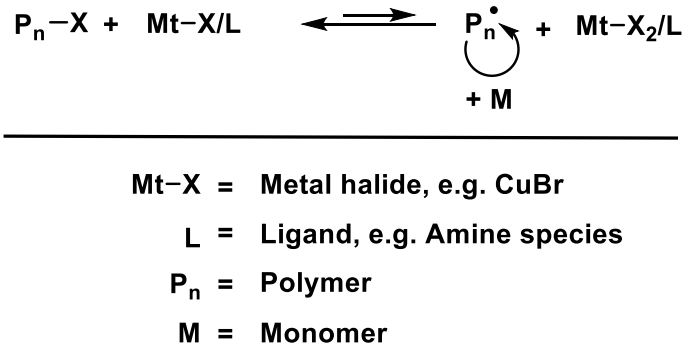

Figure 4. General scheme for ATRP mechanism.

Over time many variants of the original ATRP reaction were developed, like reverse ATRP[33], Activators Generated by Electron Transfer ATRP (AGET-ATRP[34]), Supplemental Activators and Reducing Agents ATRP (SARA-ATRP[35]), Single Electron Transfer - Living Radical Polymerization (SET-LRP[36]) or photo-ATRP[37], all with individual advantages reaching from the choice of solvent (polar/non polar), over the activation (temperature, light) to oxygen tolerance.[38] While ATRP reactions were evolved to the point where copper is only needed in ppm, the toxicity of copper makes it a great challenge to apply ATRP e.g. for bioapplications. Thus, RAFT polymerizations are strongly in the focus of research for such applications.[39]

RAFT

Of the controlled polymerizations presented so far, the reversible addition–fragmentation chain-transfer polymerization (RAFT polymerization) is the one, that was invented the latest, in 1998 by Zard *et al.*[40] and Rizzardo *et al.* in cooperation with the Australian CSIRO[41], simultaneously. The control of RAFT polymerizations is based on a thiocarbonylthio compound, called the RAFT agent, which serves as a chain transfer agent. After the initiation step, the growing polymer reacts with the thiocarbonylthio compound and builds a stabilized intermediate (see Figure 5). Here, the R-group gets cleaved off from the RAFT agent and also starts a polymerization. The growing chain end reacts with the polymer bearing RAFT agent again, which leads to cleavage and propagation of the other polymer chain. This addition-fragmentation reactions are reversible, leading to control over the polymer properties, like low dispersities.[42-43]

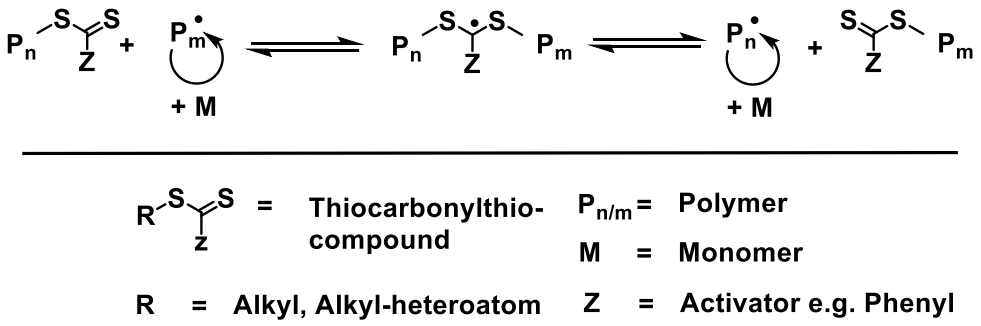

Figure 5. General scheme for RAFT mechanism.[44]

The successful RAFT polymerization depends, beside the choice of monomer, on the RAFT agent and the R- and Z-groups it is bearing. The R-group is defined as the radical leaving group and is weakly bonded to the RAFT agent due to its necessary ability to get cleaved. Also, it has an effective ability to build a radical that reinitiates polymerization. Often tertiary species that are similar to the monomer are chosen as R-groups. The Z-group has an activating function with its influence on the reactivity of the thiocarbonyl double bond and the stability of the radical bearing intermediate. Z groups are often

functional groups with electron donating effects, like phenyl groups or long alkyl chains.[18, 42-44] However, RAFT agents that are commercially available do not necessarily fit the requirements needed and typically have to be synthesized prior to the polymerization, which can be a challenging aspect of RAFT. Nevertheless, over the past 25 years, countless patents have been filed based on classical RAFT polymerization, as well as more advanced versions of RAFT, demonstrating the industrial interest in this controlled radical polymerization method.[45] One of the advances in RAFT polymerization, but also other CRPs like ATRP, was the development of light activation.

1.1.2. Radical Photopolymerizations

Light is one of the most advantageous polymerization activators that is used in research and industry alike. In contrast to activation by temperature, light has easy accessibility, low cost and direct controllability. While Blyth and Hoffman[46] already observed in 1845 that styrene undergoes self-initiated polymerization under the influence of sunlight, and in 1912 Ciamician described light-based chemistry as future-oriented,[47] photopolymers did not find real application until the 1960s, when they emerged with a vengeance, especially in the coating and printing industry.[48-49] Photoactivation is at low-cost and low-energy due to modern LED sources.[50] Also LEDs allow to irradiate at defined wavelengths dependent on the requirements. Typically, for most polymerizations this range lies between 350 and 450 nm.[51] Nevertheless, reactions were also published, that occur outside this range.[52-54] However, most advantageous for reactions activated by light is the controllability by switching the light source on and off, thus activating and deactivating the reaction instantly.[55] That results in an easy but decisive control that thermally activated reactions are not capable of.

The choice of the right photoinitiator due to the method performed is the first important step for a successful photopolymerization There are various photoinitiators available, each with defined activation wavelengths. Beside the activation of the initiator, the wavelength also has to be suited for the following steps, e.g., the polymer growth.[56] Photoinitiators are classified as Norrish type one and type two initiators (see Figure 6).[57] Type one initiators, like dibenzoyl peroxide (DBPO), get cleaved by irradiation with light, generating two radical bearing fragments, that both can initiate the polymerization. Type two initiators, like benzophenone, generate radicals by the use of an additional coinitiator. Through irradiation the initiator gets energetically excited, causing it to abstract a hydrogen from the coinitiator and generating the radical bearing species.[57-58]

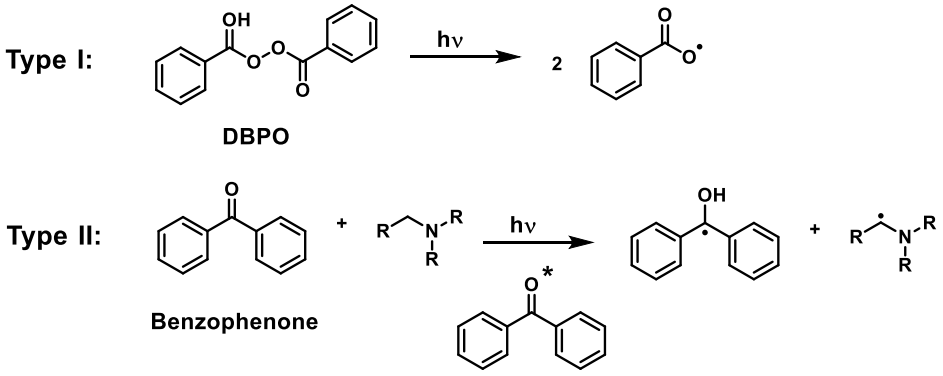

Figure 6. Examples for type I and type II photoinitiators.[57]

The free radical photopolymerization mechanism is comparable to the thermally activated FRP (see Figure 2).[58] The major difference is the activation by irradiation instead of heat. The possibility to start and stop the activation instantly leads to quick initiation and termination reactions.[59] Thus, free radical photopolymerizations are widely used in the field of coatings[60], dental restorations[61] or in 3D printings.[62]

Light activated polymerizations were shown for the whole spectra of polymerization methods. To combine the advantages of a controlled radical polymerization with the advantages of light induced reactions over thermally activated ones, photo-CRP methods were developed. In a simplified view, two mechanistic pathways are known to occur when performing photo CRPs, namely the intramolecular photo-CRP and the photoredox CRP.[21] While the intramolecular pathway mostly is metal free, the photoredox mechanism requires a photocatalyst, that often is a transition metal compound. The intramolecular mechanism is comparable to the NMP mechanism (see Figure 3), where the dormant species is cleaved by activation (here irradiation), building an active propagating species, that regenerates the dormant species, once irradiation is stopped. In the photoredox mechanism the photocatalyst is excited by irradiation and thus undergoes a redox reaction with the dormant species, generating the propagating radicals.[21] Many photoinduced counterparts of common thermal CRP methods were developed, such as photo-NMP[63], photo-ATRP[64] (see Figure 7) or PET-RAFT.[65] These reactions show that not only the polymerization can be terminated and reinitiated instantly, but also that polymer growth is at a constant rate over the whole reaction time. This was shown by comparison of the monomer conversion with the resulting molecular weight or degree of polymerization (DP) during the reaction. For controlled polymerizations this ratio is ideally linear, since it is assumed that the polymer chains grow simultaneously and thus monomer is consumed uniformly (see Figure 7).

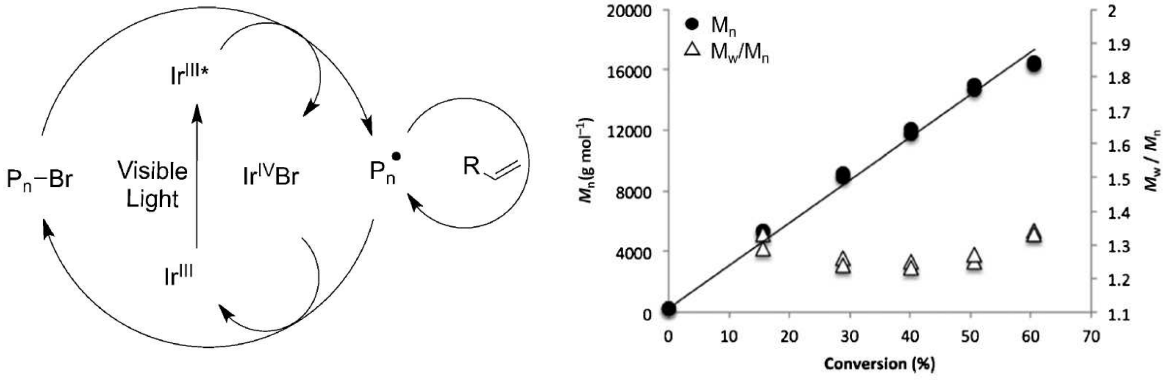

Figure 7. General mechanism photo-ATRP and plot of monomer conversion vs number average molecular weight.[64]

Beside the before mentioned common methods, many other polymerization methods were developed, that make use of unique initiators or catalysts. One major field that has been explored, due to its easy accessibility, is the use of thiols as initiators.

1.1.3. Thiol induced (photo)polymerization

Polymerization reactions with thiols as initiators are often called thiol-ene polymerizations. The "ene" describes an olefinic monomer, e.g. a vinyl monomer. The first thiol-ene reaction was discovered by Posner in 1905[66], who first described the addition of mercaptanes to olefins. However, thiol-ene polymerization gained a lot of attention in the decades from 1930 to 1950[67] as thiols as initiators are easily accessible, simple to handle and have a broad application range.[68] Marvel and Chambers were the first to publish their results on the development of a thiol induced photopolymerization, already in 1948.[69] Due to the advantages of thiol-ene reactions, namely the mild conditions to perform the polymerization, as well as the tolerance to conditions like humidity, thiol-ene polymerizations are used in several fields such as the synthesis of resins, polymers with special properties and also biomolecules.[70]

The initiation of thiol induced polymerizations is based on the lability of the sulfhydryl hydrogen. Ketley *et al.* showed that common photoinitiators (PIs) can be used in thiol-ene polymerizations to generate the radicals by hydrogen abstraction[71], the addition of PIs to the system became an established and often used tool. By activation through irradiation the photoinitiator gets cleaved and abstracts the hydrogen, thus forming a thiyl radical (R-S•). The formed thiyl radical is capable of reacting with any kind of olefinic molecule to start the polymerization (see Figure 8).[68] However, reactions with electron-rich double bonds happen faster than with electron-poor enes.[70] The reaction of a thiol with an "ene" in a click reaction is also called a thiol-Michael addition.[72]

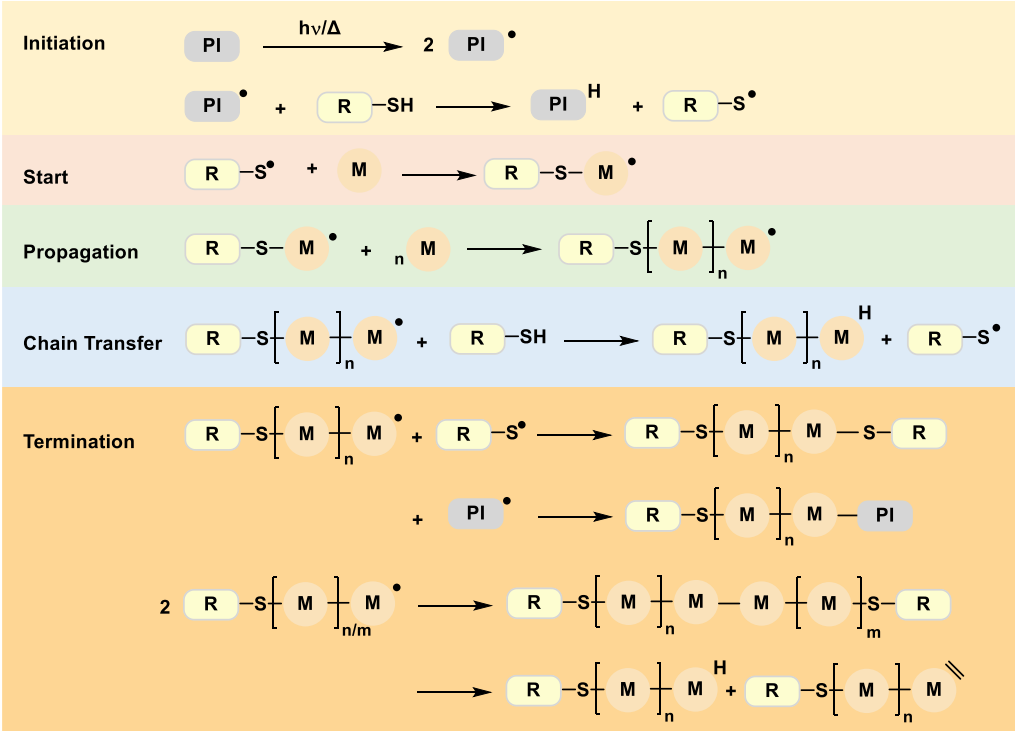

Figure 8. General mechanism of a thiol induced free radical (photo)polymerization (PI = photoinitiator, RSH = thiol compound, M = monomer).[67]

After the polymerization start, the chain propagation starts by addition of monomers, as known from the common FRP mechanism. Chain transfer reactions may occur, where the growing chain end abstracts a hydrogen from the thiol, resulting in the start of a new growing chain. Termination reactions proceed according to recombination or disproportionation reactions, but because of the potential addition of photoinitiator more recombination pathways are possible. Unwanted chain transfer reactions as well as the variety of termination reactions lead to a broad molecular weight distribution, and therefore to high dispersities.[68] However, Carslon and Knight found, that termination by recombination occurs significantly more often than termination by disproportionation, which also is a factor for higher dispersities.[73] Cramer *et al.* published, that the rate limiting step in thiol-ene polymerizations is the chain transfer reaction.[74] Thiol-ene polymerizations are mostly used for the synthesis of networks due to the ability to perform crosslinking, making it an applicable method for the synthesis of hydrogels and thin films.[75]

With the use of thiol-ene reactions, new fields of structure modification could be accessed. Thiols occur in a lot of natural substances like proteins and enzymes. Researchers have shown that protein surfaces can be modified through thiol-ene reactions, e.g. by addressing the free thiols of the cysteines the molecules are bearing.[70, 76-78] Protein-polymer conjugates that can be synthesized by thiol modification are of great interest in medicine and biotechnology.[79] An often used model protein for such modificational research is bovine serum albumin (BSA), that has one free thiol (Cys-34), that can be modified.[80] It was shown that this free thiol can be modified to a RAFT initiator[81] as well as conjugated with ATRP

polymers[80], to build protein-polymer conjugates. However, until now no native controlled polymerization from the free thiol of BSA was shown. The other thiols that BSA contains, are present as disulfides and are significantly involved in the structure stability.[82] Such disulfide bonds can be found in plenty of natural compounds.[83] Special rebridging agents were designed, that allow to open the disulfide bond and directly rebdridge it with a molecule bearing an accessible functional group.[84] This results in the preservation of protein stability, but also the possibility of follow up reactions like another thiol-ene polymerization.

Thiols tend to react with each other under oxidizing conditions and build disulfides. If previous reactions require oxidizing agents or oxygen, there are different protecting groups that can be used to prevent the formation of disulfides. These protecting groups can be cleaved again by pH adjustment, reduction/oxidation, the use of special chemicals like hydrazine or the use of UV light[85] (see Figure 9). The choice of protecting group depends on the conditions required for the whole synthetic path. Ideally orthogonal conditions are required for the deprotection reaction and the rest of the synthetic route.

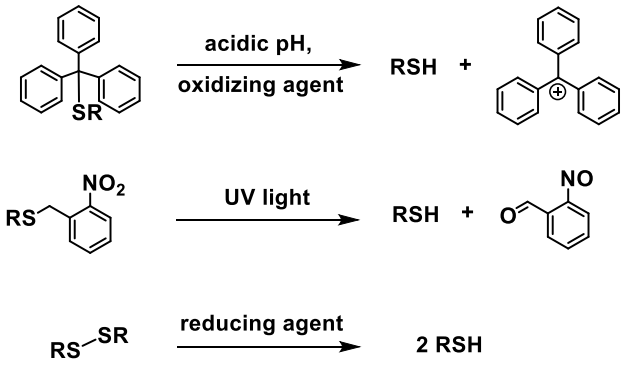

Figure 9. Different thiol protecting groups and their deprotection conditions.[85]

In 2019 the Braunschweig group showed photopolymerization with a surface-initiated thiol-acrylate (SI-TAP, see Figure 10).[55] Here, a thiol-modified surface is used to initiate a controlled radical photopolymerization, that makes use of a photoinitiator/photocatalyst-system consisting of TPO and $Ir(ppy)_3$. After functionalization of a glass surface with free thiols, *tert*-butyl methacrylate was polymerized by irradiation with UV light (405 nm wavelength). Polymer height could be detected by a CPU in real time during the reaction. Thus, uniform polymer heights at each time of the polymerization could be confirmed. By stopping irradiation, it was observed, that polymer growth also stopped and with re-irradiation the polymer growth started again. Because of the uniform growth as well as the control via UV light a controlled radical polymerization on thiol-functionalized surfaces was postulated.[55]

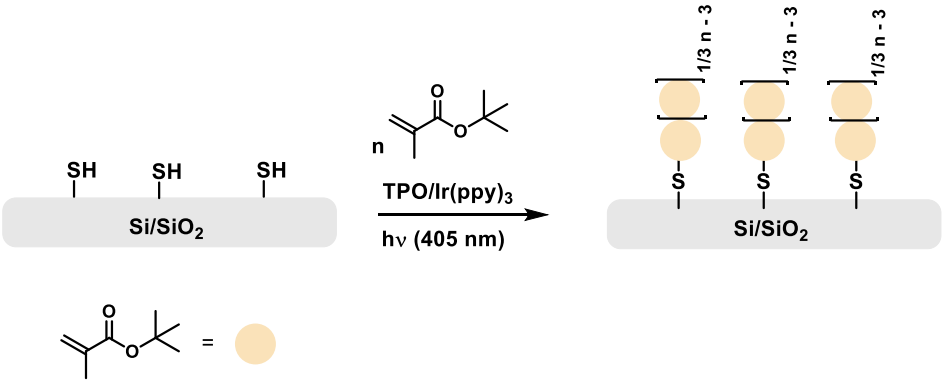

Figure 10. Schematic principle of the SI-TAP by the Braunschweig group.[55]

However, the method shown by the Braunschweig group, was exclusively performed on thiol modified surfaces and prior to this work had never been explored for solution polymerizations, limiting the applicability of the SI-TAP.

1.2 Biomimetic Polymers for Modulation of Bioadhesion

1.2.1 Concepts in the development and synthesis of biomimetic polymers

Biomimetic molecules are substances, that are designed to replace the original biomolecule by mimicking at least one of its functions, or are also capable of enhancing it, as well as adding additional functions.[86] Biomimetics often can be synthesized in a much larger scale than isolation of natural biomolecules is possible. Additionally, synthetic biomimetics allow more versatile architectures than their natural models. Thus molecular properties can be adjusted for the intended application.[87,88] There are different synthetic strategies to synthesize biomimetic polymers and materials. A promising way, is mimicking functional groups of the natural structures in a simplified synthetic polymer or dividing the biomacromolecule into different function-bearing building blocks.[86] Different approaches to generate biomimetic macromolecules are discussed in more detail in the following parts.

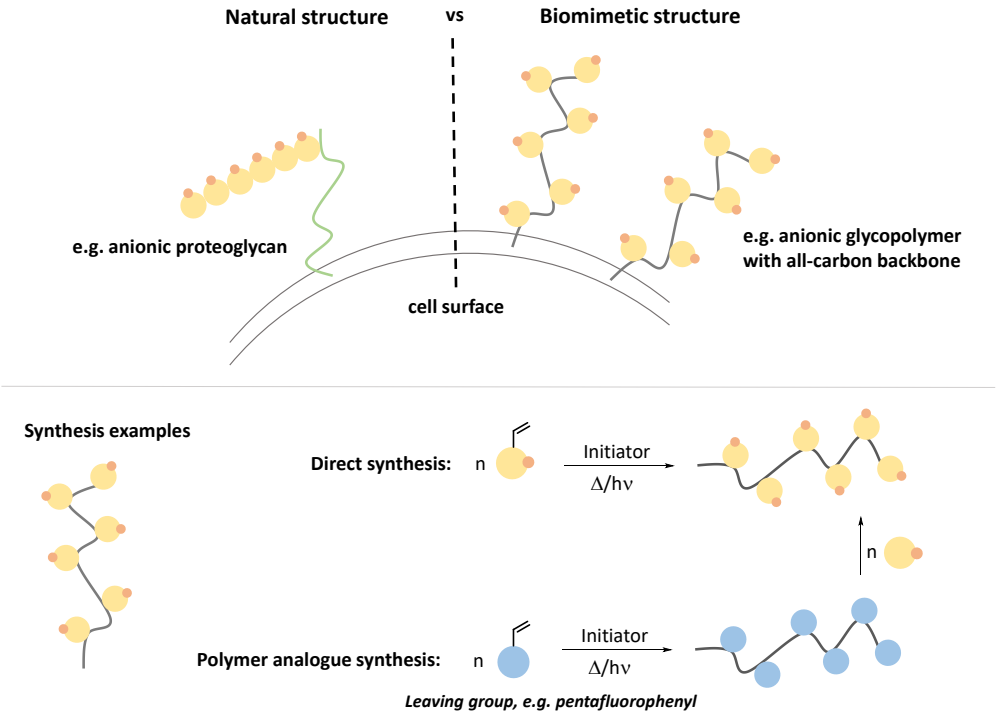

Figure 11. Schematic examples for a natural biomolecule and its biomimetic pendant and general methods for its synthesis.

1.2.1.1 Direct synthesis of Biomimetic Polymers

The mimicking of natural saccharides by direct polymerization of a carbohydrate monomer is a well-studied field of research when it comes to biomimetics. Carbohydrates are biologically important in cell adhesion, the stabilization of natural biomolecules like proteins, in ligand-receptor processes or in cell-cell communication events.[89] The principle of polymeric glycan mimetics relies on the identification of the responsible carbohydrates for the respective interactions and the synthesis of polymers, that are bearing those moieties. Carbohydrate binding to target proteins is generally weak, so it is advantageous to build polymers, which can offer the corresponding carbohydrate in multiple copies. This results in a significantly higher binding affinity or avidity from the so-called multivalency. Multivalent binding of glycans and glycan mimetics often occurs through the formation of aggregates and is also known as the cluster glycoside effect.[90] Other multivalent binding modes such as chelate binding or statistical binding can also lead to an increase in binding. Polymer glycan mimetics or glycopolymers can be directly synthesized from different CRP approaches. Fukuda *et al.* were the first to (co)polymerize a glucose functionalized methacrylate monomer via ATRP in 1998.[91] Müller *et al.* showed that also different architectures, like hyperbranched structures[92] and stars[93] are accessible. Maynard *et al.* employed a biotinylated ATRP initiator, that was used to initiate polymerization of *N*-acetyl glucosamine monomers, resulting in glycopolymers that bonded to the protein streptavidin (see Figure 12).[94]

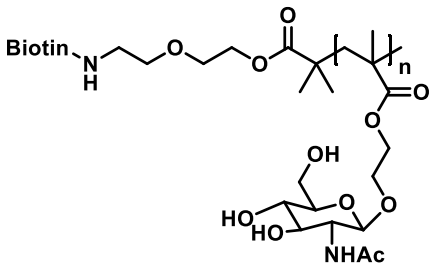

Figure 12. Biotin functionalized glycopolymer synthesized by Maynard *et al.* via ATRP.[94]

In 2003 Lowe *et al.* were the first to show linear glycopolymers synthesized by RAFT polymerization in aqueous medium.[95] Therefore, 2-methacryloxyethyl glucoside was used as a monomer, while no protecting group was needed. The resulting polymers all showed characteristics of living polymers (linear relationship of molecular weight distribution with increasing monomer conversion, low dispersities, possibility of block copolymer synthesis). In the following years a variety of glycopolymers were synthesized by direct polymerization of carbohydrate monomers using RAFT. For example, Narain *et al.* synthesized a biotin end functionalized glycopolymer via RAFT polymerization by the creation of a biotin labeled chain transfer agent. The resulting galactose polymers could be bonded to gold nanoparticles and also showed affinity to streptavidin.[96] Another example was shown by Stenzel *et al.* who created copolymers consisting of 2-hydroxyethyl acrylate and glucose, that were functionalized with a gold compound for treatment against human ovarian cancer cells.[97] Also an interesting approach came from Song *et al.* who synthesized block copolymers of mannose, *N*-acetyl glucosamine and galactose and an Alexa fluorophore to show *in vivo* targeting of alveolar macrophages (see Figure 13).[98]

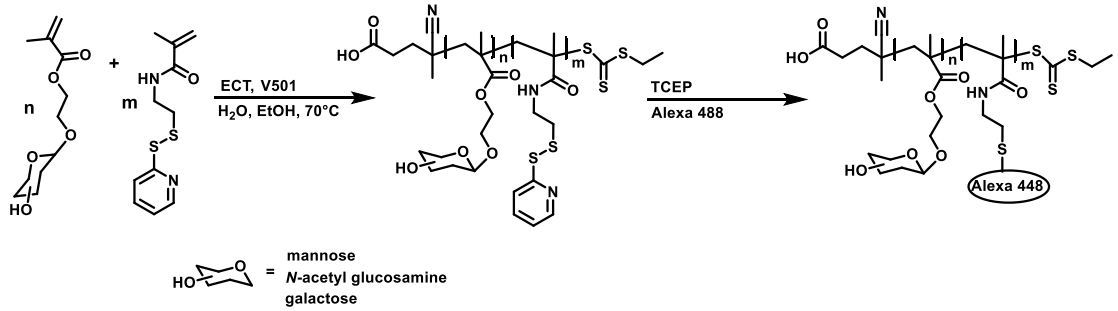

Figure 13. Block-co-polymer for macrophage targeting synthesized by Song *et al.*[98]

Polymeric biomimetics are also of interest mimicking other biopolymers, such as proteins or oligonucleotides. An example for a polymeric biomimetic of a protein are catechol-containing polymers that mimicking one of the proteins of Mussel foot proteins. A detailed description of the properties of the mussel foot protein and the resulting unique adhesion of mussels can be found in chapter 1.2.3. For example, Stepuk *et al.* synthesized a mussel inspired catechol monomer and copolymerized it with methyl methacrylate in a FRP. Thus, polymers were built, that could be adhered to metal surfaces, with an adhesive strength of 20 MPa (see Figure 14).[99] Another example, where the catechol containing

polymers showed similar adhesive strength, were synthesized by Chung *et al*.[100] through dimethacrylate crosslinking.

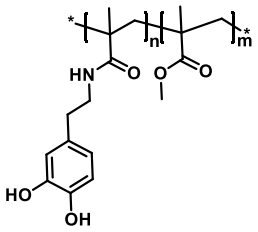

Figure 14. Catechol containing copolymer synthesized by Stepuk *et al*.[99]

One limit of the direct synthesis of biomimetics is the choice and synthesis of monomers. Bulky monomers may be sterically hindered during polymerization or special monomers designed for specific applications may not be usable under the conditions that are needed for the particular polymerization method. This challenge can be circumvented with the approach of polymer analog synthesis.

1.2.1.2 Polymer analogue Reactions to generate Biomimetics

Polymer analogue synthesis aims at pre-forming synthetic polymers and then functionalizing these with biomimetic entities afterwards.

One approach was shown by Bertozzi *et al.*, who synthesized biomimetic cell surface mucins. Mucin glycoproteins are important for cells to resist nonspecific interactions. Synthetically, a lipid was functionalized with an azo group to generate a polymer chain via FRP using methyl vinyl ketone as a monomer that was further functionalized with aminooxy-*N*-acetyl galactosamine (aminooxy-GalNAc) to create the biomimetics (see Figure 15).[101]

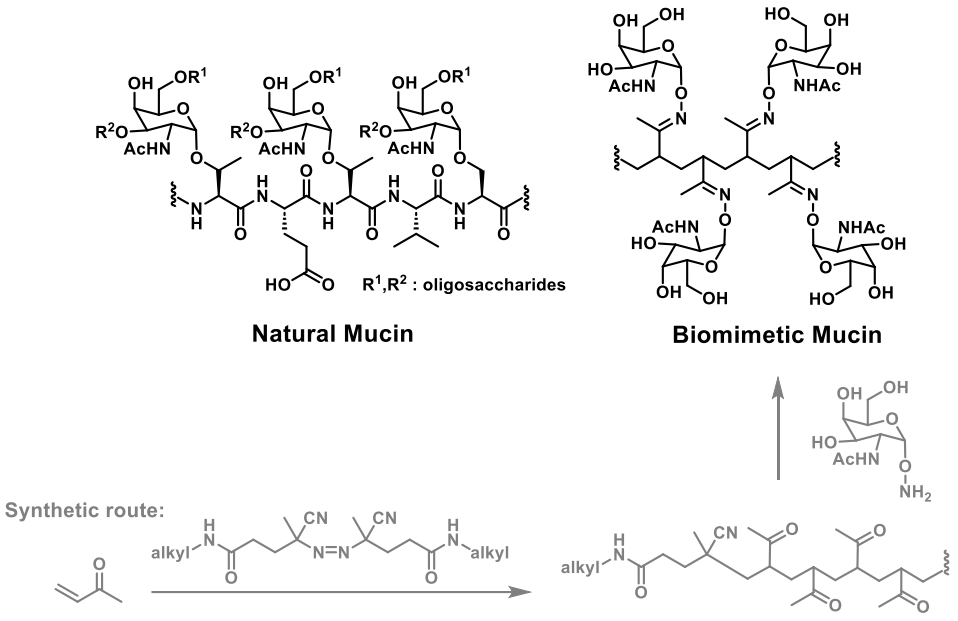

Figure 15. Structure of the native mucin and synthesis and structure of the biomimetic mucin.[101]

It was shown that the biomimetic polymers were recognized by protein receptors that also recognize the natural mucin glycoproteins. Also, nonspecific protein binding did not occur.[101] Nevertheless, it should be noted that such biomimetic systems are merely approximations of natural systems, for example, the carbon-carbon polymer backbone does not occur in nature and is also not biodegradable.[102]

Controlled radical polymerization was used in biomimetic synthesis to build defined scaffolds, that could be postfunctionalized. Haddleton *et al.* published the synthesis of a maleimide terminated methacrylate polymer scaffold by ATRP, that could be functionalized with carbohydrates by click-chemistry on the alkyne units of the side chain. Afterwards the maleimide was used in a thiol-ene addition to build a polymer-protein conjugate with bovine serum albumin (BSA).[103] Hu *et al.* also used ATRP to build defined polymers, as active ester polymers, by polymerizing N-acryloxysuccinimid. After isolation of the pre-polymer it was functionalized with galactose and ethanolamine in different ratios giving well-defined glycoconjugate polyacrylamides.[104]

An important topic where biomimetic polymers can be useful for understanding the process in detail is the infection of healthy cells by viruses. Polysaccharides also play an essential role here and mimicking them to investigate the infection process is part of the following chapter.

1.2.2 Negatively Charged Polymers as Glycosaminoglycan Mimetics for Inhibition of Virus-Cell-Adhesion

1.2.2.1. General Information on GAGs

Glycosaminoglycans (GAGs) are highly negatively charged linear polysaccharide structures, that can be found attached to proteins, for example at the cell surface, where they form proteoglycans.[105] Heparin (HP) and heparan sulfate (HS) may be the most prominent representatives of GAGs, while HS accounts for the highest proportion of GAGs at approximately 50-90 % and HP is mostly found in mast cells.[106-107] HS and HP are connected to the proteins by a linkage consisting of the tetrasaccharide GlcA-β-1,3-Gal-β-1,3-Gal-β-1,4-Xyl that is glycosylated with a serine of the protein sequence. From this linkage the main saccharides that HP and HS consist of are glucuronic acid (GlcA) and *N*-acetyl-glucosamine (GlcNAc) in an alternating sequence.[108-109] These saccharides are then modified by *N*-deacetylation, *N*- and *O*-sulfation and C5-epimerization of GlcA to L-iduronic acid (IdoA), resulting in a high structural variety.[108-109] While HP is known for the highest sulfation of GAGs, HS shows more variety in its sulfation pattern, by also having unsulfated structural sequences.[110] GAGs and especially HS takes part in many physiological processes like neurodegeneration, cancer building and infections, to list just a few.[111-112]

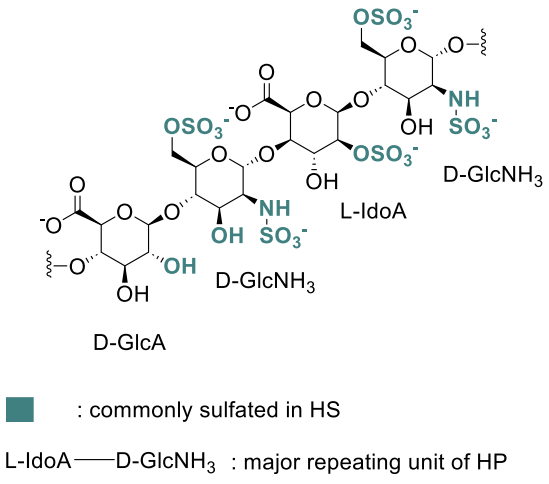

Figure 16. Structural repeating units of HS and HP.[113]

1.2.2.2. GAGs and GAG Mimetics as Viral Inhibitors

GAGs play an important role when it comes to viral infections. In 1992 Shieh *et al.* published their results on viral adhesion to the cell surface. It was shown, that HS acts as a viral receptor for herpes simplex virus (HSV) due to its anionic character.[114] Soluble HS inhibits viral adhesion by blocking the HS proteoglycan binding sites of the virus. This leads to the inhibition of the first step of a viral infection, the adhesion to the cell surface. [115-116] Other virus types, like human papilloma virus (HPV), hepatitis C virus (HCV) or corona viruses, like SARS-CoV-2 use HS binding sites to approach the cell surface and

therefore get close to more specific binding sites.[117-119] Beside this, GAGs are also known to protect cells from infection of some virus species by shielding the binding sites of specific receptors.[120-121] Because of this important role of natural GAGs in viral adhesion, GAG mimetics have been studied extensively as a mean to block and protect against viral infections (see Figure 17).[122-123] Hoffmann and coworkers have recently published an article reviewing the current status on HP and HS mimetic polymers and their use as inhibitors of viral adhesion.

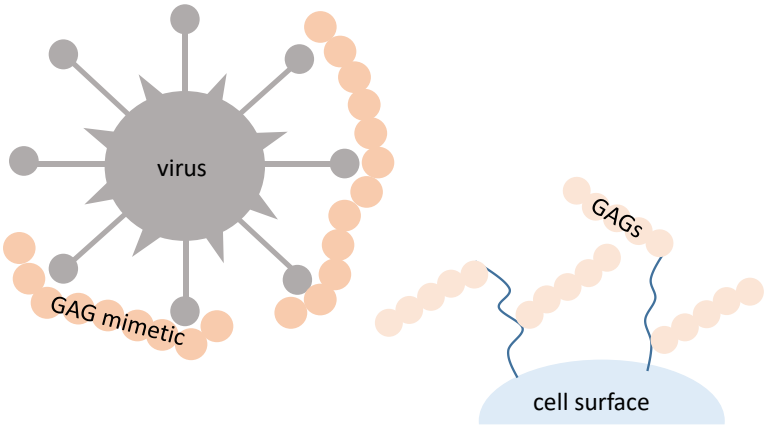

Figure 17. Schematic representation of the inhibition of viral infection by the use of synthetic highly sulfated GAG mimetics.

GAG mimetics have been shown for both, polymers made of anionic aliphatic or aromatic monomers[124], thus mimicking the negatively charged character of GAGs, but also structural mimics in form of anionic glycopolymers.[125] For example, Schandock *et al.*[126] have shown studies with carboxylated, phosphated/phosphonated and sulfonated polymers against Zika, Ebola and SARS viruses (see Figure 18). Considering the results, a high anionic character only, already shows an effect on viral inhibition.

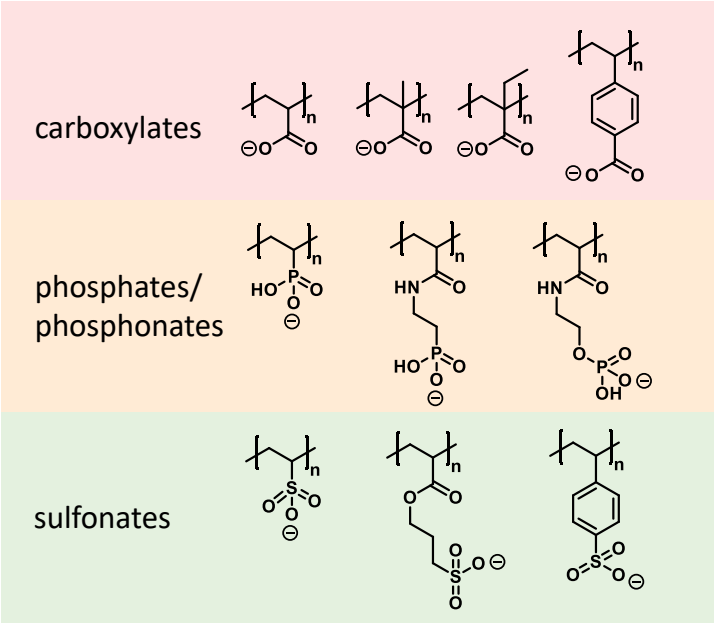

Figure 18. Selection of anionic polymers synthesized by Schandock *et al*.[126]

In a previous work from the Hartmann lab, Soria-Martinez *et al.* have shown a synthesis strategy to build both, GAG mimetic glycooligomers and glycopolymers.[127] Different examples were then analyzed against a variety of viruses as inhibitors of viral adhesion. The oligomers were synthesized via solid phase polymer synthesis (SPPoS) and functionalized with carbohydrates after cleaving off the final oligomer. To generate a highly anionic character the oligomers were then sulfated at each hydroxyl functionality. Glycopolymers were synthesized via RAFT polymerization directly from a glycomonomer. The isolated polymers were also fully sulfated afterwards. The synthesis of both, glycooligomers and glycopolymers allowed the group to investigate the effect of the chain length on the resulting viral adhesion inhibition properties.[127]

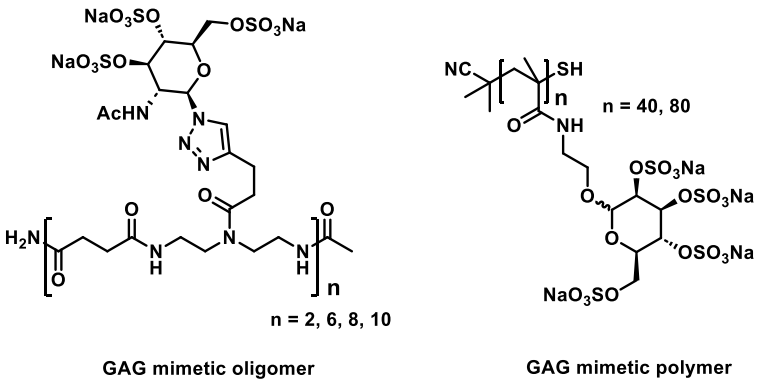

Figure 19. Structures of the GAG mimetics synthesized by Soria-Martinez *et al*.[127]

It was found, that GAG mimetic oligomers and polymers behaved differently in viral adhesion studies, but both inhibited viral infection. While the GAG mimetic polymers were able to inhibit viral adhesion

to cells and therefore also inhibit infection, the oligomers mostly could not inhibit viral adhesion. Interestingly, nevertheless cell infection was reduced. Infection experiments were also conducted *in vivo*, where GAG mimetic polymers showed higher efficiencies in inhibiting HPV infection than the oligomers.[127]

Another synthesis strategy to create GAG mimetics, is the polymerization of already sulfated monomers instead of post functionalization of the final polymers. For example, Oh *et al*. synthesized sulfated disaccharide monomers and synthesized GAG mimetics by ring opening polymerization.[128]

1.2.3. Catechol-Containing Polymers to Induce Adhesion

1.2.3.1. Mussel Adhesion in marine Environment

Another example of bioadhesion is the adhesion of mussels when sticking to a rock as their natural habitat. The blue mussel (Mytilus edulis) is also able to adhere to organic and inorganic surfaces in both dry and marine environments.[129] This is not least remarkable because seawater is slightly alkaline (pH 8.2) and has a high ion concentration. The ions form a thin layer on the marine surface, which usually complicates good adhesion.[130-131] Nevertheless, mussel adhesion is strong even under these conditions. This adhesion can be explained by certain proteins, called mussel foot proteins (Mfps), which are found in the secretion of the mussel feet (byssus). There are many variants of mussel foot proteins and about 15 are known to contribute to mussel adhesion.[132] While Mfp-2 is cross-linked to itself and thus fulfills a structuring role[133], Mfps 3 and 5 in particular could be determined to have the highest influence on adhesion to different surfaces.[134] Detailed analysis of the composition of these Mfps by Waite *et al.* determined that they contain 20-30 % *L*-3,4-dihydroxyphenylalanine (*L*-DOPA), a nonproteinogenic, catechol-containing amino acid formed from tyrosine. *L*-DOPA was thus identified as the main factor in mussel adhesion.[129, 135] Mfp-3 is considered to be the most diverse mussel foot protein with 35 different variants.[136] Mfp-3 is divided into Mfp-3 fast moving (Mfp-3f) and Mfp-3 slow moving (Mfp-3s). Here, Mfp-3f is particularly rich in *L*-DOPA (20 %), but an equally high proportion of cationically charged amino acids has been identified (25 %).[136] These occur in the form of lysine or arginine, with arginine accounting for the higher proportion.[135] Thus, adhesion can additionally be attributed to a synergy of catechols with cationically charged groups.[132] At about 18 %, the proportion of asparagine is also very high, which contains a primary amide.[137] Fischer *et al.* in a previous study from the Hartmann and Schmidt labs, described that this functionality also contributes to the synergy and thus the enhancement of adhesion.[138] In Mfp-5, that is not as versatile as Mfp-3, also a high proportion of *L*-DOPA and cationic amino acids (28 % each) were determined.[139-140]

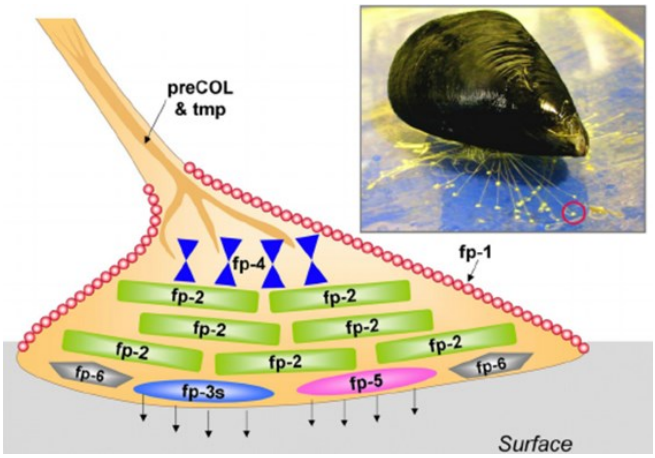

Figure 20. Schematic depiction of the Mfps found in the byssus.[133]

Chemically, mussel adhesion is explained by the fact that catechols are capable of various types of interactions. For example, under oxygen and basic pH, catechols are oxidized to quinones, which are then able to react with nucleophiles.[141] This contributes to both, adhesion with the environment and cohesion within the mfps.[142] Other interactions that catechols can engage in include π-π interactions, H-bridges, cation-π interactions, coordination to metal ions, hydrophobic interactions, and also covalent cross-linking.[143] This variety of different interactions is decisive for the good adhesion of the mussel to different surfaces. Inorganic surfaces consist to a large extent of metals or oxides, so here bonding mainly happens through interactions with the hydroxyl groups of the catechol.[144] For adhesion to organic surfaces, the interactions of the phenyl unit of the catechol (hydrophobic interactions, π-π, π-cationic) plays an important role.[143]

1.2.3.2. Catechol-Containing Polymers to Mimic Mussel Adhesion

Due to the diverse adhesive properties of the mussel, research has aimed at creating synthetic polymers inspired by the Mfps. When synthesizing catechol polymers, it is possible to incorporate catechol motifs in the main chain as well as in the side chain of the polymers to influence the properties. Incorporation into the main chain as cross-linked polydopamine was achieved both oxidatively[145] and enzymatically.[146] For example, Lee *et al.* described the crosslinking as a combination of catechol oxidation to quinone and parallel polymerization.[145]

The incorporation of catechols into polymers has also been demonstrated by ATRP and RAFT. For example, Messersmith *et al.* synthesized a catechol-containing ATRP initiator from which controlled polymerization were performed (see Figure 21A).[147] Liu *et al.* on the other hand showed a method to use catechols for RAFT polymerization and utilize them to complex metal ions (see Figure 21B).[148] A

challenge in using catecholamines as monomers, as will be presented in this thesis, is the before mentioned possible crosslinking of the catechols where they are oxidized to quinones and subsequently crosslink by forming Schiff bases.[145] To prevent this, various protecting groups are used, which can be removed after polymerization. Known protecting groups for catechols are, for example, the acetonide protecting group, which is introduced via the reaction of acetone with the catechol and cleaved off under acidic conditions[149], or also methyl protecting groups for the hydroxy functionalities, which can be removed by boron tribromide.[150]

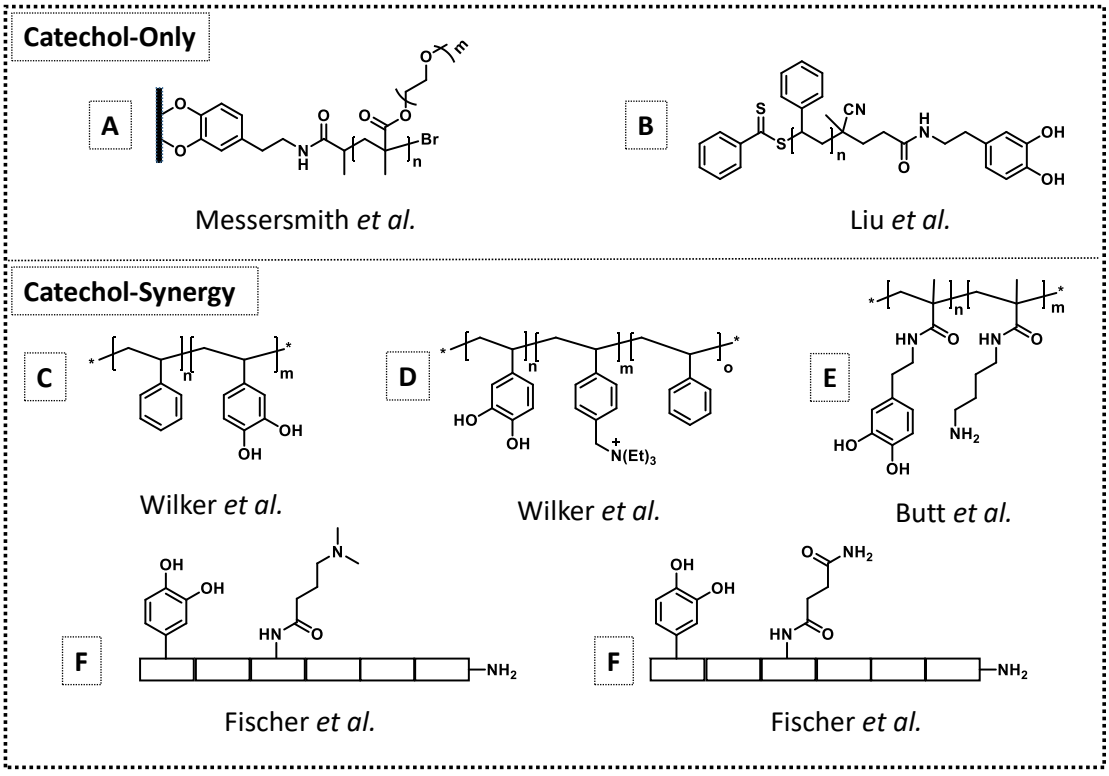

Figure 21. A. Catechol-containing ATRP polymer synthesized by Messersmith *et al.*[147]; **B.** Catechol-containing RAFT polymer synthesized by Liu *et al.*[148]; **C.** Styrene-Catechol-Copolymer by Wilker *et al.*[151]; **D.** Catechol, quart. Amine and Styrene containing Copolymer synthesized by Wilker *et al.*[152]; **E.** Copolymer of Catechol and Amine monomers synthesized by Butt *et al.*[153]; **F.** Schematic presentation of the oligomers containing catechol/amine and catechol/amide moieties synthesized by Fischer *et al.*[138]

In addition to the catechol-containing homopolymers, the development of copolymers is of interest, since here possible synergies of the comonomers to the catechol, as found in the Mfps, can be investigated. Butt *et al.* developed copolymers of a dopamine methacrylamide and butylamine methacrylamide in different monomer ratios (see Figure 21E).[153] They showed that the adhesive properties of the polymers did not increase from an incorporation of more than 10% catechol.[153] Wilker *et al.* confirmed this finding in 2012 by synthesizing crosslinked styrene-catechol copolymers that exhibited adhesion of up to 7 MPa to aluminum (see Figure 21C). The maximum was also reached at a relatively low catechol incorporation of 33% and decreased abruptly at higher incorporation levels. This can be explained by the fact that at higher incorporation levels, crosslinking of the catechols led to very high cohesion

of the polymers, which decreased the adhesion.[151] Synergy with cationically charged groups in synthetic copolymers was also studied by Wilker *et al.* Here, a copolymer of catechol, a quaternary amine, and styrene was developed and shown that adhesion increased by introducing the cationic group (see Figure 21D).[152] One reason of this synergy is, that sea surface is rich in ions, which build a layer. The cationic groups are able to break this thin salt layer, helping the catechol to interact with the pure surface.[132] However, by strongly increasing the cationic moieties, the adhesion strength decreases again.[132] Fischer *et al.* investigated not only the synergy of catechol with cationic groups, but also the additional effect of neighboring primary amides.[138] For this purpose, sequence-defined oligomers containing different combinations of catechol, amine and amide moieties were synthesized by SPPoS and examined for their adhesive properties on glass (see Figure 21F). Here, it was shown that the combination with the primary amide also resulted in a synergy that strengthened adhesion, however, no mechanism for this effect was yet proposed.[138] Overall, catechol-containing copolymers with a variety of different comonomers, such as lysine, acrylates, ethylene glycol, styrene and others, were developed.[153-157] Examples for the potential applications of such catechol-based polymers are their use as adhesives, elastomers, in resins and hydrogels, in contrast agents, layers for nanoparticles and the general functionalization of various surfaces.[100, 151, 158-162]

2. Aims and Outline

One could say that we live in the polymer age where polymer chemistry has shaped our everyday life in almost all aspects. The continuous development of new methods of polymer synthesis makes it possible to develop special products that are perfectly tailored to the required field of application. An important development was the introduction of CRPs. They enable structural and functional control in polymers and their properties that could not be addressed before, such as incorporating a wide variety of monomers into a polymer of low dispersity and with a controlled sequence. Nevertheless, CRPs have not found the breakthrough in industrial research that would have been expected. Among others, reasons are their need for special initiators, catalysts or monomers in addition to often complex reaction conditions. Thus, continuing research on new and improved CRPs is an important area in polymer chemistry.

Access to highly controlled polymer structures is particularly relevant in the design and study of polymeric biomimetics. Their natural analogues – biopolymers such as proteins and glycans – are typically monodisperse and sequence-defined and these features also control their resulting function such as bioadhesion. Bioadhesion is important on the micro scale, for example a virus attaching to a cell, and on larger scale, for example a mussel adhering to a rock. Mimicking such bioadhesion by developing synthetic polymers with biofunctional motifs can generate new functional materials, e.g., for use as inhibitors of viral attachment and thus infection, or as glues.

The goal of this study is the investigation of a potential new type of controlled radical polymerization method in solution, based on previous work by Braunschweig *et al.*[55] (TPO will be used as a photoinitiator and $Ir(ppy)_3$ as a photocatalyst). Different thiols will be explored as initiators. Acrylamides and methacrylates will be used as monomers to demonstrate the versatility of the polymerization method with classical monomers. NMR measurements and mass determinations will be used to demonstrate the controlled character of the polymers and also to propose the polymerization mechanism. SEC-MALS measurements will be carried out to show the narrow molecular weight distribution of polymers synthesized via TIRP.

In the second part of the thesis, the before mentioned photoinitiator TPO is used to prepare light-induced GAG mimetics by free radical polymerization. In this process, a mannose monomer is homo- and copolymerized with *N*-hydroxyethyl acrylamide. In order to derive GAG mimetics, the polymers will then be sulfated. Homopolymers of different chain lengths are targeted as well as copolymers with different incorporation ratios of the monomers to be able to investigate the effect of the amount of negatively charged groups as well as the charge density on the inhibitory potential in viral adhesion

studies. In light of the recent pandemics, GAG mimetic polymers are tested as inhibitors of SARS-CoV-2 adhesion and infection.

In the final part of the thesis, mussel-inspired copolymers are synthesized from four monomers in different incorporation ratios. Monomers either introduce a catechol, a tertiary amine, a primary amide or a *N*-hydroxyethyl side chain. A previous study using oligomers had shown synergistic effects of these functional groups for the resulting adhesion on glass surfaces. Here, this synergy will now be investigated for higher molecular weight polymers at different ratios of the different monomers using quartz crystal microbalance and ellipsometry measurements.

3. Results and Discussion

3.1. TIRP - Thiol-Induced, Light-Activated Controlled Radical Polymerization

Authors: L.Bonda, D.J. Valles, T.L. Wigger, J. Meisner, A.B. Braunschweig, L. Hartmann

Journal: Macromolecules

DOI: 10.1021/acs.macromol.3c00789

Impact Factor: 6.057 (2023)

Own Contribution:

Collaborative study design. Synthesis, isolation and characterization (NMR, SEC, MALDI-ToF) of all polymers and copolymers. Optimization of synthesis routes and development of optimal polymerization parameters. Performance of all kinetic studies and graphical and calculative analysis of the results. Mass spectrometric analysis of the products and collaborative establishment of a mechanistic proposal. Collaborative writing of the manuscript.

Macromolecules

pubs.acs.org/Macromolecules Article

TIRP—Thiol-Induced, Light-Activated Controlled Radical Polymerization

Lorand Bonda, Daniel J. Valles, Tillmann L. Wigger, Jan Meisner, Adam B. Braunschweig, and Laura Hartmann*

Cite This: *Macromolecules* 2023, 56, 5512–5523 Read Online

ACCESS | Metrics & More | Article Recommendations | Supporting Information

ABSTRACT: Controlled radical polymerizations (CRPs) are one of the most important ways to obtain uniform, defined molecular weight polymers with complex composition and architecture such as block copolymers. A new controlled and light-initiated radical polymerization is introduced that makes use of thiol initiators and an Ir-photocatalyst. Different reaction parameters are studied for their importance in the controlled characteristics of polymerization, such as low dispersity, control of molecular weights, and straightforward access to block copolymers. The light control furthermore allows for simple switching on and off of the polymerization. We propose a mechanism for the so-called thiol-induced, light-activated, controlled radical polymerization (TIRP), which includes the formation of dormant species and their light- and catalyst-dependent equilibrium with the active polymer chain end. TIRP enriches the portfolio of controlled and light-initiated polymerization methods by its viability at mild conditions and the possibility to grow polymers from a large variety of readily available thiols.

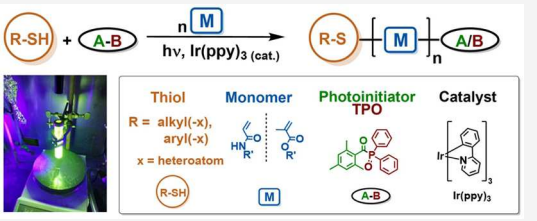

INTRODUCTION

Free radical polymerization (FRP) is typically associated with the easy and fast synthesis of polymers and compatibility with a large variety of monomers and reaction conditions.[1,2] In comparison to the ionic polymerizations, however, control over chain lengths, end groups, dispersity, and access to block copolymers is limited.[3] Combining the advantages of free radical and ionic polymerizations, reversible deactivation radical polymerizations (RDRPs) or in short CRPs were developed.[4] The most prominent representatives are atom transfer radical polymerization (ATRP),[5] reversible addition–fragmentation chain-transfer polymerization (RAFT)[6,7] and nitroxide-mediated radical polymerization (NMP).[8] The common denominator of these methods is the equilibrium between an active, growing, and a deactivated, sleeping (or dormant) form of the polymer chain end. By pushing the equilibrium to the side of the dormant species, termination reactions are drastically reduced. This results in narrow average molecular weight distributions, low dispersities, and control over end groups. Typically, these controlled polymerizations are thermally activated. In the last decade, there has been a great interest in developing alternative activation options,[9] such as redox-controlled,[10] enzymatic,[11] high voltage,[12] or directly activated polymerizations.[13] Of the emerging activation methods, photoactivated[14−17] controlled radical polymerization (photo-CRP)[18] is of particular interest because light is accessible, low-cost, low-energy, is environmentally benign compared to other activators, and polymer propagation can easily be controlled by simply turning the light on and off.[19,20]

Both metal-catalyzed and metal-free photo-CRPs[21] have been developed and demonstrated for their use in various applications.[4,22] In general, photo-CRPs occur in two different variants, the intramolecular reaction and the photoredox reaction[23,24] (Figure 1). In the intramolecular reaction, light irradiation cleaves the photoactive, dormant species, releasing the active chain end for polymerization. An example of intramolecular photo-CRPs is the UV-mediated RAFT-polymerization[16,25,26] which, compared to the thermally activated RAFT, uses special transfer reagents that can be activated through UV light. In the photoredox variant of CRPs, a photocatalyst is added, which generates a propagating radical by excitation with light. Two examples of photoredox CRPs are the photo-ATRP[18,27,28] and the photo electron transfer RAFT (PET-RAFT).[29] In photo-ATRP,[27] an air-stable copper(II) halide is reduced by light to the copper(I) species, then mediating the ATRP. Hawker et al.[30] presented a way to perform photo-ATRP by using tris(2-phenylpyridine)iridium-(III) ($Ir(ppy)_3$) as a photocatalyst.

Recently, Wong et al.[31] introduced a photoinduced thiol-acrylate polymerization (photo-TAP) exclusively used so far for grafting polymers onto solid surfaces. The polymerization

Received: April 26, 2023
Revised: May 25, 2023
Published: July 6, 2023

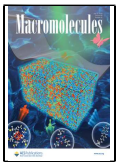

https://doi.org/10.1021/acs.macromol.3c00789
Macromolecules 2023, 56, 5512−5523

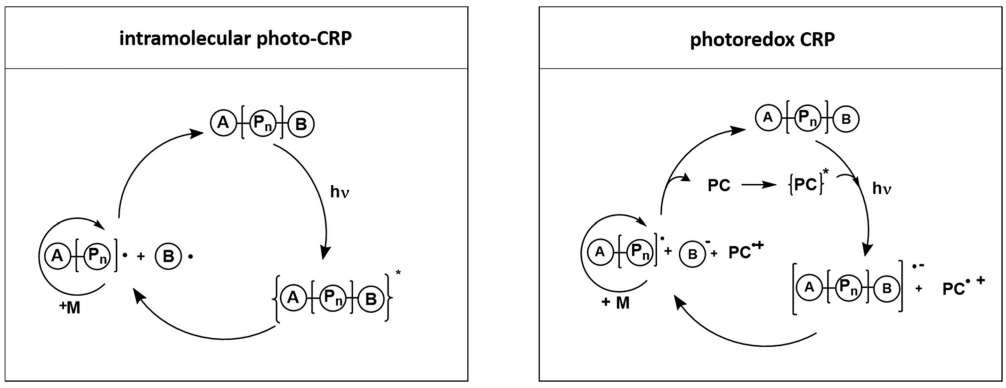

Figure 1. General mechanism of intramolecular photo-CRPs (left) and photoredox CRPs (right).[23]

was carried out on thiol-modified glass, and *tert*-butyl methacrylate (*t*BMA) was used as the monomer. With a photoinitiator/catalyst system consisting of diphenyl-(2,4,6-trimethylbenzoyl)-phosphine oxide (TPO) and $Ir(ppy)_3$, highly uniform polymer brush patterns (e.g., in terms of the height and positioning of polymers at the surface) were obtained. TPO is a known and widely used photoinitiator for light-activated FRP. $Ir(ppy)_3$ is a photocatalyst,[32,33] which is used in single electron transfer (SET) reactions, e.g., photo-ATRP[19,30] or PET-RAFT,[29] and is often used as a photoredox catalyst. The controlled surface-initiated thiol-(meth)acrylate polymerization (SI-TAP[31]) was carried out by irradiation with UV-light at 405 nm wavelength. By varying the TPO- and $Ir(ppy)_3$-concentration, a linear relationship of the resulting polymer brush height with increasing amounts of TPO or $Ir(ppy)_3$ was found. In addition, it was shown that growth on the surface was linear only up to a certain irradiance intensity (852 $\mu W/cm^2$). If this value was exceeded, polymer growth was no longer uniform. Another interesting aspect is the control of polymer growth by switching the light source on and off. If the irradiation was interrupted, the polymer growth stagnated. When the light source was switched on again, polymer growth started anew. Thus photo-TAP shows typical features of a CRP, however, this could not be further investigated as the process has been restricted to surface polymerizations. In this work, we therefore investigate this polymerization in solution. To highlight that this is a new method going beyond SI-TAP, e.g., in terms of the variety of applicable thiol initiators, analysis of molecular weights and dispersities of derived polymers, reinitiation, and accessibility of block copolymers and compatibility with other in-solution methods, we now call this thiol-induced, light-activated controlled radical polymerization (TIRP). We aim at demonstrating the controlled radical mechanism and the synthetic possibilities of TIRP, thereby adding another reaction to the small group of very impactful controlled polymerization reactions and one that is initiated from simple and widely available thiols.

EXPERIMENTAL SECTION

Materials. Chemical compounds that were not synthesized were obtained from commercial sources and used without further purification. Acetonitrile (99.9%, HPLC-grade), hydrochloric acid 1 M (p.a.), diethyl ether (p.a.), dichloromethane (99.9%, puriss., p.a.), D-(+)-mannose (99%), 2-methyl-2-propanethiol (99%), (3-nitrobenzyl)-mercaptane (97%), sodium chloride (98%), thiophenol (97%), 2-(trimethylsilyl)ethanethiol (95%), and triphenylmethanethiol (97%) were purchased from Sigma-Aldrich. Dichloromethane (p.a.), dimethylformamide (98%, for peptide synthesis), and ethyl acetate (analytical reagent grade) were purchased from ACROS Organics. Methanol (p.a.), acetic anhydride (99.7%), and pyridine were purchased from VWR Chemicals. Tris(2-phenylpyridine)-iridium(III) (99%) was purchased from BLDpharm. Diphenyl-(2,4,6-trimethylbenzoyl)-phosphine oxide (>98%) and *N*-hydroxyethylacrylamide (>98%) were purchased from TCI chemicals.

Methods. *UV-Light Source.* Samples were irradiated with a UV-LED Spot P standard (405 nm) from Opsytec Dr. Gröbel GmbH.

Irradiation Intensities. Irradiation intensities were determined with a FieldMaxII-TO Laser Power Meter from Coherent.

Nuclear Magnetic Resonance. ^1H NMR spectra were recorded at room temperature with a Bruker AVANCE III 300 (for 300 MHz) and 600 (for 600 MHz). ^{31}P NMR spectra were recorded at room temperature with a Bruker AVANCE III 300. The chemical shifts were reported relative to solvent peaks (chloroform and water) as internal standards and reported as δ in parts per million (ppm). Multiplicities were abbreviated as s for singlet, d for doublet, t for triplet, and m for multiplet.

Matrix-Assisted Laser Desorption-Ionization Time of Flight (MALDI-TOF). MALDI-TOF spectra were recorded with a MALDI-TOF Ultraflex I provided by Bruker Daltonics. The sinapinic acid matrix applied in a mixture of acetonitrile and water (ratio of 1:2) was selected.

Size Exclusion Chromatography—Multi-Angle Light Scattering (H_2O-SEC-MALS). SEC analysis was conducted with an Agilent 1200 series HPLC system and three aqueous SEC columns provided by Polymer Standards Service (PSS). The columns were two Suprema Lux analytical columns (8 mm diameter and 5 μm particle size) and one precolumn (50 mm, 2 × 160 Å of 300 mm and 1000 Å of 300 mm). The eluent was a buffer system consisting of MilliQ water and 30% acetonitrile with 50 mM, NaH_2PO_4, 150 mM NaCl, and 250 ppm NaN_3 with a pH = 7.0 (via addition of 50 mL of 3 molar aqueous sodium hydroxide solution) filtered with an inline 0.1 μm membrane filter and running at 0.8 mL per min. Multi-angle light scattering is recorded via miniDAWN TREOS and differential refractive index spectra with Optilab rEX both supplied by Wyatt Technologies EU. Data analysis was committed with Astra 5 software and a dn/dc value of 0.156 for each polymer.

Tetrahydrofuran-Size Exclusion Chromatography (THF-SEC). THF-SEC measurements were carried out with a Viscotek VE 3580 RI detector and a SYKAM S 3250 UV/Vis detector equipped with a polystyrene column (300 × 8.0 mm, 5 μm) and a polyacryl column (300 × 8.0 mm, 5 μm). A S5200 (SYKAM) sample injector as an auto sampler was utilized. THF was used as a solvent and toluene as a reference. The measurements were carried out with an injection volume of 100 μL and a flow rate of 1 mL/min. The molecular weights were determined with the Chromatographica (hs GmbH) software.

SEC (Center of Macromolecular Structure Analysis at the Leibniz Institute of Polymer Research in Dresden). SEC analysis was conducted with an Agilent 1260 series HPLC system, one precolumn, and three aqueous SEC columns provided by GE Healthcare. The

https://doi.org/10.1021/acs.macromol.3c00789
Macromolecules 2023, 56, 5512−5523

columns were three Suprema Lux analytical columns (100/100/1000). The eluent was a buffer system consisting of MilliQ water with 10 mM PBS buffer with pH = 7.4 and running at 1 mL per min. Multi-angle light scattering is recorded via DAWN Heleos-II (Wyatt), λ = 660 nm, and differential refractive index spectra with Optilab T-rEX (Wyatt), λ = 660 nm, both supplied by Wyatt Technologies EU. Data analysis was committed with Astra software and a dn/dc value of 0.163 for each polymer.

Freeze Dryer. Lyophilization was performed with an Alpha 1−4 LD instrument provided by Martin Christ Freeze Dryers GmbH. A temperature of −42 °C and a pressure of 0.1 mbar were maintained throughout the freeze-drying process.

Elemental Analysis. The ratios of carbon, hydrogen, nitrogen, and sulfur were determined using a Vario Micro Cube provided by Analysensysteme GmbH. The measurements were carried out by the Institute for Pharmaceutical and Medicinal Chemistry, Heinrich-Heine University Düsseldorf.

High-Pressure Liquid Chromatography (HPLC). RP-HPLC/MS (Reversed Phase-HPLC/Mass Spectroscopy) was performed on an Agilent Technologies 1260 Infinity System using an AT 1260 G4225A degasser, G1312B binary pump, G1329B automatic liquid sampler, G1316C thermostatted column compartment, G1314F variable wavelength detector at 214 nm, and an AT 6120 quadrupole containing an electrospray ionization (ESI) source. The mobile phase consisted of buffer C (water−acetonitrile 95:5 (v/v), 0.1 vol % formic acid) and buffer D (water−acetonitrile 5:95 (v/v), 0.1 vol % formic acid). HPLC runs were performed on a Poroshell 120 EC-C18 (3.0 × 50 mm, 2.5 μm) RP column from Agilent at a flow rate of 0.4 mL/min 95% buffer A and 5% buffer B (0−5 min), following a linear gradient to 100% buffer B (5−30 min) at 25 °C. ESI-MS for GlcNAc-oligomers and sulfates was performed using 95% buffer A and 5% buffer B without formic acid and a fragmentor voltage of 40−60 V (m/z range of 200−2000).

Computational Details. For the optimization of minimum structures and transition states, the B3LYP[34] functional was employed with the def2-TZVP[35] basis set. Electronic energies and gradients were calculated using Turbomole[36] version 7.2.1 with an accuracy of 10^{-9} atomic units and the multigrid m5. To account for dispersion, the D3 dispersion correction[37] with Becke−Johnson damping[38] was used. Stationary points have been validated in their nature by the correct number of negative eigenvalues of the corresponding Hessian matrices: zero for minima and one for transition states. Geometry optimizations were performed using the DL-FIND[39] optimization library interfaced to Turbomole via Chemshell.[40] Solvation effects were accounted by using the COSMO[41] implicit solvation model (ε_{DMF} = 37.51).[42] For the calculation of free energies, a modified rigid-rotor-harmonic-oscillator approximation was used: frequencies below 100 cm^{-1} have been set to this value to avoid divergence of the entropic term.

Synthesis. *General Procedure of TIRP.* One equivalent of *N*-hydroxyethylacrylamide monomer (HEAA, 100 mol %) or *tert*-butyl methacrylamide (TBMA, 100%) and tris(2-phenylpyridine)iridium-(III) (Ir(ppy)$_3$, z mol%) are dissolved in DMF [10 wt %] sealed in a 5 mL glass flask and flushed with argon as inert gas for 10 min. In a second step, the thiol compound (x mol%) and equimolar amounts of diphenyl-(2,4,6-trimethylbenzoyl)-phosphine oxide (TPO, y mol% = x mol%) are also dissolved in DMF [10 wt %] and sealed in a 5 mL microwave reaction vial. A spatula tip of TCEP is dissolved in a single drop of H_2O and added to the reaction solution to reduce possible disulfides. The thiol/TPO solution is flushed under an Ar-atmosphere for 10 min and irradiated with UV-light (405 nm wavelength, intensity dependent on thiol and monomer used) for 3 min. Subsequently, the monomer/Ir(ppy)$_3$ mixture is added to the TPO/thiol solution under an inert atmosphere, and the polymerization solution is irradiated further at an unchanged light intensity. After an hour, the irradiation is stopped and the polymer solution precipitated in diethyl ether (PHEAA) or H_2O/MeOH 1:3 (v/v) (PTBMA). The precipitated PHEAA is dissolved in H_2O, dialyzed against distilled water (three cycles, exclusion size-dependent on molecular weight), and subsequently lyophilized.

PHEAA-block-PHEAA. HEAA monomer (500 mg, 4.3 mmol) (1 eq) and Ir(ppy)$_3$ (0.05 mol %) are dissolved in DMF [10 wt %] sealed in a 5 mL glass flask and flushed with argon gas for 10 min. In a second step, the macro initiator polymer (55 mg, 0.0275 mmol) is also dissolved in DMF [10 wt %] and sealed in a 5 mL microwave reaction vial. A spatula tip of TCEP is dissolved in a single drop of H_2O and added to the reaction solution to reduce possible disulfides. After the monomer/Ir(ppy)$_3$ mixture is added to the vial (inert atmosphere), the solution is irradiated with UV-light (405 nm wavelength, with an intensity of 45.2 mW/cm^2 (100%)). After an hour, the irradiation is stopped and the polymer solution is precipitated in diethyl ether. The precipitated polymer is dissolved in H_2O, dialyzed against distilled water (three cycles, 10 kDa), and subsequently lyophilized.

PHEAA-block-PManAAm. AcO-ManAAm (966.6 mg, 2.17 mmol, see SI chapter 2.2 for synthesis) (1 eq) and Ir(ppy)$_3$ (0.05 mol %) are dissolved in DMF [10 wt %] sealed in a 5 mL glass flask and flushed with argon gas for 10 min. In a second step, the macro initiator polymer (0.6 g, 0.086 mmol) is also dissolved in DMF [10 wt %] and sealed in a 5 mL microwave reaction vial. A spatula tip of TCEP is dissolved in a single drop of H_2O and added to the reaction solution to reduce possible disulfides. After the monomer/Ir(ppy)$_3$ mixture is added to the vial (inert atmosphere), the solution is irradiated with UV light (405 nm wavelength, with an intensity of 45.2 mW/cm^2 (100%)). After an hour, the irradiation is stopped and 5 mL of NaOMe (0.2 M) in MeOH was added to the polymer solution and stirred one hour at room temperature. The sample solution is precipitated in diethyl ether. The precipitated polymer is dissolved in H_2O, dialyzed against distilled water (three cycles, 5 kDa), and subsequently lyophilized.

RESULTS AND DISCUSSION

Controlled Features of TIRP—Dispersity and Reinitiation. To determine if TIRP has the key features of a controlled radical polymerization (low dispersity, controllable molecular weights, linear correlation between degree of polymerization (DP) and monomer conversion, reinitiation), a first set of reactions was carried out using commercially available acrylamide (*N*-hydroxyethylacrylamide (HEAA)) and methacrylate (*tert*-butyl methacrylate) monomers, the photoinitiator/catalyst system consisting of TPO as the initiator and Ir(ppy)$_3$ as the catalyst, and tritylthiol as the thiol component, as it is easy to handle and can be easily detected in ^{1}H NMR-spectroscopy (Scheme 1). The thiol/TPO ratio was set to 1:1,

Scheme 1. TIRP in Solution (Polymerizations #1 and #2)

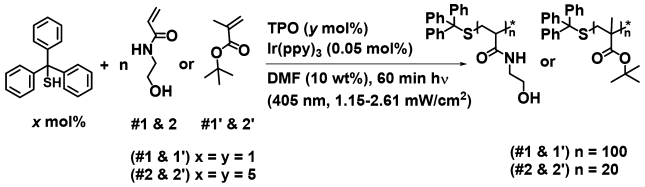

and the amount of thiol−TPO was increased from 1 mol % in the first polymerization to 5 mol % in the second polymerization to achieve different chain lengths at a similar overall monomer concentration [1.7 mmol] (Table 1). Molecular weights and dispersity of the obtained poly(*N*-hydroxyethylacrylamide) (PHEAA) were determined by aqueous size exclusion chromatography-multiangle light scattering (SEC-MALS) coupled with an RI detector, showing that both polymers are obtained with much lower dispersity ($Đ$ = 1.09−1.10, additional data via RI-MALS, see SI chapter 2) than is expected for an FRP (see the SI for control reaction performed as FRP by leaving out the thiol initiator giving $Đ$ = 1.7 at DP of

https://doi.org/10.1021/acs.macromol.3c00789
Macromolecules 2023, 56, 5512−5523

Table 1. Thiol−TPO Ratios with Average Molecular Weights and Dispersities Obtained for #1, #2, #1′, and #2′

#	thiol conc. [mol %]	TPO conc. [mol %]	irradiation intensity [mW/cm^2]	$\bar{M}_n$ [kDa][a] theoretical (via SEC)	$\bar{P}_n$ theoretical (calculated)	$Đ$[a] via SEC
1	1	1	2.61	11.8 (12)	100 (98)	1.1
2	5	5	2.61	2.7 (2.7)	20 (20)	1.09
1′	1	1	1.15	14.2 (14.6)	100 (103)	1.3
2′	5	5	1.15	2.8 (2.7)	20 (18)	1.3

[a]Via SEC-MALS-RI (precolumn (50 mm, 2 × 160 Å of 300 mm and 1000 Å of 300 mm), two main columns (8 mm diameter and 5 μm particle size), eluent: MilliQ water−acetonitrile 7:3 (v/v), 50 mM, NaH_2PO_4, 150 mM NaCl and 250 ppm NaN_3, pH = 7.0, flow rate: 0.8 mL/min; for additional measurements with SEC-MALS-RI detector, see SI, chapter 2.

70).[43] The same is found for poly(*tert*-butyl methacrylate) (PTBMA) dispersities determined by THF-SEC, with RI and UV detectors ($Đ$ = 1.0−1.4). Molecular weights for both polymers closely match the theoretically expected molecular weights (Table 1).

To further demonstrate the potentially living character of TIRP, kinetic measurements were recorded during the polymerization of HEAA with tritylthiol as the thiol source. A characteristic of controlled polymerizations is a linear relation between chain growth and conversion, in contrast to the exponential relation in FRPs. Samples were taken from the polymerization solution at defined times and the conversion was determined by ^{1}H NMR spectroscopy (see SI, chapter 2.1.3 for details). As shown in Figure 2A, reaction time is

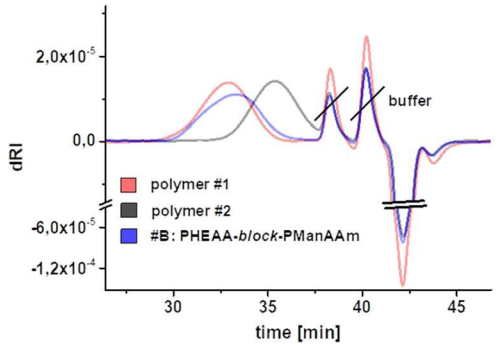

Figure 2. Aqueous SEC-MALS measurement of polymer #1, polymer #2 (Scheme 1), and PHEAA-*block*-PManAAm (Scheme 2B, copolymer #B).

plotted against the monomer conversion, showing a curve previously reported also for other light-activated CRPs such as PET-RAFT.[29] Maximum conversion is reached after 60 min for a polymer of 2.7 kDa ($\bar{P}_n$ = 20) (#2) and after 90 min for a polymer of 14.2 kDa ($\bar{P}_n$ = 100) (#1). We observed that conversion reaches a plateau at around 70%. At this time, we attribute this to deactivation of the catalyst, as has previously been shown for other CRP systems, e.g., ATRP.[44] Alternatively, a complete deactivation of the growing chains is highly unlikely, as this would have resulted in much higher dispersities than observed. It is also known that the polymerization of acrylamide monomers with full conversions is challenging in commonly used CRPs such as ATRP.[45,46] However, this phenomenon will be investigated further in future experiments.

Figure 3B shows the plot of $\ln([M]_0/[M]_t)$ against the reaction time (with $[M]_0$ = initial monomer concentration and $[M]_t$ = monomer concentration at reaction time t). An ideal living polymerization is expected to give a linear correlation in such a plot.[47] For TIRP, we observe a nearly linear correlation with a light tilt downward at higher reaction times. This has also been observed for other CRPs and indicates termination events likely by recombination and disproportionation that can occur from the radical chain ends. For example, Driessen et al.[47] showed such tilting for well-established ATRP reactions.

One of the interesting features of light-controlled polymerizations is the ability to stop polymerization by switching the light source off as well as to (re-)start the reaction again when turning the light source back on. To test whether this occurs in the TIRP, the polymerization was performed by switching repeatedly the light off and then back on again, and conversion was determined before and after each on/off cycle by ^{1}H NMR spectroscopy. We observed stagnation of the conversion during "light off" periods, with continuing conversion when the light is switched on again (Figure 3C).

The control over polymer growth by switching the light source on and off (Figure 3C), as well as the linear relationship of conversion and degree of polymerization (Figure 3D) show typical characteristics of light-controlled polymerizations. The evolution of molecular weight, respectively, the degree of polymerization was observed via ^{1}H NMR spectroscopy. SEC analysis was not suitable here as especially for the lower $\bar{P}_n$ samples, polymers could not be isolated from the reaction mixture without discriminating against parts of the sample (e.g., shorter chains).

The possibility of growth control through switching the light source on/off and comparison to other controlled systems also suggests that a dormant species is present which can be reinitiated. Thus, next, we tested whether it is possible to reinitiate, not only in the reaction solution itself but also from a polymer that is first isolated by precipitation and then used in a second, independent polymerization to derive a block copolymer (Scheme 2). Therefore, further HEAA (#A) and tetra-acetylated mannose-acrylamide monomer (AcO-ManAAm, #B, see SI, chapter 2.2 for synthesis of the monomer) were used as comonomers for two separate reinitiation reactions.

Employing the previous TIRP conditions (thiol/TPO ratio 1:1, 6 mol % each, 0.05 mol % Ir(ppy)$_3$, based on 1 eq of monomer), the PHEAA precursor of 2 kDa was purified and isolated by precipitation, dialysis, and freeze-drying. This precursor was reinitiated with the same monomer by addition of HEAA and Ir(ppy)$_3$, while not introducing any additional thiol/TPO. Molecular weight analysis by aqueous SEC-MALS shows an increase in the number averaged molecular weight ($\bar{M}_n$) from 2 to 20 kDa. Dispersity for the elongated polymer increases from 1.1 to 1.3 (Scheme 2). In a second experiment, AcO-ManAAm was used to prepare a block copolymer. Here, a PHEAA precursor of 7 kDa was again purified and isolated as described above and then reinitiated by the addition of ManAAm and Ir(ppy)$_3$. The resulting PHEAA-*block*-PManAAm (#B) was analyzed by ^{1}H NMR, showing distinct signals of both blocks, as well as by SEC-MALS, giving a mean molecular weight ($\bar{M}_n$) of 13.5 kDa and a dispersity of 1.2 (see

https://doi.org/10.1021/acs.macromol.3c00789
Macromolecules 2023, 56, 5512−5523

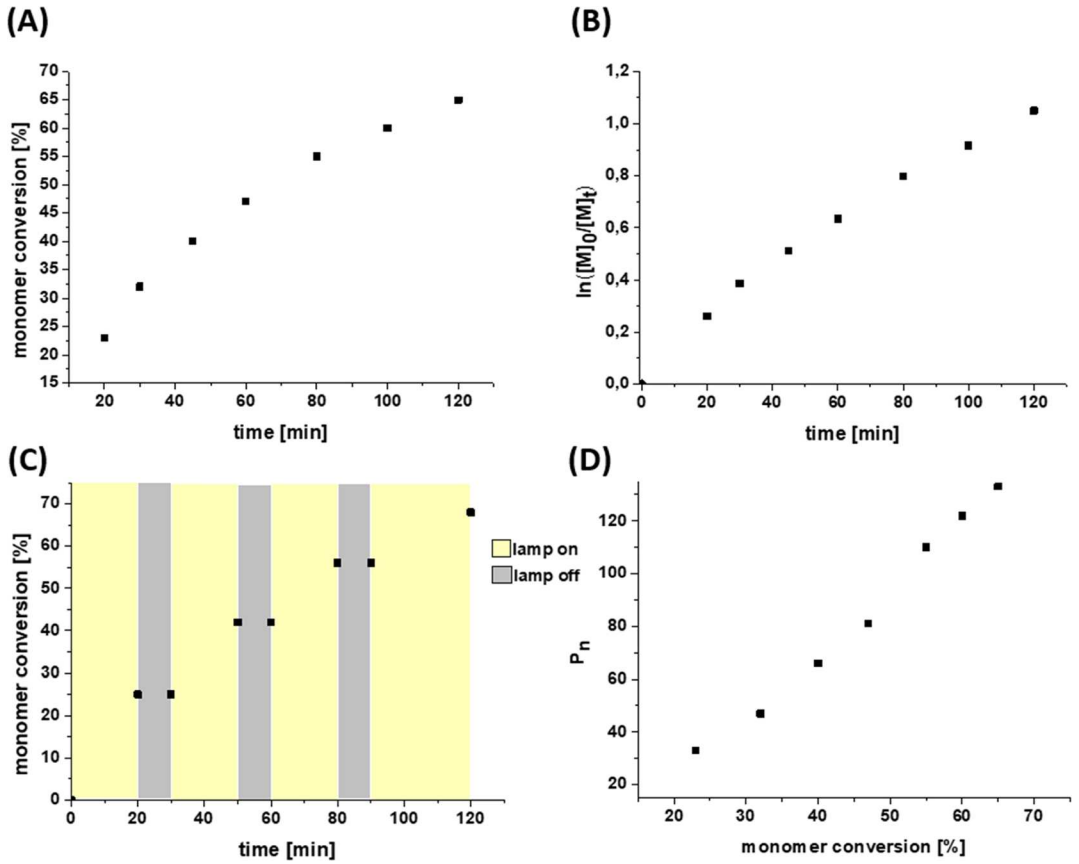

Figure 3. (A) Monomer conversion (determined by ^{1}H NMR spectroscopy) versus reaction time (#1); (B) logarithmic plot of M_0/M_t (M_0 = initial monomer concentration, M_t = monomer concentration at reaction time (t) against reaction time (#1); (C) monomer conversion (determined by ^{1}H NMR spectroscopy) versus irradiation time while light is switched on/off (#1); (D) degree of polymerization against monomer conversion [%] (determined via ^{1}H NMR spectroscopy by referencing the tritylthiol initiator protons; for further information, see SI, chapter 2.1.5).

Scheme 2. (A) Elongation of PHEAA through Reinitiation (Copolymer #A) and (B) Copolymerization with AcO-ManAAm (Copolymer #B)

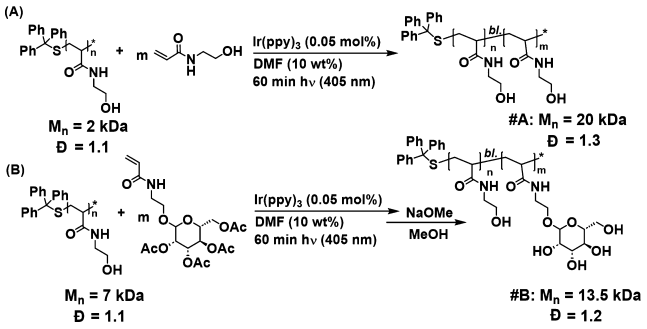

Figure 2). Thus, polymers prepared by TIRP can be reinitiated to obtain block copolymers, which is another important feature of CRPs.

For comparison, free radical copolymerization was performed by synthesis of a precursor PTBMA ($\bar{M}_n$ = 7.7 kDa) with the use of a TPO initiator but no thiol source. This FRP generates a polymer bearing TPO fragments as end groups. After isolation, the precursor polymer was reinitiated without addition of any further initiator (TPO; thiol) but ethyl acrylate as a comonomer (synthesis of precursor and copolymer, see SI, chapter 2.2.2). The resulting copolymer shows an increase in $\bar{M}_n$ (9.5 kDa), evidencing successful reinitiation. The dispersities of both polymers (precursor and copolymer, $Đ$ = 2) are higher than those obtained by TIRP ($Đ$ = 1.2−1.3) and

Scheme 3. Potential Mechanism for the Initiation and Chain Growth Reaction in TIRP via Intramolecular Photo-CRP

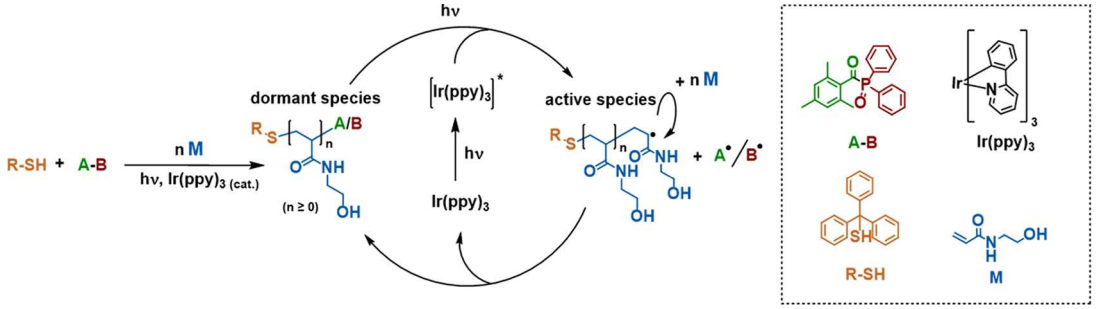

https://doi.org/10.1021/acs.macromol.3c00789
Macromolecules 2023, 56, 5512−5523

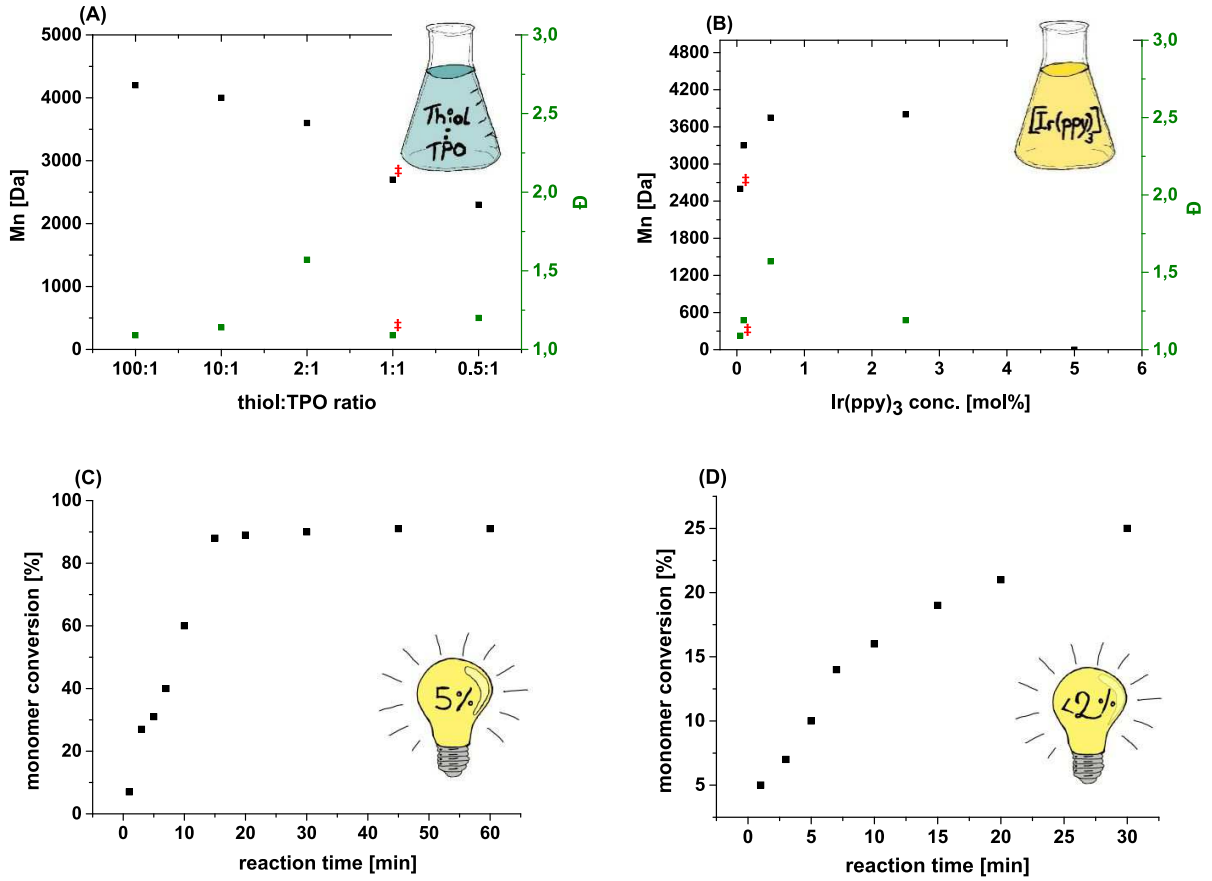

Figure 4. (A) Average molecular weights and dispersities obtained by changing thiol−TPO; $\bar{M}_n$ theory: 2700 Da; ‡highlighted data point shows optimized TIRP reaction conditions with thiol−TPO ratio 1:1, [Ir(ppy)$_3$] = 0.05 mol %, *hν* intensity = 5%; (B) average molecular weights and dispersities obtained by varying [Ir(ppy)$_3$]; $\bar{M}_{n\ theory}$: 2700 Da; ‡highlighted data point shows optimized TIRP reaction conditions with [Ir(ppy)$_3$] = 0.05 mol %, thiol−TPO ratio 1:1, *hν* intensity = 5%; (C) kinetic studies using 2-(trimethylsilyl)-ethanethiol as a thiol source at 5% irradiation intensity; (D) kinetic studies using 2-(trimethylsilyl)-ethanethiol as a thiol source at <2% irradiation intensity.

are characteristic for FRPs. Thus, this experiment shows that reinitiation of polymers bearing TPO-fragments as the end group is possible, supporting our proposed mechanism (Scheme 3). However, these polymers lack the control over the chain length and dispersity obtained by TIRP. To the best of our knowledge, the reinitiation and synthesis of block-coplymers from FRP by using TPO as the initiator have also not been demonstrated before and thus are another important findings of this study. Future studies will follow up on this methodology, while here, the focus is on demonstrating the controlled features and opportunities of TIRP.

Parameters of TIRP. Next, we explored the mechanism of TIRP by studying the effects of the different reaction conditions and components on the resulting polymers. If not stated otherwise, HEAA was used as the monomer and tritylthiol as the thiol component. All reactions were performed in DMF as the solvent, at room temperature, and with 405 nm UV-light because both, TPO and Ir(ppy)$_3$, absorb at this wavelength.[48,16]

Thiol−TPO Ratio. Our first hypothesis on the potential mechanism assumes that TPO forms radicals by photocleavage that then abstract a proton from the thiol compound, giving a thiyl radical that will start the polymerization reaction. Ideally, only the thiyl radical starts the polymer chain by reacting with a first monomer. TPO, as a photoactive radical initiator, is capable of starting polymerizations as well, forming what we call TPO-polymers in contrast to the targeted TIRP products that polymerize from the thiyl radical. If the thiol source is omitted, polymers are formed but have high dispersity, indicating that TPO-polymers are formed by FRP (see SI, chapter 2.2.2). When using a 1:1 ratio of thiol/TPO, as we have done in the first polymerization reactions (#1 and #2, Scheme 2), we observed the following features that are characteristic of controlled polymerizations: linear kinetics, low dispersity, and molecular weights that match the theoretically expected chain length. When the concentration of TPO is lower than the concentration of thiol, we observed higher molecular weights than would have expected based on the thiol−monomer ratio (Figure 4A). This suggests that only a fraction of possible thiol initiators is activated, thereby reducing the number of growing chains. If more TPO than thiol is used, all thiols are activated, but also extra TPO remains, which can initiate additional polymer chains. As a result, molecular weights are decreased and dispersity is increased (see SI, chapter 2.3). Thus, the optimal ratio of TPO−thiol to achieve controlled TIRP is equimolar (1:1) (see Scheme 1).

Ir(ppy)$_3$. To obtain TIRP with the characteristics of a CRP, the use of the photocatalyst Ir(ppy)$_3$ is mandatory. If no Ir-catalyst is used, polymers are formed but have high dispersity and do not show sulfur in the elemental analysis (see SI, Figure S49). Both results indicate that only TPO-polymers are formed. These results also suggest that the thiol source does not undergo unwanted chain transfer reactions, which are

https://doi.org/10.1021/acs.macromol.3c00789
Macromolecules 2023, 56, 5512−5523

typical for thiols in FRPs.[49] If transfers occur, the resulting dispersities would be expected to be higher than those observed. Furthermore, higher sulfur content would have been expected to be measured in the elemental analysis but was not found (see SI, chapter 2.5.1). In addition, the reaction is sensitive to the amount of Ir-catalyst: If too high of an amount of $Ir(ppy)_3$ is used (>2.5 mol % based on [monomer]), polymerization does not occur. When increasing $Ir(ppy)_3$ concentrations below this critical value (0−2.5 mol %), the average molecular weight increases with increasing Ir concentration (Figure 4B), but the yield drops with increasing Ir mol%. The optimum amount of $Ir(ppy)_3$ was found to be 0.05 mol % (based on [monomer]). Here, polymers with chain lengths, as determined by SEC, that are in very good agreement with the theoretically calculated chain lengths were obtained, in good yields, and with low dispersities (see SI, chapter 2.1).

***hν* Intensity.** The irradiation intensity is one of the most important parameters when it comes to controlling the TIRP. Based on the previously established optimized reaction conditions (equimolar ratio of thiol and TPO, 0.05 mol % photocatalyst), polymerizations were performed at either 1.15 mW/cm^2 (2%), 2.61 mW/cm^2 (5%), or 45.2 mW/cm^2 (100%) intensity at 405 nm.

At 100% intensity, we again observe features that are associated with FRP (deviation of molecular weights from theoretical values, high dispersity). At an intensity of 2%, (HEAA as the monomer, tritylthiol as the thiol source), no polymerization occurred. When using only TPO at 2% intensity, the polymer is formed. The ideal intensity was found to be 5% (2.61 mW/cm^2), where controlled polymerization characteristics were observed (see SI, chapter 2.5). To investigate this further, the reaction was carried out with a ratio thiol−TPO of 1:2. As expected, polymers are formed matching FRP characteristics (no thiol content, higher dispersity) (see SI, Table S7). To rule out potential absorption effects of the trityl group of the thiol component, the polymerization was carried out again at 2% light intensity, using triphenylmethanol or triphenylmethylchloride instead of tritylthiol at a 1:1 ratio with TPO. In both cases, polymers were obtained, indicating that the presence of phenyl substituents on the thiol group do not limit the formation of radicals from TPO fragmentation.

By varying the monomer from HEAA to TBMA (thiol−TPO 1:1, [$Ir(ppy)_3$] = 0.05 mol %), 5% intensity already led to FRP characteristics, so irradiation intensity had to be decreased to 2% to regain controlled features. This shows that light intensity has to be adapted to the monomer which we attribute to the different reactivity in radical polymerization of the monomers (methacrylate > acrylamide).[50] This is further supported by our finding that for *tert*-butyl acrylate (TBA), with a further increase in reactivity, at the lowest intensity setting possible with our set-up (1.15 mW/cm^2), we obtained polymers with typical features of FRP only ($Đ$ = 1.6−2.4) (see SI, chapter 2.5.2) We assume, that for successful TIRP of acrylate monomers, intensity has to be decreased further.

Thiol Source. One great advantage of TIRP is the availability of a large variety of different thiols that can be selected as initiators. To understand how the structure of the thiol compounds affects the TIRP, the previously used tritylthiol was replaced by 2-(trimethylsilyl)-ethanethiol (TMS-thiol). HEAA was used as the monomer. Under the reaction conditions optimized for tritylthiol (thiol−TPO ratio 1:1, 5% irradiation intensity, 0.05 mol % $Ir(ppy)_3$), polymers with molecular weights close to the theoretical value ($\bar{M}_{n\ theory}$ = 2.7 kDa), although with high dispersity (>3), were obtained. Kinetic studies show that the molecular weight first increases exponentially as the conversion progresses but then reaches a plateau. Such exponential growth is typical for FRPs (Figure 4C). However, by further reducing the light intensity to <2%, a chain growth with a constant progress relation was observed (Figure 4D). Thus, we conclude that, as in the case for monomers, for different thiols, a different light intensity is required to realize TIRP with CRP characteristics. This is likely related to the different kinetics of initiating chain growth when using different thiol sources.

We tested a first series of different thiol derivatives and show that they all can successfully be used as initiators in TIRP (Figure 5; see SI, chapter 2.7). Each thiol, however, requires its own optimal irradiation intensity to keep the controlled characteristics of the polymerization. As an example, tritylthiol did not initiate polymerization at 2% irradiation intensity, but polymerization took place at 5% irradiation intensity. Thiophenol, on the other hand, showed no polymerization at 5% irradiation intensity, so the irradiation intensity was increased to 30% (see SI, Table S10).

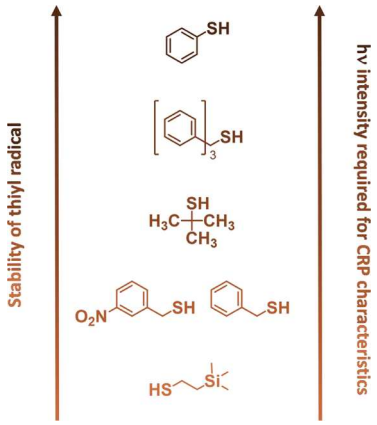

Figure 5. Thiols used to initiate TIRP (HEAA = 1 eq, $Ir(ppy)_3$ = 0.05 mol %, DMF = 10 wt %, *hν* = 60 min, varying intensities; 405 nm; for additional data, see SI, chapter 2.7).

TMS-thiol polymers were already formed at 2% irradiation intensity, but the reaction showed FRP characteristics, indicating that the intensity needs to be decreased further to regain CRP characteristics. Generally, we observed that primary thiols require less irradiation intensity than secondary or tertiary thiols. A possible explanation is that as primary thiol radicals are less stabilized than tertiary or phenylic ones, the rate-limiting step might be to initiate polymer propagation. Initiation at a more stabilized radical could require a higher light intensity, while the reaction of a primary, less-stabilized radical already occurs at a lower irradiation intensity.

Potential TIRP Mechanism. Based on our observations on the effects of the different reaction parameters and quantum chemical calculations of the different initiation and propagation steps (see SI, chapter 3), we postulate a potential mechanism for TIRP. We have seen that in the absence of thiol, upon irradiation, TPO forms two radical-bearing fragments (mesityl fragment (A) and phospine fragment (B), Scheme 3) and starts a FRP (TPO-polymers). As we have shown and discussed before, also FRP TPO-polymers can be reinitiated and give access to blockcopolymers, yet with less

https://doi.org/10.1021/acs.macromol.3c00789
Macromolecules 2023, 56, 5512−5523

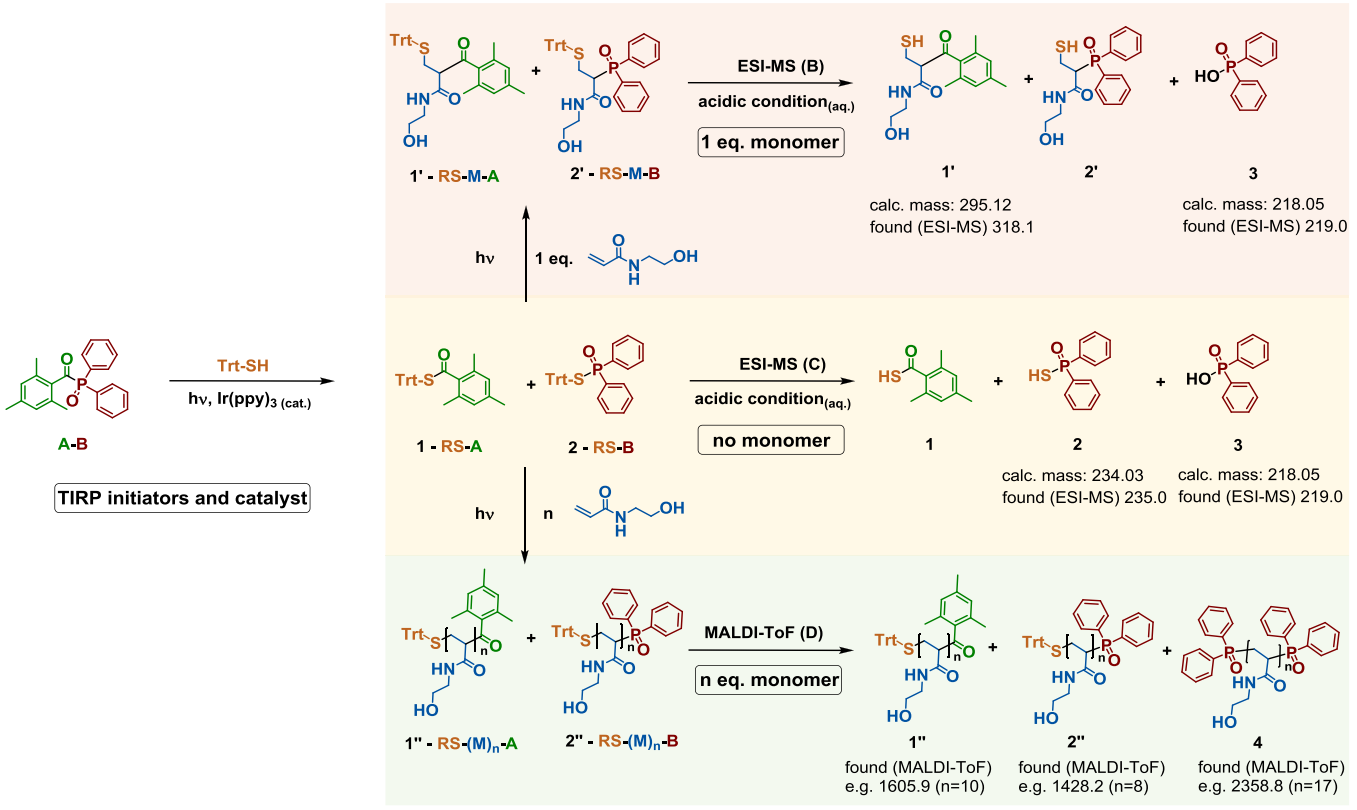

Figure 6. Reaction of tritylthiol, TPO, and Ir(ppy)$_3$ without monomers (intermediates **1** and **2**) and after adding 1 eq HEAA (intermediates **1′** and **2′**) or *n* eq. HEAA (polymers **1″** and **2″**) to the reaction. Determined molecular weights via RP-HPLC-MS and MALDI-ToF are shown (including the hydrolysis product DPPA, **3**); for RP-HPLC-MS measurement spectra of intermediates **1**, **1′**, **2**, and **3**, see SI, Figures S99 and S100. For the MALDI-ToF spectrum of polymerization performed under optimized conditions (**1″** and **4**), see SI, Figure S95.

control over the chain length and dispersity. In the case of the CRP, in the presence of both thiol and the Ir catalyst, TPO fragment(s) first abstract a hydrogen from the thiol. The resulting thiyl radical initiates chain elongation, leading to polymers with chain ends consisting of the thiol compound, as seen in MALDI-ToF-MS (see SI, Figure S95). For a controlled mechanism, a dormant species must form. We hypothesize that the dormant species in TIRP is formed by recombination of the active chain end (thiyl radical for $n = 0$) with one of the TPO fragments (A, if B abstracted the hydrogen or B, if A abstracted the hydrogen in the initiation reaction) (Figure 6). We confirm the formation of this dormant species, tritylthiol, Ir(ppy)$_3$, and TPO was irradiated in the absence of monomers (Figure 6). RP-HPLC-MS analysis of the reaction mixture indeed confirms the formation of intermediate **2** (RS-B, see SI, Figure S100). As reported by Sluggett et al.,[51] the reactivity of the two different TPO fragments in order to achieve hydrogen transfer onto a thiol is approximately equal. Therefore, we assume that also **1** (RS-A) is formed but is not detected by RP-HPLC-MS due to the detection limit. When repeating the experiment in the presence of one equivalent of monomer per TPO/thiol, polymer chains with $\overline{P}_n = 1$ were identified by RP-HPLC-MS, with end groups consisting of the thiol as well as the TPO mesityl fragment **1′** (RS-M-A, see SI, Figure S99). In all cases, an additional signal at $m/z = 219$ was found and is assigned as diphenylphosphinic acid (DPPA, **3**, see SI, Figures S99 and S100). We assume that the second dormant species, **2′** (RS-M-B), was also formed but that the TPO-end group was hydrolyzed under LC conditions (aqueous acidic conditions) releasing DPPA **3**. The trityl group is also not detected in any of the structures, as it is well known to be easily cleaved under even slightly acidic conditions.[52] Overall, these findings support our postulated mechanism (Scheme 3).

To confirm that the same end groups are also present in higher molecular weight polymers, end group analysis by MALDI-ToF-MS was performed. The MALDI-ToF (see SI, Figure S95) shows the end groups of a polymer synthesized with optimized TIRP conditions (thiol−TPO 1:1, 0.05 mol % Ir(ppy)$_3$, 5% irradiation intensity) for tritylthiol and HEAA. The signals with the highest relative intensity are spaced with $m/z = 115.13$, which corresponds to the mass of the monomer. Dormant species, RS-M$_n$-A (polymer **1″**) and RS-M$_n$-B (polymer **2″**), can be identified. In addition, chain ends formed through recombination, as known from FRP, are also found, although at lower relative intensity (see SI, Figure S98). The presence of polymers from these termination reactions is also known for other CRPs.[53,54] For comparison, MALDI-ToF end group analysis was also performed for conditions that do not follow controlled polymerization characteristics (thiol−TPO ratio not at 1:1, too high irradiation intensity for tritylthiol as well as TMS-thiol) (see SI, Figures S96 and S97). In all cases, a larger number of different end groups was observed, which were assigned to end groups from dormant species, end groups from FRPs, and mixtures thereof (TPO-initiated and recombined), as is expected for a less controlled reaction. To further confirm the phosphorus containing TPO end groups, ^{31}P NMR spectra were recorded of species 2, 2′, and 2″. For all three compounds, a phosphorus signal is found in the spectra (see SI, Figures S102−S104), supporting our findings from MS analysis.

https://doi.org/10.1021/acs.macromol.3c00789
Macromolecules 2023, 56, 5512−5523

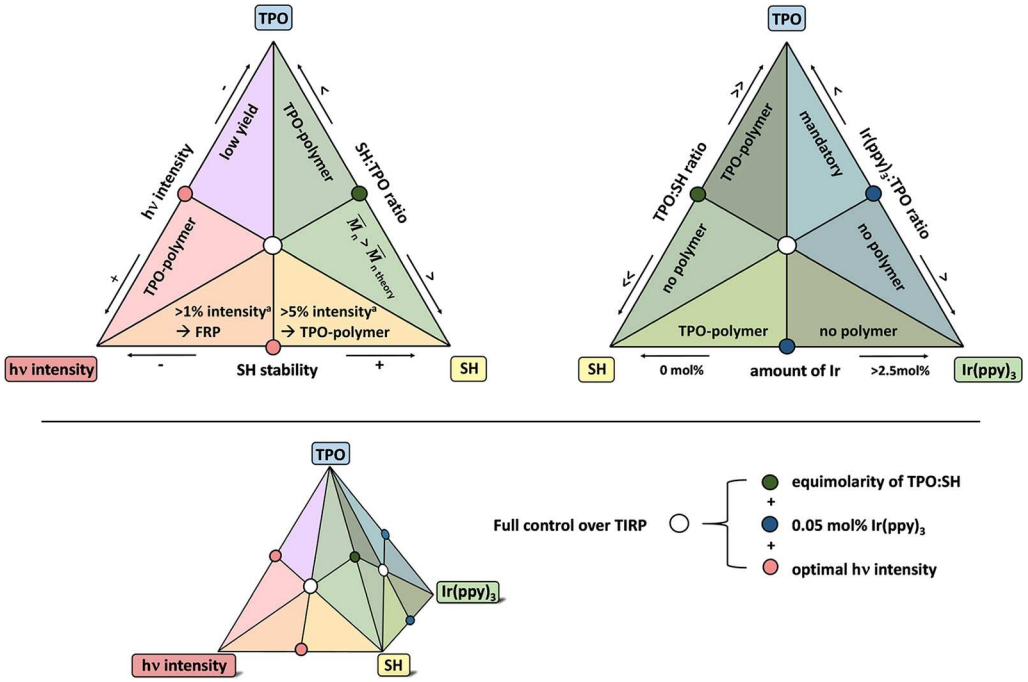

Figure 7. Triangle and tetrahedron depictions of the interrelationships and limits of TIRP when varying polymerization parameters: [a]$h\nu$ intensity (405 nm) of 2% ≙ 1.15 mW/cm^2.

Thus, our studies confirm the presence of RS-M$_n$-A species (see SI, Figure S95) and RS-M$_n$-B (see SI, Figure S97) which, according to our postulated mechanism (Scheme 3), are the dormant species of TIRP. In order to undergo controlled polymerization, dormant species have to exist in an equilibrium with the active species, the radical chain end of the growing polymer chain. We can conclude that the photocatalyst is required as well as a light source of appropriate wavelength and intensity. This is also demonstrated by performing the polymerization in two steps: first, tritylthiol, Ir(ppy)$_3$, and TPO were irradiated without any monomer, and formation of RS-B was confirmed by RP-HPLC-MS (see SI, Figure S100). Only upon addition of HEAA monomers and a second period of irradiation, polymers with end groups consistent with the proposed dormant species are formed (see SI, Figure S99). Interestingly, in comparison to the one-pot procedure, which is the general TIRP procedure used in this work (see SI, chapter 1), slightly higher irradiation intensity is required in the polymerization step of the two-step process, where first, the intermediates **1** and **2** are built, isolated, and used for initiation.

To further support our postulated mechanism, quantum chemical calculations of the individual mechanistic steps were performed. The barrier of an initial monomer reacting with tritylthiol is 10.7 kcal/mol and should therefore happen almost instantaneously. The free energy barriers for adding one monomer "M" to RS-M radicals was computed to be 17.7 kcal/mol (see SI, chapter 3 for further details), which is energetically feasible. We computed the free dissociation energy of RS-M$_n$-A to be 44.5 kcal/mol and RS-M$_n$-B 52.1 kcal/mol when following an intramolecular photo-CRP mechanism (see also Figure 1). This value is below the energy of a 405 nm photon (70.6 kcal/mol), so the dissociation of A or B from RS-M$_n$ is energetically possible. In comparison, the energy required for electron transfer from Ir(ppy)$_3$ to RS-M$_n$-A or RS-M$_n$-B, which would correspond to a photoredox CRP mechanism (also see Figure 1), is 76.7 and 80.5 kcal/mol, respectively. Therefore, we hypothesize a photocatalytic activation through an intramolecular homolytic cleavage reaction rather than a photoredox process. These computations support the postulated mechanism shown in Scheme 3.

Sweet Spot Conditions for TIRP. Taken together, our study shows that there are three rules that need to be followed to achieve TIRP with controlled characteristics: (1) a thiol−TPO ratio of 1:1 should be maintained; (2) the concentrations of Ir(ppy)$_3$ has to be ∼0.05 mol % of the overall monomer content (=100 mol %) and should not exceed 2.5 mol %; (3) the irradiation intensity needs to be optimized based on the chosen thiol initiator/monomer. Based on these parameters, a "sweet spot" for the TIRP reaction can be identified (Figure 7).

We have also seen that these parameters are interdependent. To highlight how the different reaction parameters play together in giving the "sweet spot", we have plotted a diagram (tetrahedron), as is depicted in Figure 7, showing the interrelationships that have been identified in this study. For the left triangle (Figure 7), an optimal amount of Ir(ppy)$_3$ is set, while for the right triangle, an optimum light intensity is set. Going along the sides of each triangle, we can now follow the previously described trends. For example, when more thiol than TPO is used or vice versa, noncontrolled polymerization is observed. When the light intensity is too low, no polymerization occurs. If the light intensity is too high, noncontrolled polymerization occurs. Stabilized thiyl radicals such as the tritylthiol require higher light intensities than less stabilized thiyl radicals. Increasing the amount of Ir(ppy)$_3$ increases molecular weights; however, above 2.5 mol % Ir-catalyst, polymerization no longer takes place, with an optimal amount of 0.05 mol % Ir(ppy)$_3$ relative to the monomer concentration.

We can already explain some of these correlations based on our postulated mechanism. Other parameters and their correlation are not yet understood, e.g., the necessity of a

https://doi.org/10.1021/acs.macromol.3c00789
Macromolecules 2023, 56, 5512−5523

higher irradiation intensity in the two-step polymerization process. While such optimization of reaction parameters can be tedious in solution, in the future, SI-TAP and the straightforward analysis of polymer growth on the surface by measuring the height can be used for simplified screening of optimized TIRP conditions, e.g., when varying the thiol initiators.[30]

CONCLUSIONS

We demonstrate that thiol-initiated polymerizations can be performed under controlled conditions and as light-controlled polymerizations in solution when using TPO and $Ir(ppy)_3$ as the co-initiator and catalyst, as had been initially observed on surfaces.[31] We demonstrate the use of different initiators and monomers in the synthesis of low dispersity homo- as well as block copolymers. In the future, we anticipate that TIRP will enrich the portfolio of both controlled as well as light-activated polymerization methods and can specifically make use of a variety of natural and synthetic thiols to derive complex polymer conjugates including block copolymers.

ASSOCIATED CONTENT

Supporting Information

The Supporting Information is available free of charge at https://pubs.acs.org/doi/10.1021/acs.macromol.3c00789.

^{1}H NMR spectra; H_2O-SEC data; THF-SEC data; ESI-MS; MALDI-ToF-MS; ^{31}P NMR spectra; reaction kinetic data; monomer synthesis; block copolymer synthesis and characterization; optimization studies; variation of polymerization parameters; and quantum chemical calculations (PDF)

AUTHOR INFORMATION

Corresponding Author

Laura Hartmann − *Institute of Organic Chemistry and Macromolecular Chemistry, Heinrich-Heine-University Duesseldorf, Duesseldorf D-40225, Germany; Institute for Macromolecular Chemistry, University of Freiburg, Freiburg im Breisgau D-79104, Germany;* orcid.org/0000-0003-0115-6405; Email: laura.hartmann@hhu.de

Authors

Lorand Bonda − *Institute of Organic Chemistry and Macromolecular Chemistry, Heinrich-Heine-University Duesseldorf, Duesseldorf D-40225, Germany*

Daniel J. Valles − *Advanced Science Research Center, Graduate Center, City University of New York, New York, New York 10031, United States; PhD Programs in Chemistry and Biochemistry, Graduate Center, City University of New York, New York, New York 10016, United States*

Tillmann L. Wigger − *Institute for Physical Chemistry, Heinrich-Heine-University Duesseldorf, Duesseldorf D-40225, Germany*

Jan Meisner − *Institute for Physical Chemistry, Heinrich-Heine-University Duesseldorf, Duesseldorf D-40225, Germany;* orcid.org/0000-0002-1301-2612

Adam B. Braunschweig − *Advanced Science Research Center, Graduate Center, City University of New York, New York, New York 10031, United States; PhD Programs in Chemistry and Biochemistry, Graduate Center, City University of New York, New York, New York 10016, United States; Department of Chemistry, Hunter College, New York, New York 10065, United States;* orcid.org/0000-0003-0344-3029

Complete contact information is available at: https://pubs.acs.org/10.1021/acs.macromol.3c00789

Author Contributions

The manuscript was written through contributions of all authors. All authors have given approval to the final version of the manuscript.

Notes

The authors declare the following competing financial interest(s): The authors (LB,DJV,ABB and LH) have filed for a patent application based on the findings presented in the study.

ACKNOWLEDGMENTS

We thank Susanne Boye from the polymer separation group at the Leibniz-Insitut of Polymer Research in Dresden for her great support with the SEC measurements. Also, we thank the CeMSA@HHU (Center for Molecular and Structural Analytics @ Heinrich-Heine University) for recording the mass spectrometric and the NMR-spectroscopic data. ABB acknowledges support from the US National Science Foundation (DBI-2032176), the Air Force Office of Scientific Research (FA9550-19-1-0220 and FA9550-23-1-0230), and the Army Research Office (W911NF2010271). Computational infrastructure and support were provided by the Centre for Information and Media Technology at Heinrich-Heine University Düsseldorf. J.M. is grateful for a materials cost allowance from the Fonds der Chemischen Industrie.

REFERENCES

(1) Staudinger, H. *A Source Book in Chemistry, 1900−1950*; Harvard University Press: Cambridge, MA, 2013.

(2) Nesvadba, P. Radical polymerization in industry. *Encycl. Radic. Chem., Biol. Mater.* **2012**, 1962−1997.

(3) Pan, X.; Tasdelen, M. A.; Laun, J.; Junkers, T.; Yagci, Y.; Matyjaszewski, K. Photomediated controlled radical polymerization. *Prog. Polym. Sci.* **2016**, *62*, 73−125.

(4) Destarac, M. Controlled radical polymerization: industrial stakes, obstacles and achievements. *Macromol. React. Eng.* **2010**, *4*, 165−179.

(5) Matyjaszewski, K.; Xia, J. Atom transfer radical polymerization. *Chem. Rev.* **2001**, *101*, 2921−2990.

(6) Chiefari, J.; Chong, Y.; Ercole, F.; Krstina, J.; Jeffery, J.; Le, T. P.; Mayadunne, R. T.; Meijs, G. F.; Moad, C. L.; Moad, G. Living free-radical polymerization by reversible addition− fragmentation chain transfer: the RAFT process. *Macromolecules* **1998**, *31*, 5559−5562.

(7) Moad, G.; Rizzardo, E.; Thang, S. H. Living radical polymerization by the RAFT process−a third update. *Aust. J. Chem.* **2012**, *65*, 985−1076.

(8) Hawker, C. J.; Bosman, A. W.; Harth, E. New polymer synthesis by nitroxide mediated living radical polymerizations. *Chem. Rev.* **2001**, *101*, 3661−3688.

(9) Yeow, J.; Boyer, C. Photoinitiated Polymerization-Induced Self-Assembly (Photo-PISA): New Insights and Opportunities. *Adv. Sci.* **2017**, *4*, No. 1700137.

(10) Chen, C. Redox-controlled polymerization and copolymerization. *ACS Catal.* **2018**, *8*, 5506−5514.

(11) Zhang, B.; Wang, X.; Zhu, A.; Ma, K.; Lv, Y.; Wang, X.; An, Z. Enzyme-initiated reversible addition−fragmentation chain transfer polymerization. *Macromolecules* **2015**, *48*, 7792−7802.

(12) Magenau, A. J. D.; Strandwitz, N. C.; Gennaro, A.; Matyjaszewski, K. Electrochemically Mediated Atom Transfer Radical Polymerization. *Science* **2011**, *332*, 81−84.

(13) McKenzie, T. G.; Fu, Q.; Uchiyama, M.; Satoh, K.; Xu, J.; Boyer, C.; Kamigaito, M.; Qiao, G. G. Beyond traditional RAFT: alternative activation of thiocarbonylthio compounds for controlled polymerization. *Adv. Sci.* **2016**, *3*, No. 1500394.
(14) Yagci, Y.; Jockusch, S.; Turro, N. J. Photoinitiated polymerization: advances, challenges, and opportunities. *Macromolecules* **2010**, *43*, 6245−6260.
(15) Bian, S.; Zieba, S. B.; Morris, W.; Han, X.; Richter, D. C.; Brown, K. A.; Mirkin, C. A.; Braunschweig, A. B. Beam pen lithography as a new tool for spatially controlled photochemistry, and its utilization in the synthesis of multivalent glycan arrays. *Chem. Sci.* **2014**, *5*, 2023−2030.
(16) Chapman, R.; Jung, K.; Boyer, C. *Photo RAFT Polymerization. RAFT Polymerization: Methods, Synthesis and Applications*; 2021; vol *1*, pp 611−645.
(17) Valles, D. J.; Zholdassov, Y. S.; Braunschweig, A. B. Evolution and applications of polymer brush hypersurface photolithography. *Polym. Chem.* **2021**, *12*, 5724−5746.
(18) Carbonell, C.; Valles, D.; Wong, A. M.; Carlini, A. S.; Touve, M. A.; Korpanty, J.; Gianneschi, N. C.; Braunschweig, A. B. Polymer brush hypersurface photolithography. *Nat. Commun.* **2020**, *11*, 1244.
(19) Dolinski, N. D.; Page, Z. A.; Discekici, E. H.; Meis, D.; Lee, I. H.; Jones, G. R.; Whitfield, R.; Pan, X.; McCarthy, B. G.; Shanmugam, S.; Kottisch, V.; Fors, B. P.; Boyer, C.; Miyake, G. M.; Matyjaszewski, K.; Haddleton, D. M.; de Alaniz, J. R.; Anastasaki, A.; Hawker, C. J. What happens in the dark? Assessing the temporal control of photomediated controlled radical polymerizations. *J. Polym. Sci., Part A: Polym. Chem.* **2019**, *57*, 268−273.
(20) Aydogan, C.; Yilmaz, G.; Shegiwal, A.; Haddleton, D. M.; Yagci, Y. Photoinduced Controlled/Living Polymerizations. *Angew. Chem., Int. Ed.* **2022**, No. e202117377.
(21) Junkers, T.; Laun, J. Controlled reversible deactivation radical photopolymerization. In *Photopolymerisation Initiating Systems*; The Royal Society of Chemistry: Cambridge, 2018; pp 244−273.
(22) Bagheri, A.; Jin, J. Photopolymerization in 3D printing. *ACS Appl. Polym. Mater.* **2019**, *1*, 593−611.
(23) Prier, C. K.; Rankic, D. A.; MacMillan, D. W. Visible light photoredox catalysis with transition metal complexes: applications in organic synthesis. *Chem. Rev.* **2013**, *113*, 5322−5363.
(24) Chen, M.; Zhong, M.; Johnson, J. A. Light-controlled radical polymerization: mechanisms, methods, and applications. *Chem. Rev.* **2016**, *116*, 10167−10211.
(25) Quinn, J. F.; Barner, L.; Barner-Kowollik, C.; Rizzardo, E.; Davis, T. P. Reversible addition− fragmentation chain transfer polymerization initiated with ultraviolet radiation. *Macromolecules* **2002**, *35*, 7620−7627.
(26) Otsu, T.; Matsunaga, T.; Doi, T.; Matsumoto, A. Features of living radical polymerization of vinyl monomers in homogeneous system using N, N-diethyldithiocarbamate derivatives as photoiniferters. *Eur. Polym. J.* **1995**, *31*, 67−78.
(27) Tasdelen, M. A.; Uygun, M.; Yagci, Y. Photoinduced controlled radical polymerization. *Macromol. Rapid Commun.* **2011**, *32*, 58−62.
(28) Dadashi-Silab, S.; Atilla Tasdelen, M.; Yagci, Y. Photoinitiated atom transfer radical polymerization: Current status and future perspectives. *J. Polym. Sci., Part A: Polym. Chem.* **2014**, *52*, 2878−2888.
(29) Xu, J.; Jung, K.; Atme, A.; Shanmugam, S.; Boyer, C. A robust and versatile photoinduced living polymerization of conjugated and unconjugated monomers and its oxygen tolerance. *J. Am. Chem. Soc.* **2014**, *136*, 5508−5519.
(30) Fors, B. P.; Hawker, C. J. Control of a living radical polymerization of methacrylates by light. *Angew. Chem., Int. Ed.* **2012**, *124*, 8980−8983.
(31) Wong, A. M.; Valles, D. J.; Carbonell, C.; Chambers, C. L.; Rozenfeld, A. Y.; Aldasooky, R. W.; Braunschweig, A. B. Controlled-height brush polymer patterns via surface-initiated thiol-methacrylate photopolymerizations. *ACS Macro Lett.* **2019**, *8*, 1474−1478.
(32) Lalevée, J.; Blanchard, N.; Tehfe, M. A.; Peter, M.; Morlet-Savary, F.; Fouassier, J. P. A novel photopolymerization initiating system based on an iridium complex photocatalyst. *Macromol. Rapid Commun.* **2011**, *32*, 917−920.
(33) Lee, C.-L.; Lee, K. B.; Kim, J.-J. Polymer phosphorescent light-emitting devices doped with tris (2-phenylpyridine) iridium as a triplet emitter. *Appl. Phys. Lett.* **2000**, *77*, 2280−2282.
(34) Becke, A. D. A new mixing of Hartree−Fock and local density-functional theories. *J. Chem. Phys.* **1993**, *98*, 1372−1377.
(35) Schäfer, A.; Huber, C.; Ahlrichs, R. Fully optimized contracted Gaussian basis sets of triple zeta valence quality for atoms Li to Kr. *J. Chem. Phys.* **1994**, *100*, 5829−5835.
(36) Ahlrichs, R.; Bär, M.; Häser, M.; Horn, H.; Kölmel, C. Electronic structure calculations on workstation computers: The program system turbomole. *Chem. Phys. Lett.* **1989**, *162*, 165−169.
(37) Grimme, S.; Antony, J.; Ehrlich, S.; Krieg, H. A consistent and accurate ab initio parametrization of density functional dispersion correction (DFT-D) for the 94 elements H-Pu. *J. Chem. Phys.* **2010**, *132*, 154104.
(38) Grimme, S.; Ehrlich, S.; Goerigk, L. Effect of the damping function in dispersion corrected density functional theory. *J. Comput. Chem.* **2011**, *32*, 1456−1465.
(39) Kästner, J.; Carr, J. M.; Keal, T. W.; Thiel, W.; Wander, A.; Sherwood, P. DL-FIND: an open-source geometry optimizer for atomistic simulations. *J. Phys. Chem. A* **2009**, *113*, 11856−11865.
(40) Metz, S.; Kästner, J.; Sokol, A. A.; Keal, T. W.; Sherwood, P. Chem Shell - a modular software package for QM/MM simulations. *Wiley Interdiscip. Rev.: Comput. Mol. Sci.* **2014**, *4*, 101−110.
(41) Klamt, A. The COSMO and COSMO-RS solvation models. *Wiley Interdiscip. Rev.: Comput. Mol. Sci.* **2018**, *8*, No. e1338.
(42) Corradini, F.; Marcheselli, L.; Tassi, L.; Tosi, G. Static dielectric constants of the N, N-dimethylformamide/2-methoxyethanol solvent system at various temperatures. *Can. J. Chem.* **1992**, *70*, 2895−2899.
(43) Matyjaszewski, K.; Davis, T. P. *Handbook of radical polymerization*; Wiley Online Library, 2002, p 922.
(44) Teodorescu, M.; Matyjaszewski, K. Controlled polymerization of (meth)acrylamides by atom transfer radical polymerization. *Macromol. Rapid Commun.* **2000**, *21*, 190−194.
(45) Jones, G. R.; Li, Z.; Anastasaki, A.; Lloyd, D. J.; Wilson, P.; Zhang, Q.; Haddleton, D. M. Rapid synthesis of well-defined polyacrylamide by aqueous Cu (0)-mediated reversible-deactivation radical polymerization. *Macromolecules* **2016**, *49*, 483−489.
(46) Chmielarz, P.; Park, S.; Simakova, A.; Matyjaszewski, K. Electrochemically mediated ATRP of acrylamides in water. *Polymer* **2015**, *60*, 302−307.
(47) Driessen, F. Functional and amphiphilic copolymers by means of copper-mediated polymerization. PhD Thesis, Universiteit Gent, Polymer Chemistry Research Group, 2017.
(48) Holzer, W.; Penzkofer, A.; Tsuboi, T. Absorption and emission spectroscopic characterization of $Ir(ppy)_3$. *Chem. Phys.* **2005**, *308*, 93−102.
(49) Cramer, N. B.; Reddy, S. K.; O'Brien, A. K.; Bowman, C. N. Thiol− ene photopolymerization mechanism and rate limiting step changes for various vinyl functional group chemistries. *Macromolecules* **2003**, *36*, 7964−7969.
(50) Kucharski, M.; Lubczak, R. Copolymerization of hydroxyalkyl methacrylates with acrylamide and methacrylamide I. Determination of reactivity ratios. *J. Appl. Polym. Sci.* **1997**, *64*, 1259−1265.
(51) Sluggett, G. W.; Turro, C.; George, M. W.; Koptyug, I. V.; Turro, N. J. (2, 4, 6-Trimethylbenzoyl) diphenylphosphine oxide photochemistry. A direct time-resolved spectroscopic study of both radical fragments. *J. Am. Chem. Soc.* **1995**, *117*, 5148−5153.
(52) Pathak, A. K.; Pathak, V.; Seitz, L. E.; Tiwari, K. N.; Akhtar, M. S.; Reynolds, R. C. A facile method for deprotection of trityl ethers using column chromatography. *Tetrahedron Lett.* **2001**, *42*, 7755−7757.
(53) Patten, T. E.; Xia, J.; Abernathy, T.; Matyjaszewski, K. Polymers with very low polydispersities from atom transfer radical polymerization. *Science* **1996**, *272*, 866−868.
(54) Tsujii, Y.; Ejaz, M.; Sato, K.; Goto, A.; Fukuda, T. Mechanism and kinetics of RAFT-mediated graft polymerization of styrene on a

https://doi.org/10.1021/acs.macromol.3c00789
Macromolecules 2023, 56, 5512−5523

solid surface. 1. Experimental evidence of surface radical migration. *Macromolecules* **2001**, *34*, 8872−8878.

https://doi.org/10.1021/acs.macromol.3c00789
Macromolecules 2023, 56, 5512−5523

Supporting Information

TIRP - thiol-induced, light-activated controlled radical polymerization

Lorand Bonda[1], Daniel J. Valles[2,3], Tillmann L. Wigger[4], Jan Meisner[4], Adam Braunschweig[2,3,5] and Laura Hartmann[1,6]*

[1]*Institute of Organic Chemistry and Macromolecular Chemistry, Heinrich Heine University Duesseldorf, Universitaetsstr. 1, D-40225 Duesseldorf, Germany*
[2]*Advanced Science Research Center, Graduate Center, City University of New York, 85 St. Nicholas Terrace, New York, NY 10031, USA*
[3]*PhD Programs in Chemistry and Biochemistry, Graduate Center, City University of New York, 365 5th Avenue, New York, NY 10016, USA*
[4]*Institute of Physical Chemistry, Heinrich Heine University Duesseldorf, Universitaetsstr. 1, D-40225 Duesseldorf, Germany*
[5]*Department of Chemistry, Hunter College, 695 Park Avenue, New York, NY 10065, USA*
[6]*Institute for Macromolecular Chemistry, University of Freiburg, Stefan-Meier-Str. 31, D-79104 Freiburg i.Br., Germany*

Table of Contents

1. General procedure of TIRP

Scheme S1. General polymerization scheme of TIRP

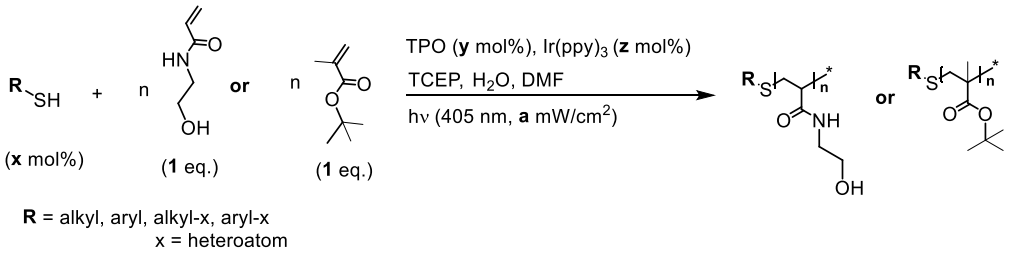

1 eq. of *N*-hydroxyethylacrylamide monomer (HEAA, 100 mol%) or *tert*-butyl methacrylamide (TBMA, 100 %)and tris(2-phenylpyridine)iridium(III) ($Ir(ppy)_3$, z mol%) are dissolved in DMF [10 wt.%] sealed in a 5 mL glass flask and flushed with argon as inert gas for 10 minutes. In a second step, the thiol (x mol%) and equimolar amounts of diphenyl-(2,4,6-trimethylbenzoyl)-phosphine oxide (TPO, y mol% = x mol%) are also dissolved in DMF [10 wt.%] and sealed in a 5 mL microwave reaction vial. A spatula tip of TCEP is dissolved in a single drop of H_2O and added to the reaction solution to reduce possible disulfides. The thiol/TPO solution is flushed under Ar-atmosphere for 10 minutes and irradiated with UV-light (405 nm wavelength, intensity dependent on thiol and monomer used) for 3 minutes. Subsequently, the monomer/$Ir(ppy)_3$ mixture is added to the TPO/thiol solution under an inert atmosphere and the polymerization solution is irradiated further at unchanged light intensity. After an hour, the irradiation is stopped and the polymer solution precipitated in diethyl ether (PHEAA) or H_2O/MeOH 1:3 (*v*/*v*) (PTBMA). The precipitated PHEAA is dissolved in H_2O, dialyzed against distilled water (three cycles, exclusion size dependent on molecular weight) and subsequently lyophilized.

2. Scheme 1: SI for optimized conditions (tritylthiol as initiator)

1 eq. of HEAA or TBMA monomer (100 mol%) and $Ir(ppy)_3$ (0.05 mol%) were dissolved in DMF [10 wt.%] sealed in a 5 mL glass flask and flushed with argon gas for 10 minutes. In a second step, tritylthiol (5 mol%) and equimolar amounts of TPO (5 mol%) were also dissolved in DMF [10 wt.%] and sealed in a 5 mL microwave reaction vial. A spatula tip of TCEP was dissolved in a single drop of H_2O and added to the reaction solution to reduce possible

disulfides. The thiol/TPO solution was flushed under Ar-atmosphere for 10 minutes and irradiated with UV-light (405 nm wavelength, with an intensity 2.61 mW/cm² (5%, HEAA) or 1.15 mW/cm² (2%, TBMA) for 3 minutes. Subsequently, the monomer/$Ir(ppy)_3$ mixture was added to the TPO/thiol solution under an inert atmosphere and the polymerization solution was irradiated further at unchanged light intensity. After an hour, the irradiation was stopped and the PHEAA solution was precipitated in diethyl ether and PTBMA in H_2O/MeOH 1:3 (v/v). The precipitated PHEAA was dissolved in H_2O, dialyzed against distilled water (three cycles, 1000 Da (polymer #2) and 3000 Da (polymer#1)) and subsequently lyophilized.

Scheme S2. Optimized TIRP parameters for tritylthiol ($Ir(ppy)_3$ = 0.05 mol%; DMF = 10 wt.%; hν = 60 min, 405 nm, 2.61 mW/cm²).

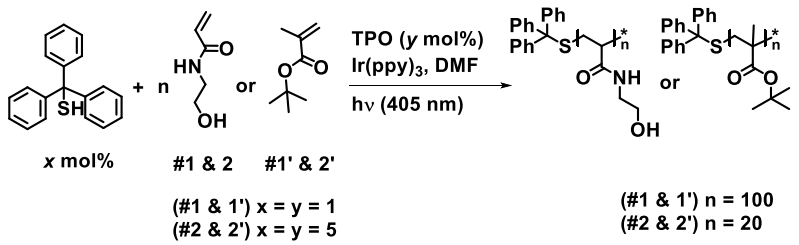

Table S1. Thiol:TPO ratios with average molecular weights and dispersities obtained for **#1** and **#2**.

#	Thiol conc. [mol%]	TPO conc. [mol%]	$\bar{P}_n$ (theoretical) calculated from SEC data	$\bar{M}_n$ [kDa] (theoretical) via H_2O-SEC, MALS coupled RI detector	Đ via H_2O-SEC, MALS coupled RI-detector	$\bar{M}_n$* [kDa] via H_2O-SEC, MALS coupled RI-detector	Đ* via H_2O-SEC, MALS coupled RI-detector	Đ via THF-SEC, RI-detector	Đ via THF-SEC UV-detector
1	1	1	(100) 98	(11.8) 12	1.1	13.6	1.2	-	-
2	5	5	(20) 20	(2.7) 2.7	1.09	3.4	1.38	-	-
1‘	1	1	(100) 103	(14.2) 14.6	-	-	-	1.4	1.3
2‘	5	5	(20) 18	(2.8) 2.7	-	-	-	1.3	1.3

SEC-MALS-RI (precolumn (50 mm, 2 x 160 Å of 300 mm and 1000 Å of 300 mm), two main columns (8 mm diameter and 5 µm particle size), eluent: MilliQ water:acetonitrile 7:3 (v/v), 50 mM, NaH_2PO_4, 150 mM NaCl and 250 ppm NaN_3, pH = 7.0, flow rate: 0.8 mL/min *measured by Dr. Boye at the Center of Macromolecular Structure Analysis at the Leibniz Insitute of polymer research in Dresden via SEC-MALS-RI (precolumn, three main columns (100/100/1000), eluent: MilliQ water, 10 mM PBS buffer, pH = 7.4, flow rate: 1 mL/min

2.1.1 Analytics

Different methods were performed to analyze the obtained polymers. With ^1H NMR-spectroscopy the building of the desired polymers and their purity could be observed. However, the proton signals of tritylthiol and TPO overlap, so the molecular weights and dispersities were analyzed by H_2O-SEC-MALS (PHEAA) and THF-

SEC (PTBMA). Elemental analysis (EA) showed, that the amount of sulfur which can be found in purified polymers equals to the theoretical amount of a thiol initiated polymer. As the theoretical values of the elemental analysis were calculated for polymers without endgroups the measured values of %C, %H and %N may differ slightly from the theoretical ones. The theoretical values were calculated for optimal DPs of 100 and 20.

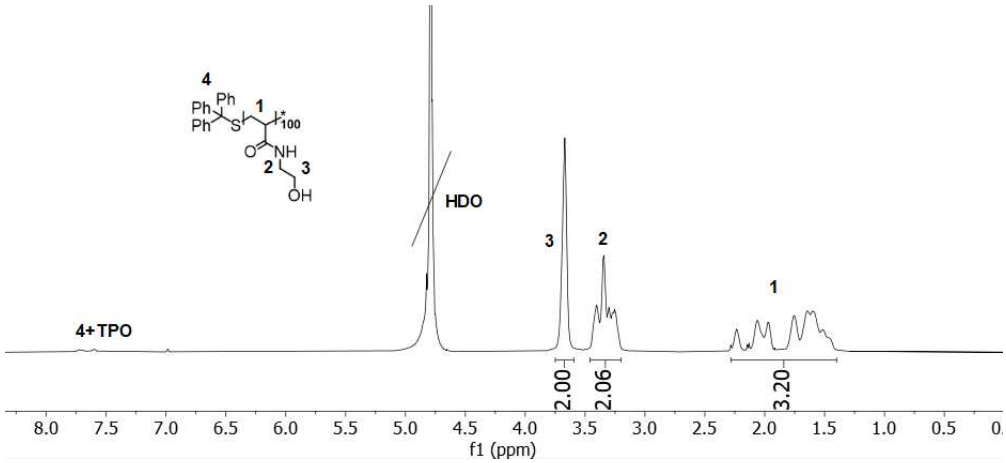

Figure S1. ^{1}H NMR (600 MHz, D_2O) of polymer **#1** synthesized under optimized conditions.

^{1}H NMR (600 MHz, D_2O) δ [ppm] 7.75-7.54 (m, **4**, **TPO** overlapping), 3.74-3.62 (m, **3**), 3.49-3.21 (m, **2**), 2.36-1.32 (m, **1**).

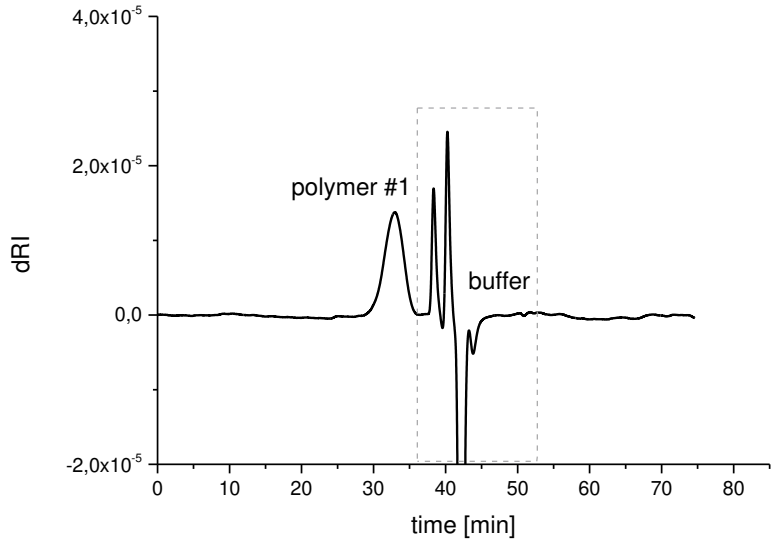

Figure S2. H_2O-SEC-MALS of polymer **#1** synthesized under optimized conditions.

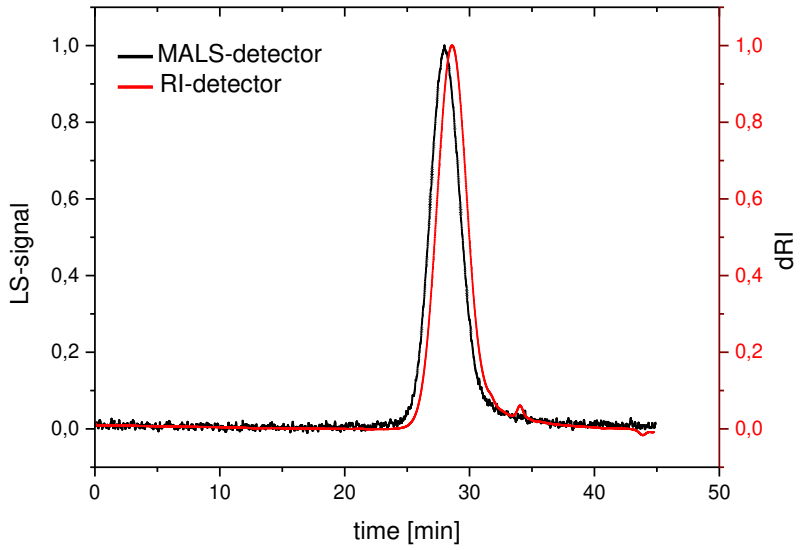

Figure S3. H_2O-SEC-MALS and H_2O-RI-SEC spectra (measured at Leibniz Insitute of polymer research in Dresden) of polymer **#1** synthesized under optimized conditions.

<u>Elemental analysis:</u>

theoretical values (n=100): %C=52.87; %H=7.83; %N=11.88; %S=0.27

measured values (n=100): %C=50.27; %H=8.11; %N=11.25; %S=0.24

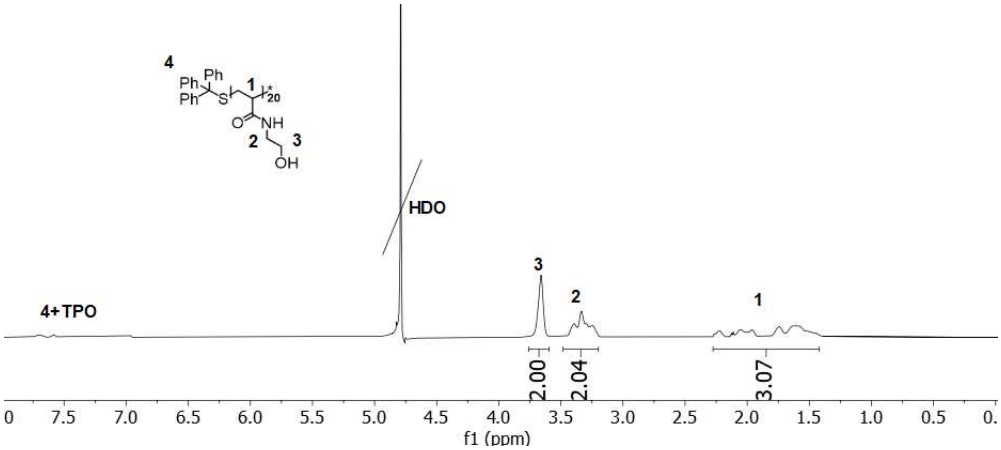

Figure S4. ^1H NMR (600 MHz, D_2O) of polymer **#2** synthesized under optimized conditions.

^1H NMR (600 MHz, D_2O) δ [ppm] 7.75-7.54 (m, **4**, **TPO** overlapping), 3.74-3.62 (m, **3**), 3.49-3.21 (m, **2**), 2.36-1.32 (m, **1**).

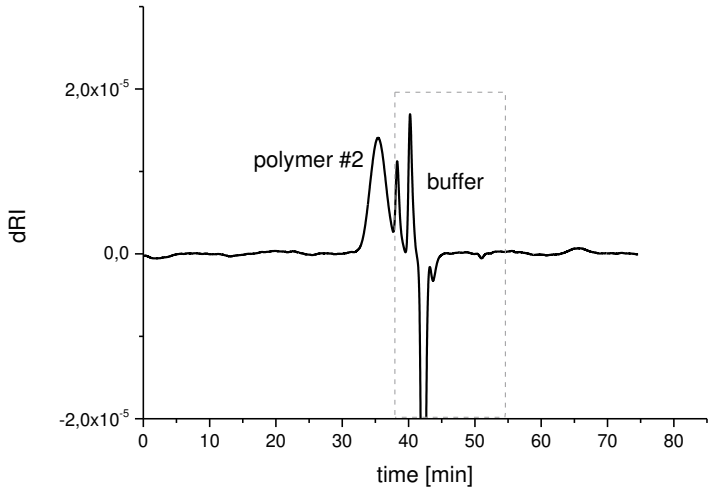

Figure S5. H_2O-SEC-MALS of polymer **#2** synthesized under optimized conditions.

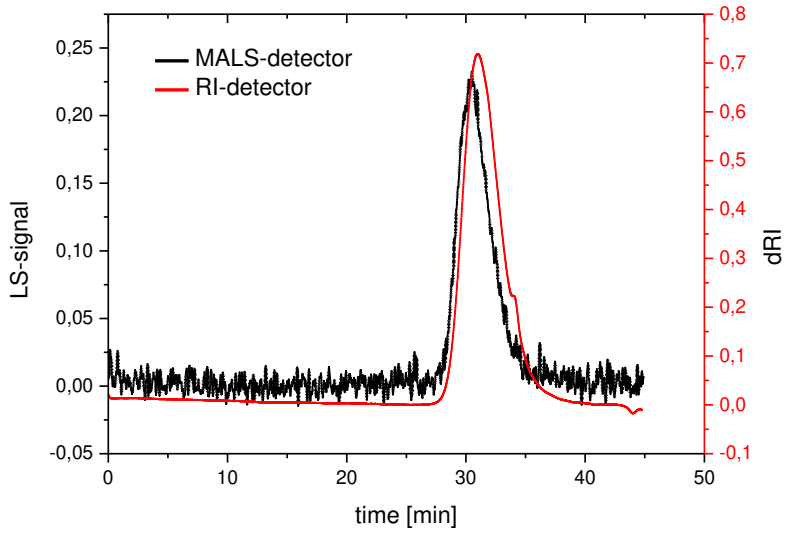

Figure S6. H_2O-SEC-MALS and H_2O-RI-SEC spectra (measured at Leibniz Insitute of polymer research in Dresden) of polymer **#2** synthesized under optimized conditions.

Elemental analysis:

theoretical values (n=20): %C=55.44; %H=7.62; %N=10.87; %S=1.24

measured values (n=20): %C=54.84; %H=7.67; %N=11.10; %S=1.02

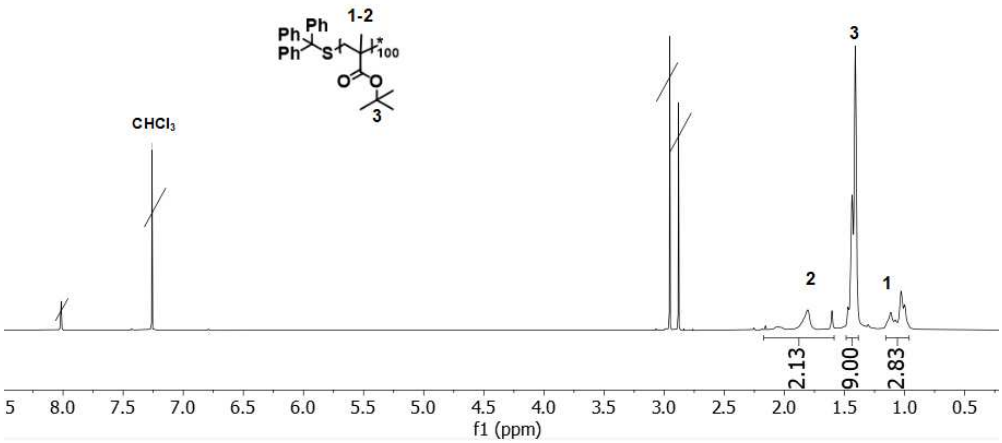

Figure S7. ^{1}H NMR (600 MHz, $CDCl_3$) of polymer **#1'** synthesized under optimized conditions.

^{1}H NMR (600 MHz, $CDCl_3$) δ [ppm] 2.16-1.58 (m, **2**), 1.48-1.38 (m, **3**), 1.15-0.96 (m, **1**).

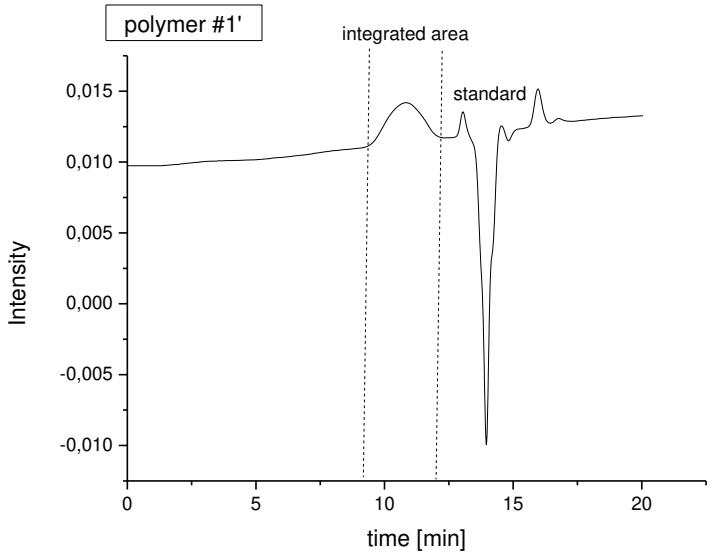

Figure S8. THF-SEC (RI detector) of polymer **#1'** synthesized under optimized conditions.

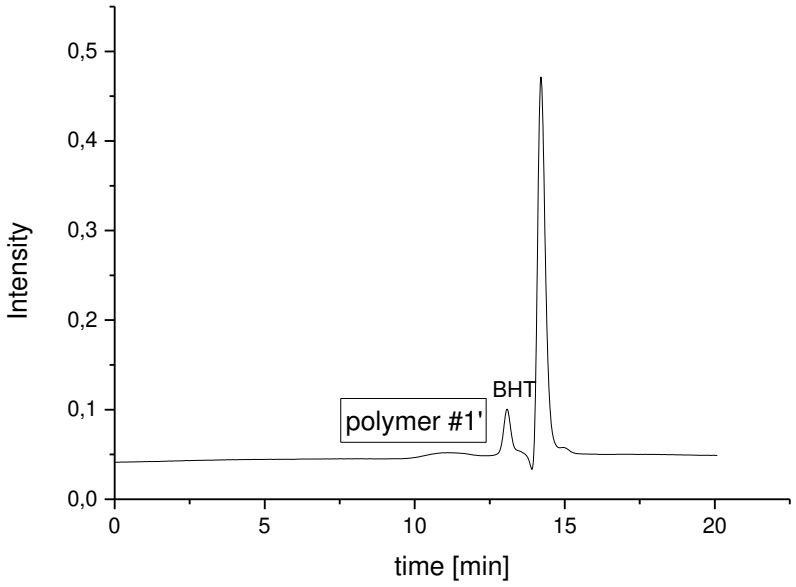

Figure S9. THF-SEC (UV detector) of polymer **#1'** synthesized under optimized conditions.

Elemental analysis:

theoretical values (n=100): %C=67.86; %H=9.85; %S=0.22

measured values (n=100): %C=67.81; %H=9.82; %S=0.22

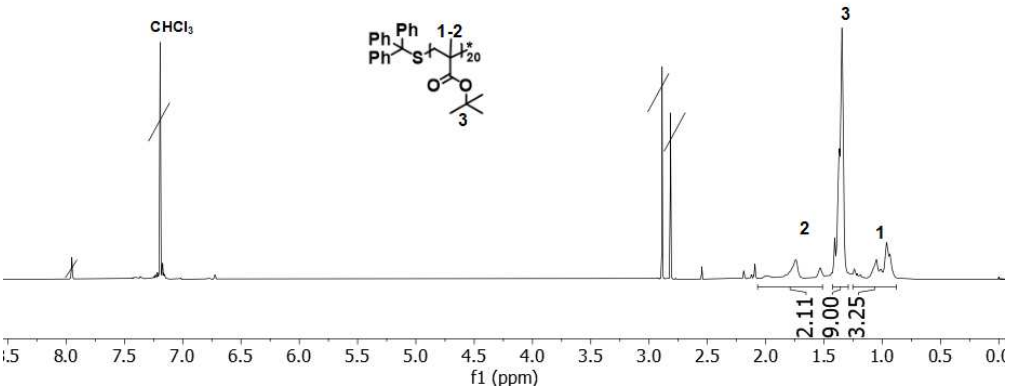

Figure S10. ^{1}H NMR (600 MHz, $CDCl_3$) of polymer **#2'** synthesized under optimized conditions.

^{1}H NMR (600 MHz, $CDCl_3$) δ [ppm] 2.16-1.58 (m, **2**), 1.48-1.38 (m, **3**), 1.15-0.96 (m, **1**).

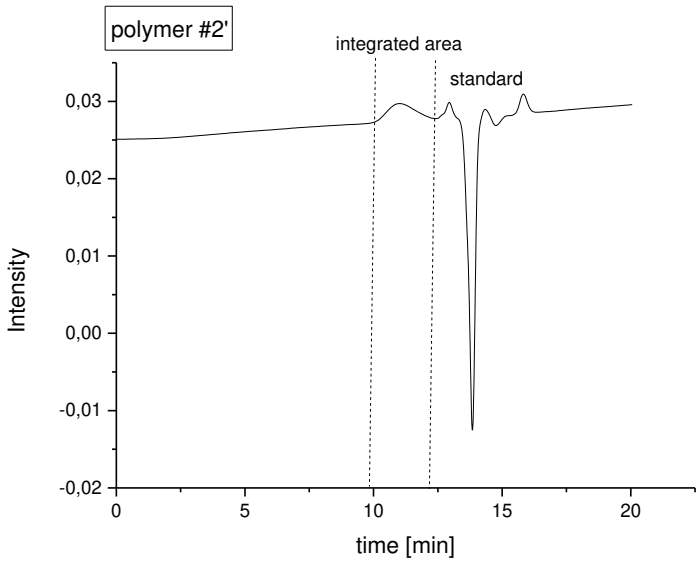

Figure S11. THF-SEC (RI detector) of polymer **#2'** synthesized under optimized conditions.

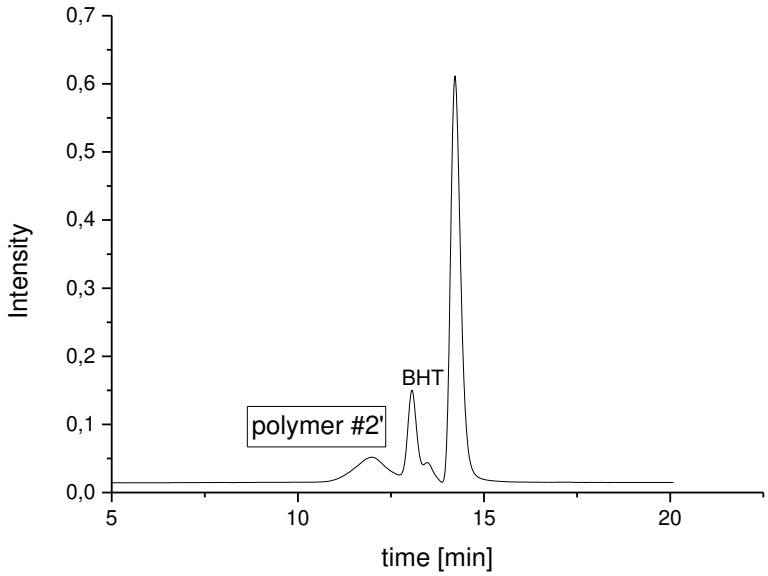

Figure S12. THF-SEC (UV detector) of polymer **#2'** synthesized under optimized conditions.

Elemental analysis:

theoretical values (n=20): %C=68.90; %H=9.56; %S=1.03

measured values (n=20): %C=68.89; %H=9.04; %S=0.98

2.1.2 Polymerization of HEAA under optimized TIRP conditions without thiol source

1 eq. of HEAA and $Ir(ppy)_3$ (0.05 mol%) were dissolved in DMF [10 wt.%] sealed in a 5 mL glass flask and flushed with argon gas for 10 minutes. In a second step TPO (1 mol%) was also dissolved in DMF [10 wt.%] and sealed in a 5 mL microwave reaction vial. A spatula tip of TCEP was dissolved in a single drop of H_2O and added to the reaction solution to reduce possible disulfides. The TPO solution was flushed under Ar-atmosphere for 10 minutes and irradiated with UV-light (405 nm wavelength, with an intensity 2.61 mW/ for 3 minutes. Subsequently, the monomer/$Ir(ppy)_3$ mixture was added to the TPO solution under an inert atmosphere and the polymerization solution was irradiated further at unchanged light intensity. After an hour, the irradiation was stopped and the PHEAA solution was precipitated in diethyl ether. The precipitated PHEAA was dissolved in H_2O, dialyzed against distilled water (three cycles, 1000 Da) and subsequently lyophilized. The resulting PHEAA was analyzed via aqueous H_2O-SEC-MALS showing, that as expected, M_n ($M_{n\ theory}$ = 11,5 kDa; $M_{n\ H2O\text{-}SEC}$ = 8 kDa) did not match the theoretically expected value and dispersity is in the range of free radical polymerizations.

Scheme S3. Reaction conditions for polymerization of HEAA without adding a thiol source ($Ir(ppy)_3$ = 0.05 mol%; DMF = 10 wt.%; hν = 60 min, 405 nm, 2.61 mW/cm²).

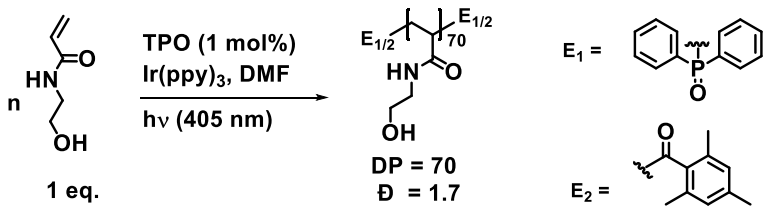

2.1.2.1 Analytics

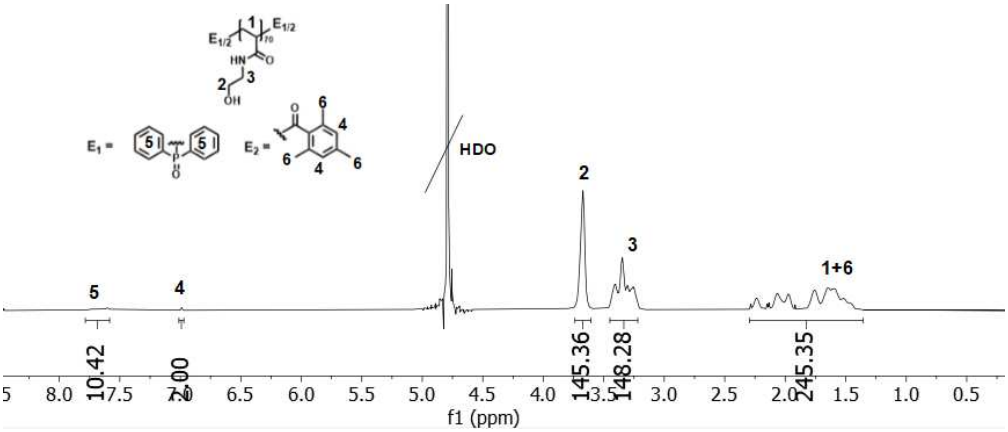

Figure S13. ^1H NMR (600 MHz, D_2O) of PHEAA with DP = 70 and TPO-fragments as endgroups synthesized under optimized TIRP conditions without thiol source.

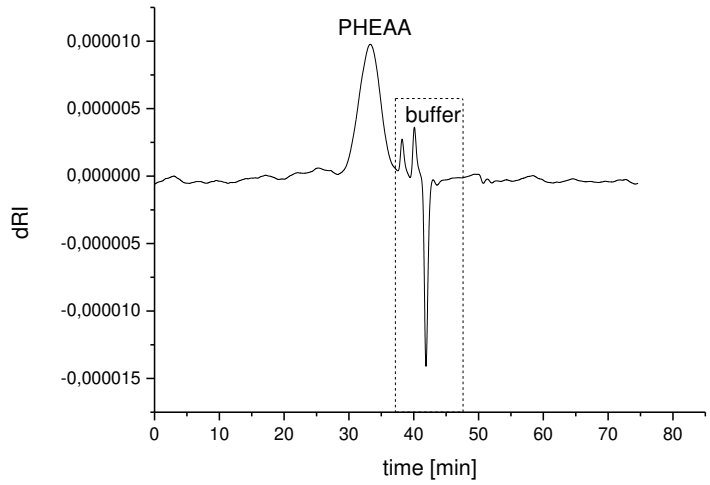

Figure S14. H_2O-SEC-MALS of PHEAA (M_n = 8 kDa) synthesized under TIRP conditions, without thiol source.

2.1.3 Figure 3 (A) and (B): SI for reaction kinetics

1 eq. of HEAA monomer (100 mol%, 200 mg) and $Ir(ppy)_3$ (0.05 mol%) were dissolved in DCM-d_2/MeOH-d_4 1:3 (*v*/*v*), [10 wt.%] sealed in a 5 mL glass flask and flushed with inert gas (Ar) for 10 minutes. In a second step, tritylthiol (5 mol%) and equimolar amounts of TPO (5 mol%) were also dissolved in DCM-d_2/MeOH-d_4 1:3 (*v*/*v*), [10 wt.%] and sealed in a 5 mL microwave reaction vial. A spatula tip of TCEP were dissolved in a single drop of H_2O and added to the reaction solution to reduce possible disulfides. The thiol/TPO solution was flushed under Ar-atmosphere for 10 minutes. After the monomer/$Ir(ppy)_3$ mixture was added to the vial the solution was irradiated with UV-light (405 nm wavelength, with an intensity of 2.61 mW/cm² (5%). Samples (0.3 mL) were taken from the reaction solution at defined times (20 min, 30 min, 45 min, 60 min, 80 min, 100 min, 120 min and the monomer conversion was determined via ^{1}H NMR-spectroscopy. Also $\ln([M]_0/[M]_t)$ against reaction time is plotted. With a linear relationship characteristics of a living polymerization can be shown.

In a second experiment 1 eq. of HEAA monomer (100 mol%, 200 mg) and $Ir(ppy)_3$ (0.05 mol%) were dissolved in DCM/MeOH 1:1 (*v*/*v*), [10 wt.%] sealed in a 5 mL glass flask and flushed with inert gas (Ar) for 10 minutes. In a second step, tritylthiol (5 mol%) and equimolar amounts of TPO (5 mol%) were also dissolved in DCM/MeOH 1:1 (*v*/*v*), [10 wt.%] and sealed in a 5 mL microwave reaction vial. A spatula tip of TCEP were dissolved in a single drop of H_2O and added to the reaction solution to reduce possible disulfides. The thiol/TPO solution was flushed under Ar-atmosphere for 10 minutes. After the monomer/$Ir(ppy)_3$ mixture was added to the vial the solution was irradiated with UV-light (405 nm wavelength, with an intensity of 2.61 mW/cm² (5%). Samples (0.3 mL) were taken from the reaction solution at defined times (1 min, 3 min, 5 min, 7 min, 10 min, 15 min, 20 min, 30 min, 45 min, 60 min and precipitated in diethyl ether. After the solvents were evaporated the monomer conversion was determined via ^{1}H NMR-spectroscopy. Also $\ln([M]_0/[M]_t)$ against reaction time is plotted. With a linear relationship characteristics of a living polymerization can be shown.

Scheme S4. TIRP conditions (experiments 1(Figure 3 (A) and (B)) and 2) for the experimental determination of monomer conversion through reaction time (tritylthiol = 5 mol%, TPO = 5 mol%, $Ir(ppy)_3$ = 0.05 mol%; DCM-d_2/MeOH-d_4 1:3 (*v*/*v*) = 10 wt.%; hν = 120 min (exp. 2; 60 min), 405 nm, 2.61 mW/cm²).

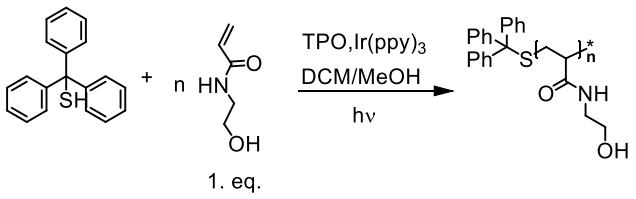

Table S2. Monomer conversion at defined reaction times and calculation of $\ln([M]_0/[M]_t)$, $[M]_0$ = initial monomer concentration, $[M]_t$ = monomer concentration at reaction time t [min].

		Experiment 1 = Figure 3 (A) and (B)			Experiment 2		
#	reaction time [min]	monomer conversion [%]	$\frac{[M]0}{[M]t}$	$\ln(\frac{[M]0}{[M]t})$	monomer conversion [%]	$\frac{[M]0}{[M]t}$	$\ln(\frac{[M]0}{[M]t})$
0	0	0	1	0	0	1	0
1	1	-	-	-	7	1.075	0.072
2	3	-	-	-	8.7	1.095	0.091
3	5	-	-	-	10.7	1.119	0.112
4	7	-	-	-	16	1.19	0.174
5	10	-	-	-	17.7	1.215	0.195
6	15	-	-	-	19.6	1.24	0.215
7	20	23	1.298	0.261	36	1.56	0.445
8	30	32	1.47	0.386	48	1.923	0.654
9	45	40	1.667	0.51	71	3.4	1.237
10	60	47	1.887	0.635	90	10	2.3
11	80	55	2.222	0.798	-	-	-
12	100	60	2.5	0.916	-	-	-
13	120	65	2.857	1.05	-	-	-

Experiment 2:

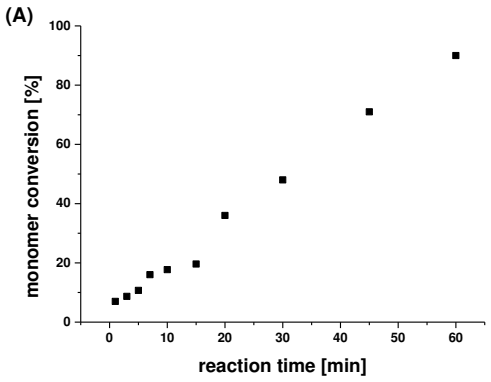

Figure S15. Experiment 2 - plot of monomer conversion [%] at defined reaction times [min] (**#1**- **#10**).

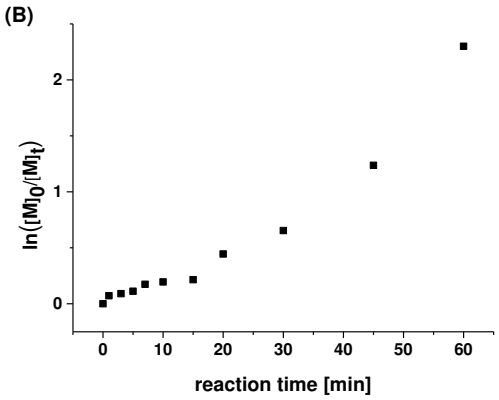

Figure S16. Experiment 2 - plot of $\ln([M]_0/[M]_t)$ ($[M]_0$ = initial monomer concentration, $[M]_t$ = monomer concentration at reaction time t [min]) versus reaction time [min] (**#1** - **#10**).

Monomer conversion was determined via ^{1}H NMR-spectroscopy by integrating the signal of one of the acrylic protons, at a chemical shift of 5.65 ppm to the value 1 (1). Then the multiplett signal from 3.59-3.77 ppm of the methylene protons of the HEAA monomer and the emerging poly-HEAA is also integrated (2) and the 2 protons of the monomer can be subtracted. Through division by two and again dividing through the total amount the conversion can be determined (3). See calculation and example below:

$$5.65\ ppm \rightarrow 1 \quad (1)$$

$$\int_{3.59\ ppm}^{3.77\ ppm} = A \quad (2)$$

$$\frac{\frac{A-2}{2}}{\left(\frac{A-2}{2}\right)+1} = X \quad (3)$$

$$X*100\% = \text{monomer conversion [\%]} \quad (4)$$

Example for 10 min (exp. 2; see ^{1}H NMR spectra below):

$$5.65\ ppm \rightarrow 1 \quad (5)$$

$$\int_{3.59\ ppm}^{3.77\ ppm} = 2.43 \quad (6)$$

$$\frac{\frac{2.43-2}{2}}{\left(\frac{2.43-2}{2}\right)+1} = 0.177 \quad (7)$$

$$0.177*100\% = 17.7\ \% \quad (8)$$

$[M]_0$ = initial monomer concentration = 100 %

$[M]_t$ = monomer concentration at reaction time t

$[M]_t$ = 100%-monomer conversion [%]

Example for t = 10 min (exp. 2):

monomer conversion = 17.7 %

$[M]_t$ = 100 % - 17.7 % = 82.3 % (9)

$$\frac{[M]0}{[M]t} = \frac{100}{82.3} = 1.215 \quad (10)$$

$$\ln(1.215) = 0.195 \quad (11)$$

2.1.3.1 Analytics

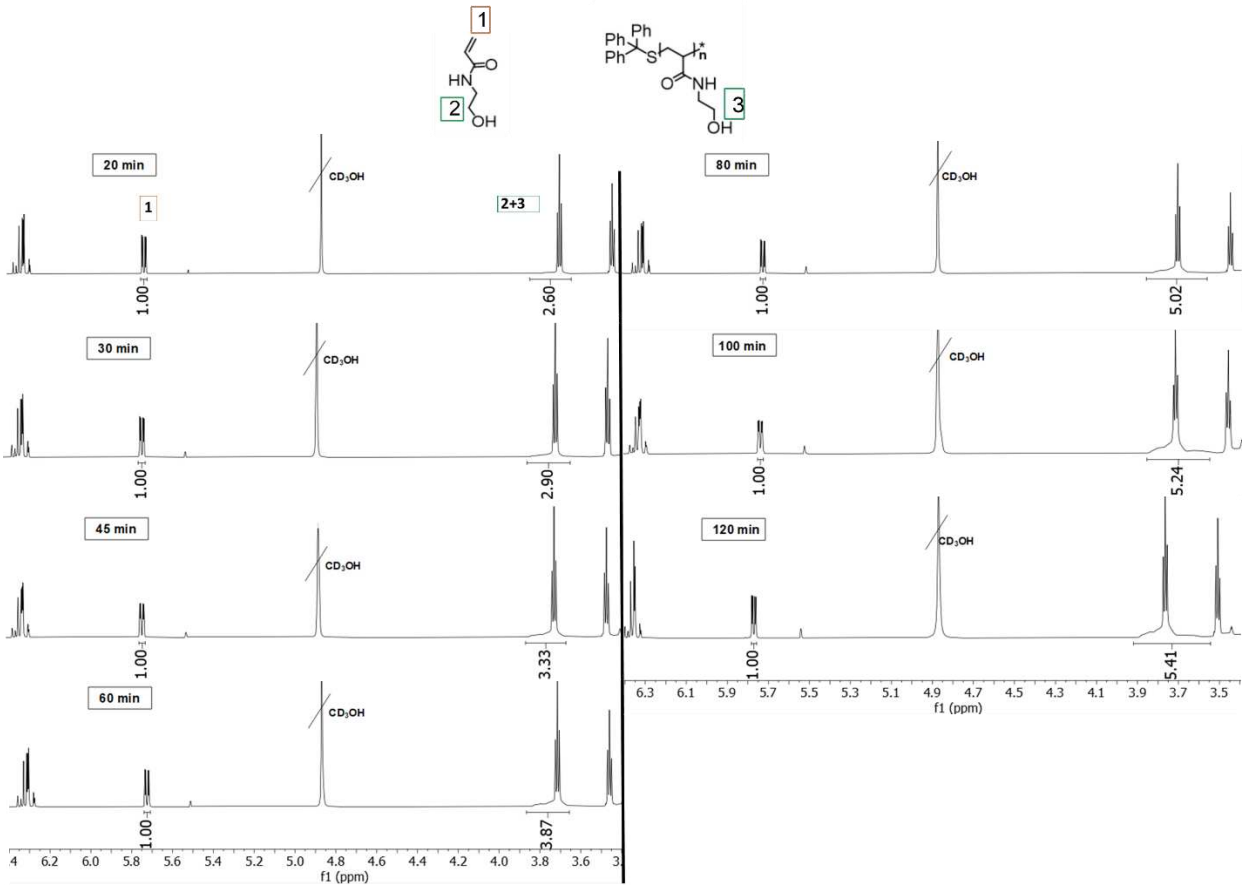

Figure S17. Experiment 1 - ^{1}H NMR-spectra (600 MHz, CD_3OD, RT) of monomer/polymer-mix (**#7** - **#13**) at different reaction times.

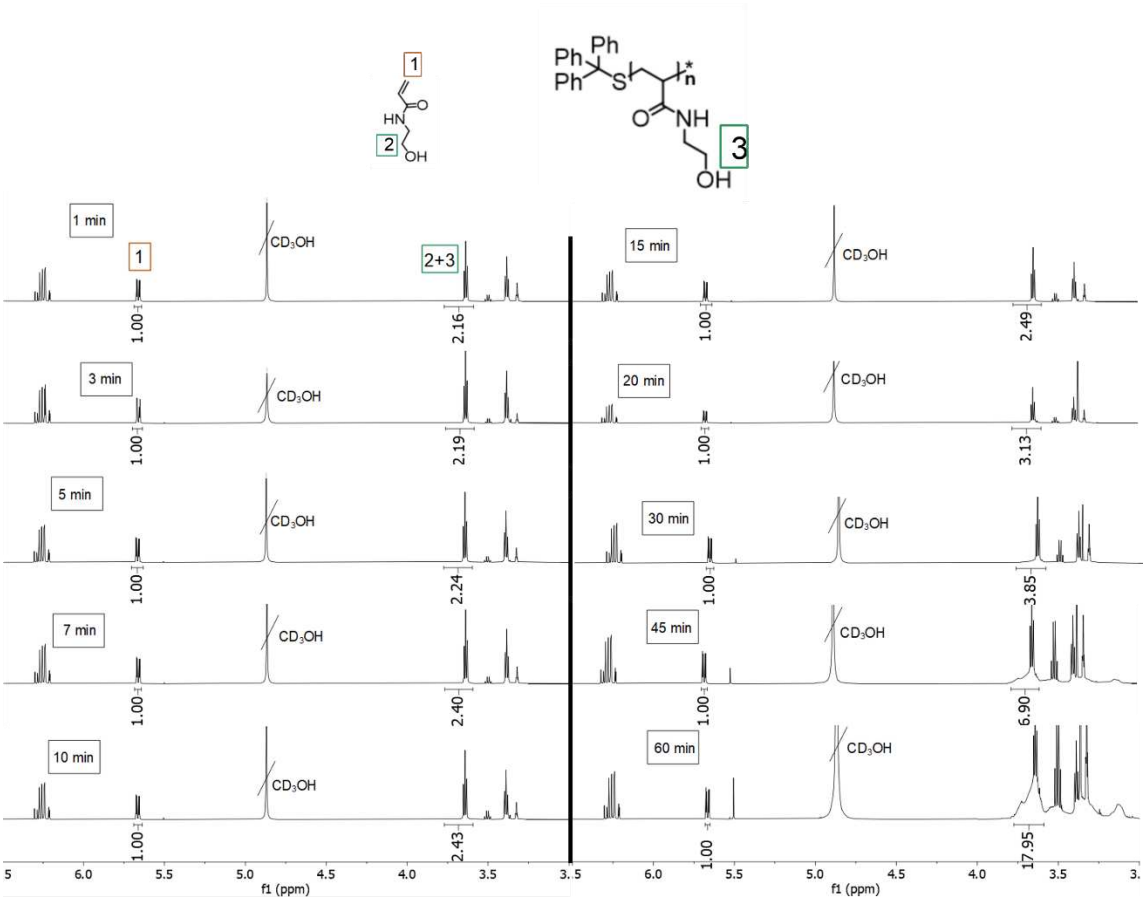

Figure S18. Experiment 2 - ^{1}H NMR-spectra (600 MHz, CD_3OD, RT) of monomer/polymer-mix (**#1 - #10**) at different reaction times.

2.1.4 Figure 3 (C): SI for light on-off experiment

1 eq. of HEAA monomer (100 mol%, 200 mg) and $Ir(ppy)_3$ (0.05 mol%) were dissolved in DCM-d_2/MeOH-d_4 1:3 (*v*/*v*), [10 wt.%] sealed in a 5 mL glass flask and flushed with argon gas for 10 minutes. In a second step, tritylthiol (5 mol%) and equimolar amounts of TPO (5 mol%) were also dissolved in DCM-d_2/MeOH-d_4 1:1 (*v*/*v*), [10 wt.%] and sealed in a 5 mL microwave reaction vial. A spatula tip of TCEP was dissolved in a single drop of H_2O and added to the reaction solution to reduce possible disulfides. The thiol/TPO solution was flushed under Ar-atmosphere for 10 minutes. After the monomer/$Ir(ppy)_3$ mixture was added to the vial the solution was irradiated with UV-light (405 nm wavelength, with an intensity of 2.61 mW/cm^2 (5%). The light source was switched on and off during the reaction at defined times to determine if polymer growth can be stopped by turning the light source off and regained by turning it on again.

Scheme S5. TIRP conditions (experiment 1 and 2) for the experimental determination of monomer conversion through reaction time while switching the light source on and off (tritylthiol = 5 mol%, TPO = 5 mol%, $Ir(ppy)_3$ = 0.05 mol%; DCM/MeOH 1:1 (*v*/*v*) = 10 wt.%; hν = 90 min (exp.1, Fig. 3 (C)) / 30 min (exp. 2), 405 nm, 2.61 mW/cm^2).

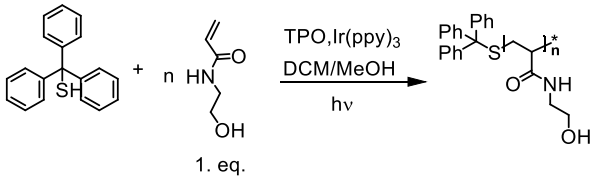

Samples (0.3 mL) were taken at 20 min, 30 min, 50 min, 60 min, 80 min, 90 min and 120 min and the monomer conversion was determined via ^{1}H NMR-spectroscopy. By plotting the monomer conversion against the reaction time a stair pattern can be observed, which indicates, that polymer growth can be controlled by turning the light source on and off. For calculation of the monomer conversion see chapter S2.1.2.

Table S3. Monomer conversion at defined reaction times after periods with the light source switched on and off.

#	reaction time [min]	Light source	monomer conversion [%]	$\frac{[M]0}{[M]t}$	$\ln(\frac{[M]0}{[M]t})$
1	0-20	ON	24	1.32	0.27
2	20-30	OFF	24	1.32	0.27
3	30-50	ON	44	1.78	0.58
4	50-60	OFF	44	1.78	0.58
5	60-80	ON	56	2.27	0.82
6	80-90	OFF	56	2.27	0.82
7	90-120	ON	70	3.33	1.2

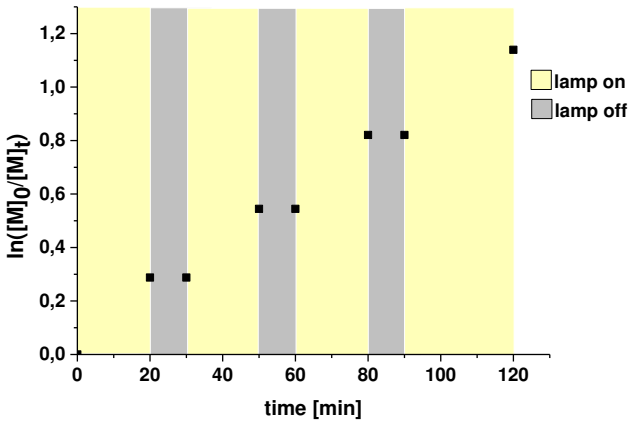

Figure S19. Plot of $\ln([M]_0/[M]_t)$ ($[M]_0$ = initial monomer concentration, $[M]_t$ = monomer concentration at reaction time t [min]) against reaction time with the light source switched on and off (**#1** - **#7**).

2.1.4.1. Analytics

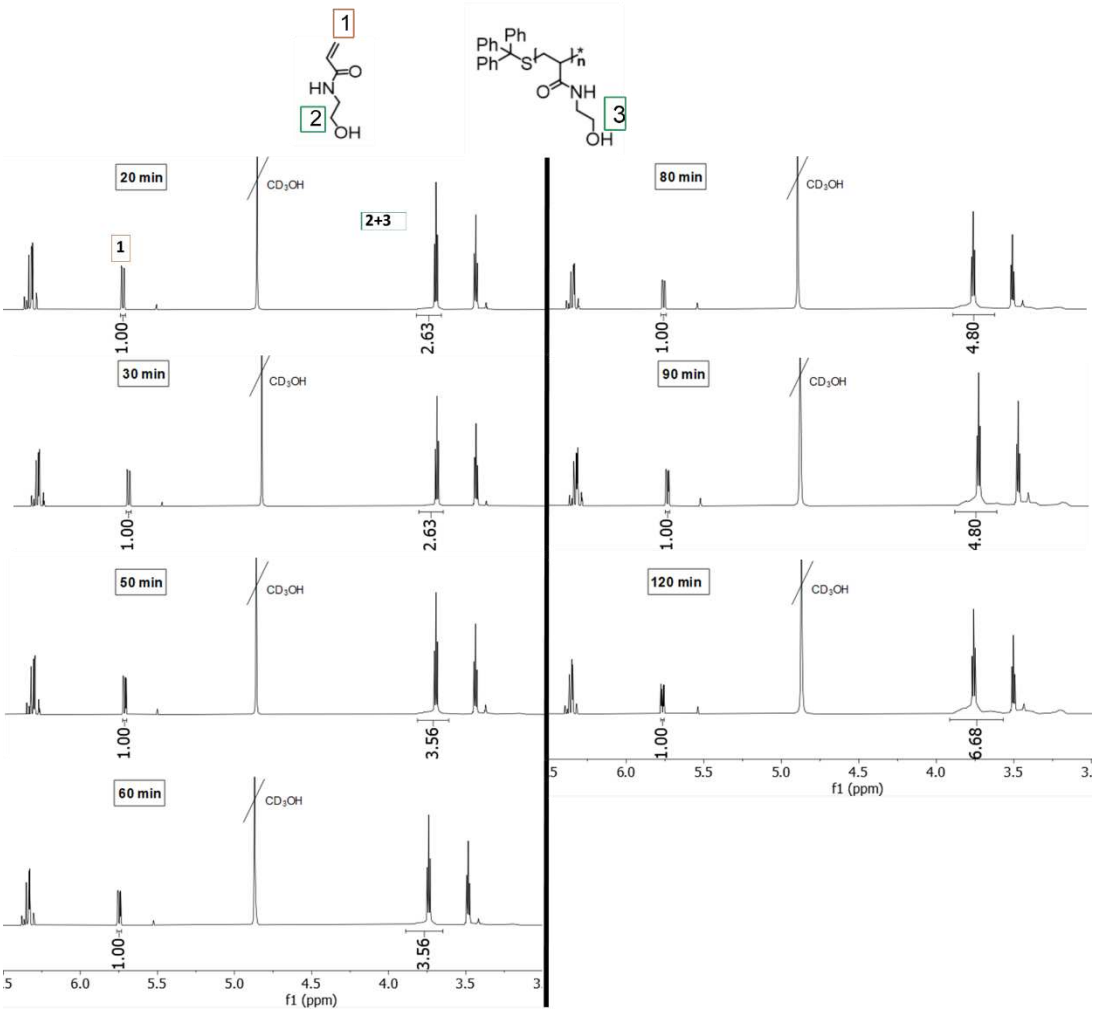

Figure S20. ^{1}H NMR-spectra (600 MHz, CD_3OD, RT) of monomer/polymer-mix (**#1**-**#7**) at different reaction times.

2.1.5 Figure 3 (D): SI for degree of polymerization against monomer conversion

The degrees of polymerization of the polymers from 3A (chapter 2.1.3, Table S2, #7-13) were calculated via the ^{1}H NMR spectra, that were also used for the calculation of monomer conversion. By doing so it is assumed, that all thiols are activated from the beginning, which is a known feature for CRPs. Determination of P_n and Đ via SEC was not possible for these polymers due to the difficulty of isolating the formed polymers e.g. by precipitation or dialysis from the monomer/initiator/catalyst mixture without discriminating against shorter chain length.

Calculation example:

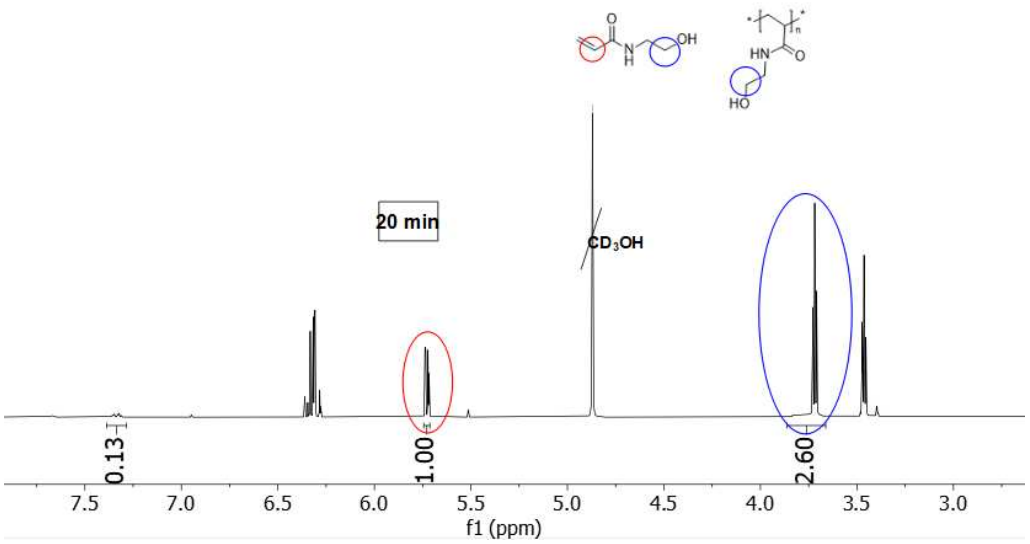

Figure S21. ^{1}H NMR of monomer polymer mix #7 (3A) for 20 min reaction time, referenced on acryl proton.

Integral = 2.60 → 2H monomer and 0.6H polymer = 77% monomer and 23% polymer

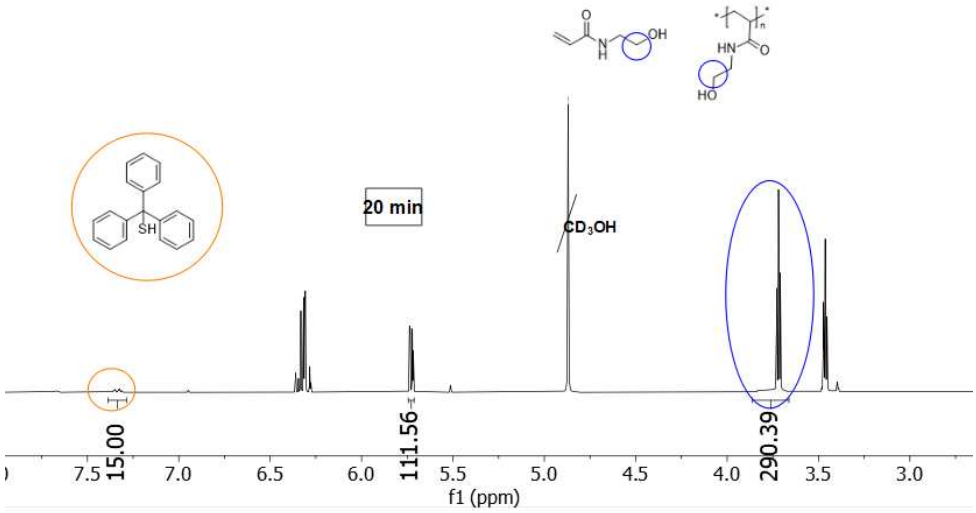

Figure S22. ^{1}H NMR of monomer polymer mix #7 (3A) for 20 min reaction time, referenced on tritylthiol initiator.

Integral = 290.39 → 23% polymer = 290.39*0.23 =66 H (2 H per repeating unit)

66 H / 2 = 33 P_n

Following this calculation results in:

Table S4. Calculated degrees of polymerization for different reaction times.

Reaction Time [min]	Monomer Conversion [%]	P_n
0	0	0
20	23	33
30	32	47
45	40	66
60	47	81
80	55	116
100	60	129
120	65	133

2.2 Scheme 2: SI for the synthesis of block-copolymers

By performing the TIRP polymerization protocol (chapter **2**) two HEAA-polymers were synthesized (**#1**: $\overline{M}_n$ = 2 kDa, **#2**: $\overline{M}_n$ = 7 kDa). The isolated and purified polymers were now used as macro initiators to perform another TIRP and build copolymers.

Scheme S6. Reaction conditions for the synthesis of PHEAA-*block*-PHEAA **#1'** ($Ir(ppy)_3$ = 0.05 mol%; DMF = 10 wt.%; hν = 60 min, 405 nm, 2.61 mW/cm²).

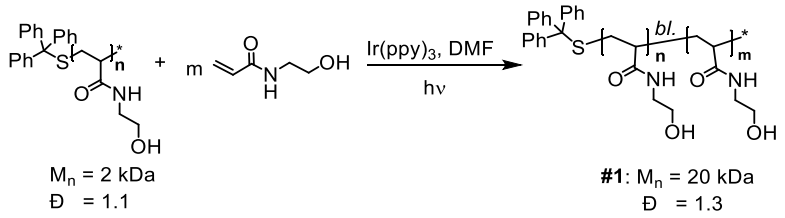

PHEAA-*block*-PHEAA **#1'**:

1 eq. of HEAA monomer (500 mg, 4.3 mmol) and $Ir(ppy)_3$ (0.05 mol%) were dissolved in DMF [10 wt.%] sealed in a 5 mL glass flask and flushed with argon gas for 10 minutes. In a second step, the macro initiator polymer (55 mg, 0.0275 mmol) was also dissolved in DMF [10 wt.%] and sealed in a 5 mL microwave reaction vial. A spatula tip of TCEP were dissolved in a single drop of H_2O and added to the reaction solution to reduce possible disulfides. After, the monomer/$Ir(ppy)_3$ mixture was added to the vial (inert atmosphere) the solution was irradiated with UV-light (405 nm wavelength, with an intensity of 45.2 mW/cm² (100%)). After an hour, the irradiation was stopped and the polymer solution was precipitated in diethyl ether. The precipitated polymer was dissolved in H_2O, dialyzed against distilled water (three cycles, 10 kDa) and subsequently lyophilized.

Scheme S7. Reaction conditions for the synthesis of PHEAA-*block*-PManAAm **#2'** ($Ir(ppy)_3$ = 0.05 mol%; DMF = 10 wt.%; hν = 60 min, 405 nm, 2.61 mW/cm², NaOMe = 0.2 M).

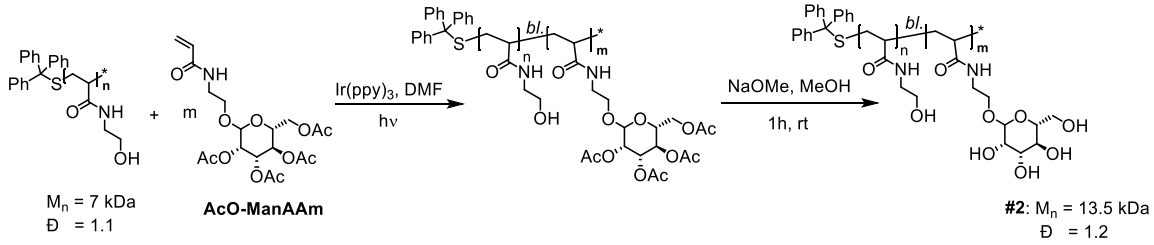

PHEAA-*block*-PManAAm **#2'**:

1 eq. of AcO-ManAAm* (966.6 mg, 2.17 mmol) and $Ir(ppy)_3$ (0.05 mol%) were dissolved in DMF [10 wt.%] sealed in a 5 mL glass flask and flushed with argon gas for 10 minutes. In a second step, the macro initiator polymer (0.6 g, 0.086 mmol) was also dissolved in DMF [10 wt.%] and sealed in a 5 mL microwave reaction vial. A spatula tip of TCEP was dissolved in a single drop of H_2O and added to the reaction solution to reduce possible disulfides. After, the monomer/$Ir(ppy)_3$ mixture was added to the vial (inert atmosphere) the solution was irradiated with UV-light (405 nm wavelength, with an intensity of 45.2 mW/cm² (100%)). After an hour, the irradiation was stopped and 5 mL NaOMe (0.2 M) in MeOH was added to the polymer solution and stirred one hour at room temperature. Solid matter that has already precipitated and the residual solution was precipitated in diethyl ether. The precipitated polymer was dissolved in H_2O, dialyzed against distilled water (three cycles, 5 kDa) and subsequently lyophilized.

<u>*AcO-ManAAm</u>

The synthesis of the mannose monomer was adapted by Gibson *et al*.[1] The acetylated mannoseacrylamide monomer was synthesized by dissolving D-mannose in a mixture of a 1:1 (*v*/*v*) mixture of pyridine/acetic anhydride [20 mL/g] and stirring at room temperature overnight. After diluting with ethylacetate the mixture was extracted three times with 1M HCl solution. Evaporation of ethylacetate resulted in 1,2,3,4,6-penta-O-acetyl-α-D-mannopyranose. Pentaacetylated mannose (1.0 eq.) and N-hydroxyethylacrylamide (1.2 eq.) were dissolved in DCM [2 mL/mmol] and flushed with argon gas for 10 minutes. BF_3*Et_2O (10.0 eq.) was added through a syringe and the mixture stirred at room temperature overnight. The reaction solution was washed three times with brine and the organic phase dried with MgSO4. The solvent was removed, which resulted in pure acetylated mannosemonomer (AcO-ManAAm) with a relative purity of 98 % and a yield of 78 %.

ESI-MS: m/z calculated for $C_{19}H_{27}NO_{11}$ $[M+H]^+$ 446.16 and $[M+Na]^+$ 468.15; found $[M+H]^+$ 446.46 and $[M+H]^+$ 468

2.2.1 Analytics

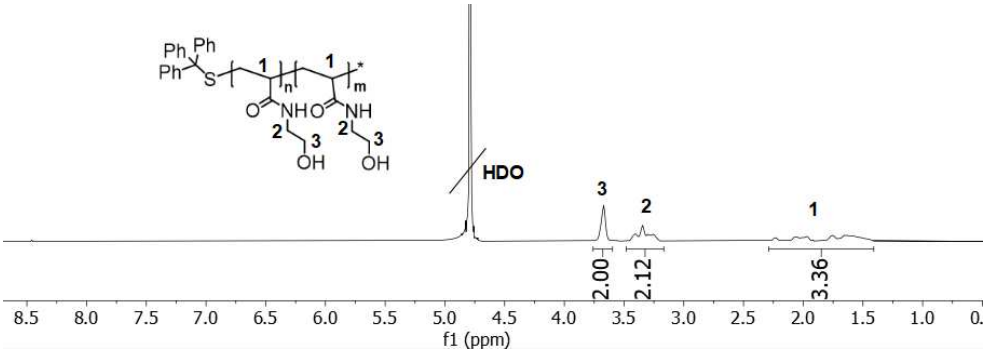

Figure S23. ^{1}H NMR (600 MHz, D_2O) of PHEAA-*block*-PHEAA **#1'**.

^{1}H NMR (600 MHz, D_2O) δ [ppm] 3.74-3.62 (m, **3**), 3.49-3.21 (m, **2**), 2.36-1.32(m, **1**).

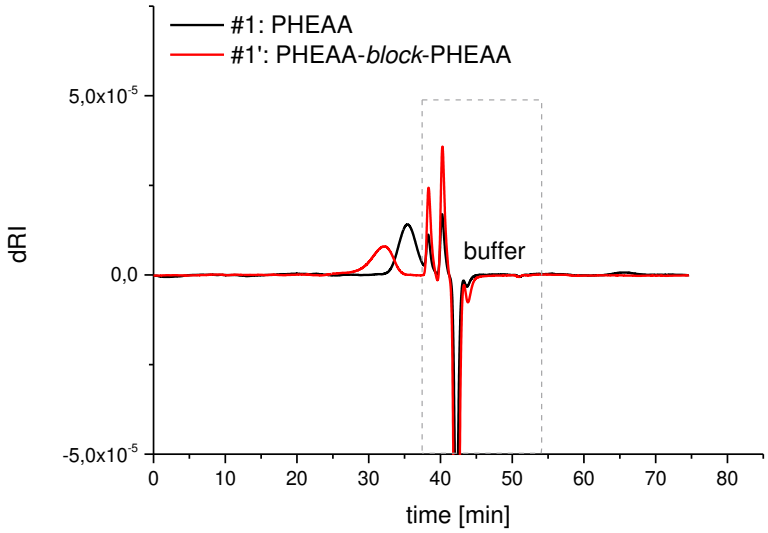

Figure S24. H_2O-SEC-MALS of the HEAA polymer **#1** and the synthesized copolymer PHEAA-*block*-PHEAA **#1'**.

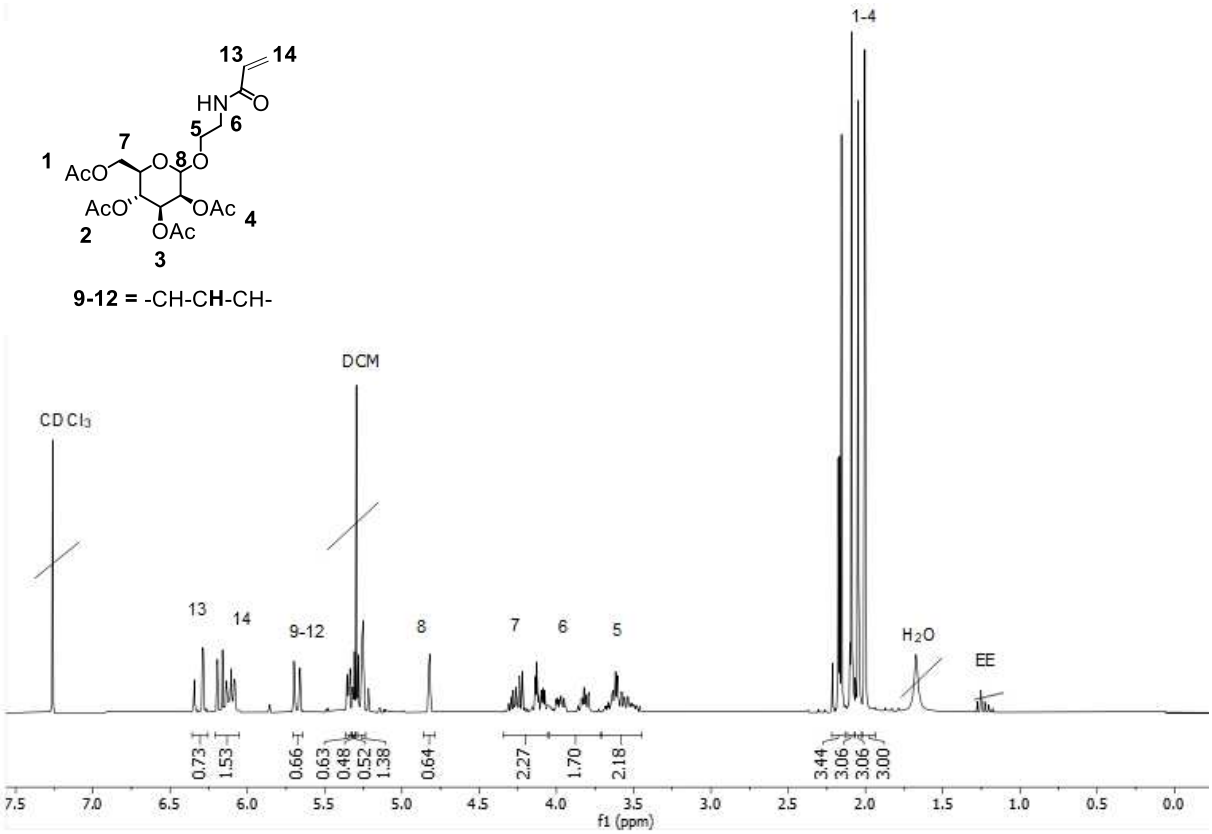

Figure S25. . ^{1}H NMR (300 MHz, $CDCl_3$) of AcO-ManAAm.

^{1}H NMR (300 MHz, $CDCl_3$): δ (ppm) 2.00-2.16 (s, 12H, C**H**$_3$ H1-4), 3.46-3.61 (m, 2H, C**H**$_2$ H5), 3.79-4.02 (m, 2H, C**H**$_2$, H6), 4.06-4.23 (m, 2H, C**H**$_2$, H7), 4.82 (s, 1H, C**H**, H8), 5.22-5.69 (m, 4H, C**H**, H9-12), 6.15 (dd, ^{2}J=10.2 Hz, ^{3}J=17.1 Hz, 2H, C**H**$_2$, H14), 6.32 (dd, ^{2}J=1.2 Hz, ^{3}J=17.1 Hz, 1H C**H**, H13)

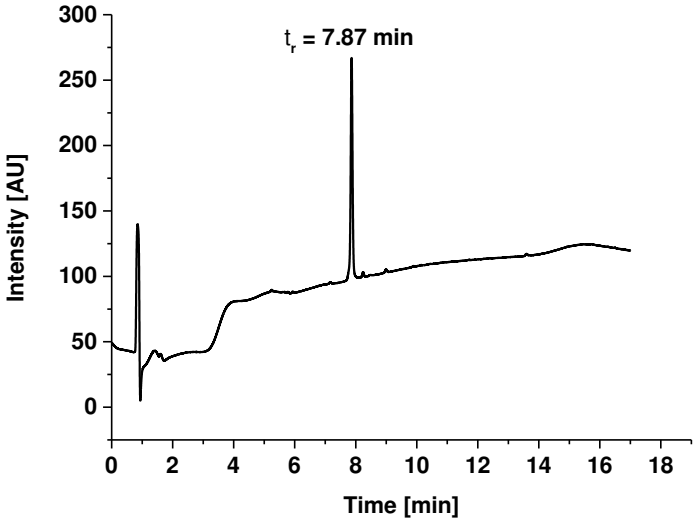

Figure S26. RP-HPLC of AcO-ManAAm (A: 95% H_2O/ 5% MeCN/ 0.1% Formic Acid; 100% A -> 50% A in 30 min): t_r = 7.87 min.

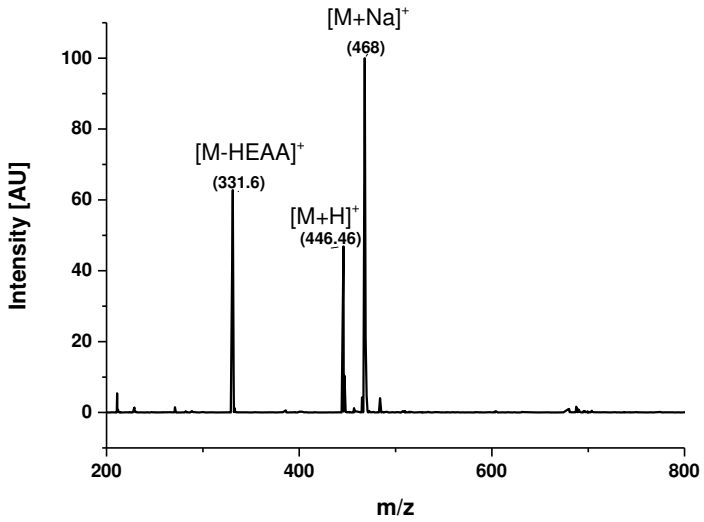

Figure S27. ESI-MS of AcO-ManAAm.

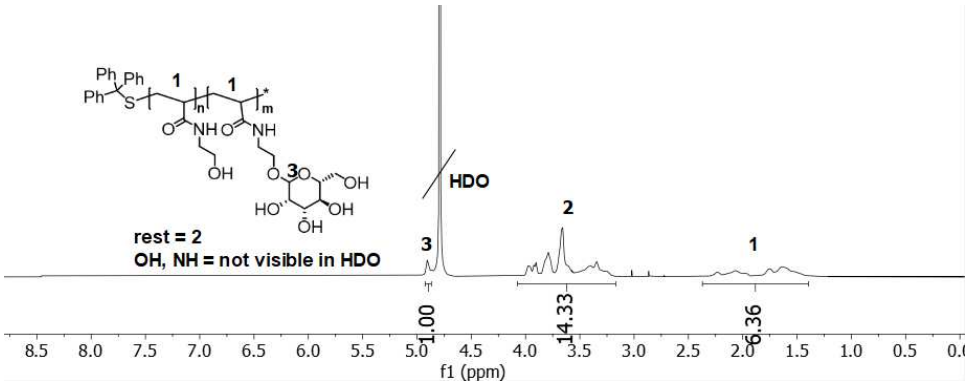

Figure S28. ^{1}H NMR (600 MHz, D_2O) of PHEAA-*block*-PManAAm **#2'**.

^{1}H NMR (600 MHz, D_2O) δ [ppm] 4.90 (s, **3**), 4.01-3.17 (m, **2**), 2.33-1.39(m, **1**).

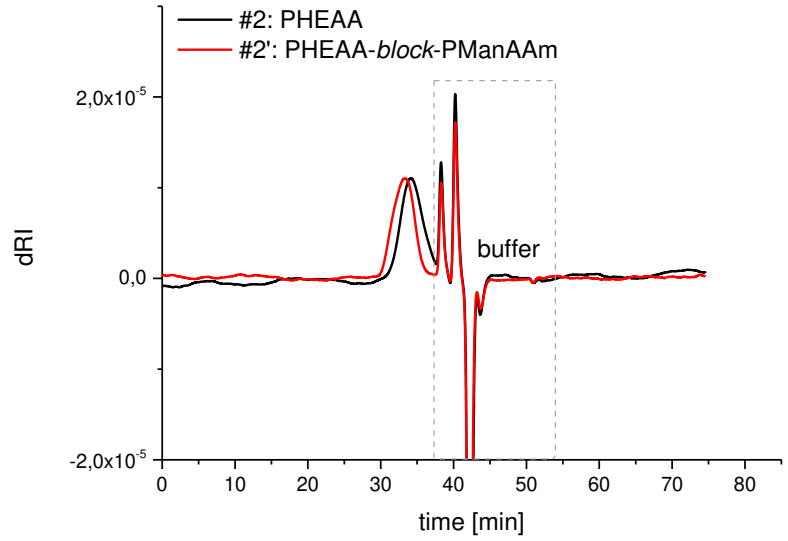

Figure S29. H_2O-SEC-MALS of the precursor polymer PHEAA **#2** and the synthesized copolymer PHEAA-*block*-PManAAm **#2'**.

2.2.2 TPO initiated block-copolymer

The optimized TIRP polymerization protocol of PTBMA (chapter 2.1; polymer #1') was performed, but without any thiol source to create TPO initiated PTBMA in a free radical polymerization that was precipitated in MeOH/H_2O 3:1 (*v:v*) and analyzed via THF-SEC. Afterwards the resulting polymer was used further as an initiator and copolymerized with ethyl acrylate (EA) by only using the comonomer and $Ir(ppy)_3$, but without additional TPO initiator to build PTBMA-*block*-PEA.

Scheme S8. Reaction conditions for the synthesis of PTBMA-*block*-PEA with TPO as initiator.

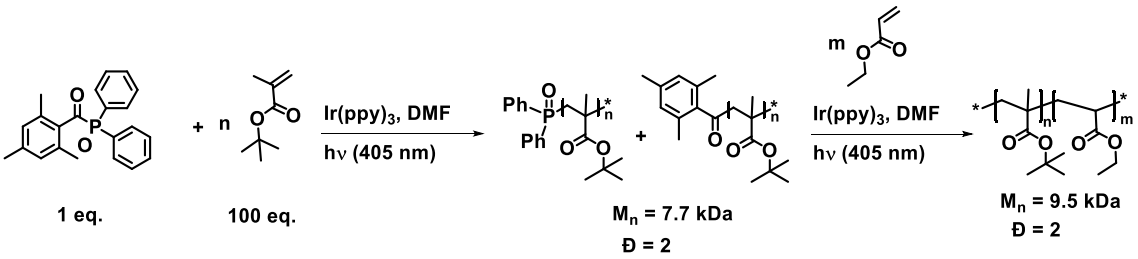

2.2.2.1 Analytics

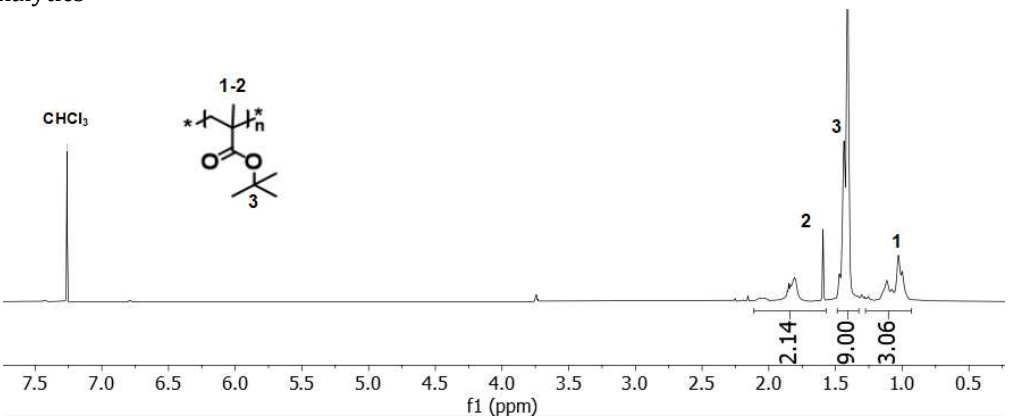

Figure S30. ^{1}H NMR (600 MHz, $CDCl_3$) of TPO initiated PTBMA.

^{1}H NMR (600 MHz, $CDCl_3$) δ [ppm] 2.16-1.58 (m, **2**), 1.48-1.38 (m, **3**), 1.15-0.96 (m, **1**).

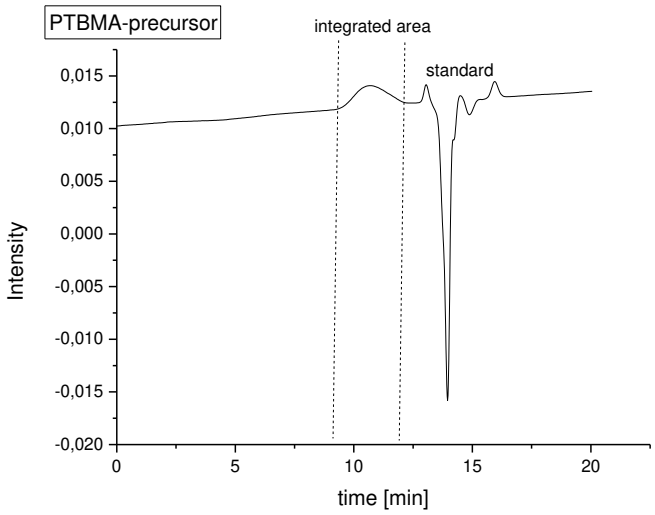

Figure S31. THF-SEC (RI detector) of the PTBMA-precursor polymer.

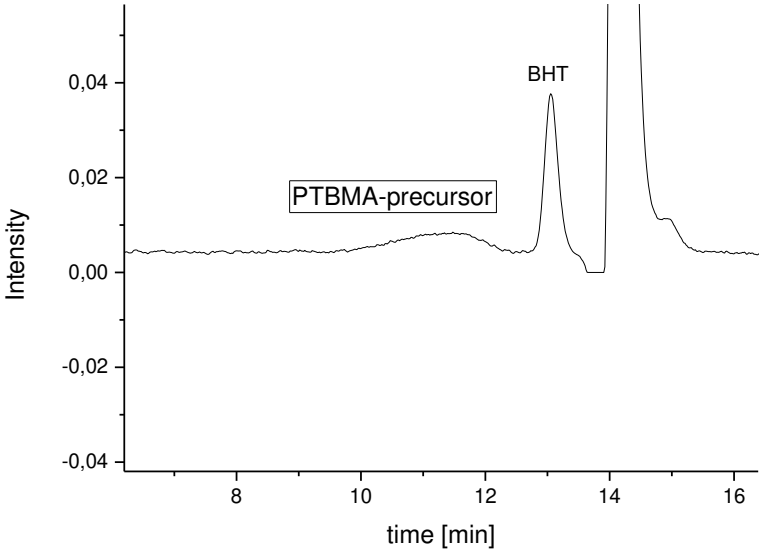

Figure S32. THF-SEC (UV detector) of the PTBMA-precursor polymer.

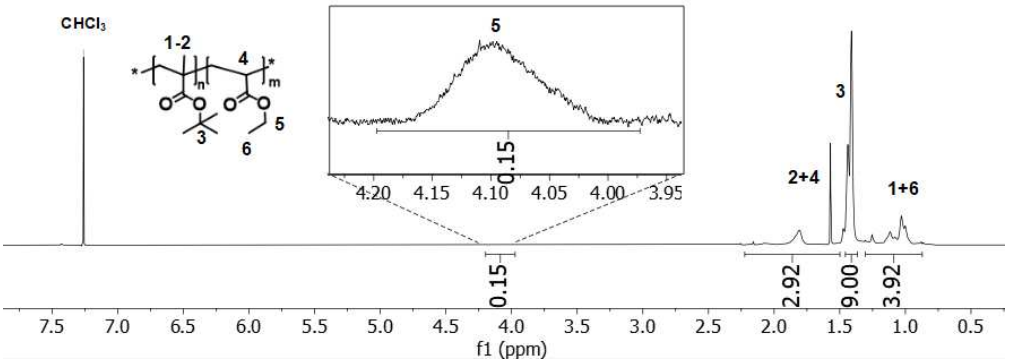

Figure S33. ^{1}H NMR (600 MHz, $CDCl_3$) of TPO initiated PTBMA-*block*-PEA.

^{1}H NMR (600 MHz, $CDCl_3$) δ [ppm] 4.17-4.01 (m, **5**), 2.16-1.58 (m, **2+4**), 1.48-1.38 (m, **3**), 1.15-0.96 (m, **1+6**).

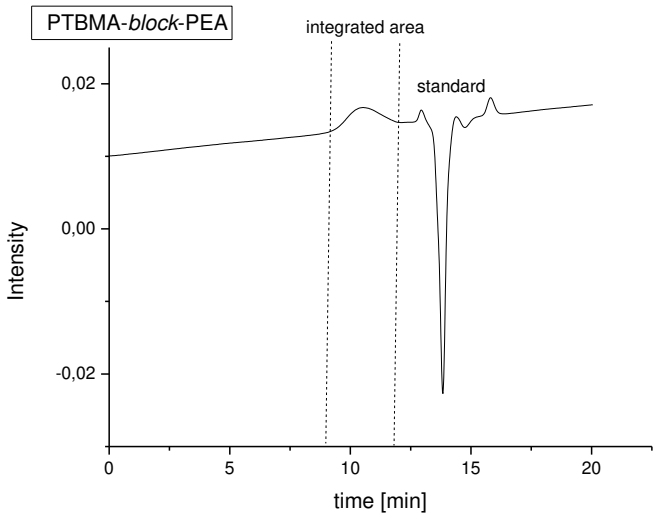

Figure S34. THF-SEC (RI detector) of PTBMA-*block*-PEA.

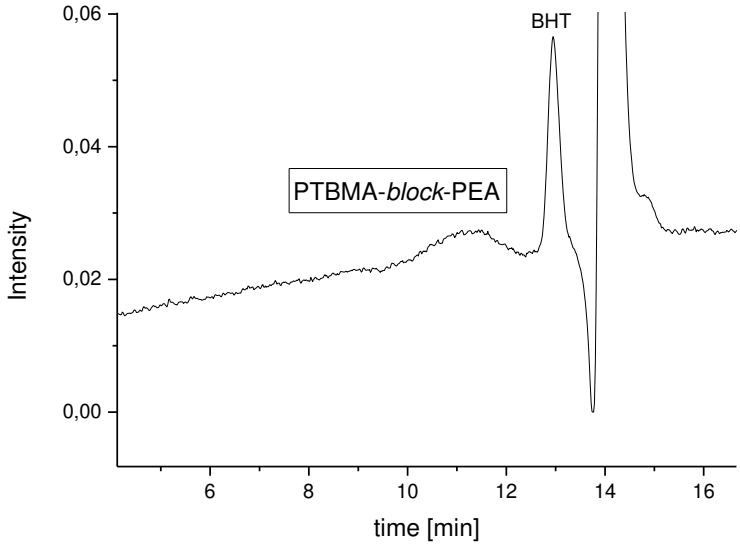

Figure S35. THF-SEC (UV detector) of PTBMA-*block*-PEA.

2.3 Figure 4 (A): SI for varying the thiol:TPO-ratio

The general procedure of TIRP (chapter 2) was carried out while varying the TPO concentration. For 1 eq. of HEAA-monomer in each reaction 5 eq. of thiol was used. The $Ir(ppy)_3$ concentration was kept at 0.05 mol%. The average molecular weights and dispersities were measured by H_2O-SEC-MALS.

Scheme S9. Polymerization parameters used while varying the thiol:TPO ratio (tritylthiol = 5 mol%, $Ir(ppy)_3$ = 0.05 mol%; DMF = 10 wt.%; hν = 60 min, 405 nm, 2.61 mW/cm²).

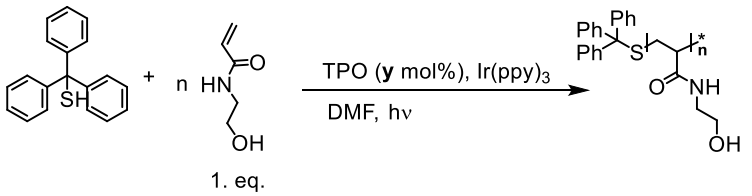

Table S5. Different thiol:TPO ratios used and the resulting average molecular weights and dispersities (**#1** - **#5**). Theoretical molecular weight: 2.7 kDa.

#	TPO conc. [mol%]	thiol:TPO ratio	$\overline{M}_n$ [kDa] via SEC	Đ via SEC
1	0.05	100:1	4.2	1.09
2	0.5	10:1	4.0	1.14
3	2.5	2:1	3.6	1.57
4	5	1:1	2.7	1.09
5	10	0.5:1	2.3	1.12

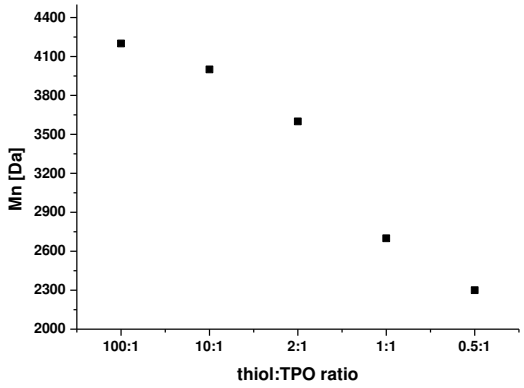

Figure S36. Average molecular weights obtained by changing thiol:TPO (**#1** - **#5**); $\overline{M}_{n\ theory}$: 2700 Da.

2.3.1. Analytics

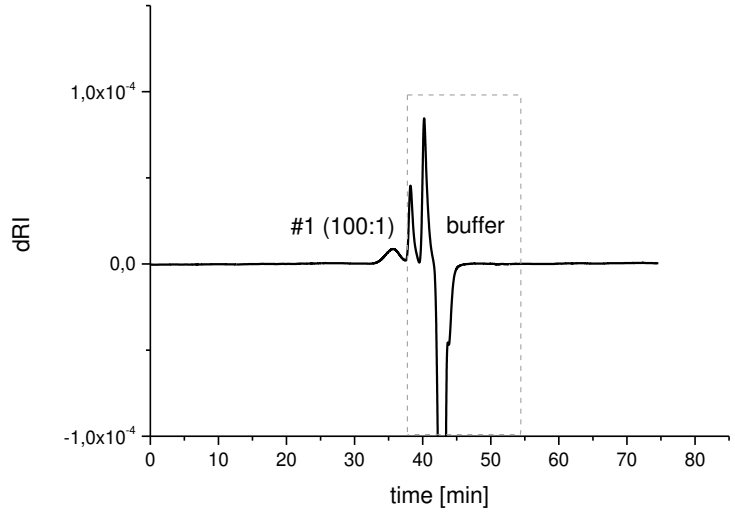

Figure S37. H_2O-SEC-MALS of **#1** (thiol:TPO ratio = 100:1).

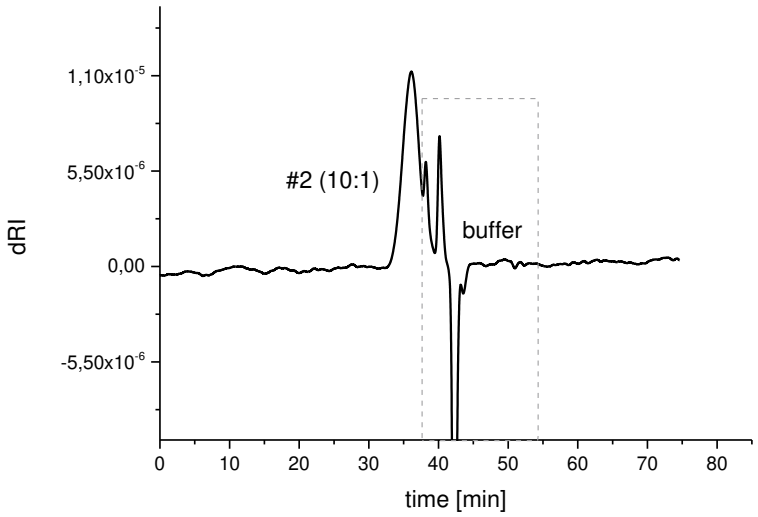

Figure S38. H_2O-SEC-MALS of **#2** (thiol:TPO ratio = 10:1).

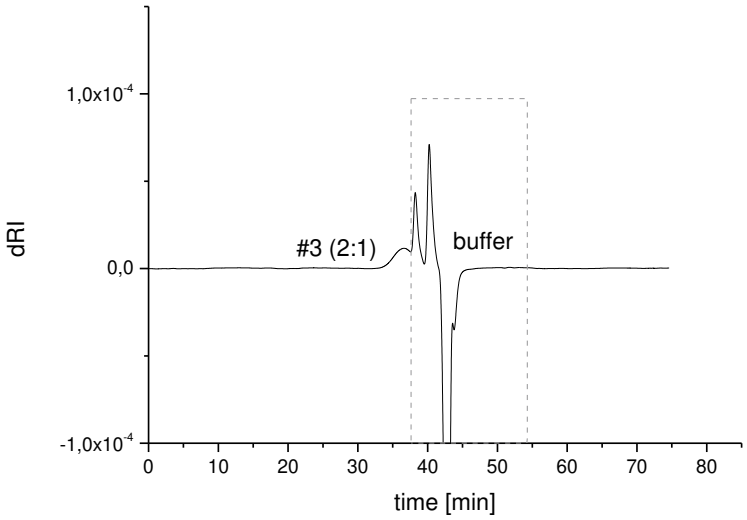

Figure S39. H_2O-SEC-MALS of **#3** (thiol:TPO ratio = 2:1).

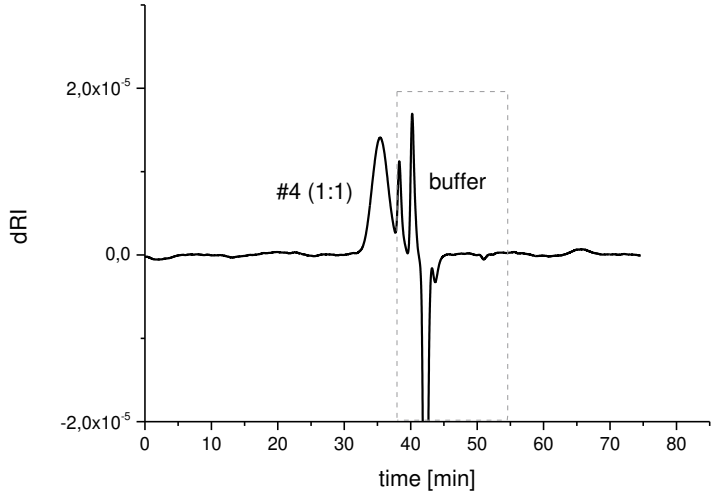

Figure S40. H_2O-SEC-MALS of **#4** (thiol:TPO ratio = 1:1).

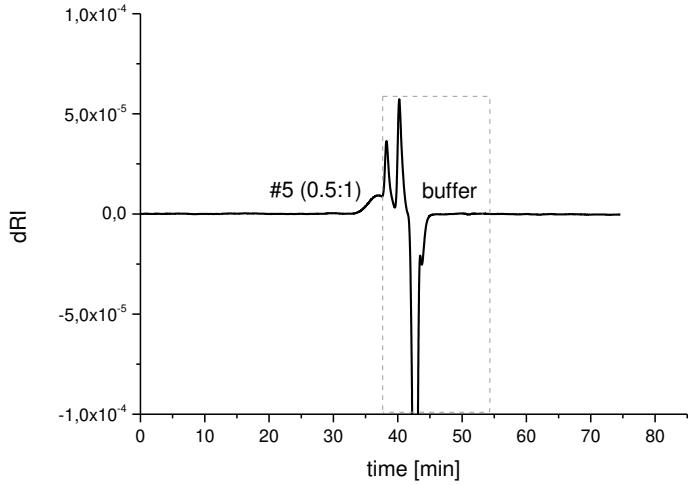

Figure S41. H_2O-SEC-MALS of **#5** (thiol:TPO ratio = 0.5:1).

2.4 Figure 4 (B): SI for varying the photocatalyst concentration: [Ir(ppy)$_3$]

The general procedure of TIRP (chapter 2) was carried out by using 1.0 eq. of HEAA-monomer and keeping the thiol:TPO ratio at 1:1 (5 mol% each). [Ir(ppy)$_3$] concentration was varied with each polymerization. The average molecular weights and dispersities were measured by H_2O-SEC-MALS.

Scheme S10. Polymerization parameters used while varying [Ir(ppy)$_3$] (tritylthiol = 5 mol%, TPO = 5 mol%; DMF = 10 wt.%; hν = 60 min, 405 nm, 2.61 mW/cm^2).

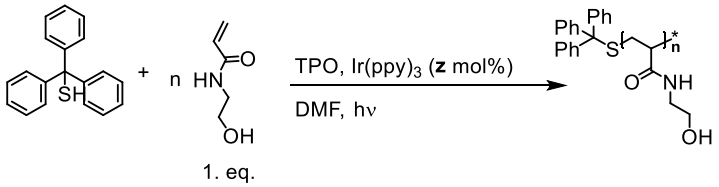

Table S6. Different [Ir(ppy)$_3$] used and the resulting average molecular weights and dispersities (**#1** - **#5**). Theoretical molecular weight: 2.7 kDa.

#	Ir(ppy)$_3$ conc. [mol%]	$\overline{M}_n$ [kDa] via SEC	Đ via SEC
1	0.05	2.7	1.09
2	0.1	3.3	1.19
3	0.5	3.75	1.57
4	2.5	3.8	1.19

5	5	no polymer	no polymer

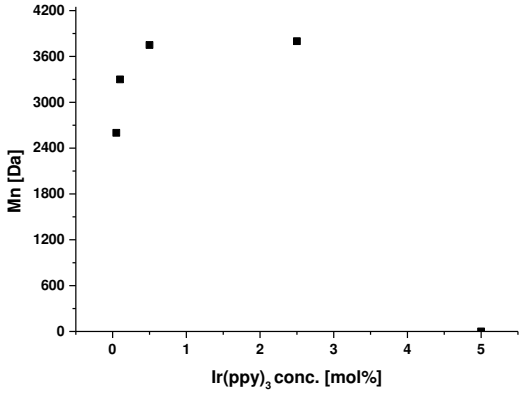

Figure S42. Average molecular weights obtained by varying [Ir(ppy)$_3$] (**#1** -**#5**); $\overline{M}_{n\ theory}$: 2700 Da.

2.4.1. Analytics

<u>H_2O-SEC-MALS:</u>

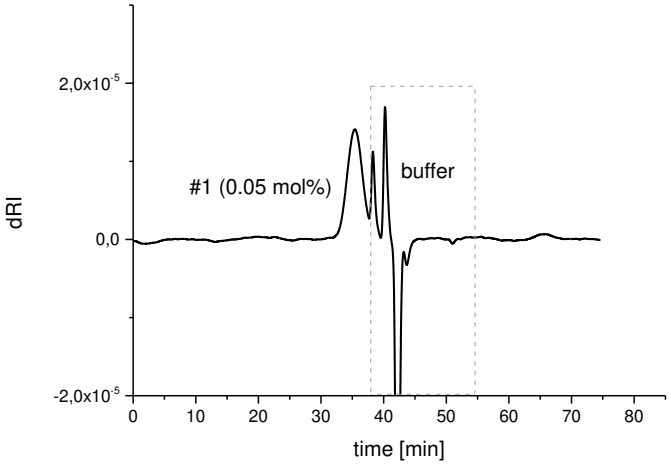

Figure S43. H_2O-SEC-MALS of **#1** ([Ir(ppy)$_3$] = 0.05 mol%).

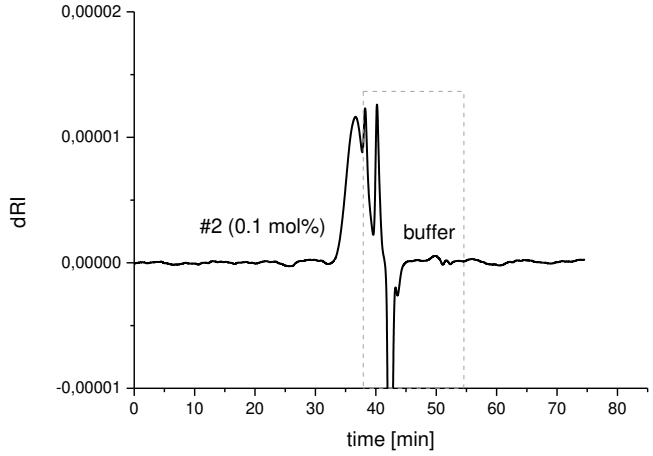

Figure S44. H_2O-SEC-MALS of **#2** ([$Ir(ppy)_3$] = 0.1 mol%).

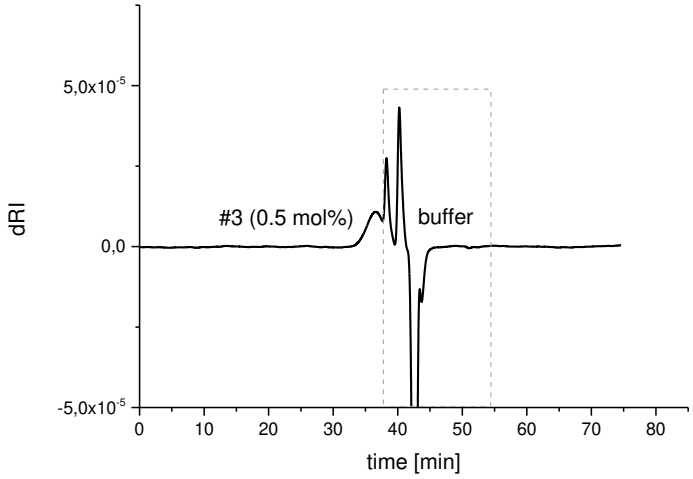

Figure S45. H_2O-SEC-MALS of **#3** ([$Ir(ppy)_3$] = 0.5 mol%).

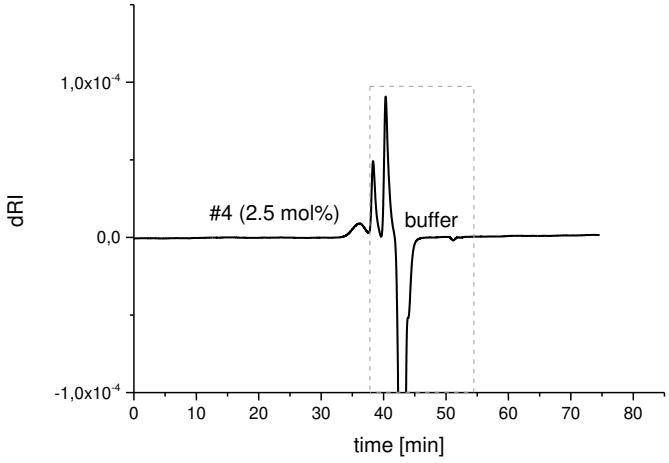

Figure S46. H_2O-SEC-MALS of **#4** ([$Ir(ppy)_3$] = 2.5 mol%).

2.5 Varying the light (hν) intensity

Scheme S11. Polymerization parameters used while varying the irradiation intensity.

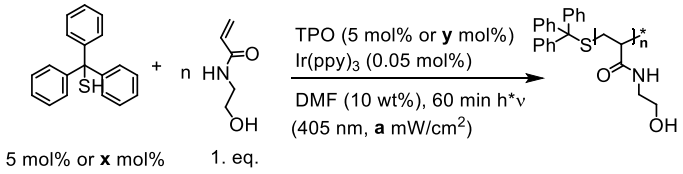

The general TIRP polymerization protocol (chapter **2**) was carried out to determine the effect of changing the light intensity. Therefore the optimized amounts of educts (1 eq. HEAA monomer, thiol:TPO 1:1 (5 eq.), [$Ir(ppy)_3$] = 0.05 mol%) were used while varying the light source (**#1** - **#4**). Also the thiol:TPO ratio and whether $Ir(ppy)_3$ was used or not was varied to determine the connections between those parameters (**#1'**, **#1''**, **#2'**, **#2''**).

Table S7. Different irradiation intensities used and the resulting average molecular weights and dispersities (**#1** - **#4**). Theoretical molecular weight: 2.7 kDa.

#	hν intensity [mW/cm²]	thiol:TPO ratio	$Ir(ppy)_3$	$\overline{M}_n$ [kDa] via SEC	Đ via SEC
1	1.15	1:1	yes	no polymer	no polymer
1'	1.15	0:1	yes	2.4	11.8
1''	1.15	0.5:1	yes	11.8	1.15
2	2.61	1:1	yes	2.7	1.09
2'	2.61	1:1	no	45.3	1.73

2‘‘	2.61	0.5:1	yes	2.3	1.12
3	26	1:1	yes	4.0	1.1
4	45.2	1:1	yes	3.7	1.5

2.5.1 Analytics

H_2O-SEC-MALS

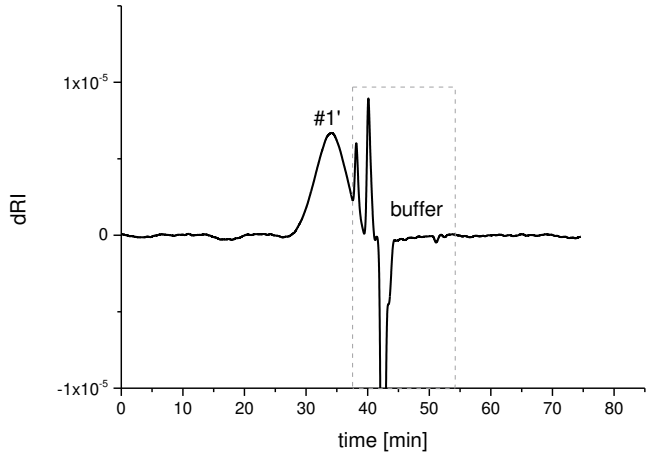

Figure S47. H_2O-SEC-MALS of **#1'** (hν intensity = 1.15 mW/cm², thiol:TPO 0:1).

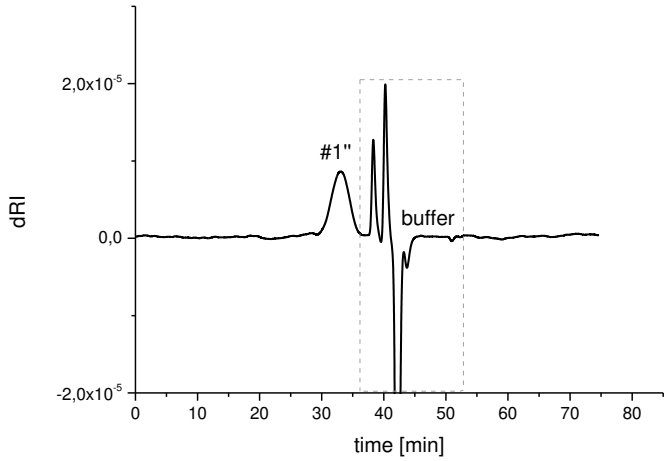

Figure S48. H_2O-SEC-MALS of **#1''** (hν intensity = 1.15 mW/cm², thiol:TPO 0.5:1).

For H_2O-SEC-MALS of **#2** (hν intensity = 2.61 mW/cm², thiol:TPO 1:1) see chapter 2.1.1 (Figure S4).

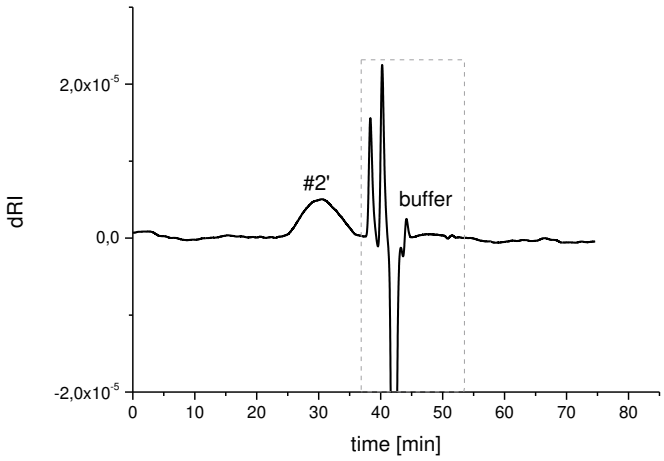

Figure S49. H_2O-SEC-MALS of **#2'** *(*hν intensity = 2.61 mW/cm², thiol:TPO 1:1, without $Ir(ppy)_3$).

Elemental analysis shows that without the iridium catalyst no polymer is built at the thiol component:

theoretical values (n=20): %C=55.44; %H=7.62; %N=10.87; %S=1.24

measured values (n=20): %C=51.41; %H=8.29; %N=11.21; %S= no sulfur found

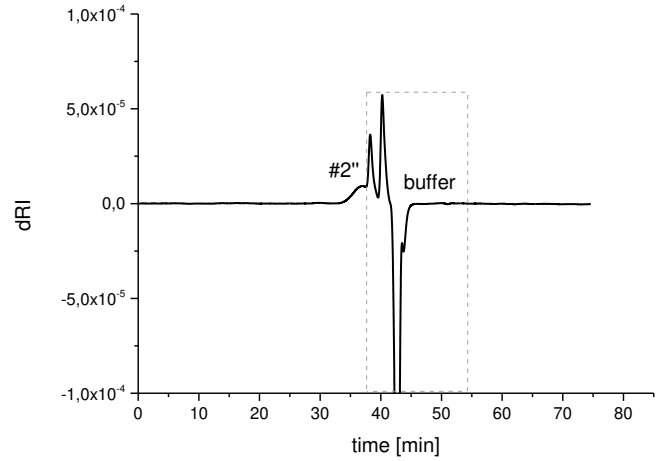

Figure S50. H_2O-SEC-MALS of **#2''** *(*hν intensity = 2.61 mW/cm², thiol:TPO 0.5:1).

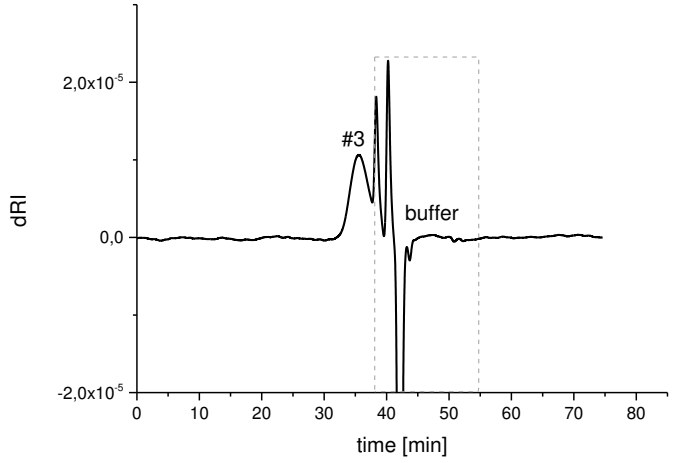

Figure S51. H_2O-SEC-MALS of **#3** *(*hν intensity = 26 mW/cm², thiol:TPO 1:1).

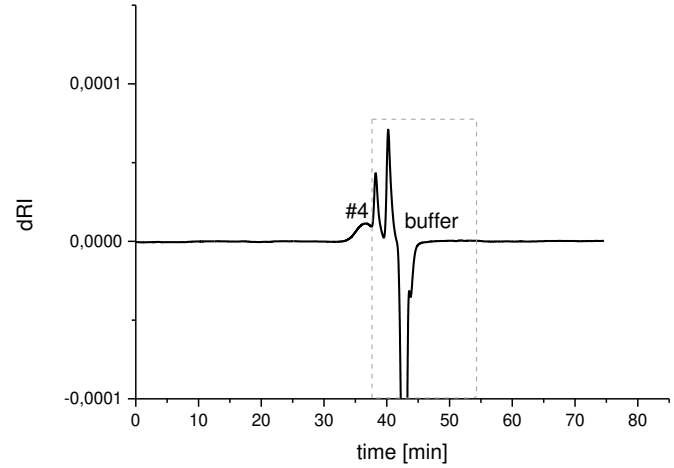

Figure S52. H_2O-SEC-MALS of **#4** *(*hν intensity = 45.2 mW/cm², thiol:TPO 1:1).

2.5.2 Variation of monomers at different hν intensities

Standard TIRP protocol (Chapter 2.1) was used to polymerize (meth)acrylate monomers. The resulting polymers were analyzed via THF-SEC and showed, that by decreasing hν intensity controlled features could be generated for methacrylate monomers. Acrylate monomers showed free radical polymerization characteristics, indicating that the irradiation intensity has to be decreased under the limit of our system to regain CRP characteristics.

Table S8. Different monomers used in TIRP while varying hν intensity.

#	monomer	hν intensity	$M_{n\ theory}$	$P_{n\ theory}$	M_n (THF-SEC)	P_n	Đ
1	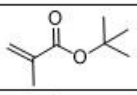	5%	14.2 kDa	100	10.2	72	1.8
2	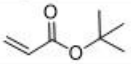	5%	2.6 kDa	20	3.7 kDa	28	1.6
3	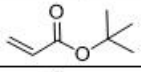	5%	12.8 kDa	100	10.8 kDa	85	1.9
4	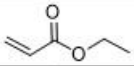	5%	2 kDa	20	5.5 kDa	55	1.4
5	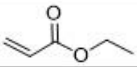	5%	10 kDa	100	10.7 kDa	106	1.6
6	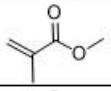	5%	2 kDa	20	2.8 kDa	25	1.4
7	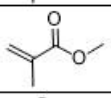	5%	10 kDa	100	9 kDa	90	1.6
8	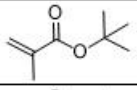	2%	14.2 kDa	100	14.6 kDa	103	1.3
9	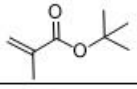	2%	2.8 kDa	20	2.7 kDa	18	1.3
10	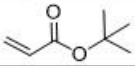	2%	2.6 kDa	20	5.3 kDa	40	1.6
11	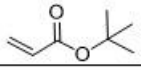	2%	12.8 kDa	100	10.4 kDa	81	2.4

*M_n determined from signals from the RI detector.

2.5.2.1 Analytics

THF-SEC measurements (for #8 and #9, see chapter 2.1.1)

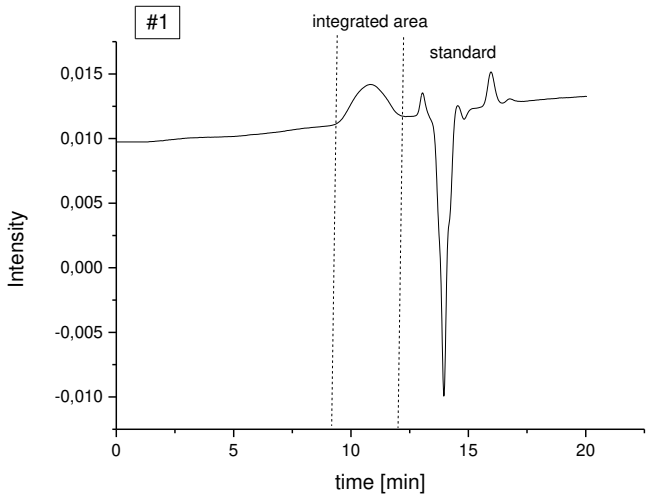

Figure S53. THF-SEC (RI detector) of PTBMA #1 (Table S7).

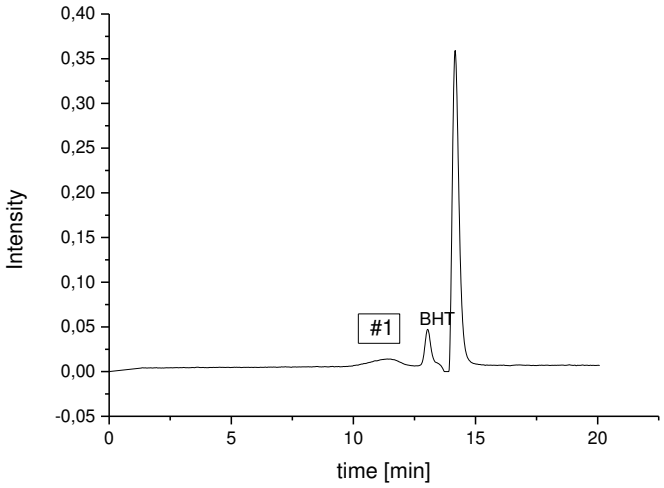

Figure S54. THF-SEC (UV detector) of PTBMA #1 (Table S7).

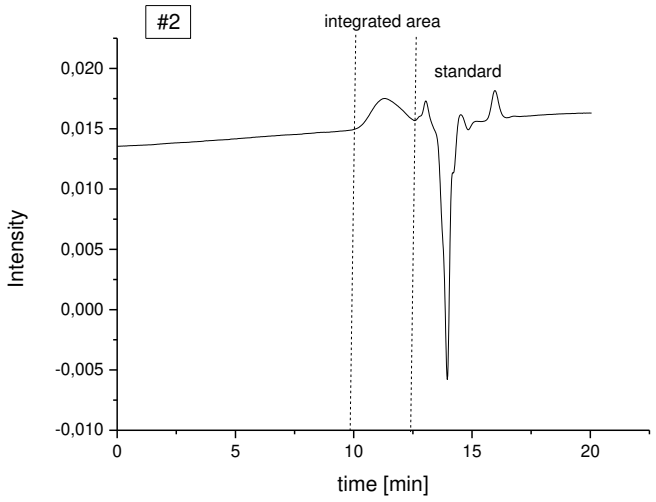

Figure S55. THF-SEC (RI detector) of poly(*tert*-butyl acrylate) (PTBA) #2 (Table S7).

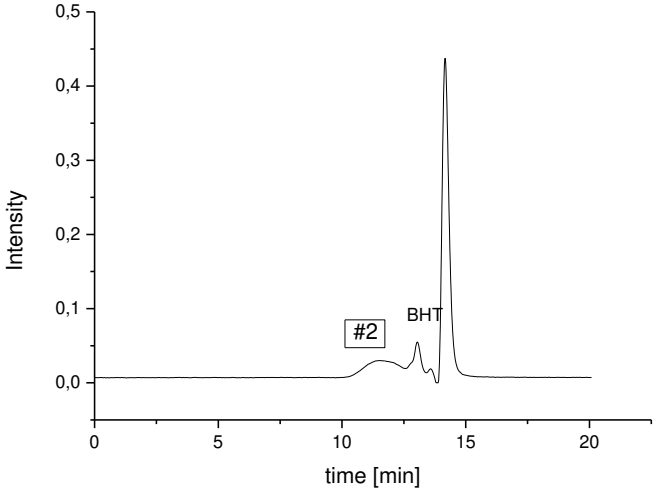

Figure S56. THF-SEC (UV detector) of poly(*tert*-butyl acrylate) (PTBA) #2 (Table S7).

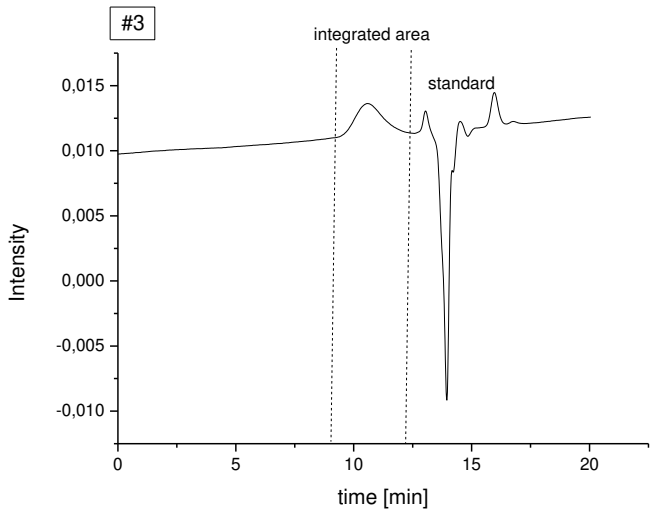

Figure S57. THF-SEC (RI detector) of PTBA #3 (Table S7).

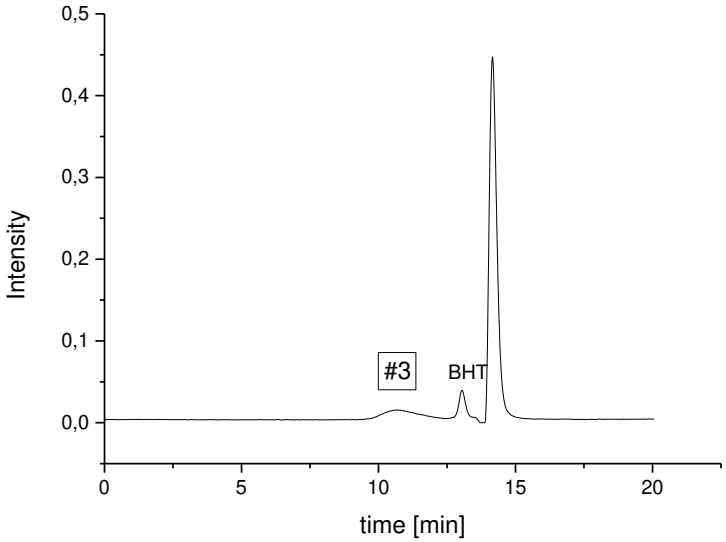

Figure S58. THF-SEC (UV detector) of PTBA #3 (Table S7).

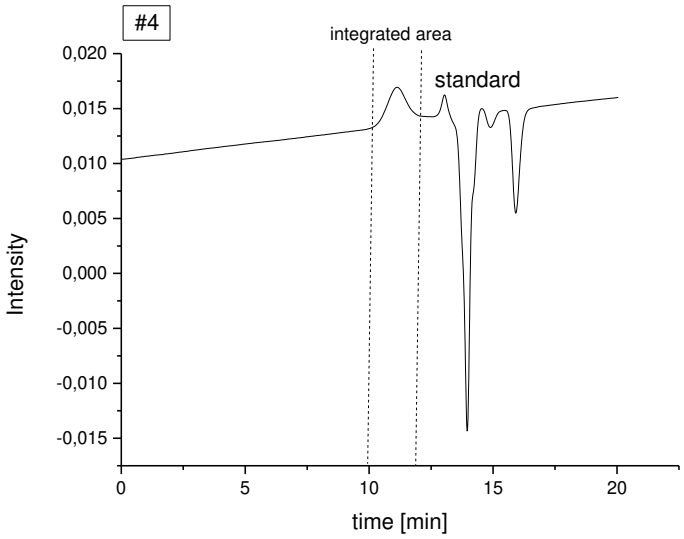

Figure S59. THF-SEC (RI detector) of PEA #4 (Table S7).

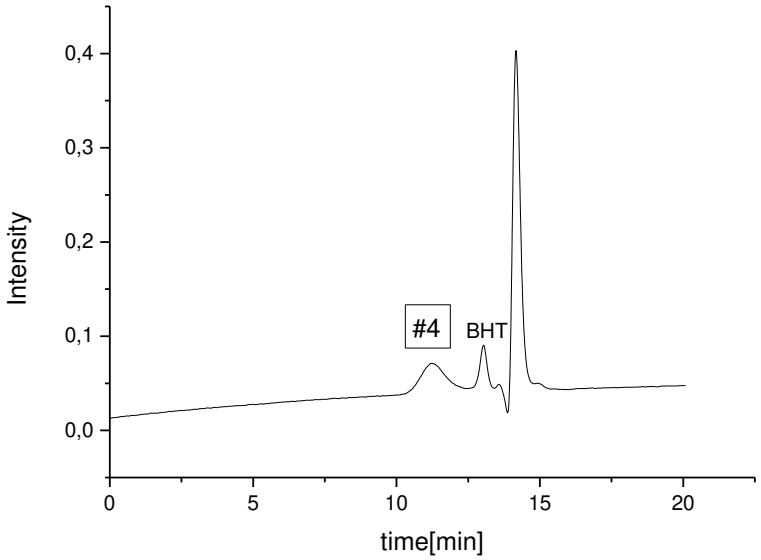

Figure S60. THF-SEC (UV detector) of PEA #4 (Table S7).

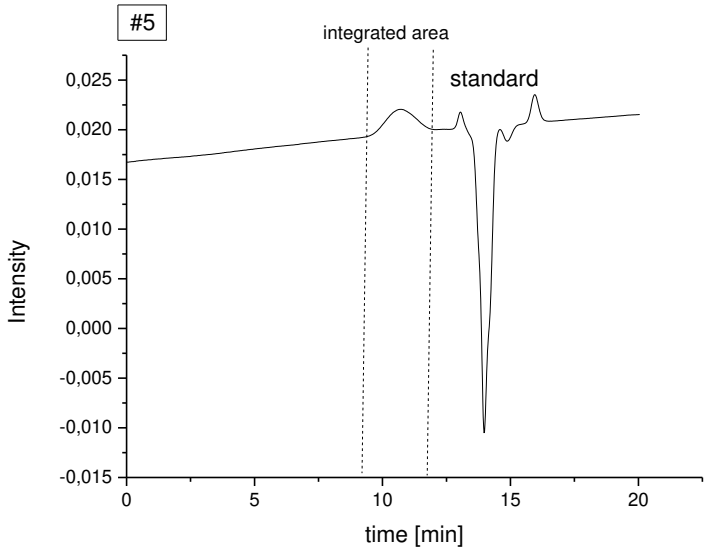

Figure S61. THF-SEC (RI detector) of PEA #5 (Table S7).

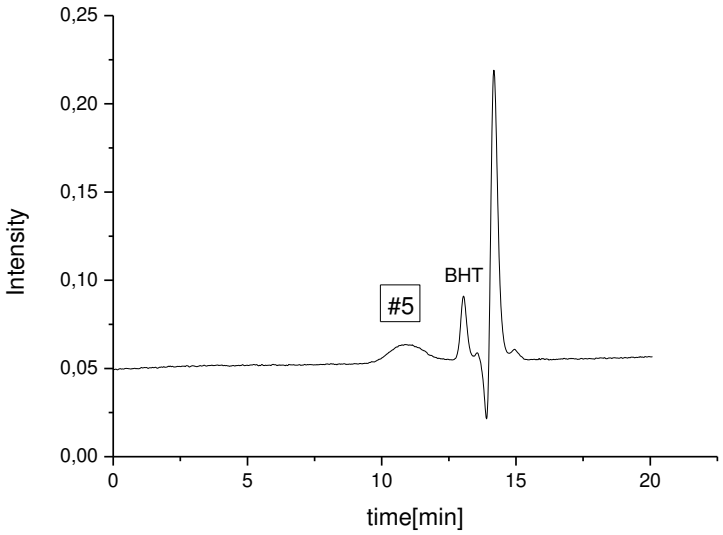

Figure S62. THF-SEC (UV detector) of PEA #5 (Table S7).

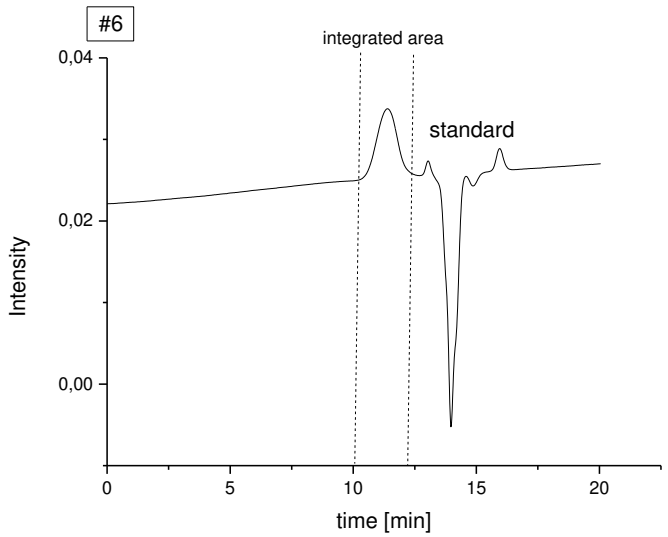

Figure S63. THF-SEC (RI detector) of poly(methyl methacrylate) (PMMA) #6 (Table S7).

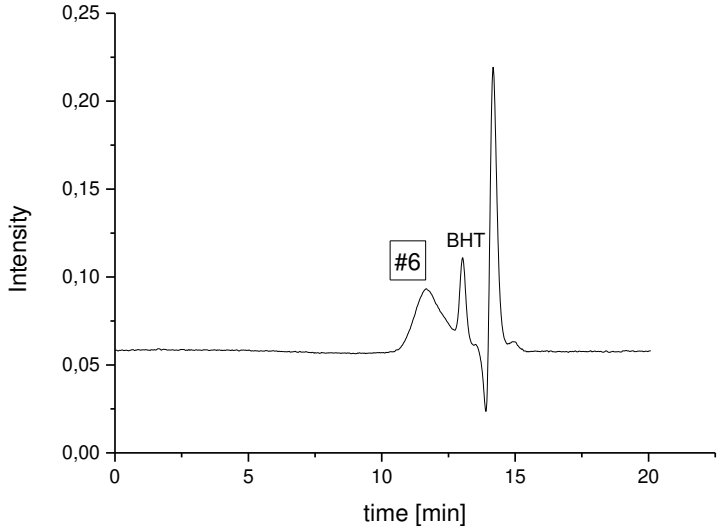

Figure S64. THF-SEC (UV detector) of poly(methyl methacrylate) (PMMA) #6 (Table S7).

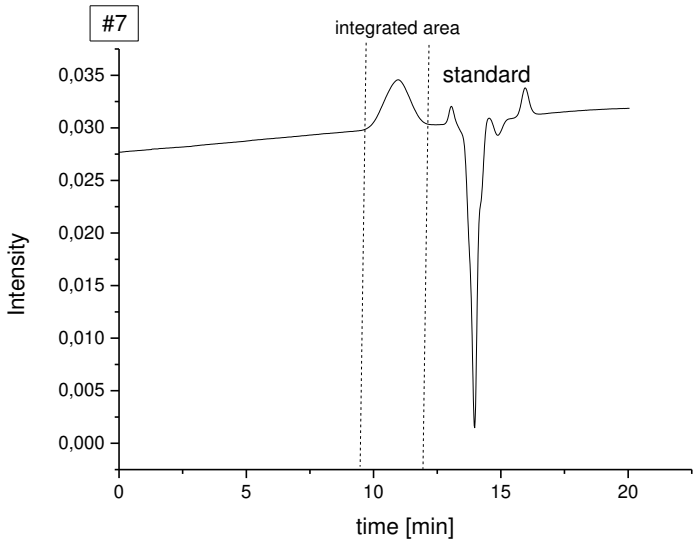

Figure S65. THF-SEC (RI detector) of PMMA #7 (Table S7).

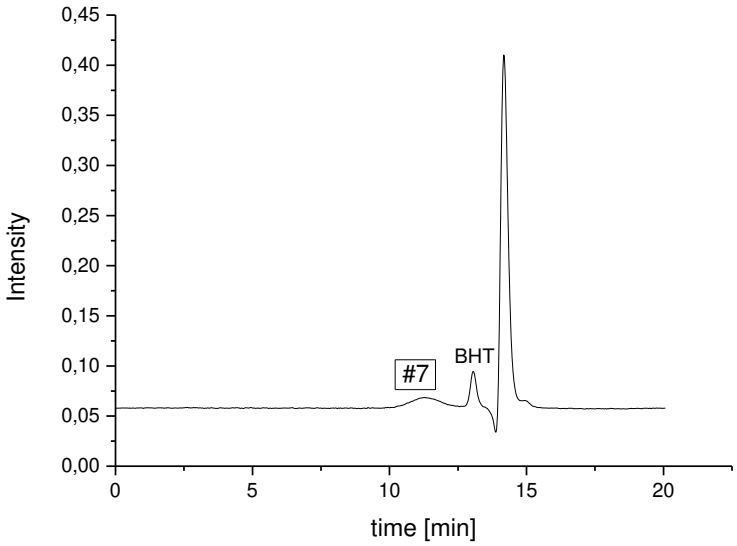

Figure S66. THF-SEC (UV detector) of PMMA #7 (Table S7).

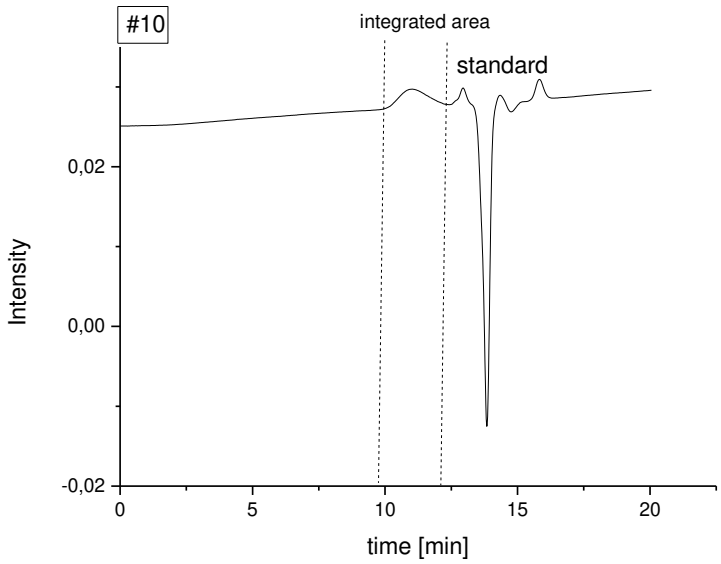

Figure S67. THF-SEC (RI detector) of PTBA #10 (Table S7).

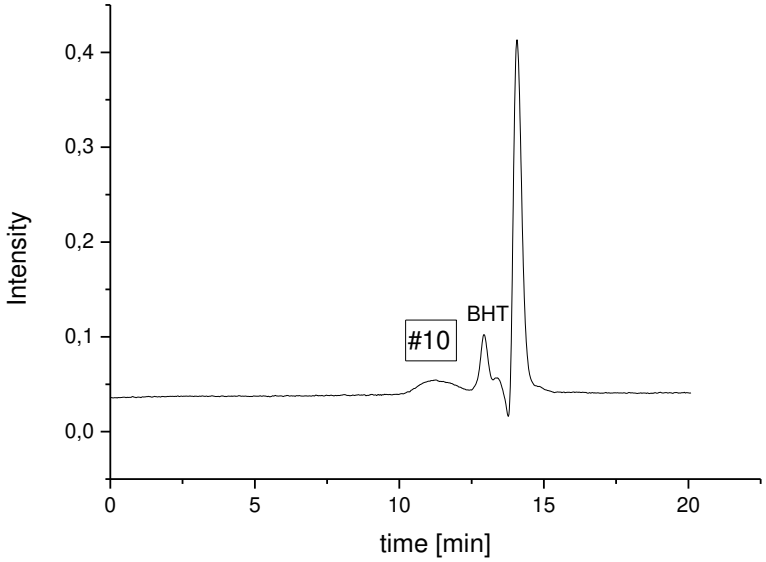

Figure S68. THF-SEC (UV detector) of PTBA #10 (Table S7).

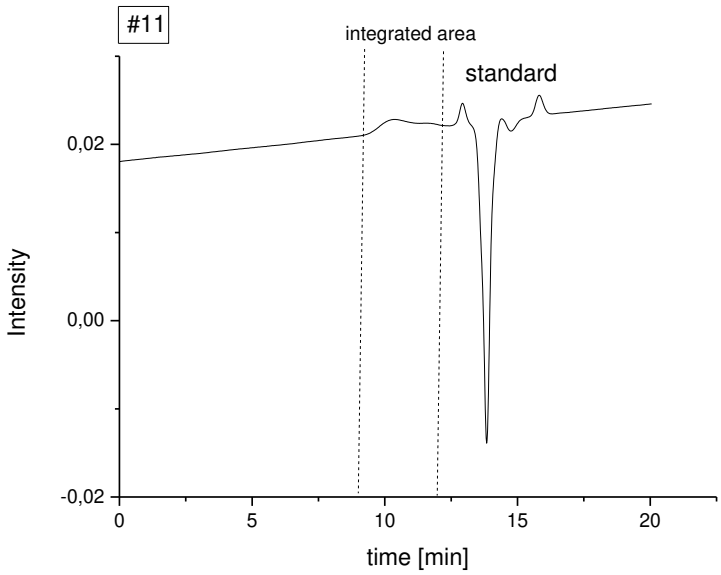

Figure S69. THF-SEC (RI detector) of PTBA #11 (Table S7).

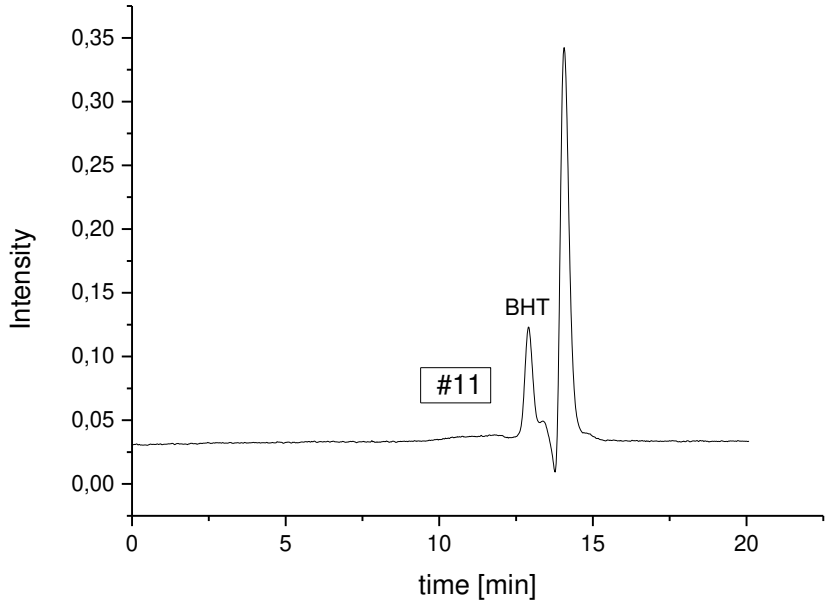

Figure S70. THF-SEC (UV detector) of PTBA #11 (Table S7).

2.6 Varying the irradiation time

Scheme S12. Polymerization parameters used while varying the irradiation time (HEAA = 1 eq., tritylthiol = 5 mol%, TPO = 5 mol%, $Ir(ppy)_3$ = 0.05 mol%; DMF = 10 wt.%; hν = 60 min, 405 nm, 2.61 mW/cm²).

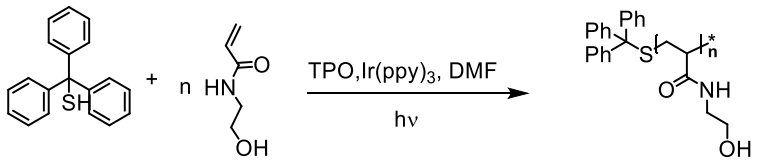

The general TIRP polymerization protocol (chapter 2) was carried out to determine the irradiation time needed to obtain the molecular weights desired in good yields. Therefore the optimized parameters (1 eq. HEAA monomer, thiol:TPO 1:1 (5 eq.), $Ir(ppy)_3$ concentration of 0.05 mol%, 2.61 mW/cm^2) were used in five separate reactions while varying the irradiation time and the average molecular weights as well as the yields at each time were determined.

Table S9. Obtained yields, average molecular weights and dispersities after purification (MWCO 1000 Da) of the polymers for different irradiation times (**#1** - **#5**). Theoretical molecular weight: 2.7 kDa.

#	Irradiation time [min]	Yield [%]	$\overline{M}_n$ [kDa] via SEC	Đ via SEC
1	15	37	2.2	1.08
2	30	42	2.24	1.03
3	45	54	2.1	1.09
4	60	85	2.7	1.06
5	90	88	2.5	1.05

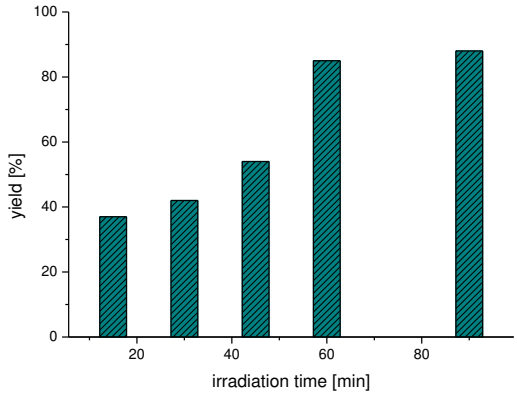

Figure S71. Obtained yields of polymerizations quenched at different reaction times (**#1** - **#5).**

2.6.1 Analytics

<u>H_2O-SEC-MALS:</u>

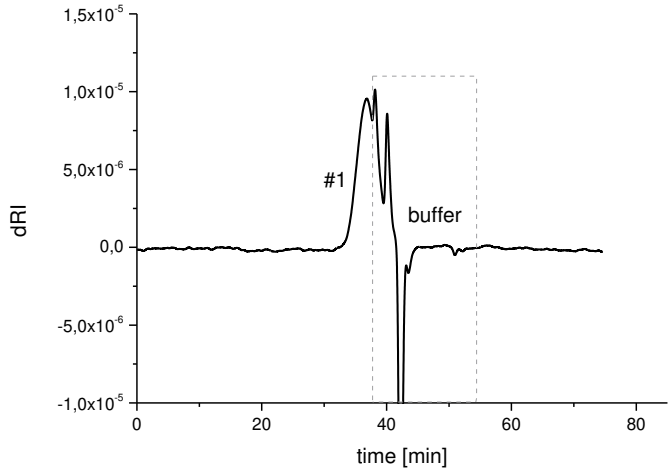

Figure S72. H_2O-SEC-MALS of **#1** (15 min irradiation time).

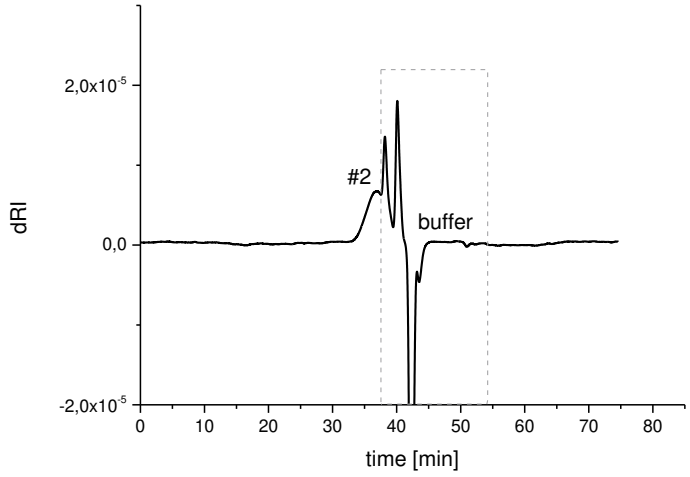

Figure S73. H_2O-SEC-MALS of **#2** (30 min irradiation time).

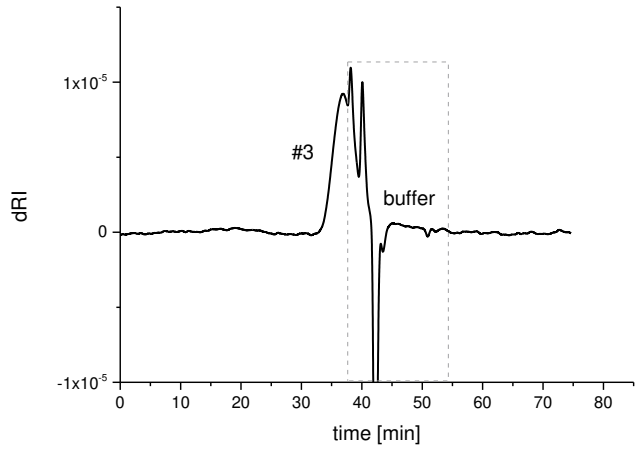

Figure S74. H_2O-SEC-MALS of **#3** (45 min irradiation time).

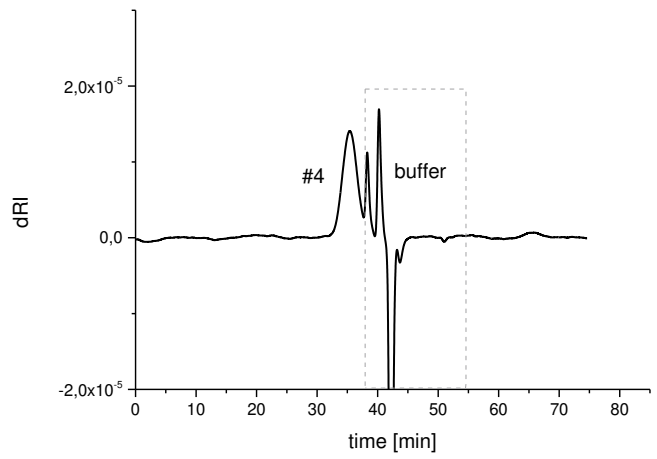

Figure S75. H_2O-SEC-MALS of **#4** (60 min irradiation time).

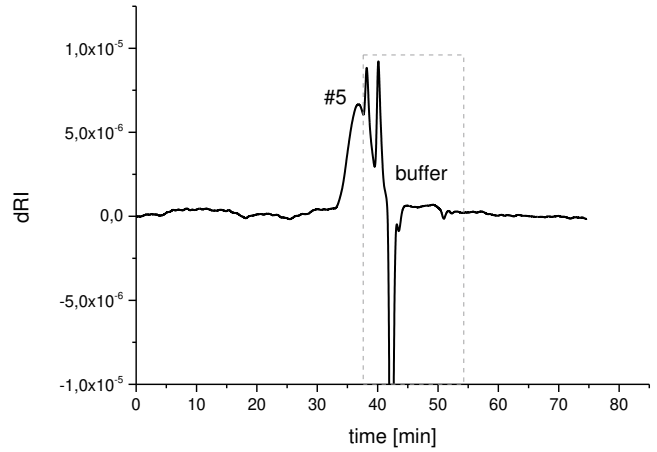

Figure S76. H_2O-SEC-MALS of **#5** (90 min irradiation time).

2.7 Figure 5: SI for varying the thiol source

Scheme S13. Polymerization parameters used while varying the thiol source (HEAA = 1 eq., $Ir(ppy)_3$ = 0.05 mol%; DMF = 10 wt.%; hν = 60 min, 405 nm).

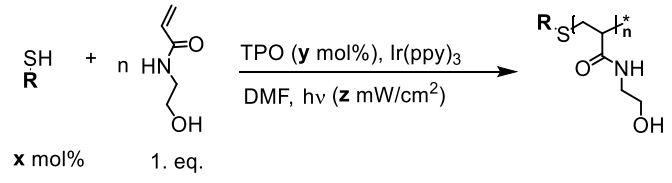

$\mathbf{R_{1\text{-}5}}$ = 1) phenyl-; 2) benzyl-; 3) 3-nitro-benzyl-; 4) *tert*-butyl-: 5) 2-(trimethylsilyl)ethane-

1 eq. of HEAA (*N*-hydroxyethylacrylamide) monomer (100 mol%) and $Ir(ppy)_3$ (0.05 mol%) were dissolved in DMF [10 wt.%] sealed in a 5 mL glass flask and flushed with argon gas for 10 minutes. In a second step, the thiolsource (**TS**) (**x** mol%) and equimolar amounts of TPO (**y**=**x** mol%) were also dissolved in DMF [10 wt.%] and sealed in a 5 mL microwave reaction vial. A spatula tip of TCEP were dissolved in a single drop of H_2O and added

to the reaction solution to reduce possible disulfides. The thiol/TPO solution was flushed under Ar-atmosphere for 10 minutes and irradiated with UV-light (405 nm wavelength, with an intensity of **z** mW/cm² for 3 minutes. Subsequently, the monomer/$Ir(ppy)_3$ mixture was added to the TPO/thiol solution under an inert atmosphere and the polymerization solution was irradiated further at unchanged light intensity. After an hour, the irradiation was stopped and the polymer solution was precipitated in diethyl ether. The precipitated polymer was dissolved in H_2O, dialyzed against distilled water (three cycles, 1000 Da) and subsequently lyophilized.

Table S10. Different thiol sources and parameters used and the resulting average molecular weights and dispersities (**#1** - **#5'**).

#	Thiol Source (TS)	Thiol conc. [mol%]	Irradiation intensity [mW/cm²]	Mn [kDa] theoretical	$\overline{M}_n$ [kDa] via SEC	Đ via SEC
1	thiophenol	1	2.61	11.6	no polymer	no polymer
1'	thiophenol	1	19.78	11.6	45	1.15
2	benzyl mercaptane	1	2.61	11.7	39	1.12
2'	benzyl mercaptane	5	1.15	2.4	3.4	3.46
3	3-nitro-benzyl mercaptan	1	1.15	11.7	19	1.24
4	*tert*-butylthiol	1	1.15	11.6	20	2.02
5	TMS-thiol	5	1.15	2.4	3.1	2.38
5'	TMS-thiol	5	2.61	2.4	2.7	4.67

2.7.1. Analytics

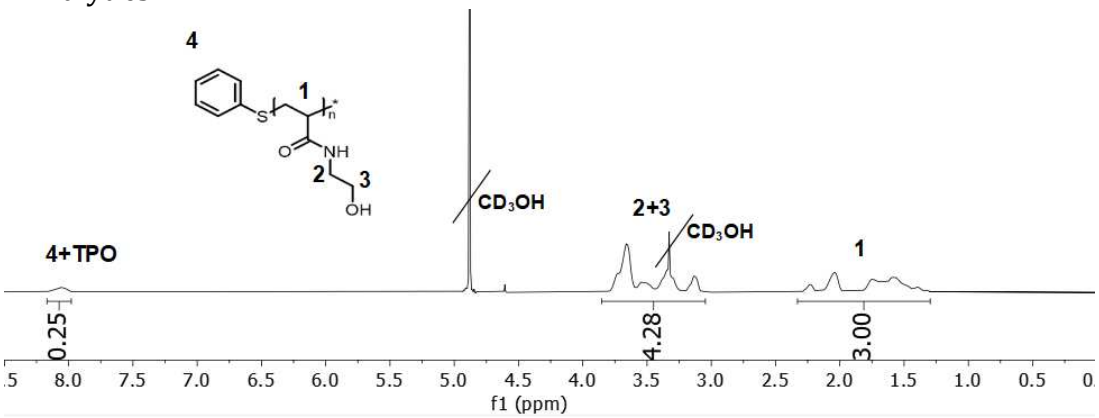

Figure S77. ^1H NMR (600 MHz, CD_3OD) of polymer **#1'** (thiol source = thiophenol (1 mol%)).

^{1}H NMR (600 MHz, CD_3OD) δ [ppm] 8.13-7.95 (m, **4, TPO** overlapping), 3.84-3.02 (m, **2+3**, **CD_3OD** overlapping), 2.32-1.28(m, **1**).

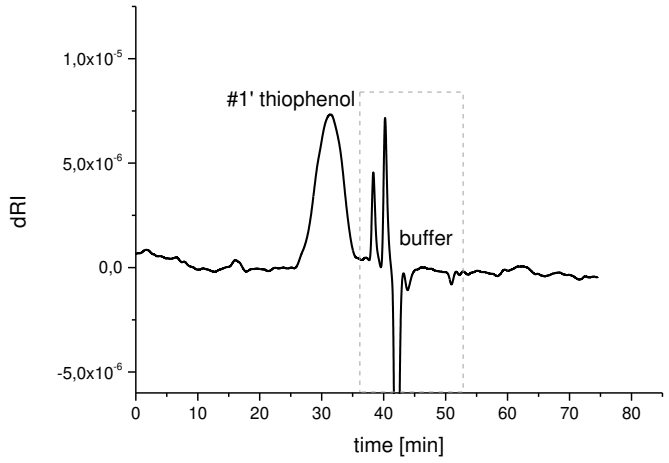

Figure S78. H_2O-SEC-MALS of polymer **#1'** (thiol source = thiophenol (1 mol%)).

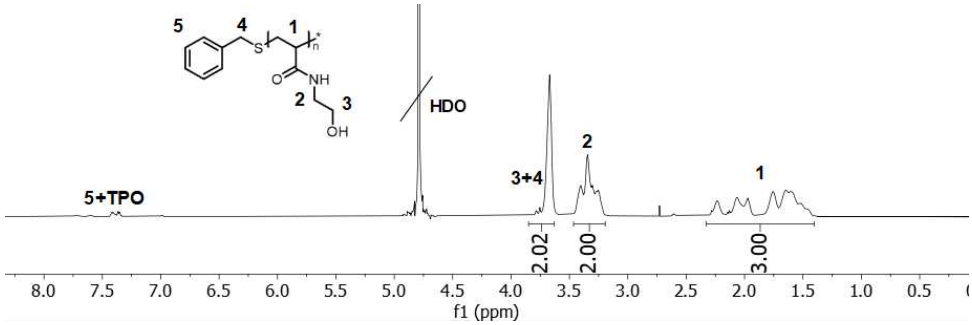

Figure S79. ^{1}H NMR (600 MHz, D_2O) of polymer **#2** (thiol source = benzyl mercaptane (1 mol%)).

^{1}H NMR (600 MHz, D_2O) δ [ppm] 7.59-7.33 (m, **5, TPO** overlapping), 3.83-3.63 (m, **3+4)**, 3.45-3.18 (m, **2)**, 2.32-1.40(m, **1**).

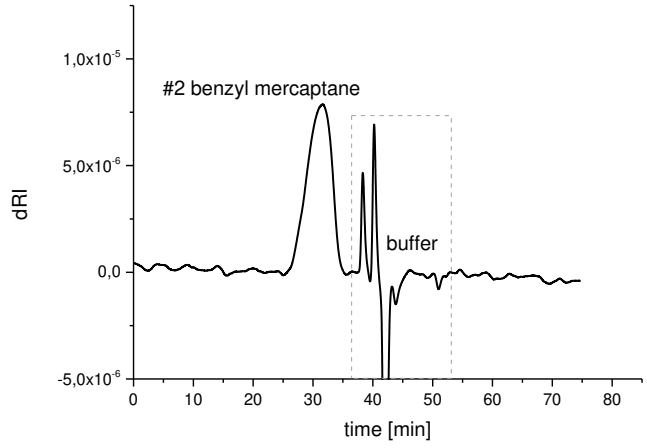

Figure S80. H_2O-SEC-MALS of polymer **#2** (thiol source = benzyl mercaptane (1 mol%)).

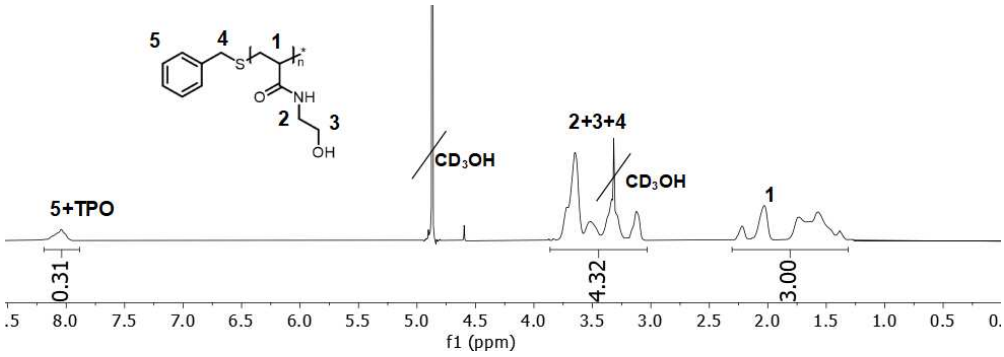

Figure S81. ^{1}H NMR (600 MHz, CD_3OD) of polymer **#2'** (thiol source = benzyl mercaptane (5 mol%)).

^{1}H NMR (600 MHz, CD_3OD) δ [ppm] 8.16-7.95 (m, **5, TPO** overlapping), 3.86-3.01 (m, **2+3+4**, **CD_3OD** overlapping), 2.29-1.30(m, **1**).

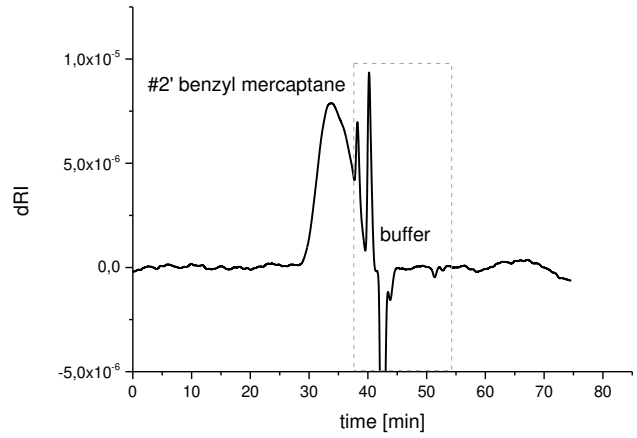

Figure S82. H_2O-SEC-MALS of polymer **#2'** (thiol source = benzyl mercaptane (5 mol%)).

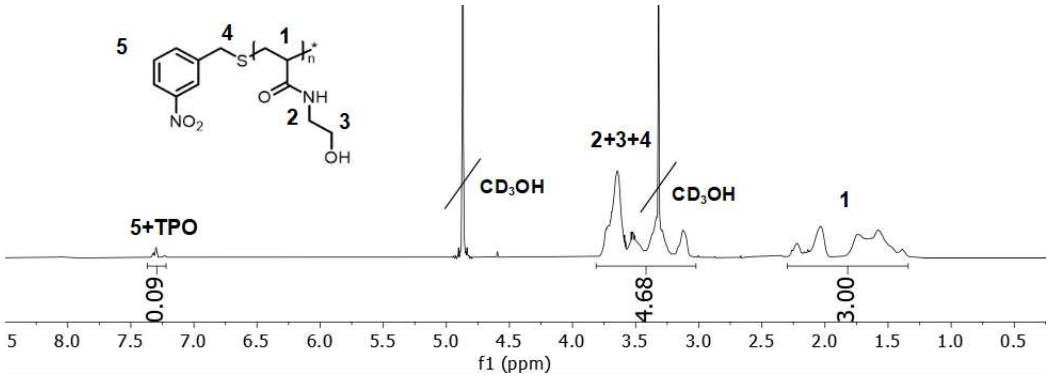

Figure S83. ^{1}H NMR (600 MHz, CD_3OD) of polymer **#3** (thiol source = 3-nitro-benzyl mercaptane (1 mol%)).

^{1}H NMR (600 MHz, CD_3OD) δ [ppm] 7.50-7.17 (m, **5, TPO** overlapping), 3.80-3.01 (m, **2+3+4**, **CD_3OD** overlapping), 2.29-1.32(m, **1**).

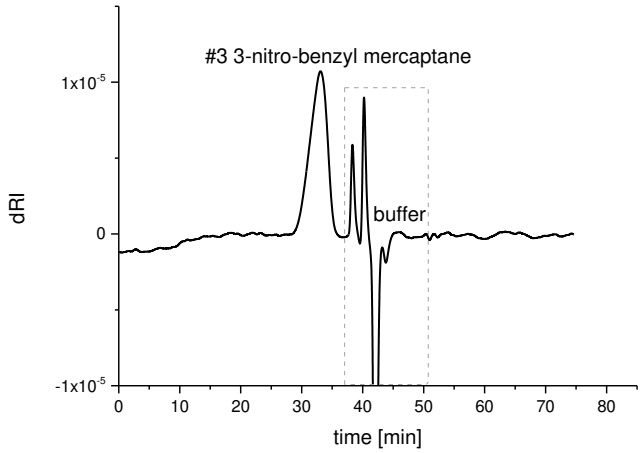

Figure S84. H_2O-SEC-MALS of polymer **#3** (thiol source = 3-nitro-benzyl mercaptane (1 mol%)).

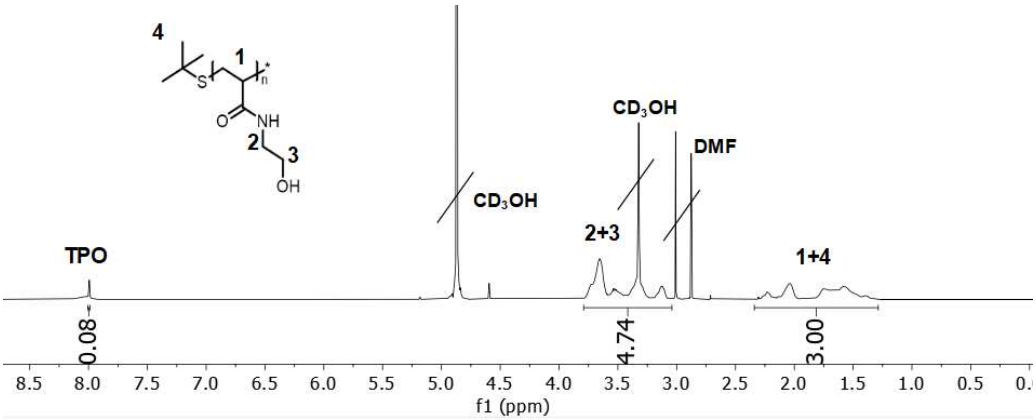

Figure S85. ^1H NMR (600 MHz, CD_3OD) of polymer **#4** (thiol source = *tert*-butyl thiol (1 mol%)).

^1H NMR (600 MHz, CD_3OD) δ [ppm] 8.05-7.95 (m, **5, TPO** overlapping), 3.77-3.04 (m, **2+3**, **CD_3OD** overlapping), 2.35-1.30(m, **1+4**).

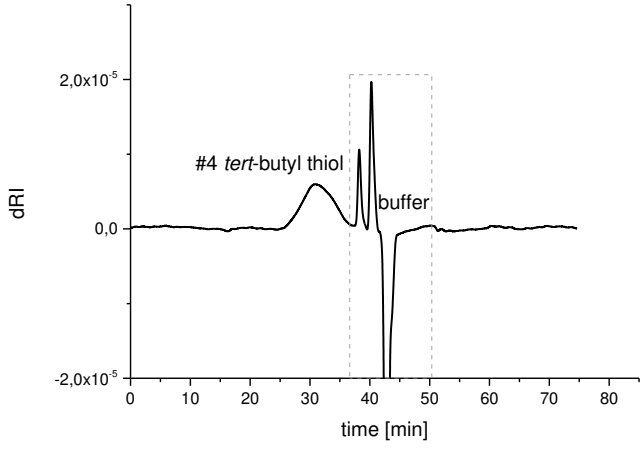

Figure S86. H_2O-SEC-MALS of polymer **#4** (thiol source = *tert*-butyl thiol (1 mol%)).

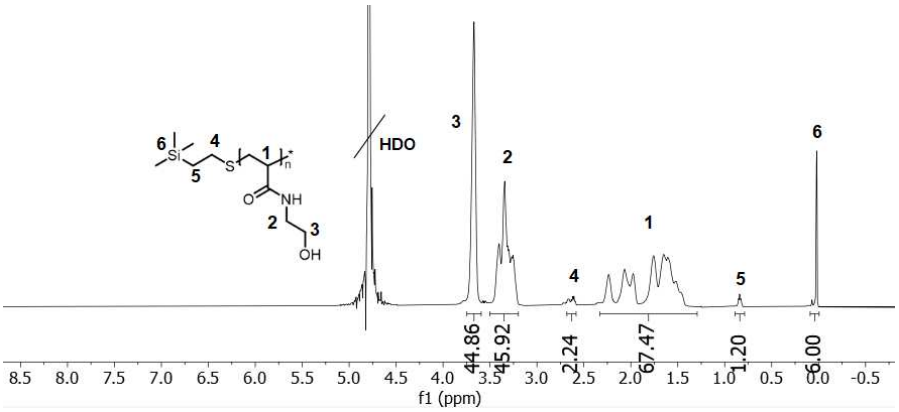

Figure S87. ^{1}H NMR (600 MHz, D_2O) of polymer **#4** (thiol source = TMS-thiol (1.15 mW/cm^2)).

^{1}H NMR (600 MHz, D_2O) δ [ppm] 3.79-3.59 (m, **3**), 3.47-3.19 (m, **2**), 2.71-2.57 (m, **4**), 2.34-1.39(m, **1**), 0.88-0.79 (m, **5**), 0.02 (s, **6**).

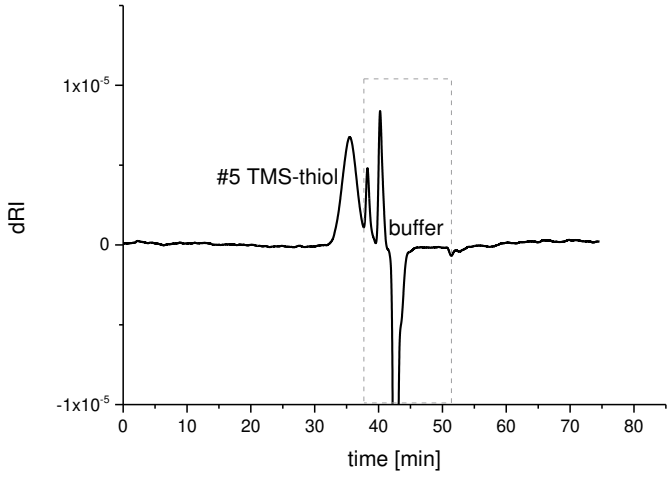

Figure S88. H_2O-SEC-MALS of polymer **#4** (thiol source = TMS-thiol (1.15 mW/cm^2)).

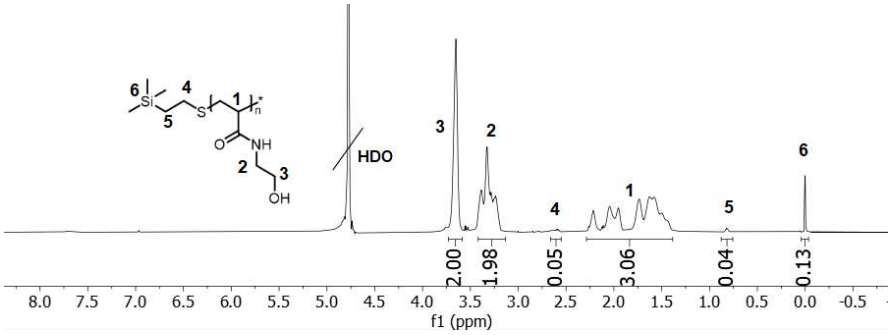

Figure S89. ^{1}H NMR (600 MHz, D_2O) of polymer **#4** (thiol source = TMS-thiol (2.61 mW/cm^2)).

^{1}H NMR (600 MHz, D_2O) δ [ppm] 3.79-3.59 (m, **3**), 3.47-3.19 (m, **2**), 2.71-2.57 (m, **4**), 2.34-1.39(m, **1**), 0.88-0.79 (m, **5**), 0.02 (s, **6**).

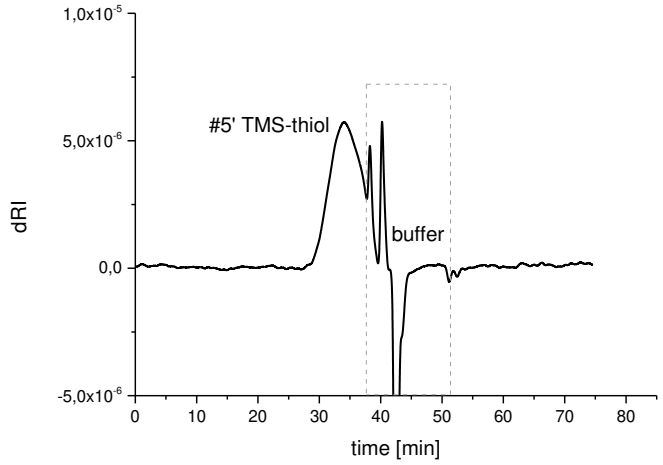

Figure S90. H_2O-SEC-MALS of polymer **#4** (thiol source = TMS-thiol (2.61 mW/cm^2)).

2.7.2. Deriving data shown in Figure 4 (C) and (D): SI for reaction kinetics of TMS-thiol

1 eq. of HEAA monomer (100 mol%, 200 mg) and $Ir(ppy)_3$ (0.05 mol%) were dissolved in DCM/MeOH 1:1 (*v*/*v*), [10 wt.%] (not DMF because of higher vapour pressure of DCM and MeOH) sealed in a 5 mL glass flask and flushed with argon gas for 10 minutes. In a second step, TMS-thiol (5 mol%) and equimolar amounts of TPO (5 mol%) were also dissolved in DCM/MeOH 1:1 (*v*/*v*), [10 wt.%] and sealed in a 5 mL microwave reaction vial. A spatula tip of TCEP was dissolved in a single drop of H_2O and added to the reaction solution to reduce possible disulfides. The thiol/TPO solution was flushed under Ar-atmosphere for 10 minutes. After the monomer/$Ir(ppy)_3$ mixture was added to the vial the solution was irradiated with UV-light (405 nm wavelength, with an intensity of **A**= 2.61 mW/cm^2 (5%), 60 min and **B** = <1.15 mW/cm^2 (<2%), 30 min. Samples (0.3 mL) were taken from the reaction solution at defined times and precipitated in diethyl ether. After the solvents were evaporated the monomer conversion was determined via ^{1}H NMR-spectroscopy to show the linear dependence of reaction time to conversion. Also $\ln([M]_0/[M]_t)$ against reaction time is plotted. With a linear relationship characteristics of a living polymerization can be shown. For calculation see chapter 2.1.2.

Scheme S14. Reaction parameters for TMS-thiol initiated polymerization with free radical polymerization characteristics (**Figure 4 (C)**, 2.61 mW/cm^2) and controlled polymerization characteristics (**Figure 4 (D)**, 1.15 mW/cm^2), (HEAA = 1 eq., TMS-thiol = 5 mol%, TPO = 5 mol%, $Ir(ppy)_3$ = 0.05 mol%; DCM/MeOH 1:1 (*v*/*v*) = 10 wt.%; hν = 60 min, 405 nm, 2.61 mW/cm^2).

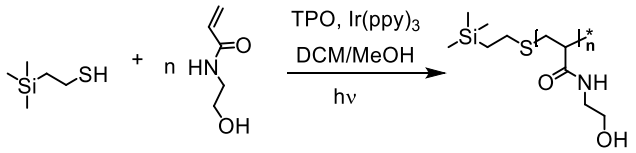

Table S11. **4(C)**: Monomer conversion at defined reaction times and calculation of $\ln([M]_0/[M]_t)$, $[M]_0$ = initial monomer concentration, $[M]_t$ = monomer concentration at reaction time t [min].

#	reaction time [min]	monomer conversion [%]	$\frac{[M]0}{[M]t}$	$\ln(\frac{[M]0}{[M]t})$
0	0	0	1	0
1	1	7	1.075	0.072
2	3	27	1.37	0.315
3	5	31	1.45	0.371
4	7	40	1.66	0.5
5	10	60	2.5	0.916
6	15	88	8.33	2.12
7	20	89	9.09	2.207
8	30	90	10	2.3
9	45	91	11.11	2.408
10	60	91	11.11	2.408

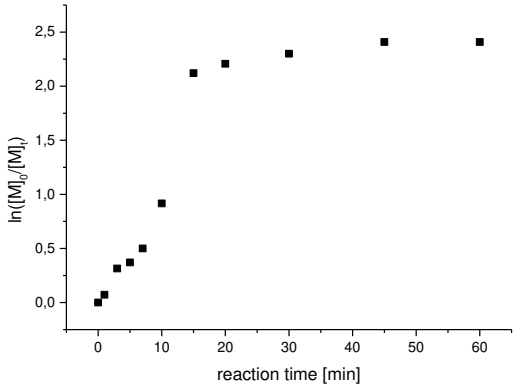

Figure S91. **A:** Plot of $\ln([M]_0/[M]_t)$ ($[M]_0$ = initial monomer concentration, $[M]_t$ = monomer concentration at reaction time t [min]) versus reaction time [min] (**#1** - **#10**).

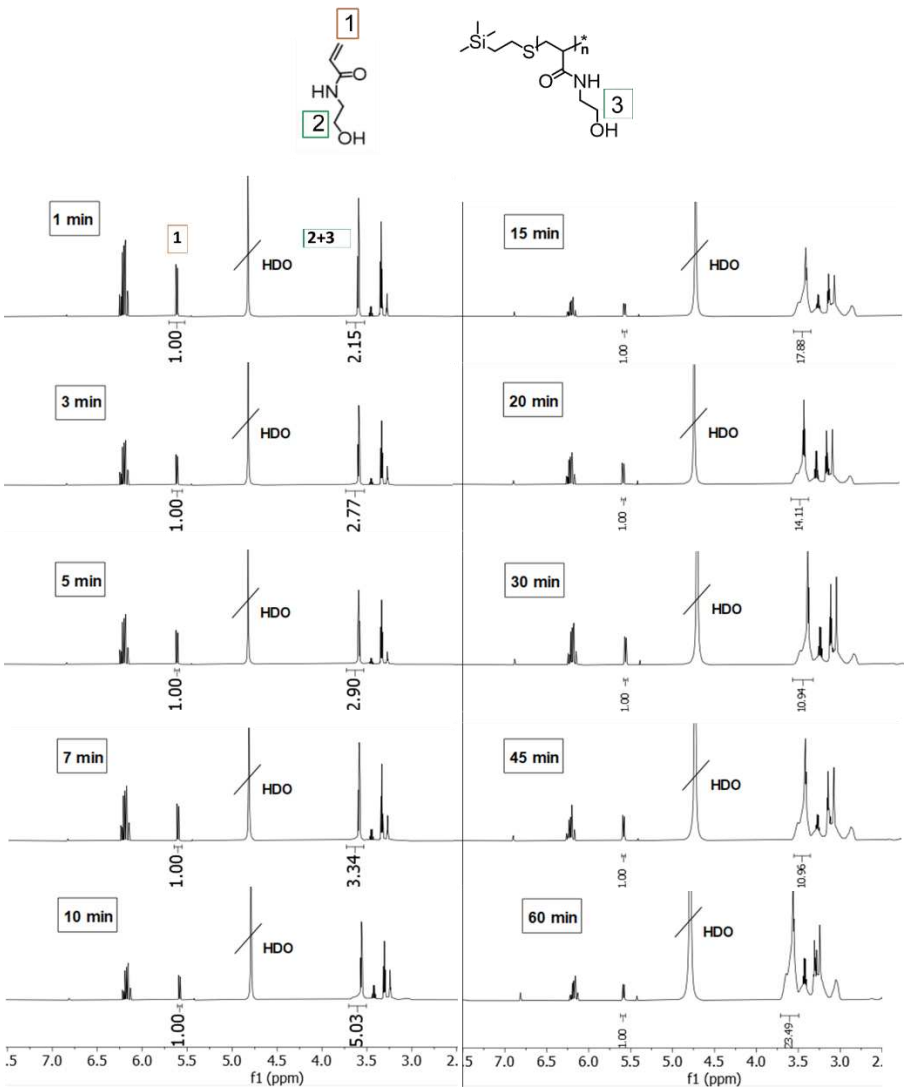

Figure S92. **4(C):** ^{1}H NMR-spectra (600 MHz, D_2O, RT) of monomer/polymer-mix (**#1** - **#10**) at different reaction times.

Table S12. **4(D)**: Monomer conversion at defined reaction times and calculation of $\ln([M]_0/[M]_t)$, $[M]_0$ = initial monomer concentration, $[M]_t$ = monomer concentration at reaction time t [min].

#	reaction time [min]	monomer conversion [%]	$\frac{[M]0}{[M]t}$	$\ln(\frac{[M]0}{[M]t})$
0	0	0	1	0
1	1	5	1.05	0.048
2	3	7	1.075	0.072
3	5	10	1.11	0.104
4	7	14	1.16	0.148
5	10	16	1.19	0.173
6	15	19	1.23	0.207

7	20	21	1.26	0.231
8	30	25	1.33	0.285

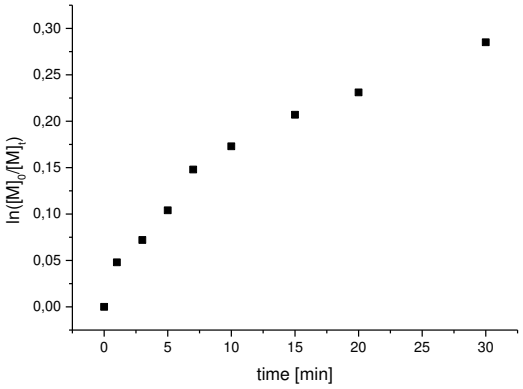

Figure S93. **B:** Plot of $\ln([M]_0/[M]_t)$ ($[M]_0$ = initial monomer concentration, $[M]_t$ = monomer concentration at reaction time t [min]) versus reaction time [min] (**#1** - **#8**).

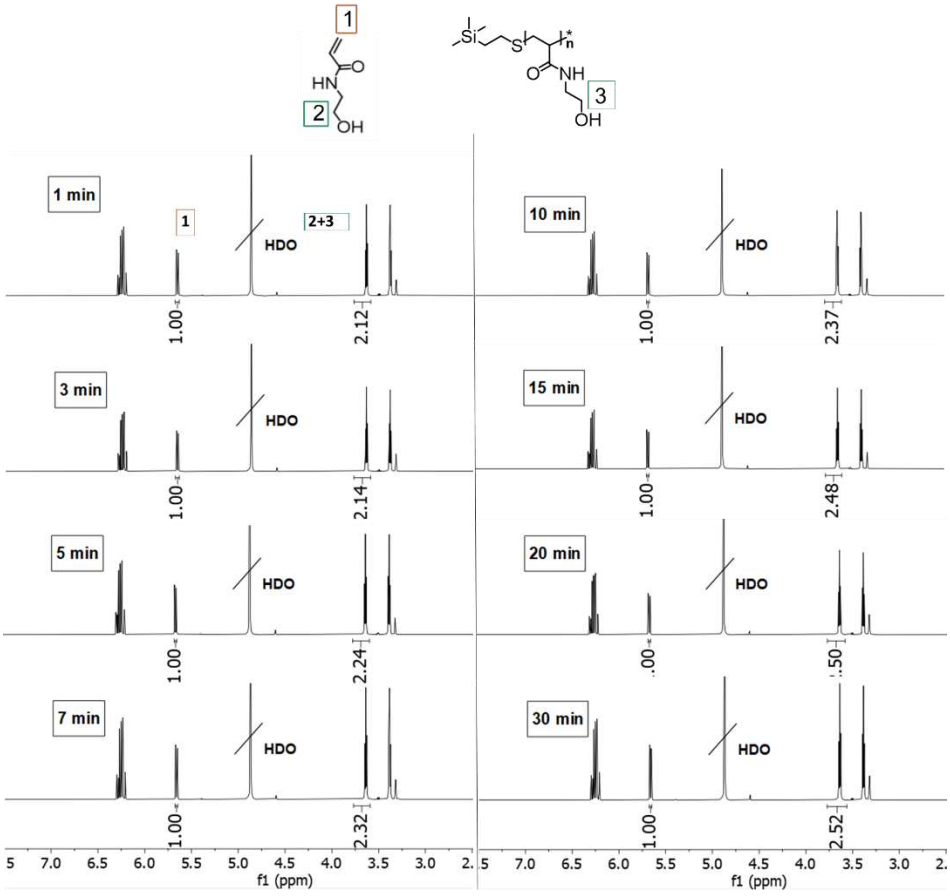

Figure S94. **4(D):** ^{1}H NMR-spectra (600 MHz, D_2O, RT) of monomer/polymer-mix (**#1** - **#8**) at different reaction times.

2.8 Endgroup analysis

Polymers which were synthesized under different conditions, either with optimized TIRP parameters (**#1**) or without (**#2**, **#3**), were analyzed via MALDI-ToF-MS to determine the endgroups obtained. ^{31}P NMR spectra were recorded of species 2, 2' and 2'' (Figure 6).

Scheme S15. Color code of possible endroups in TIRP with tritylthiol and TMS-thiol as thiol source.

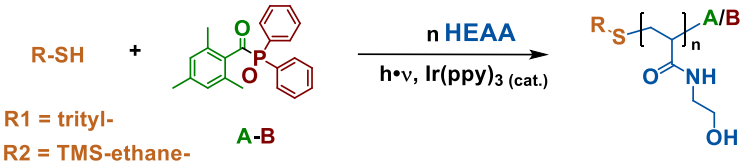

Table S13. Polymerization parameters of the synthesized polymers analyzed via MALDI-ToF-MS (**#1** - **#3**), (thiol = 5 mol%, $Ir(ppy)_3$ = 0.05 mol%)

#	R	thiol:TPO ratio	hν intensity [mW/cm^2]
1	R1	1:1	2.61
2	R1	0.5:1	2.61
3	R1	1:1	26
4	R2	1:1	1.16

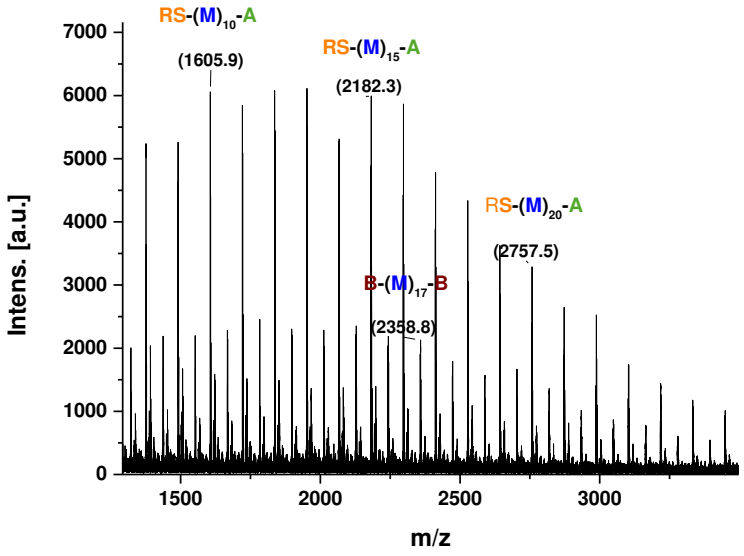

Figure S95. MALDI-ToF of **#1** (optimized TIRP).

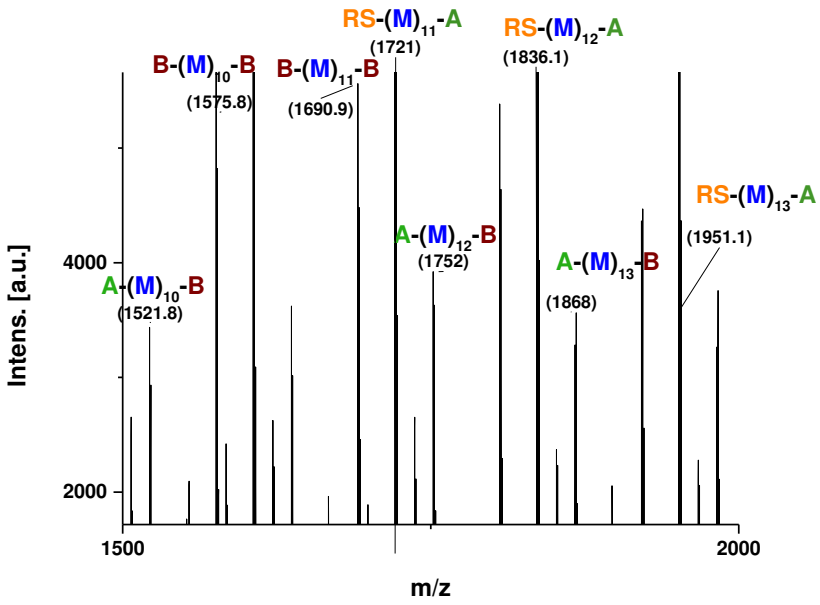

Figure S96. MALDI-ToF of **#2** (thiol:TPO ratio 0.5:1).

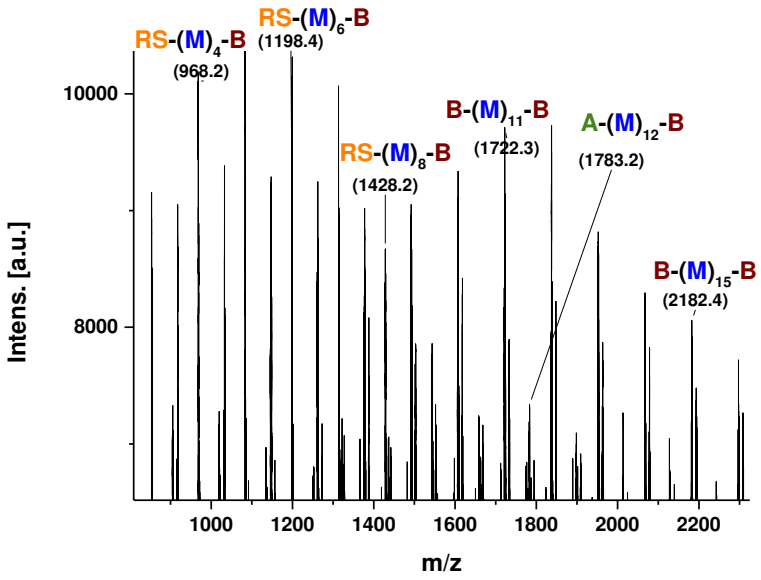

Figure S97. MALDI-ToF of **#3** (irradiation intensity 26 mW/cm^2).

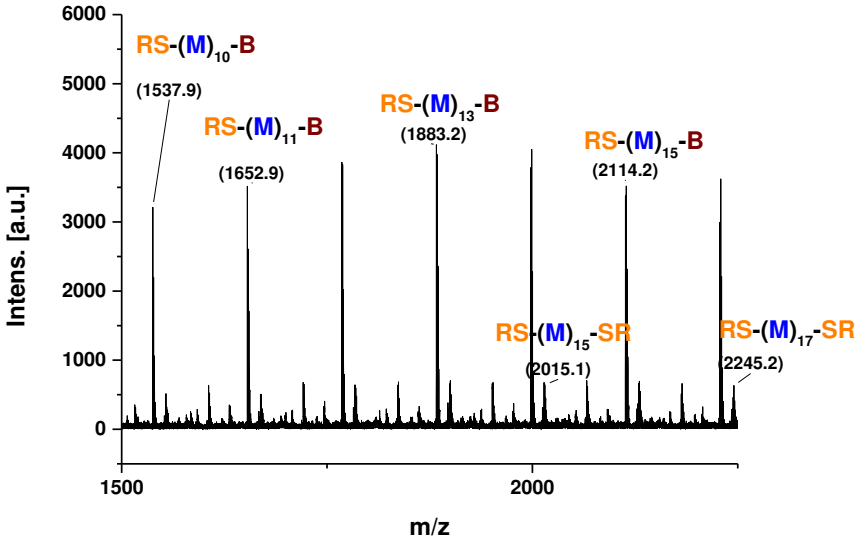

Figure S98. MALDI-ToF of **#4** (TMS-thiol).

2.9 Figure 6: Supporting RP-HPLC-MS and Maldi-ToF spectra

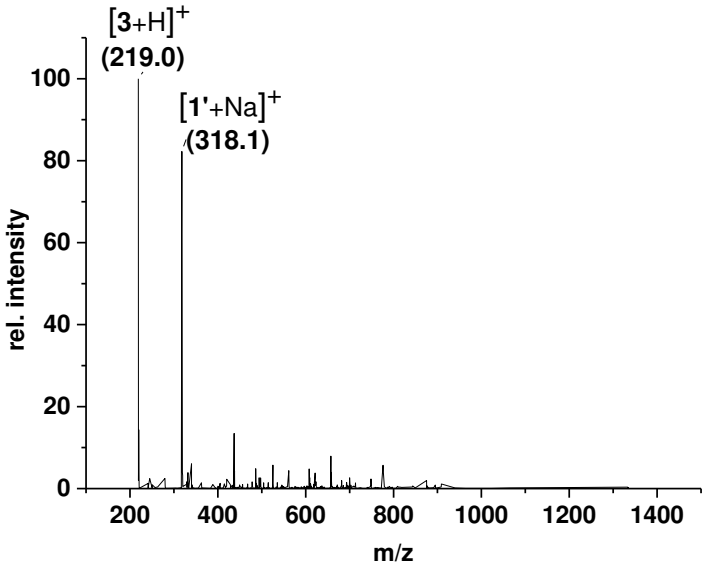

Figure S99. RP-HPLC-MS measurement: signal of intermediates **1'** and **3** (t_r = 16.02 min).

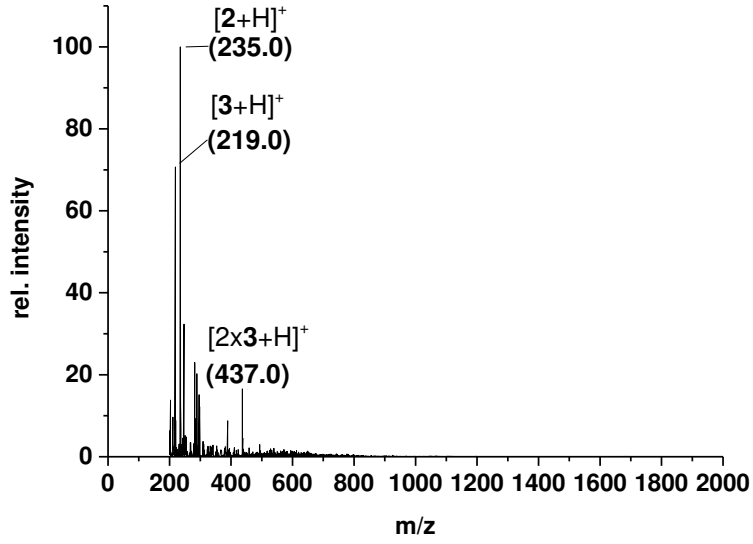

Figure S100. RP-HPLC-MS measurement intermediates **1** and **2** (t_r = 14.78 min – 16,45 min).

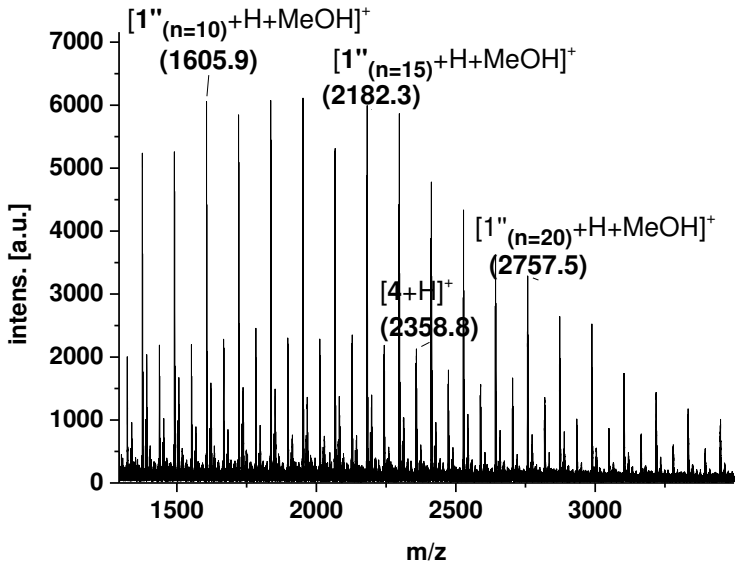

Figure S101. MALDI-ToF spectrum of a polymerization performed under optimized conditions.

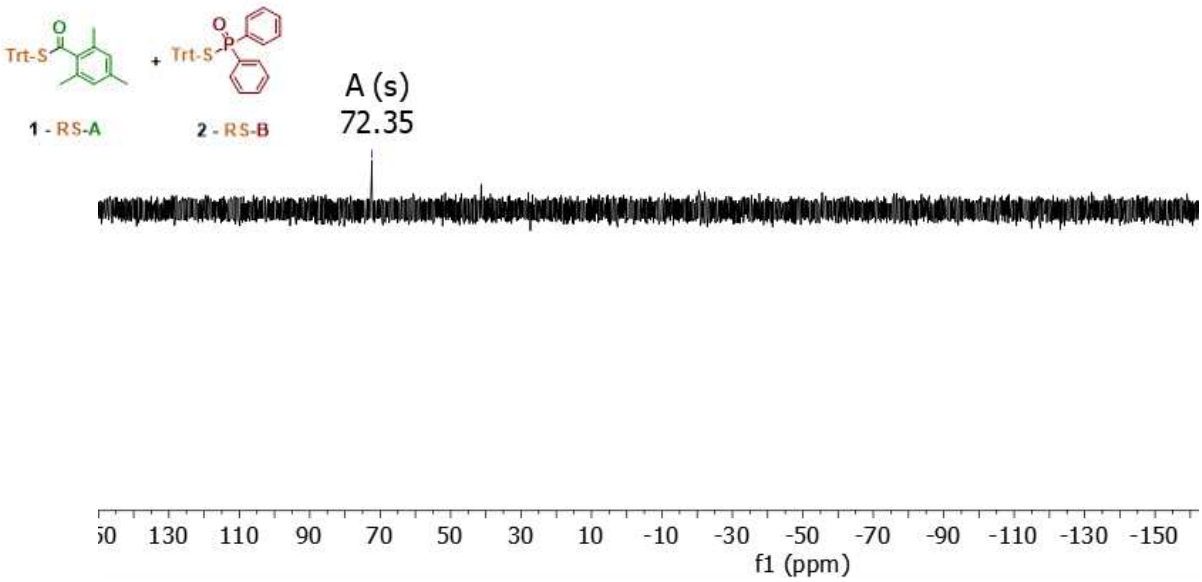

Figure S102. ^{31}P NMR spectrum of species 1 & 2 as obtained by TIRP with no monomer (Figure 6).

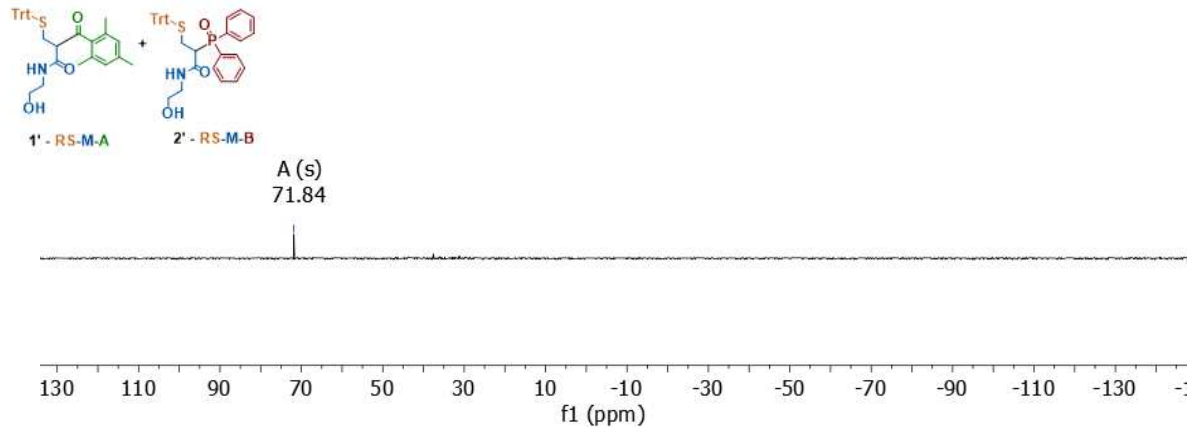

Figure S103. ^{31}P NMR spectrum of species 1' & 2 'as obtained by TIRP with 1 eq. monomer (Figure 6).

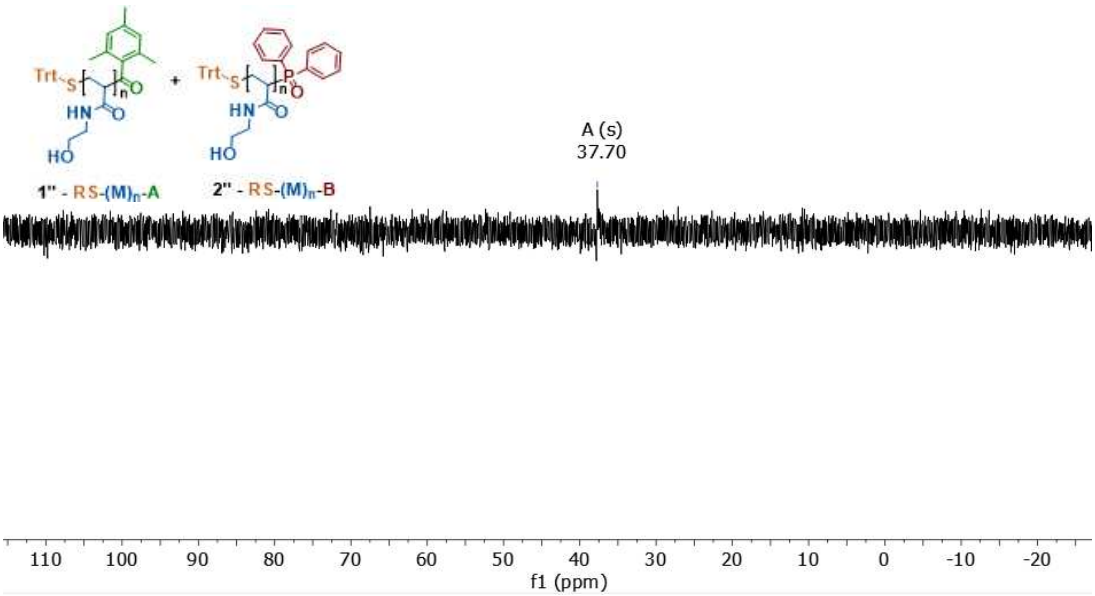

Figure S104. ^{31}P NMR spectrum of species 1" & 2" as obtained by TIRP with 20 eq. monomer (Figure 6).

3. Quantum chemical calculations

The free dissociation energies of RSMA and RSMB were computed to be the differences in free energy of these structures and the free energies of their dissociation products, i.e.

$$\Delta G_{dissoc}(\text{RSMA}) = G(\text{RSM}\bullet) + G(\text{A}\bullet) - G(\text{RSMA})$$

and

$$\Delta G_{dissoc}(\text{RSMB}) = G(\text{RSM}\bullet) + G(\text{B}\bullet) - G(\text{RSMB}),$$

respectively.

The energy required for an electron transfer from $Ir(ppy)_3$ to RSMA and RSMB are computed as

$$\Delta G_{ET}(\text{RSMA}) = EA(\text{RMSA}) + G([Ir(ppy)_3]^+) - G([Ir(ppy)_3])$$

and

$$\Delta G_{ET}(\text{RSMB}) = EA(\text{RMSB}) + G([Ir(ppy)_3]^+) - G([Ir(ppy)_3]),$$

respectively.

Where EA(RMSA) and EA(RMSB) are the electron affinities of these two species.

Table S12: Free Gibbs energies of the species and transition state structures used in this study.

Structure	Free Energy G at T = 300 K in atomic units
Monomer	-247.237644

A-Radical	-462.661383
AM-Radical	-709.906170
B-Radical	-879.631156
BM-Radical	-1126.882016
RS-Radical	-1130.816373
RSM-Radical	-1378.048247
RSMM-Radical	-1625.289326
AMSR	-1840.780472
BMSR	-2257.762478
$[Ir(ppy)_3]$	-1540.068790
$[Ir(ppy)_3]^+$	-1539.884625

Transition State Structures:

TS A radical + M -- > AM radical	-709.876909
TS B radical + M -- > BM radical	-1126.852668
RS radical + M -- > RSM radical	-1378.036964
RSM radical + M -- > RSMM radical	-1625.257762

In the following, the xyz coordinates of the species and transition state structures are given in Ångström with the respective potential energy in the second line of each coordinate-block:

Monomer:

10

Potential Energy (B3LYP+D3/def2-TZVP)= -247.291323315700

C -3.475404 1.527643 -0.000103

C -2.303517 0.902853 -0.000197

C -1.016763 1.654499 -0.000133

N 0.086294 0.880250 0.000507

H -4.407906 0.978512 -0.000005

H -3.523895 2.609907 -0.000081

H -2.248117 -0.180134 -0.000124

O -0.959073 2.886199 -0.000455

H 0.029776 -0.124412 -0.000204

H 0.998582 1.308731 0.000794

A-Radical:

22

Potential Energy (B3LYP+D3/def2-TZVP)= -462.807209995200

C -2.913396 0.222132 0.234321

C -2.588428 1.459386 -0.323937

C -1.295504 1.768692 -0.725032

C -0.289772 0.784547 -0.556026

C -0.597286 -0.474365 0.004208

C -1.906613 -0.730986 0.387636

C -1.008069 3.116612 -1.319812

H -1.917073 3.715767 -1.352524

H -0.613060 3.026655 -2.333476

H -0.256701 3.654298 -0.738612

C -4.316355 -0.065922 0.684739

H -4.524862 -1.135855 0.673354

H -5.046783 0.443570 0.055261

H -4.464128 0.288405 1.709401

C 0.456434 -1.532696 0.187717

H 0.907339 -1.811947 -0.766227

H 0.022799 -2.425450 0.637247

H 1.263378 -1.179727 0.832259

H -3.367450 2.202172 -0.451754

H -2.151655 -1.696268 0.814411

C 1.089859 1.025790 -0.952626

O 1.627812 1.970691 -1.446981

AM-Radical:

32

Potential Energy (B3LYP+D3/def2-TZVP)= -710.127149035100

C -2.149343 0.579516 0.522178

C -1.855889 1.310829 -0.629059

C -0.724463 1.053600 -1.395513

C 0.160704 0.047085 -0.967466

C -0.104800 -0.700332 0.189915

C -1.268250 -0.426322 0.907120

C -0.467429 1.865694 -2.639012

H -1.143212 2.719209 -2.679785

H -0.619255 1.266496 -3.538336

H 0.557074 2.241449 -2.674699

C -3.396467 0.866396 1.312700

H -3.419698 0.291336 2.238273

H -4.289546 0.613957 0.734820

H -3.465663 1.926989 1.564377

C 0.804458 -1.810917 0.652886

H 1.680612 -1.425000 1.178896

H 1.168515 -2.415371 -0.179723

H 0.273906 -2.472069 1.337287

H -2.529368 2.101339 -0.941246

H -1.489785 -1.017926 1.788105

C 1.388601 -0.231886 -1.769395

O 1.335991 -0.562632 -2.936981

C 3.701356 -1.103638 -1.335064

C 2.742792 -0.009364 -1.088329

H 3.803367 -1.498087 -2.337562

H 2.635407 0.182977 -0.024600

H 3.107046 0.924653 -1.545687

C 4.487539 -1.676318 -0.255694

N 5.313241 -2.692785 -0.608159

H 5.376295 -3.022236 -1.556583

H 5.889086 -3.130948 0.092554

O 4.412848 -1.269491 0.914911

B-Radical:

24

Potential Energy (B3LYP+D3/def2-TZVP)= -879.782670059500

P 3.007321 0.590203 0.272670

O 2.729329 0.111998 1.671244

C 3.683593 2.260521 0.183361

C 4.059504 -0.531337 -0.671846

C 3.569141 3.016587 -0.987434

C 4.089323 4.303557 -1.034916

C 4.708226 4.846935 0.087674

C 4.803327 4.104364 1.261887

C 4.289262 2.815133 1.315822

C 4.797714 -0.110537 -1.784065

C 5.555850 -1.027243 -2.500033

C 5.579275 -2.366654 -2.119890

C 4.840919 -2.790411 -1.017758

C 4.077077 -1.881137 -0.298637

H 4.798018 0.928272 -2.083148

H 6.133264 -0.694172 -3.352914

H 6.172133 -3.077949 -2.680531

H 4.861457 -3.830194 -0.717296

H 3.504585 -2.208225 0.559309

H 4.360296 2.235563 2.226815

H 5.109310 5.851699 0.050032

H 5.279900 4.529315 2.136093

H 3.066101 2.607596 -1.854636

H 4.003501 4.885079 -1.943712

BM-Radical:

34

Potential Energy (B3LYP+D3/def2-TZVP)= -1127.108798637000

P 2.338858 1.350276 0.004153

O 1.944458 0.570567 1.214693

C 3.565481 2.629869 0.347576

C 2.971637 0.299048 -1.324323

C 3.763437 3.738592 -0.480138

C 4.735740 4.679641 -0.164045

C 5.512429 4.522975 0.980042

C 5.314754 3.424714 1.811453

C 4.344601 2.480644 1.498328

C 3.783532 0.791468 -2.349241

C 4.140331 -0.031519 -3.410929

C 3.692266 -1.348776 -3.453297

C 2.894486 -1.846939 -2.428038

C 2.534197 -1.027092 -1.365589

H 4.142365 1.811772 -2.324885

H 4.769046 0.354865 -4.202669

H 3.968804 -1.987112 -4.282687

H 2.549518 -2.872484 -2.457083

H 1.910806 -1.409994 -0.568430

H 4.181154 1.630405 2.147320

H 6.267291 5.259035 1.225669

H 5.913006 3.304790 2.705510

H 3.163852 3.881849 -1.368804

H 4.883379 5.536250 -0.808802

C -0.180271 1.277046 -1.101066

C 0.902395 2.222983 -0.770750

H 0.571483 2.942528 -0.017252

H 1.261060 2.778295 -1.638634

H -0.838759 0.946813 -0.310178

C -0.449936 0.689320 -2.402238

N 0.385284 0.984629 -3.432963

O -1.447047 -0.032962 -2.567815

H 1.301516 1.369070 -3.276178

H 0.246622 0.490528 -4.300416

RS-Radical:

35

Potential Energy (B3LYP+D3/def2-TZVP)= -1131.056814689000

C -2.605389 1.813278 -0.767764

C -2.691498 3.260000 -0.279959

C -3.592214 4.141625 -0.875651

C -3.756738 5.432082 -0.387582

C -3.019811 5.862718 0.711952

C -2.124599 4.988209 1.317967

C -1.966459 3.695566 0.828722

C -3.714691 1.033072 -0.055411

C -4.871168 0.617911 -0.706727

C -5.890468 -0.026224 -0.008925

C -5.763010 -0.265972 1.353153

C -4.608443 0.147193 2.014509

C -3.598714 0.795092 1.316913

C -1.221988 1.172728 -0.639153

C -0.064708 1.933495 -0.876599

C 1.191015 1.349136 -0.813497

C 1.316924 -0.008680 -0.531332

C 0.175401 -0.780373 -0.323076

C -1.081912 -0.199349 -0.385796

S -2.660632 1.682331 -2.601448

H -4.978928 0.791590 -1.768953

H -6.782487 -0.340386 -0.536313

H -6.553021 -0.768674 1.896534

H -4.495318 -0.033567 3.076117

H -2.710908 1.114174 1.846610

H -1.961307 -0.807191 -0.229421

H 2.297425 -0.464451 -0.479718

H 0.266319 -1.838318 -0.113310

H -0.155569 2.986010 -1.103299

H 2.072329 1.952905 -0.987227

H -4.172328 3.816582 -1.730597

H -1.544538 5.309652 2.173939

H -1.266612 3.030183 1.315415

H -4.459888 6.101188 -0.867420

H -3.141929 6.869353 1.091193

RSM-Radical:

45

Potential Energy (B3LYP+D3/def2-TZVP)= -1378.363218234000

C -2.426656 1.793976 -1.331060

C -2.479905 3.159918 -0.639626

C -3.601639 3.982366 -0.803615

C -3.668671 5.235734 -0.214076

C -2.615263 5.700326 0.569851

C -1.506901 4.887261 0.761270

C -1.442172 3.629604 0.164878

C -3.665485 0.944690 -1.040215

C -4.013056 -0.120268 -1.875024

C -5.083737 -0.949641 -1.570445

C -5.828871 -0.736775 -0.413934

C -5.484224 0.308955 0.432847

C -4.411961 1.140637 0.121905

C -1.152094 1.012857 -0.978423

C 0.092045 1.405275 -1.485178

C 1.251911 0.719768 -1.148186

C 1.196383 -0.370233 -0.284901

C -0.030714 -0.762555 0.234719

C -1.193062 -0.079172 -0.111528

S -2.249007 2.087779 -3.199412

H -3.437188 -0.298656 -2.772866

H -5.335696 -1.764307 -2.237773

H -6.666115 -1.380675 -0.176222

H -6.046819 0.482381 1.341586

H -4.153896 1.939563 0.801547

H -2.134842 -0.405337 0.304086

H 2.099809 -0.904509 -0.019505

H -0.091227 -1.605535 0.911627

H 0.162170 2.264097 -2.138899

H 2.200829 1.043136 -1.557133

H -4.445791 3.635830 -1.379866

H -0.684449 5.224104 1.379939

H -0.570953 3.017251 0.340136

H -4.548873 5.848713 -0.362484

H -2.665779 6.678340 1.031281

C -3.912864 2.680381 -3.752584

C -4.054151 2.301685 -5.164375

H -3.981100 3.755662 -3.619233

H -4.651280 2.165183 -3.137474

C -3.873812 3.276877 -6.230048

H -4.242433 1.265926 -5.416945

N -4.017245 2.803094 -7.491275

H -4.227819 1.836745 -7.675453

H -3.910778 3.429456 -8.273013

O -3.609160 4.467427 -6.001090

RSMM-Radical:

55

Potential Energy (B3LYP+D3/def2-TZVP)= -1625.682521937000

C -2.277527 1.533642 -1.303080

C -2.174437 3.039185 -1.027259

C -3.160946 3.902449 -1.520319

C -3.089678 5.272489 -1.314914

C -2.031150 5.819966 -0.594888

C -1.058422 4.974852 -0.078272

C -1.131637 3.599900 -0.290381

C -3.679442 1.001352 -0.987807

C -4.203517 -0.113729 -1.641653

C -5.439389 -0.639387 -1.283538

C -6.174148 -0.064565 -0.252019

C -5.656358 1.038019 0.418125

C -4.422742 1.564865 0.051649

C -1.214784 0.714856 -0.549885

C 0.136227 0.796846 -0.909273

C 1.104994 0.067254 -0.232951

C 0.747032 -0.760955 0.826365

C -0.588529 -0.847070 1.197572

C -1.558824 -0.118522 0.514415

S -1.821117 1.222900 -3.109797

H -3.637820 -0.575346 -2.439162

H -5.826851 -1.500451 -1.813536

H -7.137745 -0.471769 0.026985

H -6.210489 1.492062 1.230108

H -4.034056 2.416695 0.591272

H -2.590093 -0.209484 0.820313

H 1.500832 -1.331347 1.354095

H -0.885223 -1.486505 2.019489

H 0.438794 1.443498 -1.721061

H 2.141679 0.149924 -0.534273

H -4.012329 3.501534 -2.049112

H -0.237149 5.379366 0.500160

H -0.367125 2.969343 0.136513

H -3.868464 5.912400 -1.710698

H -1.975055 6.888481 -0.429945

C -3.172026 1.985010 -4.063579

C -3.245179 1.359362 -5.462688

H -3.013583 3.060363 -4.130594

H -4.111448 1.800276 -3.543559

C -4.488629 1.887447 -6.176169

N -4.447409 3.167952 -6.583888

H -3.637974 3.749935 -6.450757

H -5.247765 3.571617 -7.045051

O -5.475964 1.173758 -6.344220

C -1.943957 1.581995 -6.277752

H -3.402474 0.286523 -5.361670

C -2.029999 1.029235 -7.648690

C -1.819201 -0.389126 -7.892276

N -1.973661 -0.799696 -9.175395

O -1.516719 -1.176989 -6.982231

H -1.859666 -1.774366 -9.402992

H -2.239610 -0.163715 -9.908084

H -1.138551 1.079839 -5.737991

H -1.708450 2.647742 -6.312593

H -2.308263 1.669393 -8.476295

AMSR:

67

Potential Energy (B3LYP+D3/def2-TZVP)= -1841.272124

C -0.239944 1.570296 -0.234108

O -0.750184 1.643473 0.866626

C 1.124940 2.118418 -0.489665

C 1.393996 2.955232 -1.588996

C 2.678274 3.474691 -1.738253

C 3.707259 3.168007 -0.854172

C 3.424459 2.315516 0.211126

C 2.151764 1.797247 0.425132

H 4.217753 2.048884 0.900368

H 2.875328 4.141709 -2.569605

C -1.357428 -0.580067 -0.748522

C -0.961501 0.794009 -1.338931

S -1.663726 -1.839199 -2.031433

C -3.214321 -3.086920 -0.013080

C -4.388173 -3.264601 0.724588

C -4.353128 -3.793748 2.008760

C -3.141607 -4.165685 2.582355

C -1.969575 -4.010204 1.851610

C -2.008670 -3.479714 0.566619

C -3.527257 -3.866910 -2.318584

C -2.497530 -4.567837 -2.942211

C -2.755101 -5.749289 -3.634829

C -4.045563 -6.256342 -3.703841

C -5.080076 -5.570657 -3.071828

C -4.821742 -4.390951 -2.389214

C -4.344993 -1.528093 -1.731083

C -4.725442 -0.611336 -0.750508

C -5.598954 0.431940 -1.043264

C -6.119853 0.572832 -2.321874

C -5.750301 -0.336890 -3.310586

C -4.869476 -1.367259 -3.018175

H -4.348305 -0.703604 0.257345

H -5.866861 1.134451 -0.264814

H -6.802402 1.381523 -2.549838

H -6.142816 -0.238043 -4.314906

H -4.576603 -2.048706 -3.804639

H -6.091962 -5.953995 -3.111346

H -5.639802 -3.871572 -1.910303

H -1.480373 -4.206995 -2.887800

H -1.938193 -6.271100 -4.117296

H -4.246133 -7.174714 -4.240810

H -1.089500 -3.378113 0.007024

H -5.342637 -2.990877 0.299061

H -5.277071 -3.914779 2.560243

H -3.112796 -4.573746 3.584663

H -1.018247 -4.301582 2.278772

C -2.195809 1.560710 -1.840389

N -2.653244 1.158113 -3.040501

O -2.700928 2.479900 -1.209160

H -3.558880 1.496667 -3.330612

H -2.358437 0.265744 -3.409728

C 1.938410 0.889548 1.610621

H 1.350393 0.007787 1.353580

H 1.406362 1.403603 2.412005

H 2.899993 0.555280 1.999035

C 0.342748 3.359179 -2.590612

H 0.706096 4.186504 -3.198538

H -0.581582 3.676100 -2.108675

H 0.098242 2.541449 -3.272304

C 5.079309 3.758481 -1.023961

H 5.225293 4.138700 -2.035147

H 5.855778 3.021342 -0.812582

H 5.226321 4.591739 -0.330516

C -3.290495 -2.604301 -1.470340

H -0.280936 0.635776 -2.174614

H -2.235714 -0.476019 -0.120050

H -0.548528 -0.945952 -0.119878

BMSR:

69

Potential Energy (B3LYP+D3/def2-TZVP)= -2258.258931

P -0.459630 0.654871 0.194137

O -0.807638 1.501111 1.372006

C 0.247707 1.590431 -1.178534

C 0.691528 -0.671735 0.631793

C 0.370688 1.071535 -2.471086

C 0.930013 1.839241 -3.483120

C 1.368536 3.132972 -3.214226

C 1.245301 3.657441 -1.931784

C 0.686402 2.890082 -0.916259

C 1.498057 -1.318782 -0.306200

C 2.290209 -2.393001 0.076266

C 2.285676 -2.826773 1.398868

C 1.500023 -2.173112 2.342333

C 0.707016 -1.097411 1.962532

H 1.520062 -0.987700 -1.334640

H 2.912556 -2.889669 -0.656930

H 2.900778 -3.667216 1.694209

H 1.502042 -2.501954 3.373589

H 0.096582 -0.586181 2.694932

H 0.581025 3.296063 0.081006

H 1.802140 3.731647 -4.005006

H 1.581641 4.664541 -1.721603

H 0.033448 0.069849 -2.701002

H 1.020061 1.431221 -4.481471

C -2.573713 -1.115419 0.581320

C -1.901794 -0.251845 -0.513622

S -2.081260 -2.858197 0.618774

C -2.747721 -5.130703 -0.804623

C -3.575218 -5.956216 -1.571152

C -3.365782 -7.326673 -1.623422

C -2.316626 -7.902884 -0.911056

C -1.480951 -7.090452 -0.156413

C -1.692254 -5.714008 -0.108370

C -0.992153 -2.955116 -2.292330

C -0.404725 -2.591317 -3.497002

C -1.185960 -2.431182 -4.638052

C -2.551489 -2.676880 -4.560711

C -3.134907 -3.047525 -3.352029

C -2.371471 -3.154434 -2.188748

C -4.459733 -3.262030 -0.648193

C -5.231477 -4.025872 0.234488

C -6.544950 -3.684846 0.520845

C -7.122789 -2.559721 -0.063616

C -6.363928 -1.779804 -0.924703

C -5.045252 -2.126142 -1.208642

H -4.796880 -4.894569 0.708984

H -7.118725 -4.297583 1.204819

H -8.148843 -2.294187 0.156804

H -6.789749 -0.893698 -1.378100

H -4.480117 -1.494333 -1.875821

H -4.195313 -3.248127 -3.328673

H 0.665714 -2.434602 -3.544725

H -0.733934 -2.134900 -5.575657

H -3.172239 -2.582212 -5.442530

H -1.016724 -5.105536 0.476705

H -4.395896 -5.525274 -2.128469

H -4.023842 -7.945765 -2.220183

H -2.153694 -8.972489 -0.947486

H -0.657932 -7.521686 0.399397

C -2.898892 0.706309 -1.144536

N -2.982608 0.650887 -2.487575

O -3.590082 1.458440 -0.466495

H -3.617413 1.266256 -2.972722

H -2.439435 0.007168 -3.037062

C -2.987700 -3.611454 -0.852864

H -0.375181 -3.067388 -1.412572

H -1.492742 -0.897844 -1.284426

H -3.655360 -1.048033 0.495771

H -2.327115 -0.750372 1.578047

[$Ir(ppy)_3$]:

61

Potential Energy (B3LYP+D3/def2-TZVP)= -1540.497434013000

C -4.333320 1.487536 1.246318

C -4.250955 2.321882 2.350223

C -2.994512 2.708833 2.820252

C -1.838168 2.263207 2.190567

C -1.882374 1.416068 1.074217

C -3.169500 1.037791 0.610144

C -4.356491 -0.376080 -1.140033

C -4.255602 -1.211372 -2.238649

C -2.996222 -1.513770 -2.750041

C -1.889284 -0.962436 -2.131850

N -1.984836 -0.152127 -1.071337

C -3.202519 0.154168 -0.556105

H -5.309101 1.191478 0.881200

H -5.152239 2.669862 2.839059

H -2.921313 3.363115 3.682106

H -0.875746 2.577193 2.574900

H -5.326651 -0.137963 -0.729241

H -5.147361 -1.625801 -2.690592

H -2.870927 -2.163948 -3.604351

H -0.888185 -1.168728 -2.484395

Ir -0.323323 0.687743 0.011206

C -0.171190 -1.059766 1.018243

C -0.920720 -1.479008 2.126510

C -0.727172 -2.723167 2.715468

C 0.231202 -3.604207 2.210906

C 0.988715 -3.224752 1.113765

C 0.794989 -1.971898 0.518599

H -1.669988 -0.813694 2.536967

H 1.729305 -3.911104 0.721963

H -1.325554 -3.013195 3.572224

H 0.381576 -4.574122 2.668079

C 1.570278 -1.523021 -0.638765

N 1.227980 -0.297531 -1.111033

C 1.876514 0.223014 -2.159269

C 2.899919 -0.443155 -2.807584

C 3.265791 -1.703079 -2.340948

C 2.598816 -2.241703 -1.254729

H 2.876083 -3.215564 -0.878700

H 3.395981 0.016731 -3.650609

H 4.064382 -2.256236 -2.817920

H 1.556221 1.205703 -2.476797

N -0.251226 2.559304 -1.051181

C -1.030068 2.893440 -2.086605

C -0.970568 4.134287 -2.693378

C -0.064304 5.067807 -2.197156

C 0.739737 4.725488 -1.124240

C 0.637505 3.454803 -0.550933

H -1.719376 2.133666 -2.428169

H -1.619716 4.360258 -3.527522

H 0.010891 6.051945 -2.641032

H 1.443015 5.441695 -0.725400

C 1.418714 2.971208 0.588283

C 2.406292 3.747727 1.207226

C 3.118413 3.246574 2.285794

C 2.840077 1.958680 2.747508

C 1.859824 1.186533 2.135009

C 1.116987 1.661336 1.044794

H 2.626260 4.745778 0.848590

H 3.882656 3.848260 2.761514

H 3.394133 1.558253 3.589489

H 1.662247 0.191056 2.512609

$[Ir(ppy)_3]^+$:

61

Potential Energy (B3LYP+D3/def2-TZVP)= -1540.314536572000

C -4.325759 1.483423 1.257205

C -4.240285 2.339191 2.344590

C -2.990705 2.767222 2.796505

C -1.831122 2.338670 2.165086

C -1.886858 1.450375 1.084441

C -3.163402 1.037121 0.622301

C -4.332553 -0.352431 -1.150886

C -4.219043 -1.185611 -2.248811

C -2.954957 -1.503003 -2.739513

C -1.851079 -0.967679 -2.105863

N -1.961159 -0.154756 -1.047892

C -3.183292 0.160943 -0.547206

H -5.299935 1.169288 0.907070

H -5.142379 2.677161 2.837583

H -2.925266 3.435978 3.646091

H -0.871573 2.675943 2.532630

H -5.306581 -0.100347 -0.759358

H -5.106704 -1.587478 -2.718742

H -2.824232 -2.152397 -3.592978

H -0.848396 -1.185028 -2.445066

Ir -0.317204 0.690884 0.074744

C -0.189207 -1.079565 1.030246

C -0.977045 -1.502979 2.106600

C -0.775947 -2.745408 2.692449

C 0.203077 -3.609114 2.198092

C 0.978899 -3.226177 1.114868

C 0.791641 -1.972263 0.525795

H -1.737044 -0.844997 2.505413

H 1.725601 -3.908972 0.731881

H -1.381602 -3.045536 3.538885

H 0.354653 -4.578261 2.655089

C 1.552132 -1.518176 -0.636680

N 1.222473 -0.280717 -1.089403

C 1.864383 0.252133 -2.136656

C 2.864061 -0.423769 -2.807408

C 3.212539 -1.698264 -2.366852

C 2.555714 -2.245328 -1.279716

H 2.818363 -3.231491 -0.927307

H 3.355974 0.039421 -3.650433

H 3.991710 -2.257279 -2.867597

H 1.558274 1.244335 -2.435851

N -0.256228 2.548408 -1.029174

C -1.039340 2.869063 -2.066596

C -0.966970 4.099392 -2.689354

C -0.050078 5.031639 -2.209933

C 0.753960 4.703085 -1.133738

C 0.638939 3.444832 -0.539939

H -1.735387 2.111697 -2.397883

H -1.614507 4.319086 -3.525835

H 0.033502 6.006211 -2.672043

H 1.467792 5.417278 -0.751733

C 1.415376 2.977293 0.606443

C 2.395365 3.754713 1.229413

C 3.120058 3.239481 2.293247

C 2.879571 1.936626 2.734000

C 1.915462 1.153197 2.115170

C 1.148380 1.658101 1.058327

H 2.599720 4.760930 0.888612

H 3.874138 3.846649 2.776686

H 3.447103 1.535708 3.564908

H 1.737101 0.148593 2.473719

Transition state structures:

TS A radical + M -- > AM radical:

32

Potential Energy (B3LYP+D3/def2-TZVP)= -710.0958106

C 2.750020 -0.176601 0.740681

C 2.456302 0.735429 -0.271388

C 1.170727 1.223173 -0.465887

C 0.159375 0.811253 0.418453

C 0.427737 -0.092944 1.466941

C 1.724422 -0.579549 1.593393

C 0.897686 2.164882 -1.605922

H 1.786408 2.753251 -1.835534

H 0.078520 2.850983 -1.392053

H 0.634349 1.590442 -2.496768

C 4.143839 -0.716372 0.897676

H 4.866260 0.094873 1.014090

H 4.439000 -1.285101 0.012013

H 4.220155 -1.372256 1.764535

C -0.638907 -0.561752 2.418131

H -1.504509 -0.960594 1.884705

H -1.001279 0.254851 3.044789

H -0.246818 -1.343307 3.067413

H 3.248055 1.065924 -0.934487

H 1.940102 -1.291145 2.382237

C -1.216662 1.268352 0.200194

O -2.065308 1.595801 0.964134

C -1.767982 -0.933298 -1.462243

C -2.103549 0.374873 -1.638048

H -2.358502 -1.568926 -0.812843

H -1.566845 0.969926 -2.363207

H -3.067374 0.741849 -1.316139

C -0.538974 -1.493650 -2.040953

N -0.211769 -2.736716 -1.611820

H -0.735939 -3.201575 -0.890347

H 0.640976 -3.164305 -1.934112

O 0.150407 -0.891610 -2.873333

TS B radical + M -- > BM radical:

34

Potential Energy (B3LYP+D3/def2-TZVP)= -1127.077130021000

P 2.487492 1.285711 0.136143

O 2.079275 0.516803 1.355724

C 3.719765 2.559673 0.418679

C 2.886872 0.271593 -1.289362

C 3.962079 3.556430 -0.534693

C 4.876392 4.565631 -0.266850

C 5.536778 4.601249 0.958923

C 5.279288 3.627203 1.919542

C 4.370746 2.610184 1.657145

C 3.790784 0.663827 -2.283901

C 3.935199 -0.105621 -3.430981

C 3.182499 -1.264763 -3.597967

C 2.292770 -1.665573 -2.605279

C 2.139242 -0.901992 -1.457597

H 4.389079 1.555387 -2.163781

H 4.638137 0.200606 -4.194977

H 3.291242 -1.854933 -4.498691

H 1.710029 -2.568991 -2.730732

H 1.440865 -1.209241 -0.690440

H 4.163858 1.854395 2.402844

H 6.245684 5.392334 1.167389

H 5.787980 3.659463 2.874618

H 3.432788 3.555271 -1.478370

H 5.066479 5.329330 -1.009649

C -0.479158 1.337434 -1.429650

C 0.200188 2.388812 -0.936123

H 0.015634 2.739121 0.070461

H 0.803399 3.035200 -1.561848

H -1.150393 0.774117 -0.793777

C -0.430194 0.837673 -2.819601

N 0.522766 1.329279 -3.644333

O -1.269792 0.020655 -3.213604

H 1.327065 1.814110 -3.285634

H 0.608927 0.920436 -4.561369

TS RS radical + M -- > RSM radical:

45

Potential Energy (B3LYP+D3/def2-TZVP)= -1378.351421918000

C -2.154275 2.440428 -0.841081

C -0.655758 2.107021 -0.881616

C -0.060100 1.126403 -0.097680

C 1.307750 0.871804 -0.188260

C 2.100095 1.598502 -1.065967

C 1.514815 2.590646 -1.850444

C 0.154484 2.842810 -1.753639

C -2.869485 2.047871 -2.138928

C -4.219057 2.373800 -2.317450

C -4.910009 1.973444 -3.450307

C -4.272056 1.213619 -4.430055

C -2.937306 0.873317 -4.259851

C -2.241963 1.291406 -3.125848

C -2.275322 3.932134 -0.486176

C -1.822170 4.356208 0.769507

C -1.868485 5.695124 1.131196

C -2.351243 6.644951 0.234495

C -2.777508 6.238427 -1.024027

C -2.741799 4.892885 -1.381036

S -3.068954 1.582495 0.540206

H -4.739507 2.927220 -1.548912

H -5.952197 2.244626 -3.564696

H -4.813252 0.890051 -5.309979

H -2.427461 0.276414 -5.005477

H -1.207390 1.003871 -3.013832

H -3.070857 4.603558 -2.367684

H -2.384278 7.690889 0.511672

H -3.139162 6.968080 -1.737734

H -1.416128 3.631326 1.462991

H -1.518416 5.998240 2.109943

H -0.660149 0.567977 0.605284

H 2.120404 3.170723 -2.535562

H -0.285317 3.620065 -2.365002

H 1.748389 0.103753 0.435041

H 3.162505 1.402344 -1.136207

C -3.129197 -0.767421 -0.208890

C -4.197949 -0.728905 -1.048250

H -3.257548 -1.081795 0.817731

H -2.124776 -0.761499 -0.605370

C -5.581441 -0.858442 -0.544520

H -4.058382 -0.526819 -2.101303

N -6.538529 -0.641829 -1.471339

H -6.306671 -0.340025 -2.403107

H -7.510180 -0.673649 -1.205591

O -5.842435 -1.142556 0.627735

TS RSM radical + M -- > RSMM radical:

55

Potential Energy (B3LYP+D3/def2-TZVP)= -1625.646695170000

C -1.884365 1.448541 -1.477451

C -1.137996 2.788533 -1.493559

C -1.793612 3.950820 -1.918521

C -1.134229 5.169869 -1.979870

C 0.203420 5.263914 -1.605589

C 0.861507 4.124745 -1.162136

C 0.196790 2.902048 -1.105128

C -3.260684 1.556834 -0.812387

C -4.273152 0.639981 -1.102102

C -5.491198 0.682717 -0.436206

C -5.720229 1.641096 0.546308

C -4.714721 2.548344 0.857041

C -3.497632 2.505326 0.183858

C -1.063852 0.333248 -0.807461

C 0.026024 -0.252714 -1.460755

C 0.786825 -1.238245 -0.844531

C 0.481061 -1.655324 0.446839

C -0.592974 -1.075300 1.110184

C -1.358677 -0.093897 0.487448

S -2.056787 0.851988 -3.262605

H -4.105335 -0.113678 -1.859104

H -6.261982 -0.035428 -0.686427

H -6.670193 1.677798 1.064294

H -4.871915 3.293533 1.626694

H -2.725915 3.212703 0.450604

H -2.191078 0.337083 1.023361

H 1.073937 -2.422077 0.929123

H -0.844055 -1.386313 2.116479

H 0.297153 0.070493 -2.456396

H 1.623153 -1.675588 -1.375096

H -2.840215 3.915530 -2.180094

H 1.897446 4.180357 -0.851749

H 0.733466 2.036973 -0.747006

H -1.670298 6.049861 -2.312661

H 0.719105 6.214766 -1.649306

C -3.253269 2.015253 -3.997474

C -3.993423 1.373666 -5.121433

H -2.731704 2.920626 -4.308142

H -3.969390 2.292278 -3.216192

C -4.886121 2.138317 -6.003418

N -4.692861 3.474262 -6.088806

H -3.981847 3.956837 -5.568018

H -5.281102 4.016699 -6.700695

O -5.764626 1.566039 -6.659784

C -2.361145 0.850087 -6.623151

H -4.303073 0.346097 -4.990038

C -2.989806 0.509449 -7.777384

C -3.493768 -0.859131 -7.995456

N -4.125427 -1.058075 -9.172930

O -3.349165 -1.763923 -7.165361

H -4.514994 -1.962953 -9.384066

H -4.270120 -0.309562 -9.829312

H -2.035270 0.067937 -5.951182

H -1.902851 1.823562 -6.517084

H -3.209046 1.257577 -8.529108

4. Supporting References

1. Wilkins, L. E.; Phillips, D. J.; Deller, R. C.; Davies, G.-L.; Gibson, M. I., Synthesis and characterisation of glucose-functional glycopolymers and gold nanoparticles: study of their potential interactions with ovine red blood cells. *Carbohydr. Res.* **2015,** *405*, 47-54.

3.2. Sulfated glycosaminoglycan mimetic glycopolymers as inhibitors of SARS-CoV-2 cell attachment and infection

Own Contribution:

Collaborative study design. Synthesis, isolation and characterization of all glycomonomers (NMR, HPLC-MS). Synthesis, isolation and characterization (NMR, SEC, MALDI-ToF) of all polymers and copolymers. Sulfation of all polymers and characterization of sulfated polymers (NMR, elemental analysis). Dynamic Light Scattering measurements. Collaborative writing of the manuscript.

Comment:

This chapter is part of a manuscript draft with the same title. Lorand Bonda is shared first author together with Miriam Hoffmann. This chapter only gives information on the synthesis and physicochemical analysis of the glycopolymers as were synthesized and performed by Lorand Bonda, but shows no data on the study of glycopolymers as viral inhibitors and their anticoagulant activity that were performed by other co-authors of the manuscript. Main results in this area are shortly highlighted in a conclusion at the end of this chapter.

Sulfated glycosaminoglycan mimetic glycopolymers as inhibitors of SARS-CoV-2 cell attachment and infection

(This chapter is part of a manuscript draft with the same title. Lorand Bonda is shared first author together with Miriam Hoffmann. This chapter only gives information on the synthesis and physicochemical analysis of the glycopolymers as were synthesized and performed by Lorand Bonda, but shows no data on the study of glycopolymers as viral inhibitors and their anticoagulant activity that were performed by other co-authors of the manuscript. Main results in this area are shortly highlighted in a conclusion at the end of this chapter.)

ABSTRACT:

Carbohydrate-mediated attachment is used by many pathogens, including viruses, as one of the first steps in an infection process. Macromolecules that mimic these carbohydrates can serve as decoy, thus reducing or preventing this process. Here we report the synthesis and biological evaluation of several synthetic glycopolymers designed to mimic sulfated glycosaminoglycans (sGAGs), which have been shown to play a role in SARS-CoV-2 engagement. Several structures were shown to efficiently inhibit SARS-CoV-2 infection. Here, the synthesis of sGAG mimetics both as homopolymers of different lengths and copolymers with various monomer ratios is presented. All sGAG mimetics were utilized in cell infection assays and evaluated against the inhibition of SARS-CoV-2 infection. In addition, the anticoagulant effect of the sGAG mimetics was investigated as natural GAGs like Heparin are known to serve as anticoagulants, which may be undesired when treating a viral infection. It has been shown that both the length and the charge density of the sGAG mimetics enhance the viral adhesion inhibition as well as influence the anticoagulant effect. To the best of our knowledge this work provides the first examples of GAG mimetic glycopolymers as inhibitors of SARS-CoV-2.

1. INTRODUCTION:

The severe acute respiratory syndrome coronavirus 2 (SARS-CoV-2) continues to threaten our health and challenge our economy worldwide. Despite the availability of vaccines as the gold standard of protection against SARS-CoV-2 and other virus infections, new mutations of the virus keep developing. This leads to a continuous cycle: new therapeutics are made available, yet the virus evolves and circumvents the therapeutics' function. Alternatively, therapeutics are being developed that target mechanisms of the infection process that are less likely to be prone to such fast mutations. One such mechanism is the first step of the infection process – the attachment of the virus to the cell surface that is then typically followed by the entry into the cell. Developing inhibitors to block this attachment can thus lead to therapeutics for the protection against and treatment of SARS-CoV-2 infection. SARS-CoV-2, like many other viruses, is

known to use proteoglycans composed of a membrane anchored protein with long polysaccharide brush-like side chains as attachment factors at the cell surface.[1-2] One of the primary polysaccharides engaged by SARS-CoV-2 is heparan sulfate (HS).[1] HS is a member of the GAG family, which is a family of linear and negatively charged polysaccharides that are characterized by a high structural diversity.[3-4] Structurally closely related to HS is the GAG heparin (HP), which is more highly sulfated and charged and often used as analogue in several applications.[3]

The role of HS proteoglycans in viral infection has already been investigated for various virus families.[5-7] Besides their role in cell attachment, for SARS-CoV-2 and other viruses engaging HS proteoglycans, it has been demonstrated that soluble polysaccharides such as HS/HP can act as inhibitors of this cell attachment most likely by blocking the according HS binding sites on the virus capsid.[8] By inhibiting cell attachment, infection can be significantly reduced or even completely blocked which opens up new therapeutic approaches both in prophylactic treatments or for the acute infection.[8] These findings have even led to the recommendation of using HS and HP in the treatment against SARS-CoV-2 infections.[9-10] However, especially HP is also well known for its anticoagulant activity, leading to the risk of undesired side effects when using it for its antiviral properties.[11] Furthermore, HS/HP – like many other glycosaminoglycans – are a rather ill-defined materials, with high structural heterogeneity.[12-14] Thus, HS/HP or more generally mimetic materials of sulfated GAGs (sGAGs) have been developed allowing for more structural control and exploring potential benefits of such synthetic structures, e.g., reduced side-effects, higher reproducibility and long-term stability.[15-19]

In 2020 we have demonstrated the use of a first generation of sulfated glycooligomers and glycopolymers as sGAG mimetics and their activity as broadband antivirals.[20] We initially focused on targeting Human Papilloma Virus 16 (HPV16) given the importance of this virus in the development of invasive cancers such as cervical cancer.[2,3] Our experiments revealed that our sGAG mimetics could prevent HPV infection, both *in vitro* and *in vivo*. We then explored the generalizability of this approach. Additional studies with Herpes Simplex Virus (HSV), Influenza A Virus (IAV), and Merkel Cell Polyomavirus (MCPyV) showed that our compounds could also serve as broad-spectrum inhibitors of viral infection. Due to the Corona pandemics the use of glycopolymers and sGAG mimetics as antivirals has regained tremendous interest. Recent results presenting the use of sGAG mimetic polymers as inhibitor of SARS-CoV-2 infections have focused on sulfated polymers such as linear and branched polyglycerols. These types of mimetics retain the charged groups of HS and thus can drive interaction with the virus mainly by electrostatic charges. This is indeed particularly relevant for SARS-CoV-2 as it has been observed that during mutation of the virus an

increase in cationic amino acids in and near the region identified as primary HS recognition site occurred. Another class of sGAG mimetic polymers not only carries the charged groups of HS but also retains carbohydrate motifs, mostly presented as side-chains on a synthetic polymer backbone. While sGAG mimetic glycopolymers have been extensively studied in the context of tissue engineering and cancer therapy, to the best of our knowledge, so far no sGAG mimetic glycopolymers have been demonstrated as inhibitors of SARS-CoV-2.

Here, we designed a library of sGAG mimetic glycopolymers systematically varying structural parameters such as the chain length, density of carbohydrate side chains and linker connecting the carbohydrate and polymer scaffold. These glycopolymers are then studied as inhibitors of SARS-CoV-2 infection. Through these structural variations, on the one hand, we aimed at maximizing the inhibitory potency by maximizing the interactions with the virus receptors e.g., by synthesizing long chain glycopolymers. On the other hand, we explored the variation of selected structural parameters such as the charge density to reduce off-target effects, specifically anticoagulant properties, while maintaining high antiviral activity.

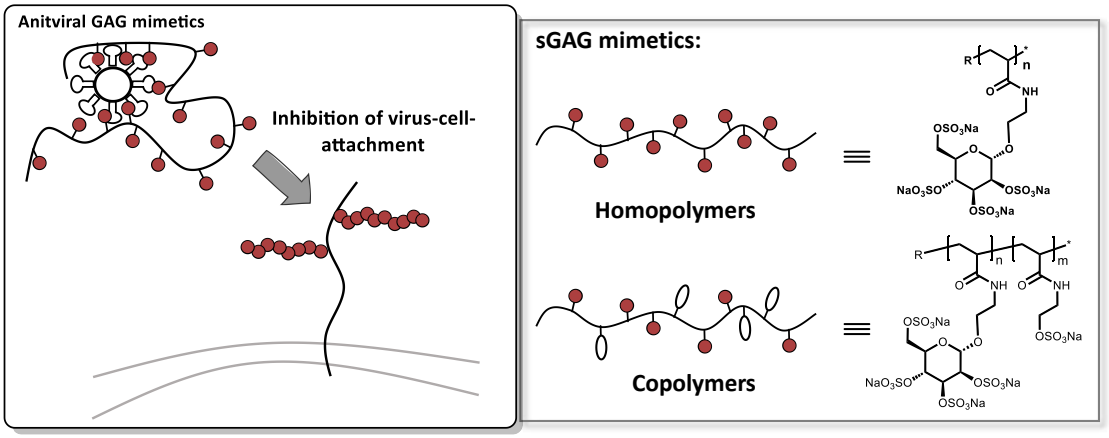

Figure 1. Schematic presentation of the inhibition of viral infection by GAGs and the glycopolymers designed and studied as inhibitors of SARS-CoV-2 infections.

2. RESULTS AND DISCUSSION:

2.1 Design and synthesis of sGAG mimetic glycopolymers

sGAG mimetic glycopolymers are composed of a synthetic backbone decorated with sulfated carbohydrate motifs thereby retaining two key features of their natural analogues – the carbohydrate motifs and sulfate groups. This simplified structure allows for straightforward synthesis from polymerizable carbohydrate motifs, so-called glycomonomers, and their free radical polymerization

followed by global sulfation. Thereby, they are also accessible at high molecular weights similar e.g., to natural HS. Synthesis proceeds following previously established protocols starting from tailor-made glycomonomers exclusively focusing on mannose as carbohydrate motif. As polymerizable unit, acrylamide groups are introduced at the anomeric position. Two different monomers were synthesized selectively varying the linker between the polymerizable unit and the mannose. First, using mannose-amine (for synthesis see SI) and reaction with acryloyl chloride afforded M1, a mannose acrylamide monomer with no additional linker (see Scheme 1). Secondly, using a *N*-hydroxyethyl acrylamide and glycosylation with acetylated mannose gave M2, a mannose acrylamide monomer with an ethyl linker between the acrylamide unit and the anomeric center of the mannose. Both monomers were then applied in free radical photopolymerizations. After polymerization both glycopolymers were deacetylated by treatment with sodium methanolate. Both monomers were homopolymerized, however, M1 showed much lower yield and chain lengths indicating that this monomer is not well suited for radical polymerization, likely due to sterical effects as it is less mobile without the ethyl linker. Therefore, we continued synthesis of a small library of homopolymers only with M2 selectively varying the chain length from 10 to 800. In addition, M2 was copolymerized with *N*-hydroxyethyl acrylamide (HEAA) at two different chain length (70 and 300) with varying ratios of mannose/HEAA (from 30 to 50 to 70% mannose). All glycopolymers were characterized by aqueous SEC-MALS and ^{1}H NMR (see SI for details on the synthesis and analytical data). Finally, glycopolymers were globally sulfated using a previously established protocol.[20] Degree of sulfation was measured by elemental analysis and successful sulfation was further confirmed by ^{1}H NMR spectroscopy (see SI). In total eleven sGAG mimetic glycopolymers (GPs) and their according non-sulfated precursors were isolated (see Table 1). Nomenclature gives the degree of polymerization e.g., GP-10, and for the non-sulfated precursor OH is added, e.g., GP-10-OH. Copolymers (coGP) additionally carry the information of the ratio of Mannose/HEAA as the theoretical (number) percentage of mannose monomers, e.g. coGP-70 (30%). As additional control compound without a carbohydrate motif, HEAA was homopolymerized (PHEAA-200-OH) and globally sulfated giving PHEAA-200.

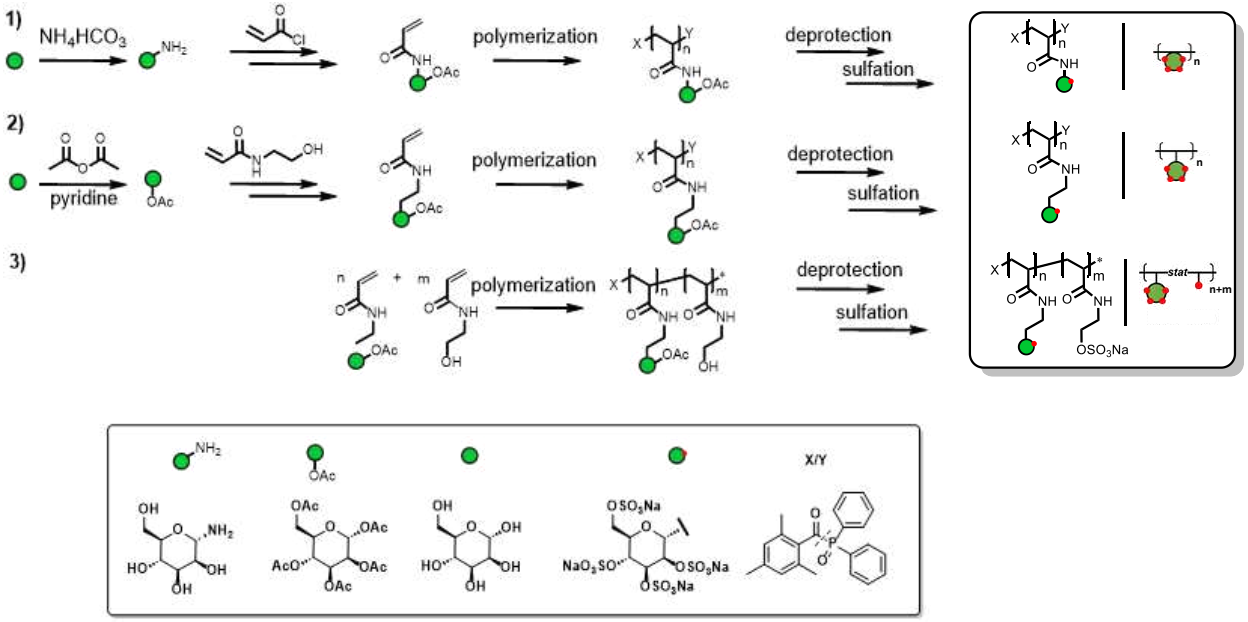

Scheme 1. Synthesis of glycomonomers and homo- and co-glycopolymers and their global sulfation. 1) Homopolymers from glycomonomer with no linker: polymerization (1eq. M1, 1.4 mol% TPO, DMF [10 wt.%], 1h hν (λ = 405 nm, 45.2 mW/cm²), deprotection (NaOMe/MeOH (0.2 M), 1h, rt), sulfation (40 eq./OH TMA*SO_3, 18h, 70°C); 2) Homopolymers from glycomonomer with ethyl linker: polymerization (1 eq. M2, x mol% TPO (for x, see SI), DMF [10 wt.%], 1h hν (λ = 405 nm, 45.2 mW/cm²), deprotection (NaOMe/MeOH (0.2 M), 1h, rt), sulfation (40 eq./OH TMA*SO_3, 18h, 70°C); 3) Copolymers from glycomonomer with ethyl linker and HEAA: polymerization (1 eq. M2, x eq. HEAA (for x, see SI), 1.4 mol% TPO, DMF [10 wt.%], 1h hν (λ = 405 nm, 45.2 mW/cm²), deprotection (NaOMe/MeOH (0.2 M), 1h, rt), sulfation (40 eq./OH TMA*SO_3, 18h, 70°C).

Table 1. Overview on structural parameters of precursor and sulfated glycopolymers.

Name	Structure	M_n[a] precursor (sulfated)[b] [kDa]	Đ[c]	$N_{theor.}$ (Man)	Copolymers		Degree of sulfation [%][d]
					n	m	
GP-60-NL	60	14 (31.2)	1.03	60	60	-	70
GP-10	10	2.8 (6.08)	1.41	10	10	-	80
GP-30	30	8.3 (19.6)	1.24	30	30	-	92
GP-70	70	19.4 (42.3)	1.29	70	70	-	80
GP-200	200	55.5 (125.6)	1.13	200	200	-	86
GP-300	300	83.2 (198.4)	1.16	300	300	-	94
GP-800	800	221.8 (530.3)	2.16	800	800	-	94

CoGP-70 (30%)	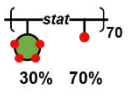	11.5 (23.4)	1.51	21	21	49	88
CoGP-70 (50%)	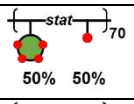	13.8 (29.3)	1.56	35	35	35	87
CoGP-70 (70%)	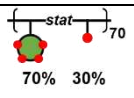	14.8 (34.95)	1.41	46	46	19	98
CoGP-300 (50%)	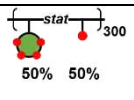	58.8 (135.4)	1.46	150	150	150	100

[a] M_n determined by aqueous SEC-MALS, [b] M_n determined by calculation based on degree of sulfation, [c] Đ determined by aqueous SEC-MALS, [d]degree of sulfation determined by elemental analysis via S/C ratio (for detail, see SI)

With this library of sGAG mimetic polymers and controls we then investigated their biological activity as inhibitors of viral adhesion and as anticoagulants. For both types of activity, we base our polymer design on previous structure property correlations, e.g., it has been shown for both, natural and mimetic sGAGs that their chain length strongly impacts their antiviral and anticoagulant properties. While high molecular weight HP is the more potent inhibitor of virus adhesion, it also shows highly increased anticoagulant properties in comparison to its lower molecular weight fragments. In pharmaceutical application of HP as anticoagulant, unfractionated heparin shows variable dose-response relationships due to its structural heterogeneity and requires close monitoring during administration furthermore side-effects are observed such as heparin-induced thrombocytopenia. Therefore, typically fractionated lower molecular weight HP is used instead of unfractionated heparin. A structural parameter that has been less studied is the positioning and related density of the sulfate groups along the sGAG chain. For example, HS consists of highly, less or non-sulfated segments.[4] For natural sGAGs, it is highly challenging to analyze or even control such segments of sulfation. For glycopolymers, this could be more readily controlled through the density of carbohydrate motifs along the polymer chain e.g. in a copolymer with non-carbohydrate monomers where segments with no carbohydrate side chains represent non-sulfated segments. Indeed, for other types of glycopolymers e.g. as inhibitors of bacterial adhesion, it has been shown that the density of carbohydrate motifs can strongly impact their binding affinity (or avidity) and thus their biological activity.[21] Surprisingly, it is not the highest density and thus highest number of carbohydrates that leads to the highest activity, but it is often a reduced density that leads to optimal binding.[22] Here, we systematically investigate the effect of carbohydrate density and thus sulfate density by including a first series of copolymers. Furthermore, by varying the linker length from M1 to M2, we also expect to affect the chain conformation and carbohydrate accessibility and thus can further explore how these structural parameters affect sGAG mimetic glycopolymers. To gain a first insight into the potential accessibility of

sulfated carbohydrate motifs within the glycopolymers, we performed dynamic light scattering experiments to measure the hydrodynamic radii (see Figure 2). It can be expected that a larger hydrodynamic radius indicates a larger and less densely coiled polymer structure in solution and thus would afford higher accessibility to bind e.g., to the viral capsid proteins.

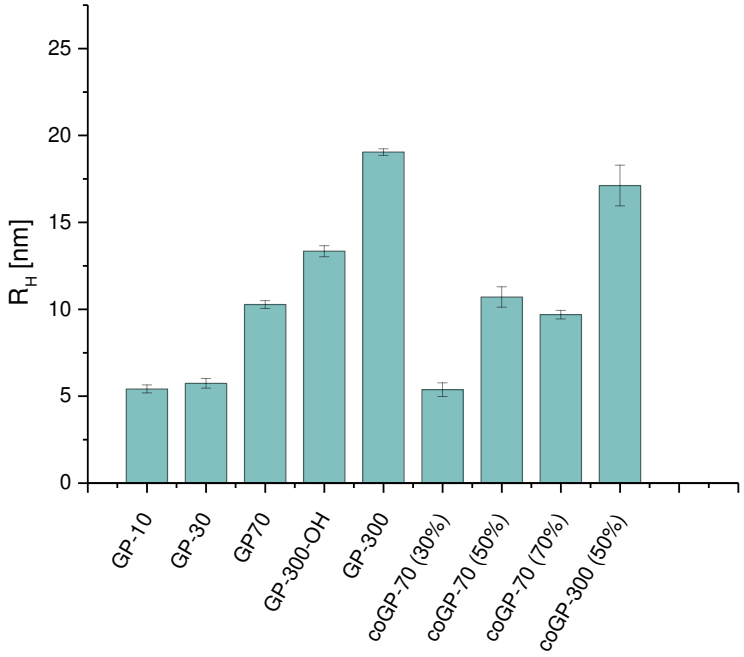

Figure 2. Hydrodynamic radii for selected compounds determined by DLS in PBS buffer: LGP-10, LGP-30, LGP-70, LG-300, LGP-300-US, LGCoP-70-30/70 and LGCoP-70-50/50.

As expected, with an increase in chain length the hydrodynamic radii increase from GP-10 to GP-300. Interestingly, when retaining the same degree of polymerization and thus chain length (DP 70) but reducing the number of mannose units by replacing them with HEAA, we see a decrease in hydrodynamic radius. We tentatively explain this by a lower number and density of sulfate groups and thus less intramolecular electrostatic repulsion leading to a more coiled polymer conformation.[23]

CONCLUSION

We demonstrated the synthesis of sGAG mimetics as mannose homopolymers of different chain lengths with and without linker and as mannose-HEAA copolymers of different monomer ratios. Also it was shown, that all polymers were highly sulfated like their natural models. Due to the different chain lengths of the homopolymers and variable monomer ratios with constant chain length of the copolymers, we were able to investigate the effect of the number of carbohydrates to the sheer number of charge density in viral inhibition and anticoagulation studies. To determine the hydrodynamic radii, all sGAGs were

measured by DLS. In the viral assays, cell infection was increasingly inhibited as the chain length, i.e., the number of carbohydrates, increased. The copolymers with a total chain length of 70 also showed that a higher sugar content (70%>50%>30%) leads to less cell infection. Also a reduction of sulfate density while retaining high molecular weight could still afford highly potent viral inhibitors. In the anticoagulation studies, both activated partial thromboplastin time (APTT), and thrombin clotting time (TCT) were performed, which measure the blood clotting time and both assays showed similar trends. Since long-chain heparins as anticoagulants may have undesirable side effects, we investigated to use shorter sGAGs as anticoagulants, which can also act as potent viral inhibitors. We have shown that charge density plays as an important role in coagulation as the chain length. GAG mimetics with lower sulfated mannose density showed similar inhibition effects but clearly decreased anticoagulant properties.

ACKNOWLEDGMENTS

The authors thank the DFG for financial support through the research group 'Virocarb' (HA5950/5-2), the National Science Foundation (International Research Experience for Scientists Award # 1854028), and the Research Corporation for Science Advancement (RSCA) organization for financial support through the award #27368. We thank Susanne Boye from the polymer separation group at the Leibniz-Insitut of Polymer Research in Dresden for her great support with the SEC measurements. Also we thank the CeMSA@HHU (Center for Molecular and Structural Analytics @ Heinrich-Heine University) for recording the mass spectrometric and the NMR-spectroscopic data.

CONTRIBUTIONS

Lorand Bonda (shared first author with Miriam Hoffmann)**,** *Department of Organic and Macromolecular Chemistry, Heinrich-Heine-University Düsseldorf, Universitätsstraße 1, 40225 Düsseldorf, Germany*:

> Synthesis, isolation and characterization (HPLC-MS, NMR, SEC, elemental analysis) of all monomers, homopolymers and/or copolymers. Performance of all sulfations and calculative analysis of the results. DLS measurements of the polymers and graphical presentation of the results. Writing of the experimental section. Collaborative project development and writing of the manuscript.

Miriam Hoffmann (shared first author with Lorand Bonda), *Department of Organic and Macromolecular Chemistry, Heinrich-Heine-University Düsseldorf, Universitätsstraße 1, 40225 Düsseldorf, Germany*:

Anticoagulation assays as well as analysis and presentation of the results. Collaborative project development and writing of the manuscript.

Stephan Ludwig and **Mario Schelhaas**, *Institute of Cellular Virology, ZMBE and Cells in Motion Interfaculty Centre CiMIC, University of Münster, Münster 48149, Germany*.

Project idea and organization. Plan, performance and evaluation of all viral assays including SARS-CoV-2. Collaborative project development and writing of the manuscript. Not included in this early version of the manuscript.

Nicole Snyder, *Department of Chemistry, Davidson College, Davidson, North Carolina 28035, United States:*

Project idea, evaluation and organization. Collaborative project development and writing of the manuscript.

Laura Hartmann*, Institute for Macromolecular Chemistry, University of Freiburg, Stefan-Meier-Str. 31, 79104 Freiburg i.Br., Germany*:

Project idea, evaluation and organization. Collaborative project development and writing of the manuscript.

REFERENCES

1. Clausen, T. M.; Sandoval, D. R.; Spliid, C. B.; Pihl, J.; Perrett, H. R.; Painter, C. D.; Narayanan, A.; Majowicz, S. A.; Kwong, E. M.; McVicar, R. N., SARS-CoV-2 infection depends on cellular heparan sulfate and ACE2. *Cell* **2020,** *183* (4), 1043-1057. e15.
2. Schuurs, Z. P.; Hammond, E.; Elli, S.; Rudd, T. R.; Mycroft-West, C. J.; Lima, M. A.; Skidmore, M. A.; Karlsson, R.; Chen, Y.-H.; Bagdonaite, I., Evidence of a putative glycosaminoglycan binding site on the glycosylated SARS-CoV-2 spike protein N-terminal domain. *Computational and Structural Biotechnology Journal* **2021,** *19*, 2806-2818.
3. Gandhi, N. S.; Mancera, R. L., The structure of glycosaminoglycans and their interactions with proteins. *Chemical biology & drug design* **2008,** *72* (6), 455-482.
4. Kreuger, J.; Kjellén, L., Heparan sulfate biosynthesis: regulation and variability. *Journal of Histochemistry & Cytochemistry* **2012,** *60* (12), 898-907.
5. Hoffmann, M.; Snyder, N. L.; Hartmann, L., Polymers inspired by heparin and heparan sulfate for viral targeting. *Macromolecules* **2022,** *55* (18), 7957-7973.

6. Cagno, V.; Tseligka, E. D.; Jones, S. T.; Tapparel, C., Heparan sulfate proteoglycans and viral attachment: true receptors or adaptation bias? *Viruses* **2019,** *11* (7), 596.
7. Koganti, R.; Memon, A.; Shukla, D. In *Emerging roles of heparan sulfate proteoglycans in viral pathogenesis*, Seminars in Thrombosis and Hemostasis, Thieme Medical Publishers, Inc. 333 Seventh Avenue, 18th Floor, New York, NY …: 2021; pp 283-294.
8. Guimond, S. E.; Mycroft-West, C. J.; Gandhi, N. S.; Tree, J. A.; Le, T. T.; Spalluto, C. M.; Humbert, M. V.; Buttigieg, K. R.; Coombes, N.; Elmore, M. J., Synthetic heparan sulfate mimetic pixatimod (PG545) potently inhibits SARS-CoV-2 by disrupting the spike–ACE2 interaction. *ACS central science* **2022,** *8* (5), 527-545.
9. Ackermann, M.; Verleden, S. E.; Kuehnel, M.; Haverich, A.; Welte, T.; Laenger, F.; Vanstapel, A.; Werlein, C.; Stark, H.; Tzankov, A., Pulmonary vascular endothelialitis, thrombosis, and angiogenesis in Covid-19. *New England Journal of Medicine* **2020,** *383* (2), 120-128.
10. Barrett, C. D.; Moore, H. B.; Yaffe, M. B.; Moore, E. E., ISTH interim guidance on recognition and management of coagulopathy in COVID-19: A Comment. *Journal of Thrombosis and Haemostasis* **2020,** *18* (8), 2060-2063.
11. Mohamed, S.; Coombe, D. R., Heparin mimetics: Their therapeutic potential. *Pharmaceuticals* **2017,** *10* (4), 78.
12. Liu, H.; Zhang, Z.; Linhardt, R. J., Lessons learned from the contamination of heparin. *Natural product reports* **2009,** *26* (3), 313-321.
13. Guerrini, M.; Beccati, D.; Shriver, Z.; Naggi, A.; Viswanathan, K.; Bisio, A.; Capila, I.; Lansing, J. C.; Guglieri, S.; Fraser, B., Oversulfated chondroitin sulfate is a contaminant in heparin associated with adverse clinical events. *Nature biotechnology* **2008,** *26* (6), 669-675.
14. Kjellén, L.; Lindahl, U., Specificity of glycosaminoglycan–protein interactions. *Current Opinion in Structural Biology* **2018,** *50*, 101-108.
15. Wang, Z.; Hsieh, P.-H.; Xu, Y.; Thieker, D.; Chai, E. J. E.; Xie, S.; Cooley, B.; Woods, R. J.; Chi, L.; Liu, J., Synthesis of 3-O-sulfated oligosaccharides to understand the relationship between structures and functions of heparan sulfate. *Journal of the American Chemical Society* **2017,** *139* (14), 5249-5256.
16. Pongener, I.; O'Shea, C.; Wootton, H.; Watkinson, M.; Miller, G. J., Developments in the chemical synthesis of heparin and heparan sulfate. *The Chemical Record* **2021,** *21* (11), 3238-3255.
17. Miura, Y.; Fukuda, T.; Seto, H.; Hoshino, Y., Development of glycosaminoglycan mimetics using glycopolymers. *Polymer journal* **2016,** *48* (3), 229-237.
18. Paluck, S. J.; Nguyen, T. H.; Maynard, H. D., Heparin-mimicking polymers: synthesis and biological applications. *Biomacromolecules* **2016,** *17* (11), 3417-3440.
19. Liu, Q.; Chen, G.; Chen, H., Chemical synthesis of glycosaminoglycan-mimetic polymers. *Polymer Chemistry* **2019,** *10* (2), 164-171.
20. Soria-Martinez, L.; Bauer, S.; Giesler, M.; Schelhaas, S.; Materlik, J.; Janus, K.; Pierzyna, P.; Becker, M.; Snyder, N. L.; Hartmann, L., Prophylactic antiviral activity of sulfated glycomimetic oligomers and polymers. *Journal of the American Chemical Society* **2020,** *142* (11), 5252-5265.
21. Pramudya, I.; Chung, H., Recent progress of glycopolymer synthesis for biomedical applications. *Biomaterials science* **2019,** *7* (12), 4848-4872.
22. Salvadó, M.; Reina, J. J.; Rojo, J.; Castillón, S.; Boutureira, O., Topological defects in hyperbranched glycopolymers enhance binding to lectins. *Chemistry–A European Journal* **2017,** *23* (62), 15790-15794.
23. Murdoch, T. J.; Willott, J. D.; de Vos, W. M.; Nelson, A.; Prescott, S. W.; Wanless, E. J.; Webber, G. B., Influence of anion hydrophilicity on the conformation of a hydrophobic weak polyelectrolyte brush. *Macromolecules* **2016,** *49* (24), 9605-9617.

Supporting Information

GAG mimetic glycopolymers as inhibitors of SARS-CoV-2 cell attachment and infection

1. Material and Mehtods

Materials:

Acetonitrile (99.9 %, HPLC-grade), hydrochloric acid 1M (p.a.), diethyl ether (p.a.), dichloromethane (99.9 %, puriss., p.a.), D-(+)-mannose (99 %), sodium chloride (98 %), thiophenol (97%) were purchased from Sigma-Aldrich. Dichloromethane (p.a.), dimethylformamide (98 %, for peptide synthesis), ethyl acetate (analytical reagent grade) were purchased from ACROS Organics. Methanol (p.a.), acetic anhydride (99.7 %) and pyridine were purchased from VWR Chemicals. Diphenyl-(2,4,6-trimethylbenzoyl)-phosphine oxide (>98%) and *N*-hydroxyethylacrylamide (>98%) were purchased from TCI chemicals.

Methods:

UV-light source

Samples were irradiated with a UV-LED Spot P standard (405 nm) from Opsytec Dr. Gröbel GmbH.

Irradiation Intensities

Irradiation intensities were determined with a FieldMaxII-TO Laser Power Meter from Coherent.

^{1}H-NMR

^{1}H-NMR spectra were recorded at room temperature with a Bruker AVANCE III 300 (for 300 MHz) and 600 (for 600 MHz). The chemical shifts were reported relative to solvent peaks (chloroform and water) as internal standards and reported as δ in parts per million (ppm). Multiplicities were abbreviated as s for singlet, d for doublet, t for triplet and m for multiplet**.**

Size Exclusion Chromatography - Multi-angle Light Scattering (H_2O-SEC-MALS)

SEC analysis was conducted with an Agilent 1200 series HPLC system and three aqueous SEC columns provided by Polymer Standards Service (PSS). The columns were two Suprema Lux analytical columns (8 mm diameter and 5 µm particle size) and one precolumn (50 mm, 2 x 160 Å of 300 mm and 1000 Å

of 300 mm). The eluent was a buffer system consisting of MilliQ water and 30 % acetonitrile with 50 mM, NaH2PO4, 150 mM NaCl and 250 ppm NaN3 with a pH = 7.0 (via addition of 50 mL 3 molar aqueous sodium hydroxide solution) filtered with inline 0.1 µm membrane filter and running at 0.8 mL per minute. Mullti-angle light scattering is recorded via mimDAWN TREOS and differential refractive index spectra with Optilab rEX both supplied by Wyatt Technologies EU. Data analysis was committed with Astra 5 software and a dn/dc value of 0.156 for each polymer.

Size Exclusion Chromatography (Center of Macromolecular Structure Analysis at the Leibniz Insitute of polymer research in Dresden).

SEC analysis was conducted with an Agilent 1260 series HPLC system, one precolumn and three aqueous SEC columns provided by GE Healthcare. The columns were three Suprema Lux analytical columns (100/100/1000). The eluent was a buffer system consisting of MilliQ water with 10 mM PBS-buffer with pH = 7.4 and running at 1 mL per minute. Mullti-angle light scattering is recorded via DAWN Heleos-II (Wyatt), λ=660 nm and differential refractive index spectra with Optilab T-rEX (Wyatt), λ=660 nm, both supplied by Wyatt Technologies EU. Data analysis was committed with Astra software and a dn/dc value of 0.163 for each polymer.

Freeze Dryer

Lyophilization was performed with an Alpha 1-4 LD instrument provided by Martin Christ Freeze Dryers GmbH. A temperature of –42 °C and a pressure of 0.1 mbar were maintained throughout the freezedrying process.

Elemental Analysis

The ratio of carbon, hydrogen, nitrogen and sulfur were determined using a Vario Micro Cube provided by Analysensysteme GmbH. The measurements were carried out by the Institute for Pharmaceutical and Medicinal Chemistry, Heinrich-Heine University Düsseldorf.

High Pressure Liquid Chromatography (HPLC)

RP-HPLC/MS (Reversed Phase-HPLC/Mass Spectroscopy) was performed on an Agilent Technologies 1260 Infinity System using an AT 1260 G4225A degasser, G1312B binary pump, G1329B automatic

liquid sampler, G1316C thermostated column compartment, G1314F variable wavelength detector at 214 nm and an AT 6120 quadropole containing an electrospray ionisation (ESI) source. The mobile phase consisted of buffer C (water:acetonitrile 95:5 (*v*/*v*), 0.1 vol.% formic acid) and buffer D (water:acetonitrile 5:95 (*v*/*v*), 0.1 vol.% formic acid). HPLC runs were performed on a Poroshell 120 EC-C18 (3.0 × 50 mm, 2.5 µm) RP column from Agilent at a flow rate of 0.4 ml/min 95% buffer A and 5% buffer B (0-5 min), following a linear gradient to 100% buffer B (5-30 min) at 25 °C. ESI-MS for GlcNAc-oligomers and sulfates was performed using 95% buffer A and 5% buffer B without formic acid and a fragmentor voltage of 40-60 V (m/z range of 200 to 2000).

Dynamic Light Scattering

DLS measurements were performed on a Zetasizer Nano – ZS from Malvern. Samples were prepared by solving the polymers in PBS buffer (pH 7.4) with a concentration of 0.5 mg/mL. Before measuring the samples were filtered through Whatman Puradisc 13 PTFE filters (5.0 mm, 13 diameter) from cytiva. Measurements were performed in SARSTEDT polystyrene cuvettes.

2. Monomer Synthesis

2.1 Mannose monomer without linker (M1)

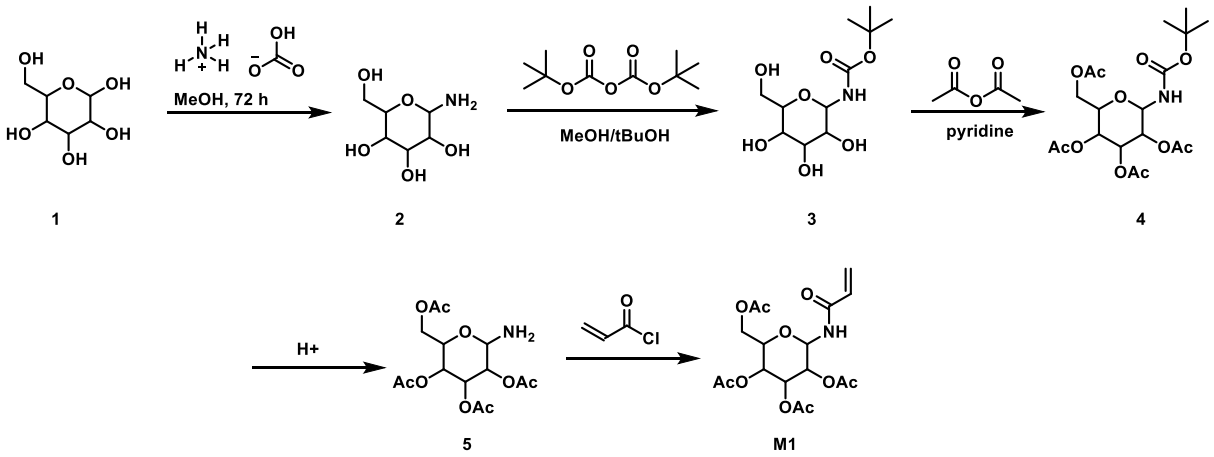

To synthesize monomer M1, commercially purchased mannose **1** (1 g, 0.55 mmol) was stirred with ammonium bicarbonate (2 eq.) and magsnesium sulfate for 72 h at 45°C. The solution was then filtered and heated to 61°C to decompose residual ammonium bicarbonate. By adding Di-*tert*-butyl dicarbonate (1.3 eq.) and stirring overnight, Boc-protected mannoseamine **3** precipitated and was filtered afterwards. The sugar was then stirred with pyridine [10 ml/g] and acetic anhydride [10 ml/g] overnight, and after dilution with ethyl acetate extracted with 1M HCl three times. After the Boc protecting group was removed by using TFA/DCM 1:1 (v/v) for 2h at room temperature, compound **5** was isolated after evaporating the DCM and TFA under reduced pressure. Monomer **M1** was obtained

by reaction of **5** with acryloyl chloride. For this, **5** (1 eq.) was dissolved with NEt_3 (2.5 eq.) in DCM [10 mL/g], and the solution was cooled in an ice bath. Acryloyl chloride (1.3 eq.) was then added and the reaction was carried out at room temperature for 2h. After extraction with $NaHCO_3$, **M1** was purified by column chromatography (EE/Hexan 1:1 (*v:v*)).
M1 was deprotected for RP-HPLC and ESI-MS measurements in aqueous atmosphere.

ESI-MS: m/z calculated for $C_9H_{15}NO_6$ $[M+H]^+$ 234.09 and $[M+Na]^+$ 256.08; found $[M+H]^+$ 234.24 and $[M+Na]^+$ 256.05

2.1.1 Analytics

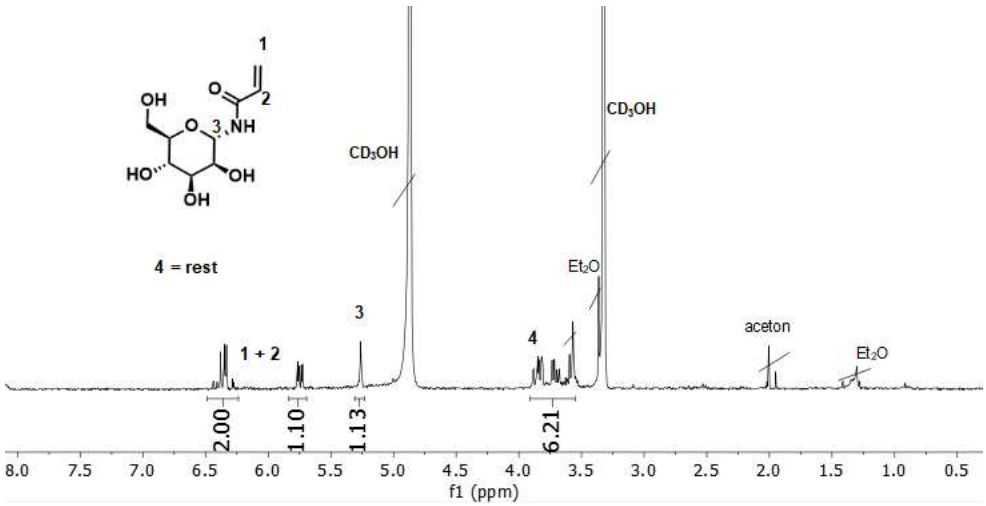

Figure S1. ^1H NMR spectrum (600 MHz, CD_3OD) of M1.

^{1}H-NMR (600 MHz, CD_3OD): δ (ppm) 6.50 – 6.27 (m, 2H), 5.75 (dd, J = 9.2, 2.8 Hz, 1H), 5.26 (d, J = 1.3 Hz, 1H).3.9-3.55 (m, 6H).

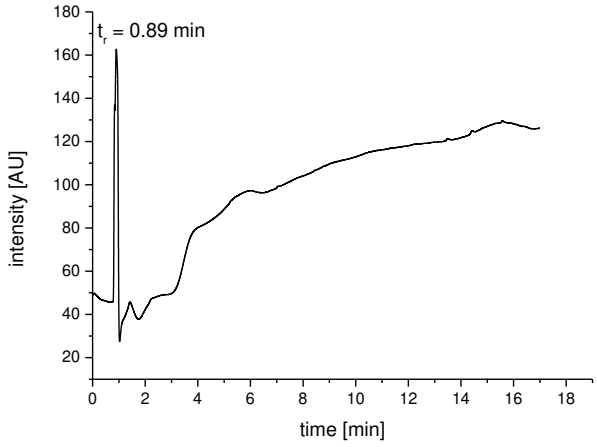

Figure S2. RP-HPLC of M2 (A: 95% H_2O/ 5% MeCN/ 0.1% Formic Acid; 100% A -> 50% A in 30 min): t_r = 0.89 min.

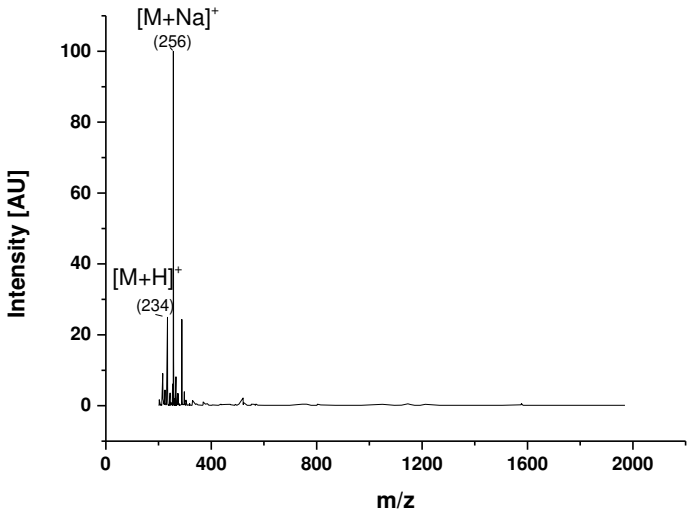

Figure S3. ESI-MS of M1.

2.2 Mannose monomer with linker

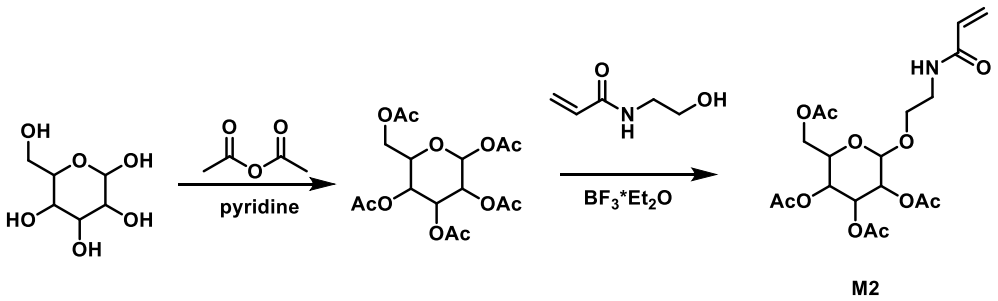

The synthesis of the mannose monomer was adapted by Wilkins *et al*.[1] The acetylated mannoseacrylamide monomer was synthesized by dissolving D-mannose in a mixture of a 1:1 (*v*/*v*) mixture of pyridine/acetic anhydride [20 mL/g] and stirring at room temperature overnight. After diluting with ethylacetate the mixture was extracted three times with 1M HCl solution. Evaporation of ethylacetate resulted in 1,2,3,4,6-penta-O-acetyl-α-D-mannopyranose. Pentaacetylated mannose (1.0 eq.) and N-hydroxyethylacrylamide (1.2 eq.) were dissolved in DCM [2 mL/mmol] and flushed with argon gas for 10 minutes. BF_3*Et_2O (10.0 eq.) was added through a syringe and the mixture stirred at room temperature overnight. The reaction solution was washed three times with brine and the organic phase dried with MgSO4. The solvent was removed, which resulted in pure acetylated mannosemonomer (AcO-ManAAm) with a relative purity of 98 % and a yield of 78 %.

ESI-MS: m/z calculated for $C_{19}H_{27}NO_{11}$ $[M+H]^+$ 446.16 and $[M+Na]^+$ 468.15; found $[M+H]^+$ 446.46 and $[M+H]^+$ 468

2.2.1 Analytics

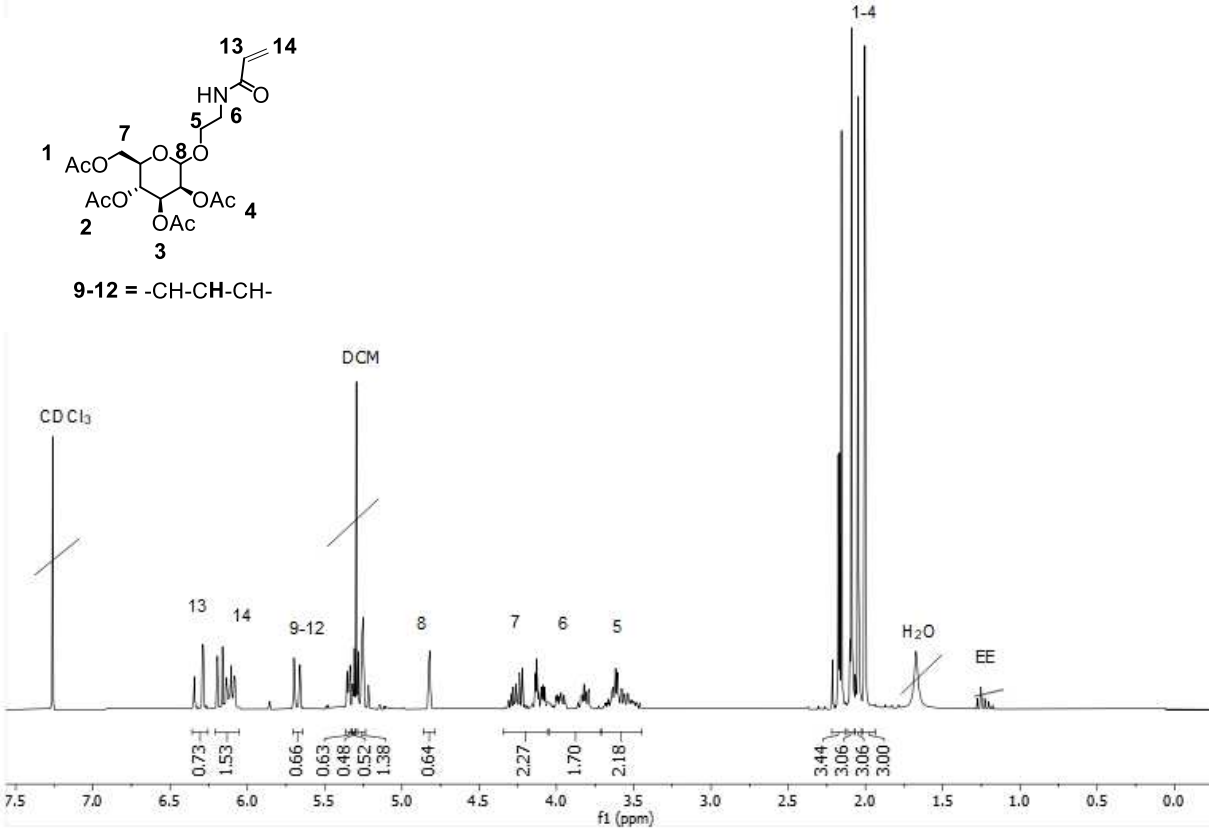

Figure S4. ^{1}H NMR (300 MHz, $CDCl_3$) spectrum of M2.

^{1}H-NMR (300 MHz, $CDCl_3$): δ (ppm) 2.00-2.16 (s, 12H, C**H**$_3$ H1-4), 3.46-3.61 (m, 2H, C**H**$_2$ H5), 3.79-4.02 (m, 2H, C**H**$_2$, H6), 4.06-4.23 (m, 2H, C**H**$_2$, H7), 4.82 (s, 1H, C**H**, H8), 5.22-5.69 (m, 4H, C**H**, H9-12), 6.15 (dd, ^{2}J=10.2 Hz, ^{3}J=17.1 Hz, 2H, C**H**$_2$, H14), 6.32 (dd, ^{2}J=1.2 Hz, ^{3}J=17.1 Hz, 1H C**H**, H13)

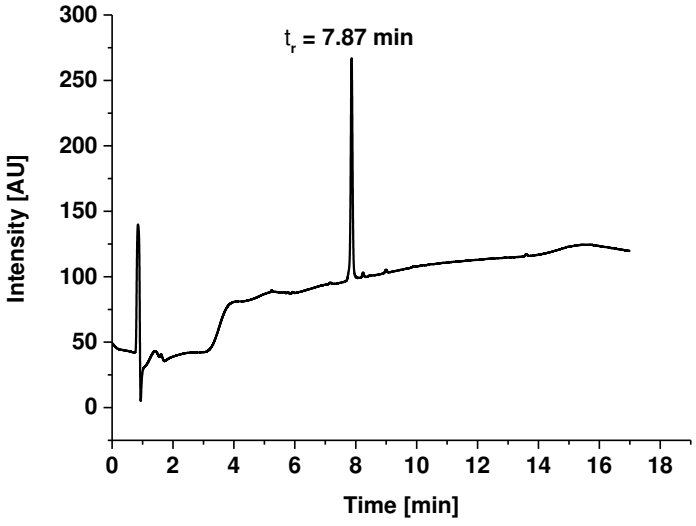

Figure S5. RP-HPLC of M2 (A: 95% H_2O/ 5% MeCN/ 0.1% Formic Acid; 100% A -> 50% A in 30 min): t_r = 7.87 min.

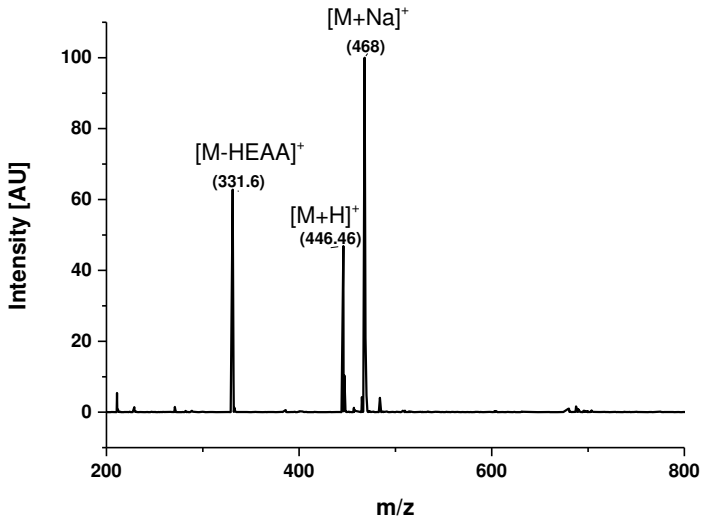

Figure S6. ESI-MS of M2.

3. Polymer Synthesis

3.1 Homopolymersynthesis

GP60-nl

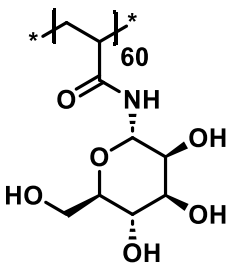

100 mg of monomer M1 (0.4 mmol) and 1.99 mg of TPO (1.4 mol%, 0.0056 mmol) were dissolved in DMF [10 wt.%] and the solution was flushed with Argon for 10 minutes and irradiated with UV-light (405 nm wavelength, with an intensity 45.2 mW/cm^2). After an hour, the irradiation was stopped and 5 mL NaOMe (0.2 M) in MeOH was added to the polymer solution and stirred one hour at room temperature. Solid matter that has already precipitated and the residual solution was precipitated in diethyl ether. The precipitated polymer was dissolved in H_2O, dialyzed against distilled water (three cycles, 2 kDa) and subsequently lyophilized.

3. Polymer Synthesis

GP-10-OH

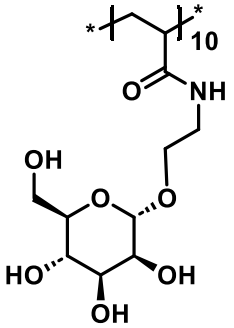

222.7 mg of monomer M2 (0.5 mmol) and TPO (10 mol%, 0.05 mmol) were dissolved in DMF [10 wt.%] and the solution was flushed with Argon for 10 minutes and irradiated with UV-light (405 nm wavelength, with an intensity 45.2 mW/cm^2). After an hour, the irradiation was stopped and 5 mL NaOMe (0.2 M) in MeOH was added to the polymer solution and stirred one hour at room temperature. Solid matter that has already precipitated and the residual solution was precipitated in diethyl ether. The precipitated polymer was dissolved in H_2O, dialyzed against distilled water (three cycles, 2 kDa) and subsequently lyophilized.

GP-30-OH

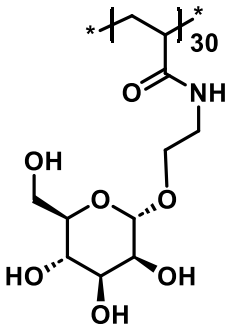

222.7 mg of monomer M2 (0.5 mmol) and TPO (3 mol%, 0.015 mmol) were dissolved in DMF [10 wt.%] and the solution was flushed with Argon for 10 minutes and irradiated with UV-light (405 nm wavelength, with an intensity 45.2 mW/cm^2). After an hour, the irradiation was stopped and 5 mL NaOMe (0.2 M) in MeOH was added to the polymer solution and stirred one hour at room temperature. Solid matter that has already precipitated and the residual solution was precipitated in diethyl ether. The precipitated polymer was dissolved in H_2O, dialyzed against distilled water (three cycles, 2 kDa) and subsequently lyophilized.

3. Polymer Synthesis

GP-70-OH

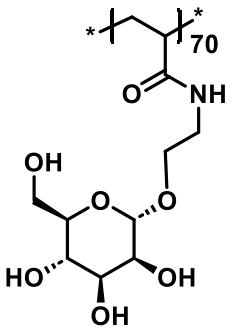

222.7 mg of monomer M2 (0.5 mmol) and TPO (1.4 mol%, 0.007 mmol) were dissolved in DMF [10 wt.%] and the solution was flushed with Argon for 10 minutes and irradiated with UV-light (405 nm wavelength, with an intensity 45.2 mW/cm^2). After an hour, the irradiation was stopped and 5 mL NaOMe (0.2 M) in MeOH was added to the polymer solution and stirred one hour at room temperature. Solid matter that has already precipitated and the residual solution was precipitated in diethyl ether. The precipitated polymer was dissolved in H_2O, dialyzed against distilled water (three cycles, 2 kDa) and subsequently lyophilized.

GP-200-OH

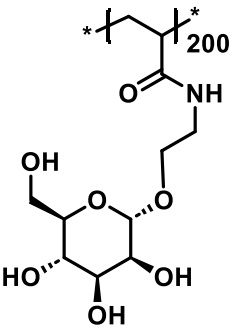

445.4 mg of monomer M2 (1 mmol) and TPO (0.5 mol%, 0.005 mmol) were dissolved in DMF [10 wt.%] and the solution was flushed with Argon for 10 minutes and irradiated with UV-light (405 nm wavelength, with an intensity 45.2 mW/cm^2). After an hour, the irradiation was stopped and 5 mL NaOMe (0.2 M) in MeOH was added to the polymer solution and stirred one hour at room temperature. Solid matter that has already precipitated and the residual solution was precipitated in diethyl ether. The precipitated polymer was dissolved in H_2O, dialyzed against distilled water (three cycles, 2 kDa) and subsequently lyophilized.

GP-300-OH

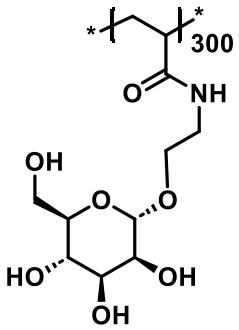

445.4 mg of monomer M2 (1 mmol) and TPO (0.33 mol%, 0.0033 mmol) were dissolved in DMF [10 wt.%] and the solution was flushed with Argon for 10 minutes and irradiated with UV-light (405 nm wavelength, with an intensity 45.2 mW/cm^2). After an hour, the irradiation was stopped and 5 mL NaOMe (0.2 M) in MeOH was added to the polymer solution and stirred one hour at room temperature. Solid matter that has already precipitated and the residual solution was precipitated in diethyl ether. The precipitated polymer was dissolved in H_2O, dialyzed against distilled water (three cycles, 2 kDa) and subsequently lyophilized.

GP-800-OH

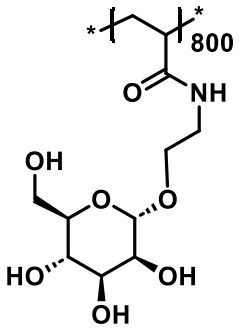

890.8 mg of monomer M2 (2 mmol) and TPO (0.12 mol%, 0.0025 mmol) were dissolved in DMF [10 wt.%] and the solution was flushed with Argon for 10 minutes and irradiated with UV-light (405 nm wavelength, with an intensity 45.2 mW/cm^2). After an hour, the irradiation was stopped and 5 mL NaOMe (0.2 M) in MeOH was added to the polymer solution and stirred one hour at room temperature. Solid matter that has already precipitated and the residual solution was precipitated in diethyl ether. The precipitated polymer was dissolved in H_2O, dialyzed against distilled water (three cycles, 2 kDa) and subsequently lyophilized.

PHEAA-200-OH

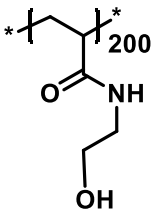

1151.3 mg of N-hydroxyethylacrylamide (10 mmol) and TPO (0.5 mol%, 0.005 mmol) were dissolved in DMF [10 wt.%] and the solution was flushed with Argon for 10 minutes and irradiated with UV-light (405 nm wavelength, with an intensity 45.2 mW/cm^2). After an hour, the irradiation was stopped and the solution was precipitated in diethyl ether. The precipitated polymer was dissolved in H_2O, dialyzed against distilled water (three cycles, 2 kDa) and subsequently lyophilized.

3.1.2 Analytics

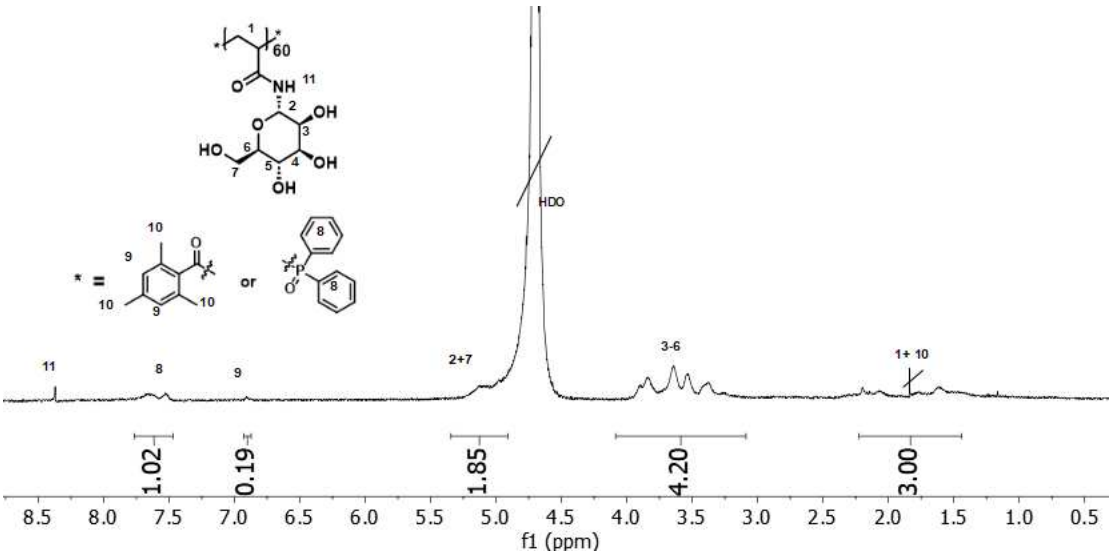

Figure S7. ^{1}H NMR spectrum (600 MHz, D_2O) of GP-60-OH-nl.

^{1}H-NMR (600 MHz, D_2O) δ [ppm] 7.79-7.59 (m, **8**), 7.00-6.99 (m, **9**), 5.31-4.89 (m, **2+7,** D_2O overlapping), 4.01-3.15 (m, **3-6**), 2.32-1.33 (m, **1+10**).

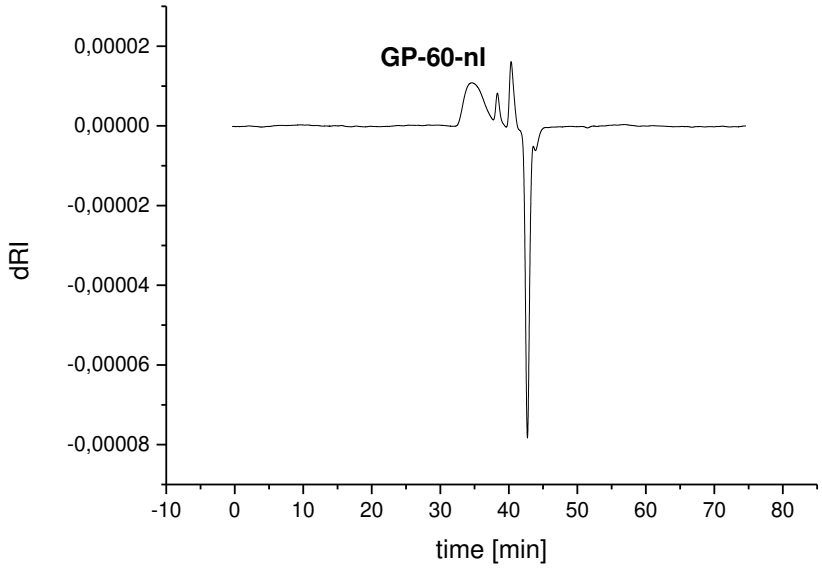

Figure S8. H_2O-SEC spectrum of GP-60-OH-nl.

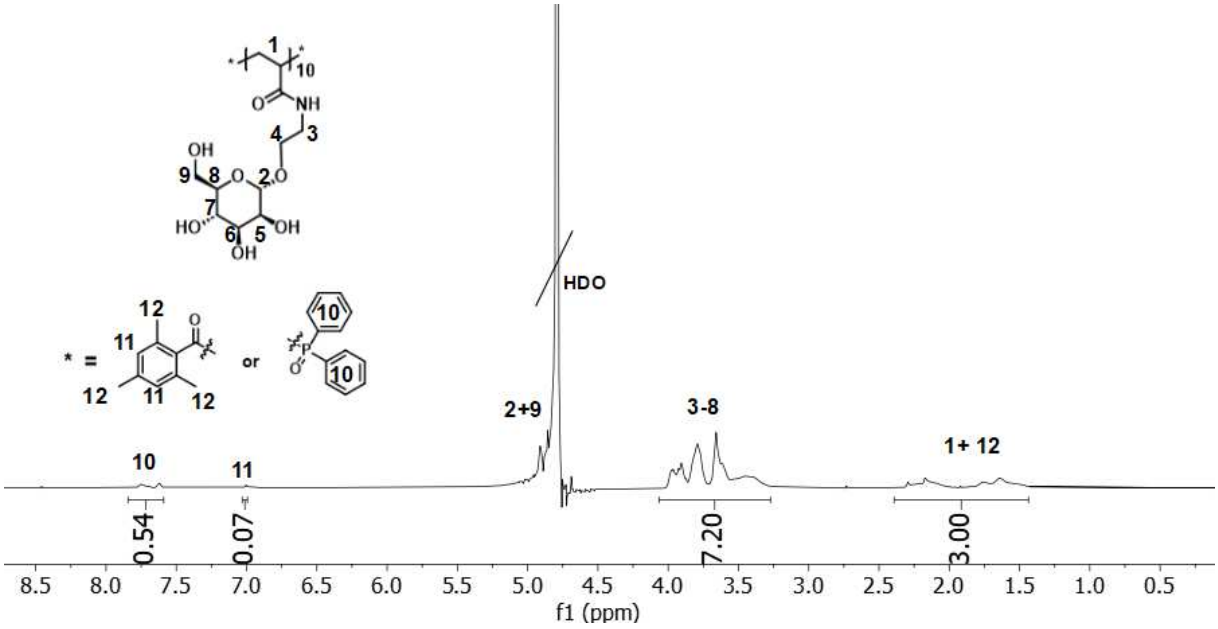

Figure S9. ^1H NMR spectrum (600 MHz, D_2O) of GP-10-OH.

^1H-NMR (600 MHz, D_2O) δ [ppm] 7.79-7.59 (m, **10**), 7.00-6.99 (m, **11**), 5.00-4.83 (m, **2+9,** D_2O overlapping), 4.04-3.27 (m, **3-8**), 1.42-1.32 (m, **1+12**).

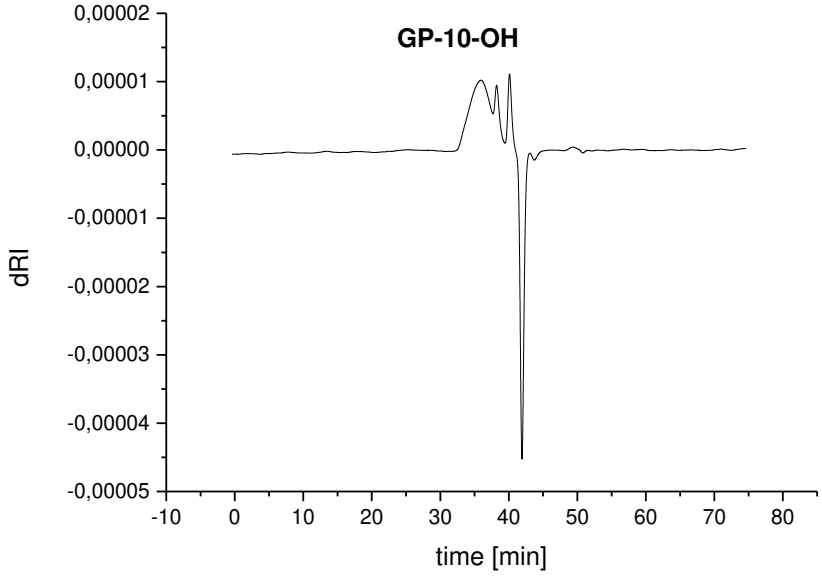

Figure S10. H_2O-SEC spectrum of GP-10-OH.

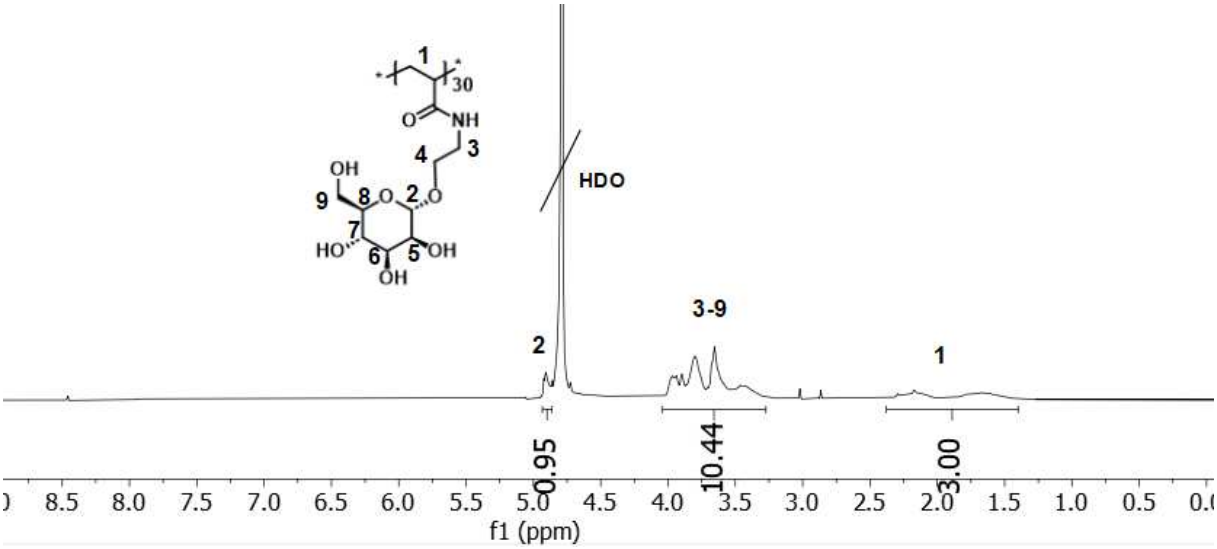

Figure S11. ^1H NMR spectrum (600 MHz, D_2O) of GP-30-OH.

^1H-NMR (600 MHz, D_2O) δ [ppm] 4.93-4.88 (m, **2,** D_2O overlapping), 4.04-3.25 (m, **3-9**), 2.37-1.38 (m, **1**).

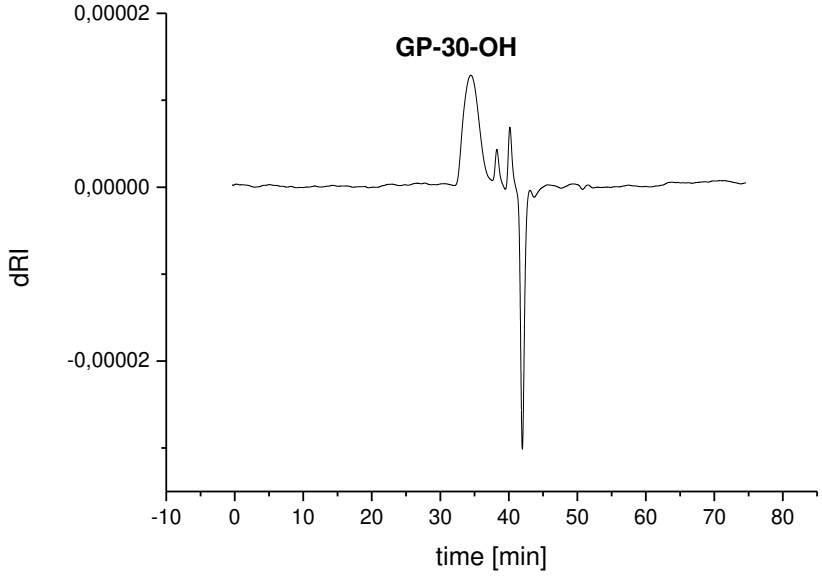

Figure S12. H_2O-SEC spectrum of GP-30-OH.

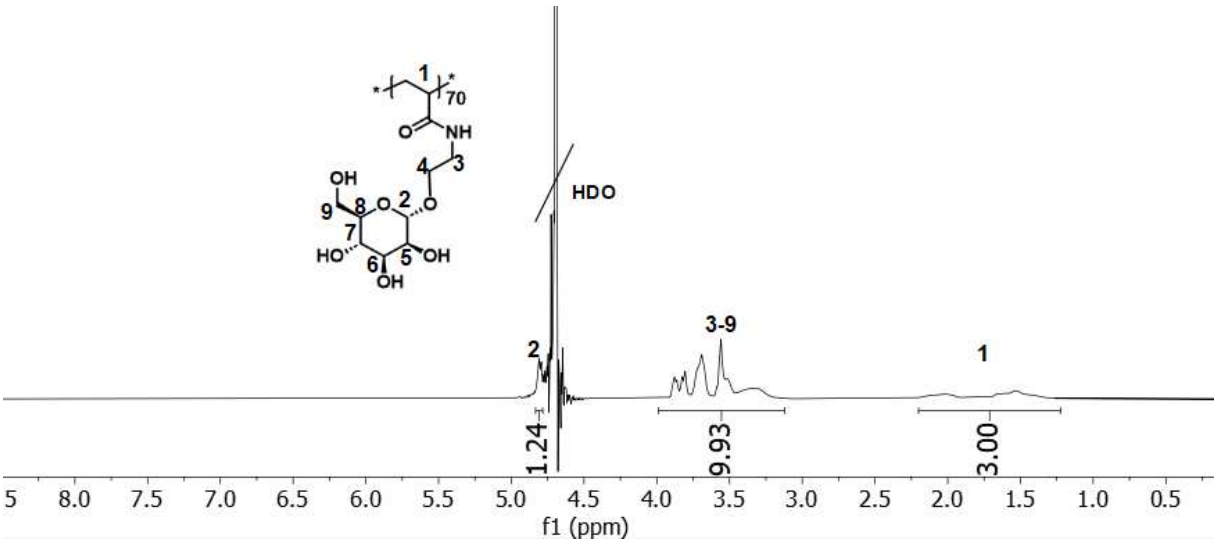

Figure S13. ^{1}H NMR spectrum (600 MHz, D_2O) of GP-70-OH.

^{1}H-NMR (600 MHz, D_2O) δ [ppm] 4.85-4.77 (m, **2,** D_2O overlapping), 3.98-3.11 (m, **3-9**), 2.19-1.22 (m, **1**).

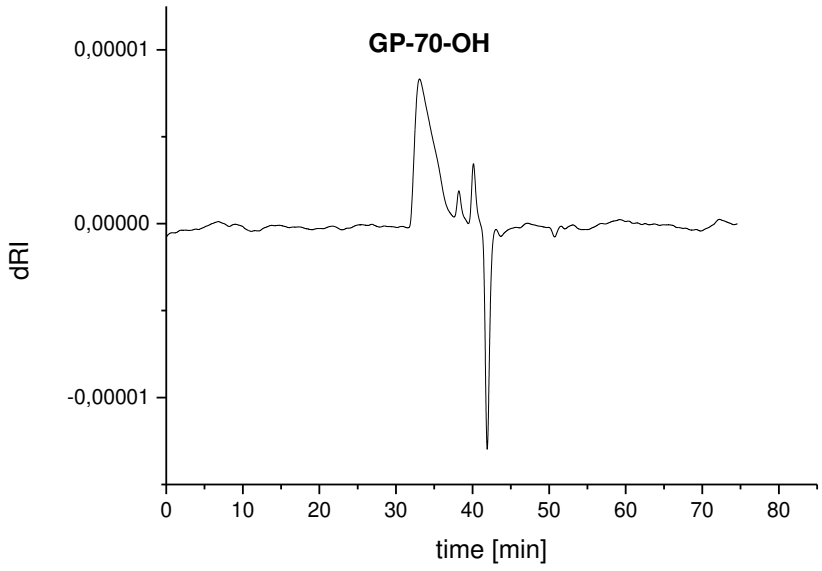

Figure S14. H_2O-SEC spectrum of GP-30-OH.

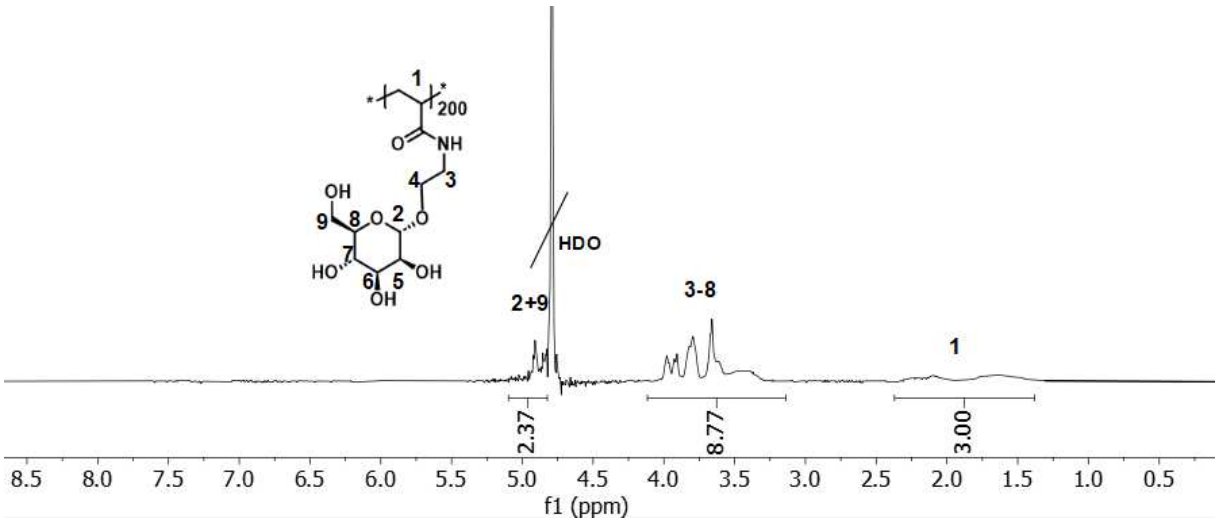

Figure S15. ^{1}H NMR spectrum (600 MHz, D_2O) of GP-200-OH.

^{1}H-NMR (600 MHz, D_2O) δ [ppm] 5.00-4.83 (m, **2+9,** D_2O overlapping), 4.1-3.21 (m, **3-8**), 2.35-1.38 (m, **1**).

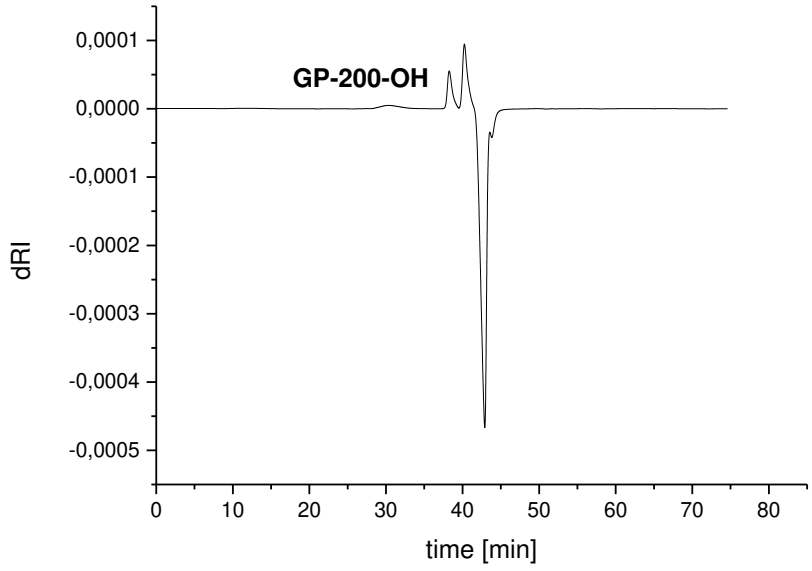

Figure S16. H_2O-SEC spectrum of GP-200-OH.

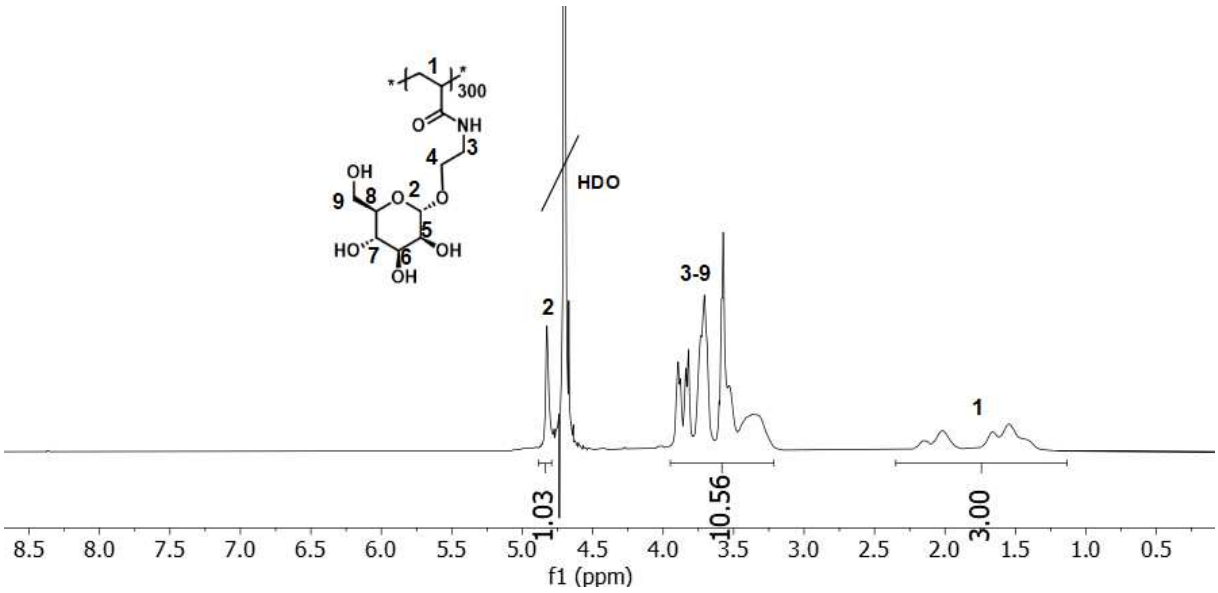

Figure S17. ^{1}H NMR spectrum (600 MHz, D_2O) of GP-300-OH.

^{1}H-NMR (600 MHz, D_2O) δ [ppm] 4.87-4.79 (m, **2,** D_2O overlapping), 3.95-3.2 (m, **3-9**), 2.3-1.19 (m, **1**).

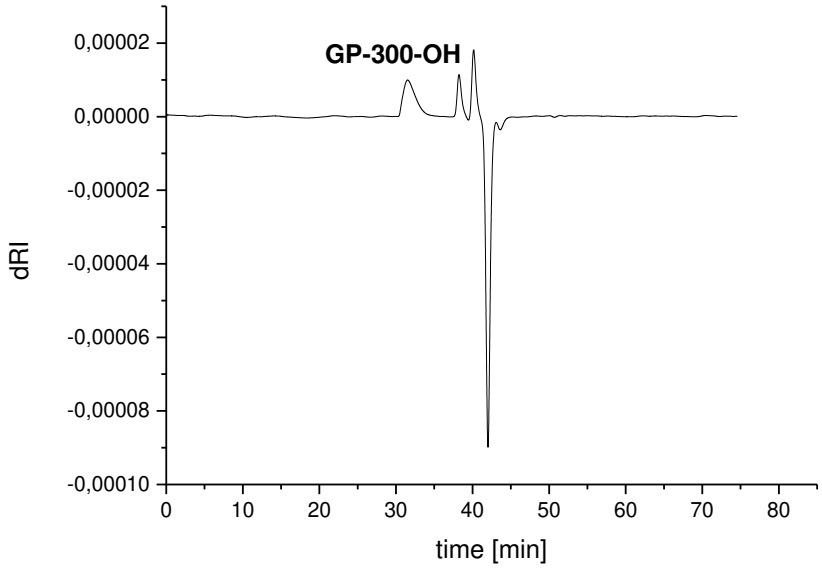

Figure S18. H_2O-SEC spectrum of GP-300-OH.

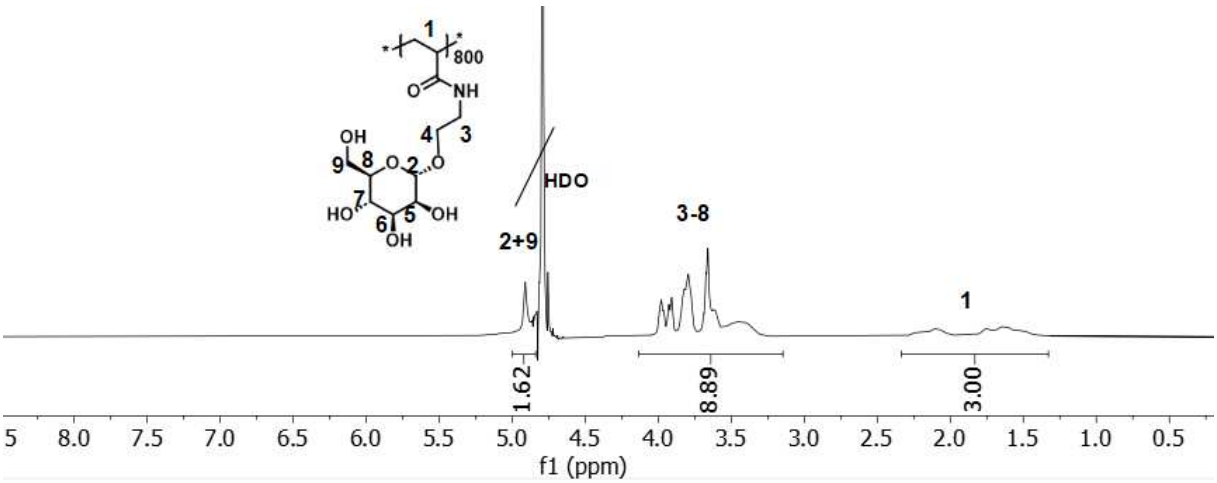

Figure S19. ^{1}H NMR spectrum (600 MHz, D_2O) of GP-800-OH.

^{1}H-NMR (600 MHz, D_2O) δ [ppm] 5.00-4.83 (m, **2+9,** D_2O overlapping), 4.07-3.24 (m, **3-8**), 2.3-1.32 (m, **1**).

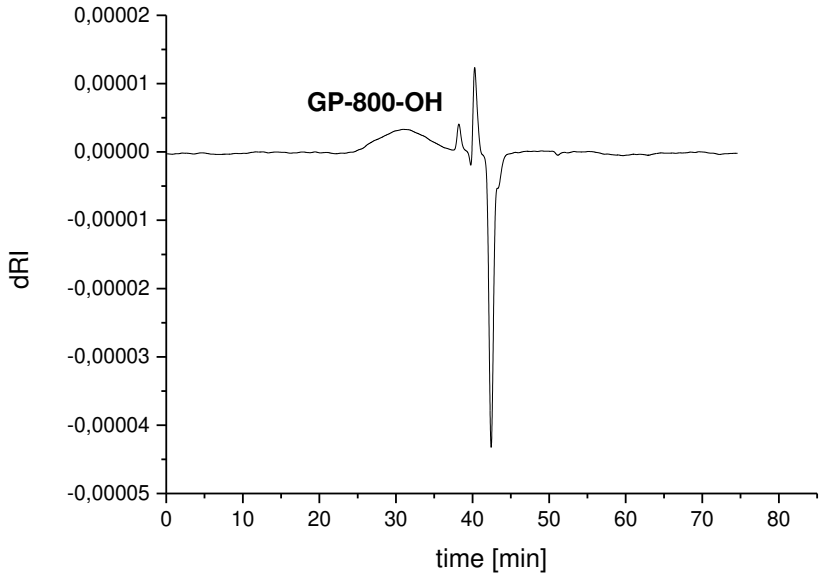

Figure S20. H_2O-SEC spectrum of GP-800-OH.

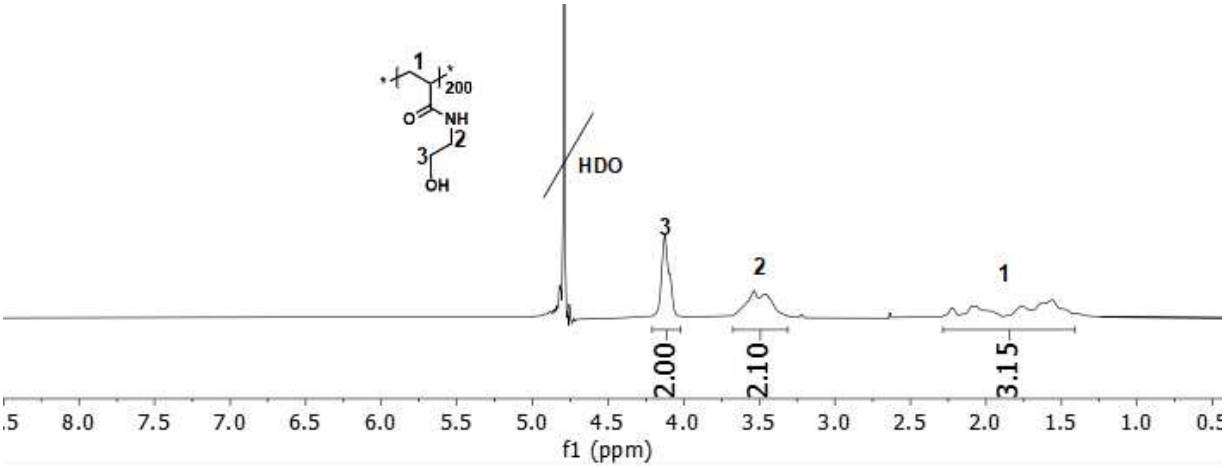

Figure S21. ^{1}H NMR spectrum (600 MHz, D_2O) of PHEAA-200-OH.

^{1}H-NMR (600 MHz, D_2O) δ [ppm] 4.18-4.02 (m, **3**), 3.64-3.30 (m, **2**), 2.25-1.36 (m, **1**).

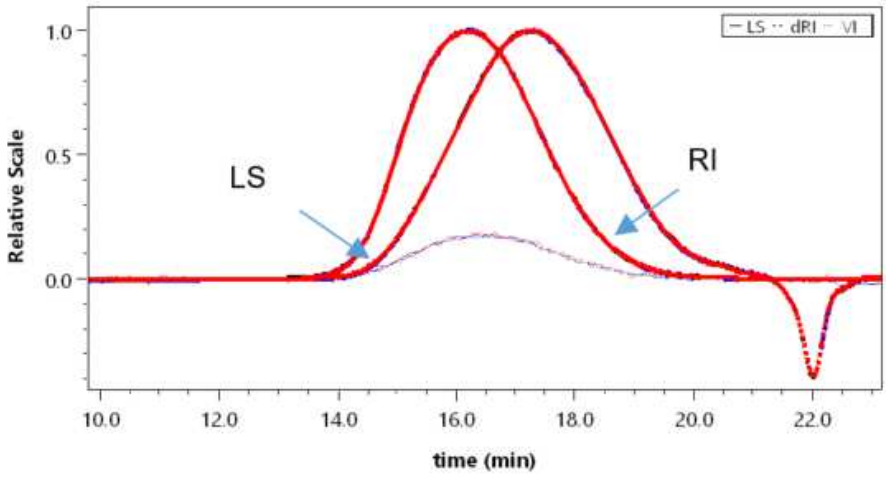

Figure 22. H_2O-SEC-MALS and H_2O-RI-SEC spectra (measured at Leibniz Insitute of polymer research in Dresden) of PHEAA-200-OH.

3.2 Copolymersynthesis

coGP-70-OH (30%)

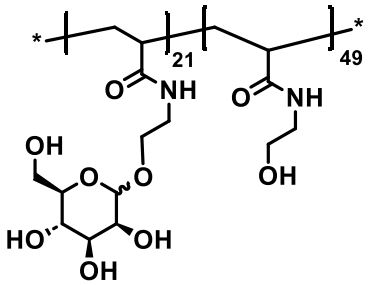

133.6 mg of monomer M2 (0.3 mmol), 80.6 mg of HEAA (0.7 mmol) and TPO (1.4 mol%, 0.007 mmol) were dissolved in DMF [10 wt.%] and the solution was flushed with Argon for 10 minutes and irradiated with UV-light (405 nm wavelength, with an intensity 45.2 mW/cm^2). After an hour, the irradiation was stopped and 5 mL NaOMe (0.2 M) in MeOH was added to the polymer solution and stirred one hour at room temperature. Solid matter that has precipitated and the residual solution that was precipitated in diethyl ether were collected. The precipitated polymer was dissolved in H_2O, dialyzed against distilled water (three cycles, 2 kDa) and subsequently lyophilized.

3. Polymer Synthesis

coGP-70-OH (50%)

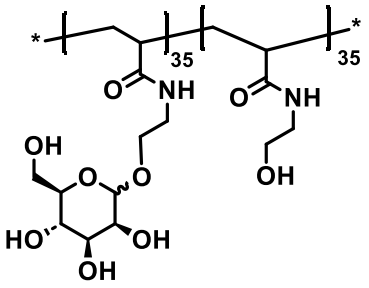

222.7 mg of monomer M2 (0.5 mmol), 57.56 mg of HEAA (0.5 mmol) and TPO (1.4 mol%, 0.007 mmol) were dissolved in DMF [10 wt.%] and the solution was flushed with Argon for 10 minutes and irradiated with UV-light (405 nm wavelength, with an intensity 45.2 mW/cm^2). After an hour, the irradiation was stopped and 5 mL NaOMe (0.2 M) in MeOH was added to the polymer solution and stirred one hour at room temperature. Solid matter that has precipitated and the residual solution that was precipitated in diethyl ether were collected. The precipitated polymer was dissolved in H_2O, dialyzed against distilled water (three cycles, 2 kDa) and subsequently lyophilized.

coGP-70-OH (70%)

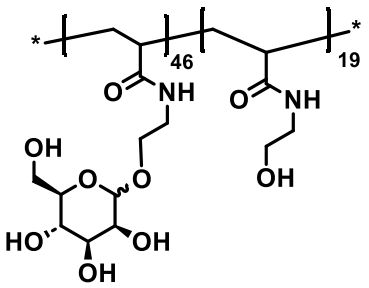

311.8 mg of monomer M2 (0.7 mmol), 34.54 mg of HEAA (0.3 mmol) and TPO (1.4 mol%, 0.007 mmol) were dissolved in DMF [10 wt.%] and the solution was flushed with Argon for 10 minutes and irradiated with UV-light (405 nm wavelength, with an intensity 45.2 mW/cm^2). After an hour, the irradiation was stopped and 5 mL NaOMe (0.2 M) in MeOH was added to the polymer solution and stirred one hour at room temperature. Solid matter that has precipitated and the residual solution that was precipitated in diethyl ether were collected. The precipitated polymer was dissolved in H_2O, dialyzed against distilled water (three cycles, 2 kDa) and subsequently lyophilized.

3. Polymer Synthesis

coGP-300-OH (50%)

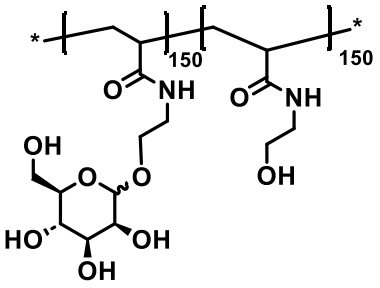

445.4 mg of monomer M2 (1 mmol), 115.13 mg of HEAA (1 mmol) and TPO (0.33 mol%, 0.006 mmol) were dissolved in DMF [10 wt.%] and the solution was flushed with argon for 10 minutes and irradiated with UV-light (405 nm wavelength, with an intensity 45.2 mW/cm^2). After an hour, the irradiation was stopped and 5 mL NaOMe (0.2 M) in MeOH was added to the polymer solution and stirred one hour at room temperature. Solid matter that has precipitated and the residual solution that was precipitated in diethyl ether were collected. The precipitated polymer was dissolved in H_2O, dialyzed against distilled water (three cycles, 2 kDa) and subsequently lyophilized.

3.2.1 Analytics

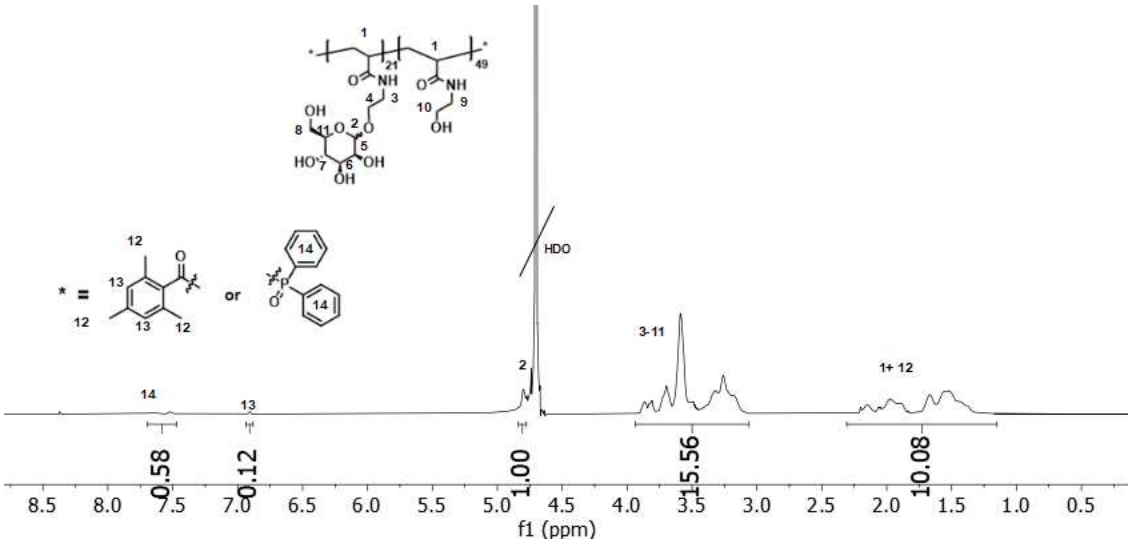

Figure S23. ^{1}H NMR spectrum (600 MHz, D_2O) of coGP-70 (30%)-OH.

^{1}H-NMR (600 MHz, D_2O) δ [ppm] 7.79-7.59 (m, **14**), 7.00-6.99 (m, **13**), 4.82-4.80 (m, **2,** D_2O overlapping), 3.93-3.04 (m, **3-11**), 2.20-1.17 (m, **1+12**).

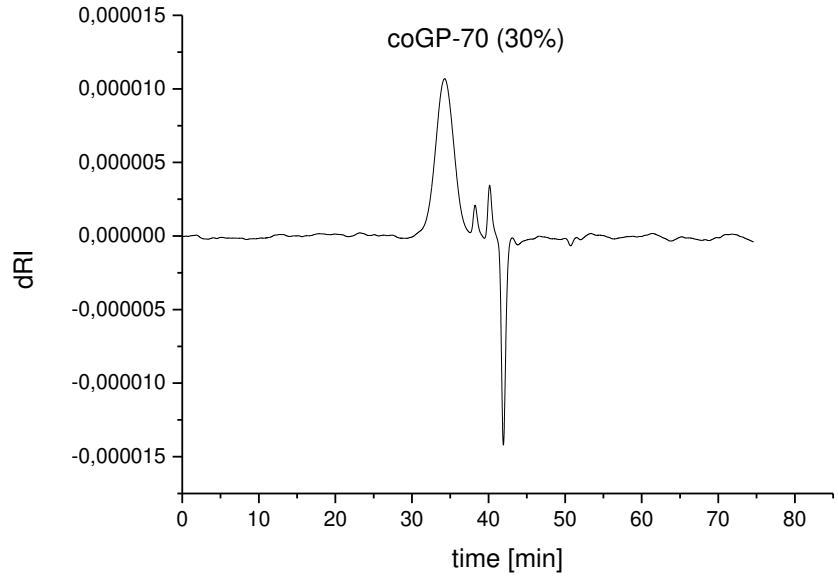

Figure S24. H_2O-SEC spectrum of coGP-70 (30%)-OH.

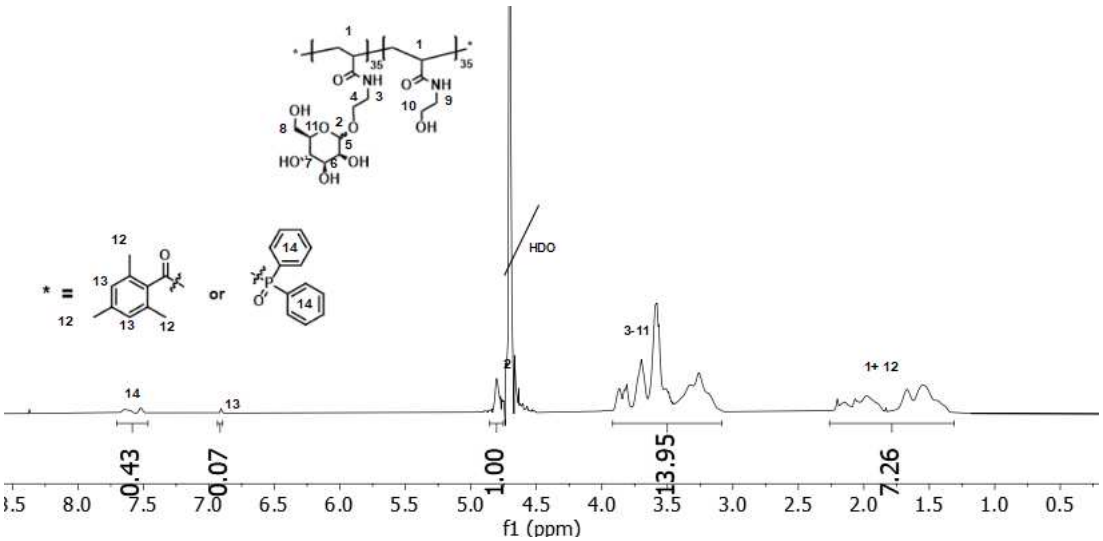

Figure S25. ^{1}H NMR spectrum (600 MHz, D_2O) of coGP-70 (50%)-OH.

^{1}H-NMR (600 MHz, D_2O) δ [ppm] 7.79-7.59 (m, **14**), 7.00-6.99 (m, **13**), 4.82-4.80 (m, **2,** D_2O overlapping), 3.93-3.04 (m, **3-11**), 2.20-1.17 (m, **1+12**).

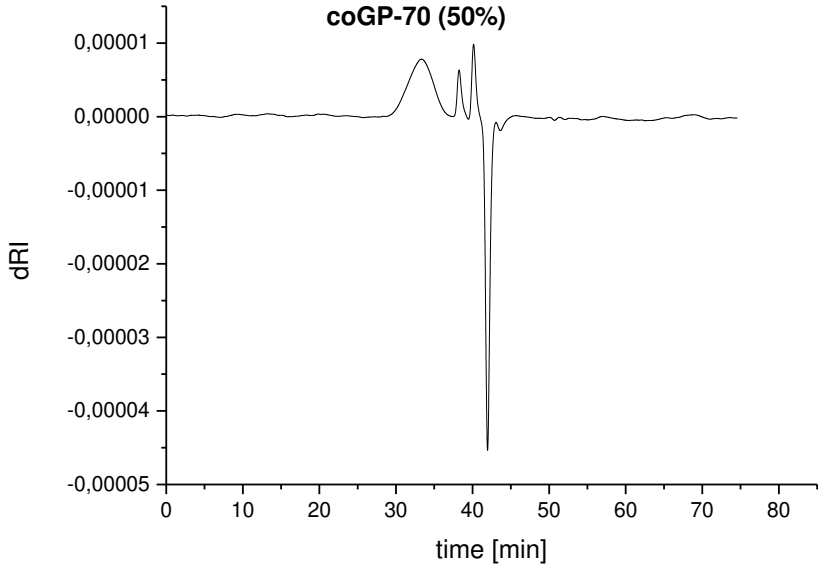

Figure S26. H_2O-SEC spectrum of coGP-70 (50%)-OH.

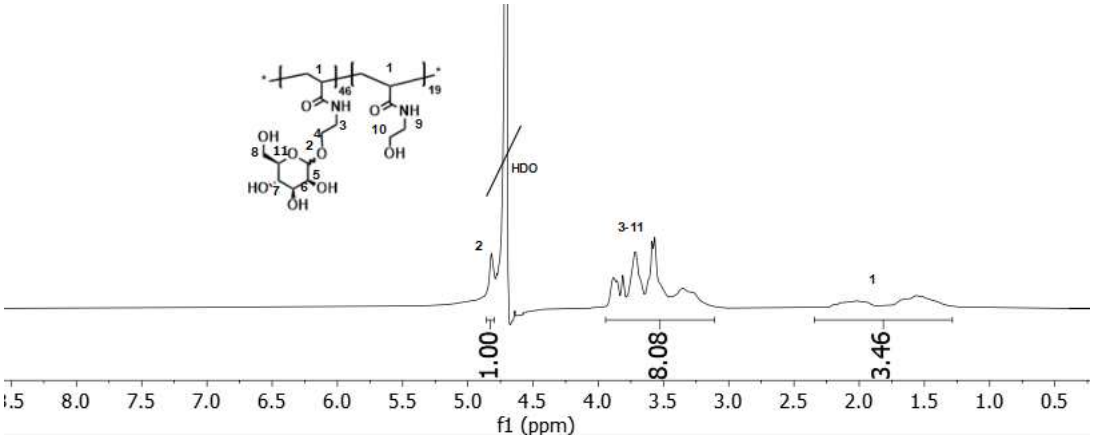

Figure S27. ^{1}H NMR spectrum (600 MHz, D_2O) of coGP-70 (70%)-OH.

^{1}H-NMR (600 MHz, D_2O) δ [ppm] 4.82-4.80 (m, **2,** D_2O overlapping), 3.95-3.13 (m, **3-11**), 2.34-1.29 (m, **1**).

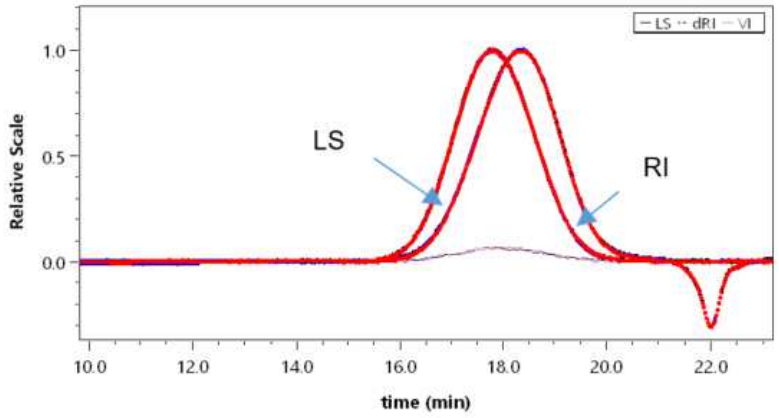

Figure 28. H_2O-SEC-MALS and H_2O-RI-SEC spectra (measured at Leibniz Insitute of polymer research in Dresden) of coGP-70 (70%)-OH

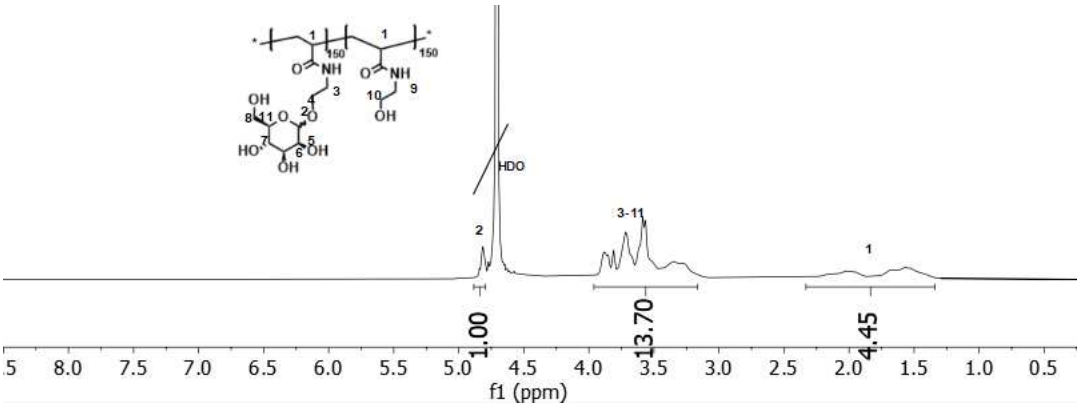

Figure S29. ^{1}H NMR spectrum (600 MHz, D_2O) of coGP-300 (50%)-OH.

^{1}H-NMR (600 MHz, D_2O) δ [ppm] 4.82-4.80 (m, **2,** D_2O overlapping), 3.97-3.10 (m, **3-11**), 2.34-1.31 (m, **1**).

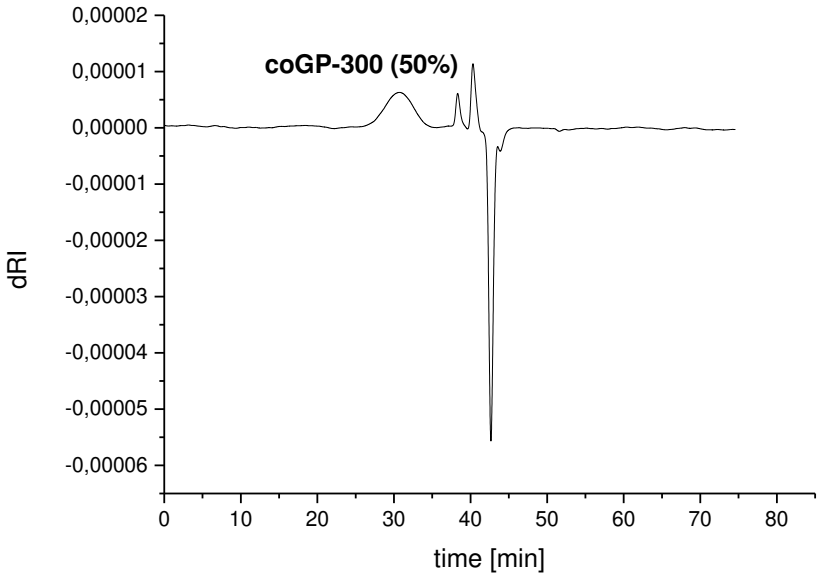

Figure S30. H_2O-SEC spectrum of coGP-300 (50%)-OH.

4. Sulfation of Glycopolymers

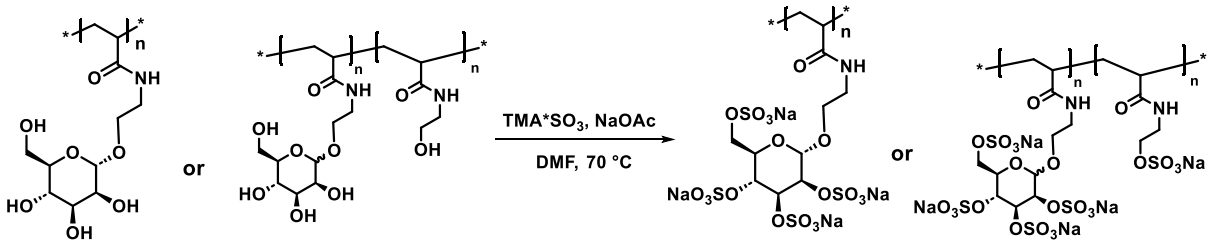

Sulfation of glycopolymers and glycol copolymers was performed as in an earlier published protocol.[2] TMA*SO3 (40 eq. per OH-group) was used as a sulfating agent and dissolved with the polymer in DMF and stirred for 18h at 70°C. After the solution was cooled down to room temperature, 20 eq. of aqueous sodium acetate solution (20 %) was added for quenching at 0°C. The solvent mixture was evaporated under reduced pressure, dialyzed (MWCO 5-10 kDa) and lyophilized.

The degree of sulfation was determined via elemental analysis. Theoretical values were calculated for 100% sulfation (without considering the end groups) and the degree of sulfation was calculated from the obtained values. For this purpose, the S/C ratio was calculated for optimal (100%) sulfation and also the S/C ratio was calculated for actual sulfatization. $((S/C)_{actual}/(S/C)_{optimal})*100$ forms the actual degree of sulfation.

4. Sulfation of Glycopolymers

4.1 Analytics

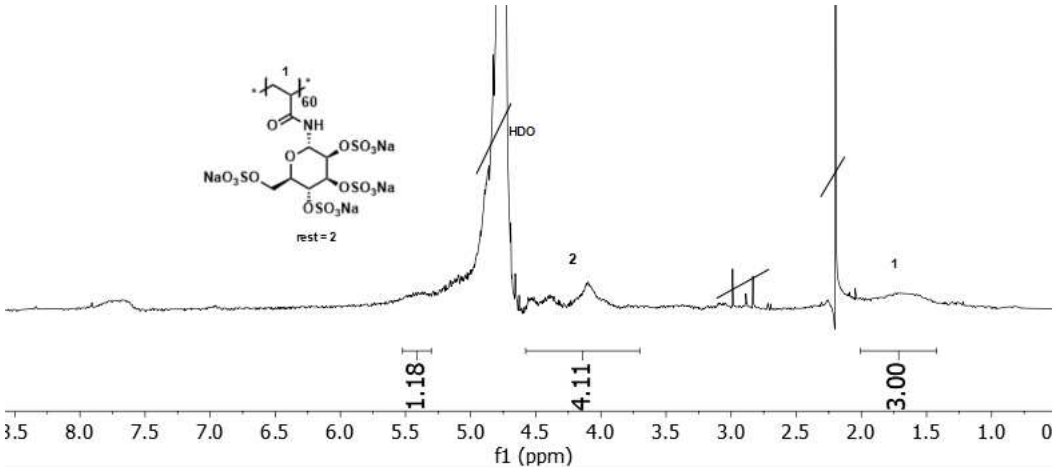

Figure S31. ^{1}H NMR spectrum (600 MHz, D_2O) of GP-70-nl.

^{1}H-NMR (600 MHz, D_2O) δ [ppm] 5.51-3.68 (m, **2**, D_2O overlapping), 1.98-1.42 (m, **1**).

<u>Elemental analysis GP-70-nl:</u>

theoretical values (n=60): %C=17.19; %H=1.76; %N=2.17; %S=19.88

measured values (n=60): %C=21.40; %H=3.52; %N=2.67; %S=16.74

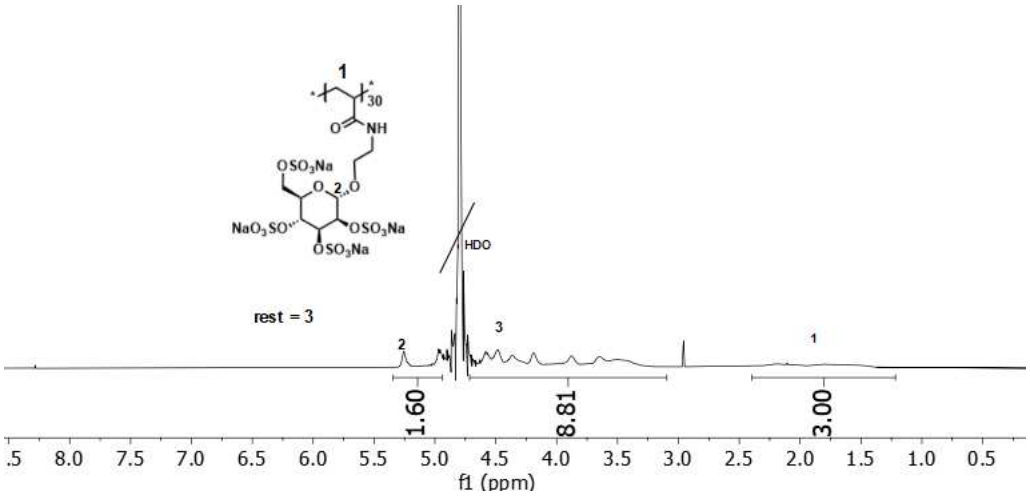

Figure S32. ^{1}H NMR spectrum (600 MHz, D_2O) of GP-30.

^{1}H-NMR (600 MHz, D_2O) δ [ppm] 5.29-5.18 (m, **2**), 5.01-3.23 (m, **3**, D_2O overlapping), 2.40-1.23 (m, **1**).

<u>Elemental analysis GP-30:</u>

theoretical values (n=30): %C=19.27; %H=2.21; %N=2.04; %S=18.71

measured values (n=30): %C=18.48; %H=3.34; %N=2.28; %S=16.57

4. Sulfation of Glycopolymers

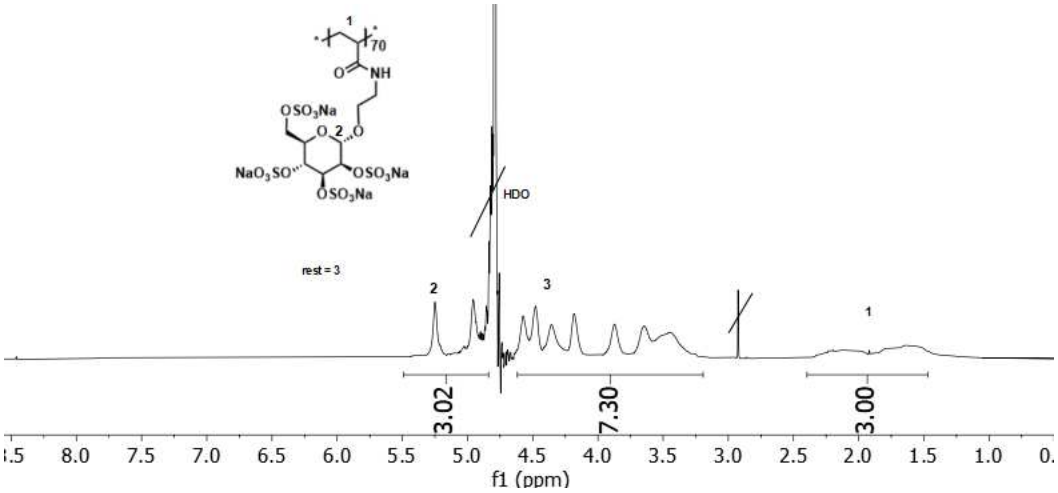

Figure S33. ^{1}H NMR spectrum (600 MHz, D_2O) of GP-70.

^{1}H-NMR (600 MHz, D_2O) δ [ppm] 5.30-5.18 (m, **2**), 5.09-3.22 (m, **3**, D_2O overlapping), 2.38-1.38 (m, **1**).

Elemental analysis GP-70:

theoretical values (n=70): %C=19.27; %H=2.21; %N=2.04; %S=18.71

measured values (n=70): %C=17.23; %H=3.34; %N=1.74; %S=15.51

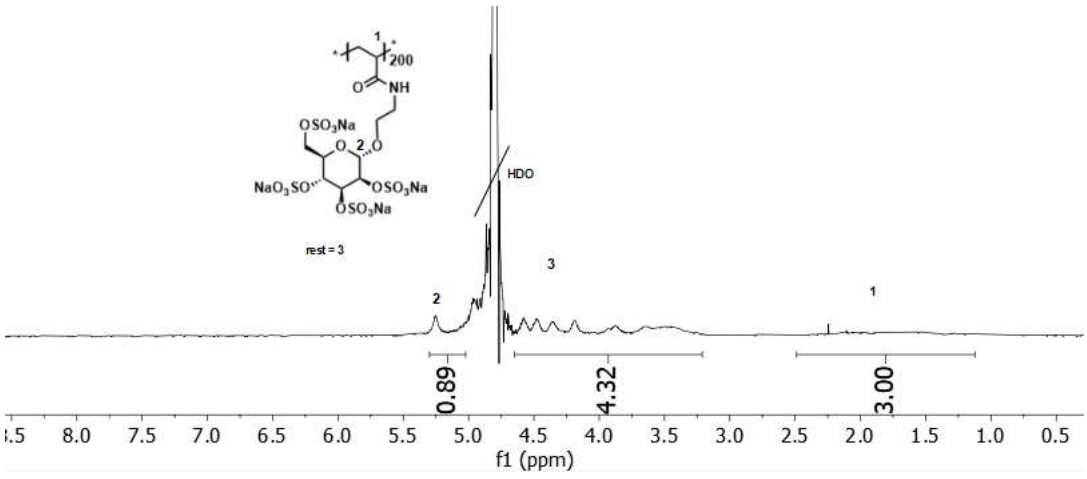

Figure S34. ^{1}H NMR spectrum (600 MHz, D_2O) of GP-200.

^{1}H-NMR (600 MHz, D_2O) δ [ppm] 5.30-5.18 (m, **2**), 5.05-3.19 (m, **3**, D_2O overlapping), 2.46-1.12 (m, **1**).

Elemental analysis GP-200:

theoretical values (n=200): %C=19.27; %H=2.21; %N=2.04; %S=18.71

measured values (n=200): %C=17.56; %H=3.11; %N=1.96; %S=15.28

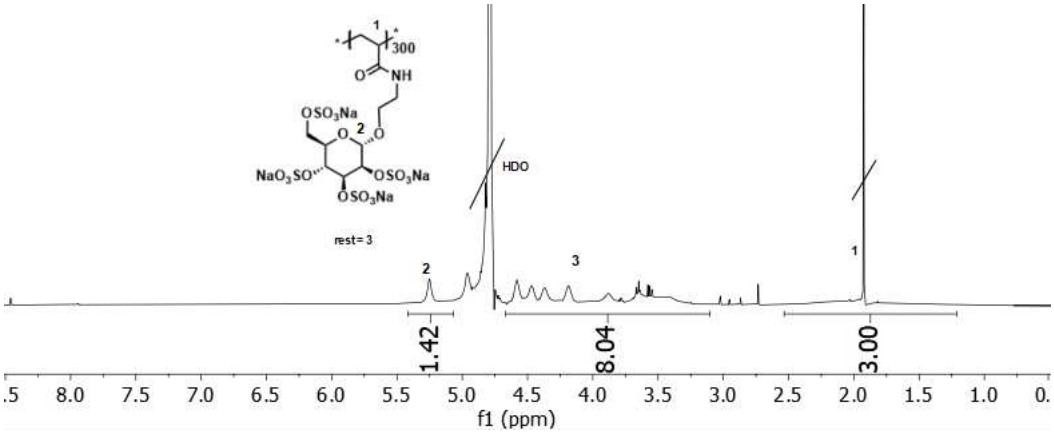

Figure S35. ^{1}H NMR spectrum (600 MHz, D_2O) of GP-300.

^{1}H-NMR (600 MHz, D_2O) δ [ppm] 5.32-5.21 (m, **2**), 5.04-3.14 (m, **3**, D_2O overlapping), 2.50-1.22 (m, **1**).

Elemental analysis GP-300:

theoretical values (n=300): %C=19.27; %H=2.21; %N=2.04; %S=18.71

measured values (n=300): %C=17.71; %H=3.28; %N=1.74; %S=16.20

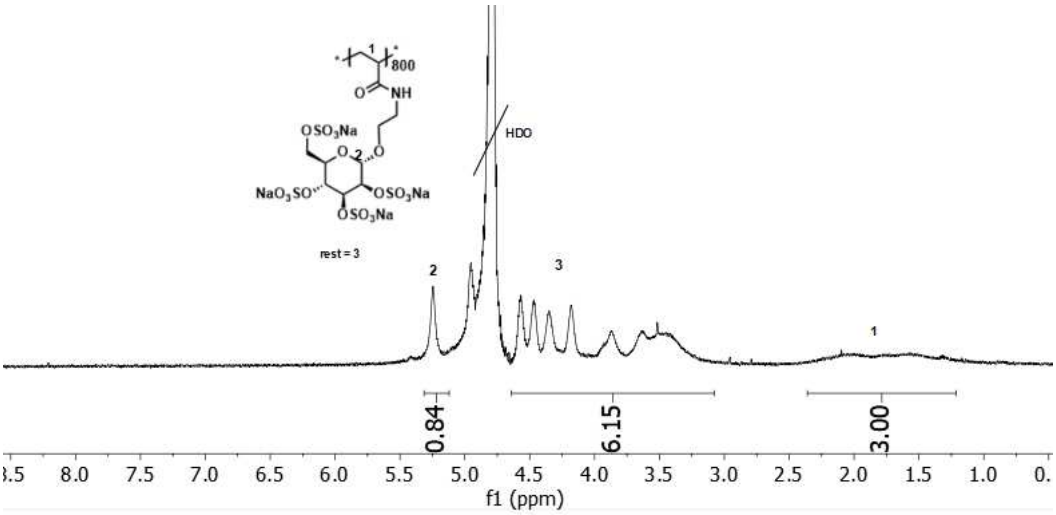

Figure S36. ^{1}H NMR spectrum (600 MHz, D_2O) of GP-800.

^{1}H-NMR (600 MHz, D_2O) δ [ppm] 5.30-5.18 (m, **2**), 5.02-3.11 (m, **3**, D_2O overlapping), 2.35-1.23 (m, **1**).

Elemental analysis GP-800:

theoretical values (n=800): %C=19.27; %H=2.21; %N=2.04; %S=18.71

measured values (n=800): %C=18.31; %H=2.87; %N=2.05; %S=15.21

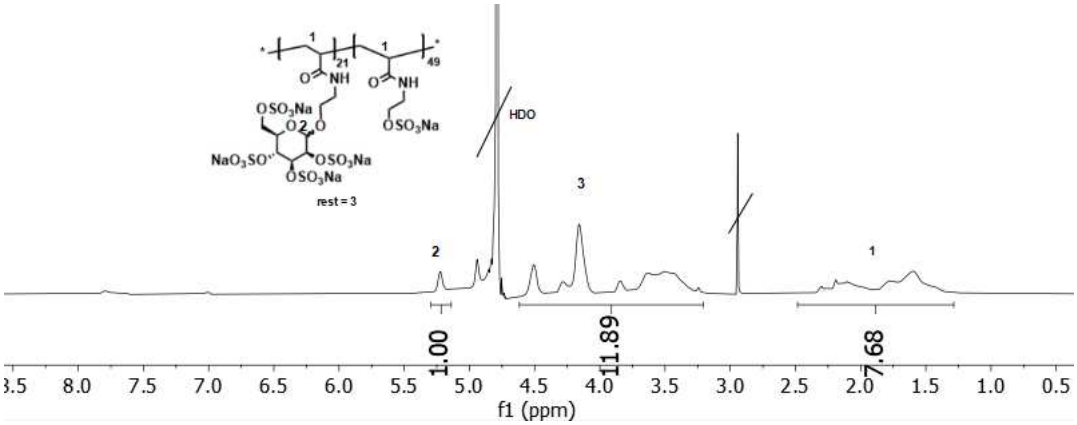

Figure S37. ^{1}H NMR spectrum (600 MHz, D_2O) of coGP-70 (30%).

^{1}H-NMR (600 MHz, D_2O) δ [ppm] 5.27-5.17 (m, **2**), 4.96-3.21 (m, **3**, D_2O overlapping), 2.42-1.31 (m, **1**).

Elemental analysis coGP-70 (30%):

theoretical values (n=21, m=49): %C=22.84; %H=2.85; %N=3.92; %S=17.03

measured values (n=21, m=49): %C=20.91; %H=4.04; %N=3.41; %S=13.43

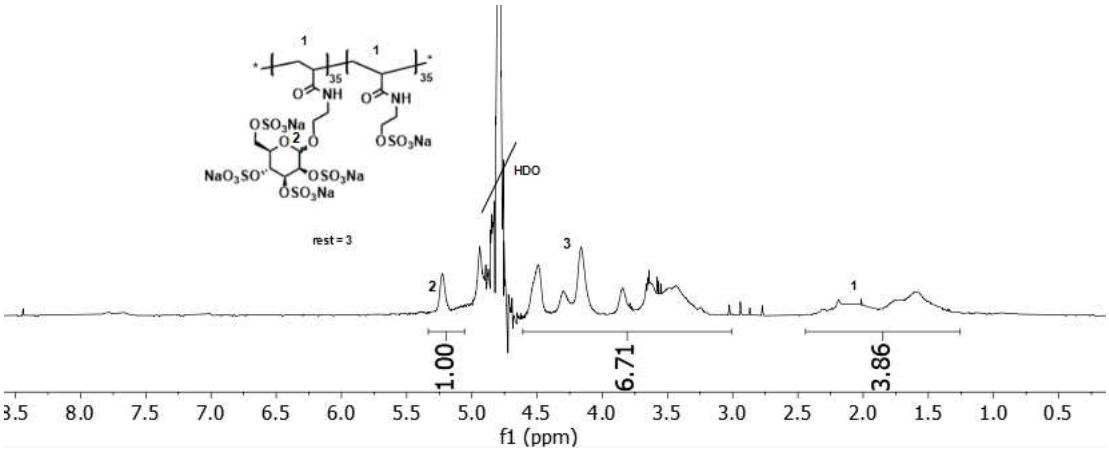

Figure S38. ^{1}H NMR spectrum (600 MHz, D_2O) of coGP-70 (50%).

^{1}H-NMR (600 MHz, D_2O) δ [ppm] 5.27-5.17 (m, **2**), 4.98-3.04 (m, **3**, D_2O overlapping), 2.42-1.24 (m, **1**).

Elemental analysis coGP-70 (50%):

theoretical values (n=35, m=35): %C=21.29; %H=2.58; %N=3.1; %S=17.76

measured values (n=35, m=35): %C=19.71; %H=3.58; %N=2.71; %S=14.05

4. Sulfation of Glycopolymers

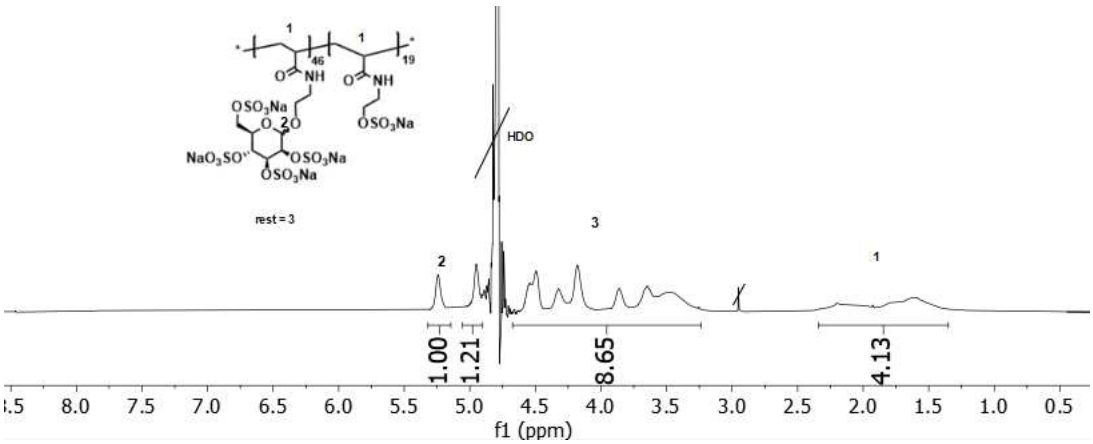

Figure S39. ^{1}H NMR spectrum (600 MHz, D_2O) of coGP-70 (70%).

^{1}H-NMR (600 MHz, D_2O) δ [ppm] 5.29-5.19 (m, **2**), 5.03-3.24 (m, **3**, D_2O overlapping), 2.33-1.35 (m, **1**).

Elemental analysis coGP-70 (70%):

theoretical values (n=46, m=19): %C=20.24; %H=2.39; %N=2.55; %S=18.25

measured values (n=46, m=19): %C=17.98; %H=3.7; %N=2.19; %S=15.81

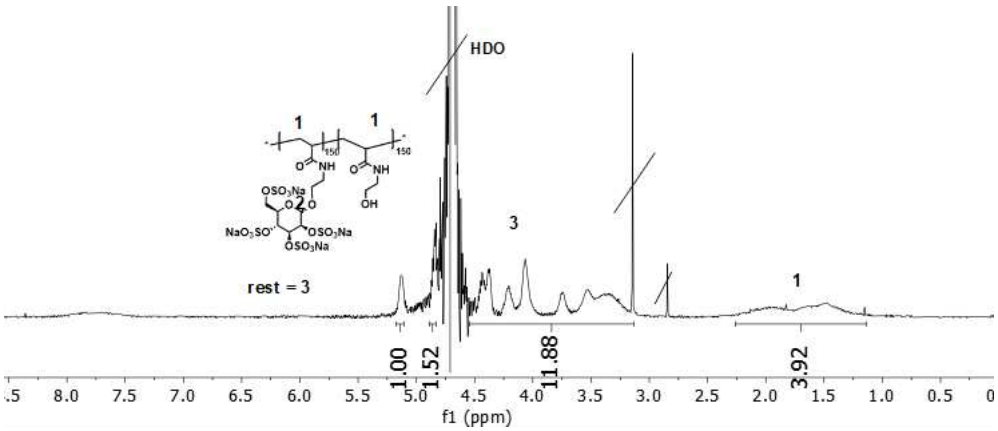

Figure S40. ^{1}H NMR spectrum (600 MHz, D_2O) of coGP-300 (50%).

^{1}H-NMR (600 MHz, D_2O) δ [ppm] 5.17-5.08 (m, **2**), 5.03-3.11 (m, **3**, D_2O overlapping), 2.24-1.12 (m, **1**).

Elemental analysis coGp-300 (50%):

theoretical values (n=150, m=150): %C=21.29; %H=2.57; %N=3.1; %S=17.76

measured values (n=150, m=150): %C=18.24; %H=3.69; %N=2.46; %S=15.29

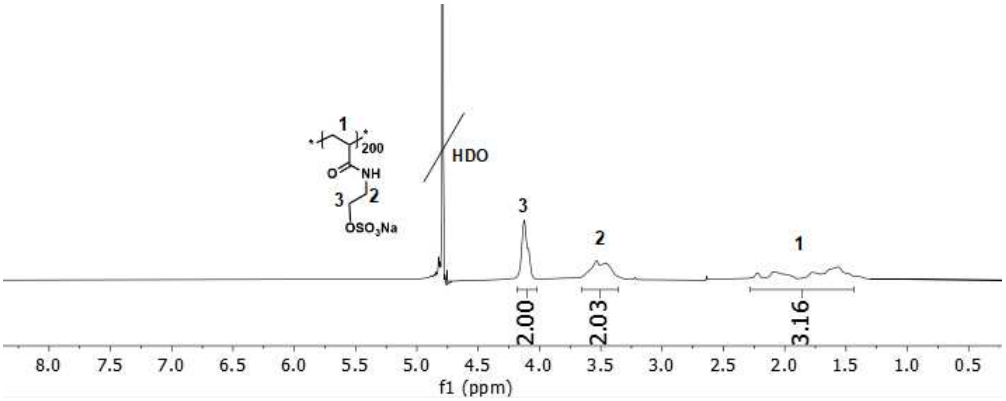

Figure S41. ^{1}H NMR spectrum (600 MHz, D_2O) of PHEAA-200.

^{1}H-NMR (600 MHz, D_2O) δ [ppm] 4.18-4.03 (m, **3**), 3.62-3.33 (m, **2**), 2.25-1.36 (m, **1**).

Elemental analysis PHEAA-200:

theoretical values (n=200): %C=27.65; %H=3.72; %N=6.45; %S=14.76

measured values (n=200): %C=23.59; %H=3.94; %N=5.16; %S=11.49

5. Dynamic Light Scattering

Each polymer was dissolved in PBS buffer (pH =7.4) with a concentration of 0.5 mg/mL. 0.8 mL each was filtered into a polystyrene cuvette and the hydrodynamic radius of the samples, as well as the PDI were determined via DLS measurement. Unsulfated GP-300-OH was measured as a control sample.

Sample	Hydrodynamic Radius [nm]	PDI
GP-10	5.74	0.211
	5.26	0.268
	5.24	0.258
GP-30	5.37	0.248
	5.79	0.272
	6.05	0.28
GP-70	10.17	0.233
	10.06	0.214
	10.58	0.233
GP-300-OH	13	0.141
	13.25	0.153
	13.77	0.187
GP-300	19.27	0.164
	18.8	0.139
	19.66	0.149
coGP-70 (30%)	4.98	0.227
	5.24	0.21

	5.91	0.255
coGP-70 (50%)	10.54	0.3
	10.08	0.298
	11.49	0.323
coGP-70 (70%)	10.04	0.473
	9.49	0.661
	9.55	0.76
coGP-300 (50%)	15.82	0.173
	16.88	0.255
	18.66	0.321

1. Wilkins, L. E.; Phillips, D. J.; Deller, R. C.; Davies, G.-L.; Gibson, M. I., Synthesis and characterisation of glucose-functional glycopolymers and gold nanoparticles: study of their potential interactions with ovine red blood cells. *Carbohydrate research* **2015,** *405*, 47-54.
2. Soria-Martinez, L.; Bauer, S.; Giesler, M.; Schelhaas, S.; Materlik, J.; Janus, K.; Pierzyna, P.; Becker, M.; Snyder, N. L.; Hartmann, L., Prophylactic antiviral activity of sulfated glycomimetic oligomers and polymers. *Journal of the American Chemical Society* **2020,** *142* (11), 5252-5265.

3.3. Facile Synthesis of Catechol-Containing Polyacrylamide Copolymers: Synergistic Effects of Amine, Amide and Catechol Residues in Mussel-Inspired Adhesives

Authors: L.Bonda, J. Müller, L. Fischer, M. Löwe, A. Kedrov, S. Schmidt, L. Hartmann

Journal: Polymers

DOI: 10.3390/polym15183663

Impact Factor: 5.0 (2022)

Own Contribution:

Synthesis, isolation and characterization (HPLC-MS, NMR, SEC) of all monomers, homopolymers and copolymers. Acetonide deprotection and characterization (^{1}H NMR) of the final polymers. Optimization of the synthesis routes and development of optimal polymerization parameters. Performance of ellipsometry measurements and graphical presentation of the results. Collaborative project development and writing of the manuscript.

Comment:

Parts of this publication were performed prior to this thesis. This includes: monomer/polymer synthesis and characterization; polymerization optimization. Part of this thesis are: DMAc-SEC measurements, acetonide deprotection and characterization; ellipsometry measurements of all polymers; quarz crystal microbalance measurements of all polymers; writing of manuscript.

polymers

MDPI

Article

Facile Synthesis of Catechol-Containing Polyacrylamide Copolymers: Synergistic Effects of Amine, Amide and Catechol Residues in Mussel-Inspired Adhesives

Lorand Bonda [1], Janita Müller [1], Lukas Fischer [2], Maryna Löwe [3], Alexej Kedrov [3], Stephan Schmidt [1,4,*] and Laura Hartmann [1,4,*]

[1] Institut für Organische und Makromolekulare Chemie, Heinrich-Heine-Universität Düsseldorf, Universitätsstr. 1, 40225 Düsseldorf, Germany; bolor100@hhu.de (L.B.); janita.mueller@hhu.de (J.M.)
[2] Lehrstuhl für Technische Chemie II, Universität Duisburg-Essen, Universitätsstr. 7, 45141 Essen, Germany; lukas.fischer@uni-duesseldorf.de
[3] Synthetische Membransysteme, Institut für Biochemie, Heinrich-Heine-Universität Düsseldorf, Universitätsstr. 1, 40225 Düsseldorf, Germany; loewe@hhu.de (M.L.); kedrov@hhu.de (A.K.)
[4] Institut für Makromolekulare Chemie, Albert-Ludwigs-Universität Freiburg, Stefan-Meier-Str. 31, 79104 Freiburg, Germany
* Correspondence: stephan.schmidt@hhu.de (S.S.); laura.hartmann@hhu.de (L.H.)

Abstract: The straightforward synthesis of polyamide-derived statistical copolymers with catechol, amine, amide and hydroxy residues via free radical polymerization is presented. In particular, catechol, amine and amide residues are present in natural mussel foot proteins, enabling strong underwater adhesion due to synergistic effects where cationic residues displace hydration and ion layers, followed by strong short-rang hydrogen bonding between the catechol or primary amides and SiO_2 surfaces. The present study is aimed at investigating whether such synergistic effects also exist for statistical copolymer systems that lack the sequence-defined positioning of functional groups in mussel foot proteins. A series of copolymers is established and the adsorption in saline solutions on SiO_2 is determined by quartz crystal microbalance measurements and ellipsometry. These studies confirm a synergy between cationic amine groups with catechol units and primary amide groups via an increased adsorptivity and increased polymer layer thicknesses. Therefore, the free radical polymerization of catechol, amine and amide monomers as shown here may lead to simplified mussel-inspired adhesives that can be prepared with the readily scalable methods required for large-scale applications.

Keywords: mussel foot proteins (Mfps); free radical polymerization; underwater adhesive; DOPA; QCM; ellipsometry

Citation: Bonda, L.; Müller, J.; Fischer, L.; Löwe, M.; Kedrov, A.; Schmidt, S.; Hartmann, L. Facile Synthesis of Catechol-Containing Polyacrylamide Copolymers: Synergistic Effects of Amine, Amide and Catechol Residues in Mussel-Inspired Adhesives. *Polymers* **2023**, *15*, 3663. https://doi.org/10.3390/polym15183663

Academic Editors: Angels Serra and Asterios (Stergios) Pispas

Received: 11 July 2023
Revised: 27 August 2023
Accepted: 1 September 2023
Published: 6 September 2023

1. Introduction

Underwater adhesion is significantly limited by hydration layers and associated salt ions that prevent the adhesive groups' direct contact with the surfaces of the materials [1,2]. Marine adhesive proteins secreted by barnacles, sandcastle worms, mussels and similar organisms nevertheless show excellent binding to inorganic and organic surfaces, even in the presence of high salt concentrations [3,4]. Particularly for mussels, sticky proteins known as mussel foot proteins (Mfps) have evolved that get around this issue by displacing the hydration layers and surface salts before bridging to surfaces via strong bonding, primarily through L-3,4-dihydroxyphenylalanine (DOPA) groups [5–7]. The catechol units of DOPA bind to minerals using short-range bidentate hydrogen bonding via the hydroxy groups. According to recent findings, the presence of DOPA close to the cationic amino acids lysine and arginine is crucial for strong binding. Indeed, mussel adhesion proteins comprise a large amount of DOPA and amine residues. For example, Mfp-5 contains 30 mol% DOPA and 28 mol% cationic residues that are usually in close proximity along the protein chain [8].

The cationic residues are capable of displacing the hydration and salt layer and assisting the catechol residues in binding to the surface (Figure 1). The synergy between catechol and charged groups was confirmed using various adhesion assays [8–13] and led to the development of various bioinspired adhesive polymers, coatings and hydrogels [3,14–36].

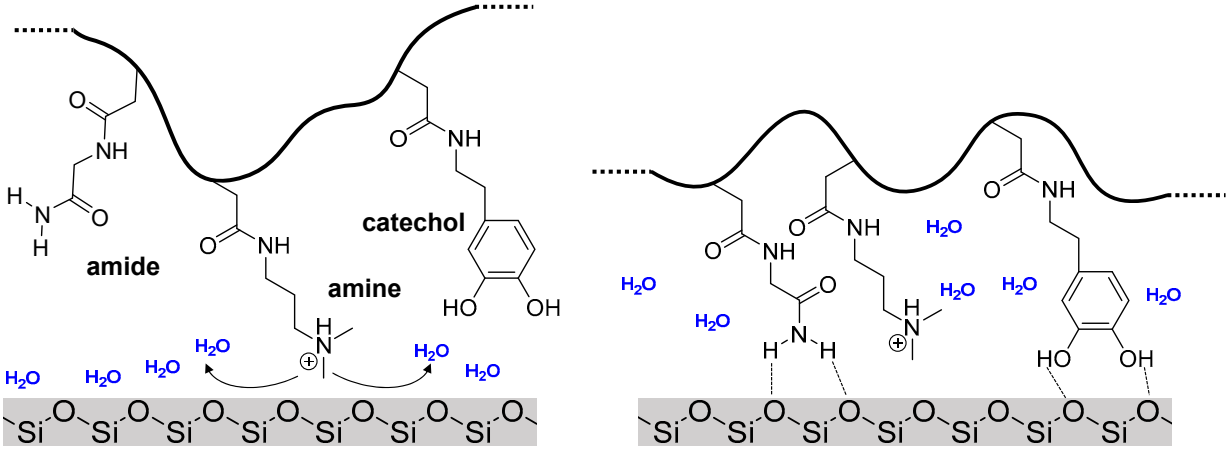

Figure 1. Charged amine residues on polymers as synthesized in this work displace the ion layer and hydration layer on SiO_2 surfaces (**left**), thereby enabling close range hydrogen bonding of catechol or amide units (**right**).

Besides cationic and catechol residues, primary amides in the form of asparagine are another type of residue often present at higher than 10 mol% (in Mfp-2, Mfp-3, Mfp-4 and Mfp-6) [37–40]. The role of asparagine in Mfps is not entirely understood, but it could be argued that its "helix-breaker" function ensures disordered coil-like conformations to increase the accessibility of the adhesive groups. Importantly, however, for Mfp-3, the amide residues are mostly positioned next to amine and DOPA residues, pointing toward a more sophisticated role of the primary amides [40]. Mfp-3 most likely serves as the adhesion primer, i.e., Mfp-3 binds to the mineral surface and then links to the other Mfps [6,41]. Therefore, we have recently studied the adhesive properties of short sequence-defined oligomers containing catechol, amide and amine residues at different positions [42]. These studies confirmed a significant adhesion enhancement in the case of adjacent catechol and amine groups, but also amide groups were able to strongly increase the adhesion when positioned next to catechol units. Additional hydrogen bonding, favorable conformations or the partially ionic character may explain the observed amide–catechol synergy, but the precise mechanism still awaits detailed analysis.

Nevertheless, to first test the potential benefit of the primary amide function for underwater adhesion, here we establish the synthesis of polyacrylamide-derived statistical copolymers with catechol, amine, amide and hydroxy side chain residues and investigate their adsorption to SiO_2 surfaces. We focus on free radical polymerization, which is often preferred for larger scale synthesis and applications. Various studies showed the feasibility of free and controlled radical polymerization routes toward uncharged [43–47] and charged [24,30,34,35] catechol-containing copolymers. Importantly, however, the effect of additional primary amide units was not yet studied in such copolymer systems.

2. Materials and Methods

Acetone and ethanol were purchased from Carl Roth. Acetonitrile, 2,2-dimethoxypropane, *p*-toluenesulfonic acid, tetrahydrofuran and sodium chloride (98%) were purchased from Sigma Aldrich (Taufkirchen, Germany). Acryloyl chloride (96%) was purchased from Merck (Darmstadt, Germany). Azobis(isobutyronitril) (98%), triethylamine and trifluoroacetic acid were purchased from Acros Organics (Geel, Belgium). Dichlormethane, diethylether, ethyl acetate, methanol, hexane and dimethylformamide were purchased from VWR Prolabo (Darmstadt, Germany). Dopamine hydrochloride (99.96%) and glycinamide hydrochloride

were purchased from BLD Pharmatech (Kaiserslautern, Germany). Hydroquinone was purchased from J.T. Baker (Phillipsburg, NJ, USA). Potassium carbonate, lithium hydroxide and magnesium sulfate were purchased from Fisher Scientific. Methyl trifluoroacetate was purchased from Fluorochem (Hadfield, UK). *N*-[3-(Dimethylamino)propyl]acrylamide (98%) and *N*-(2-hydroxyethyl)acrylamide (98%) were purchased from TCI (Tokyo, Japan). Sodium hydrogencarbonate, hydrochloric acid (37%) and toluene were purchased from VWR Chemicals.

2.1. ^1H NMR

^{1}H NMR spectra were recorded at room temperature with a Bruker AVANCE III 300 (Hercules, CA, USA) (for 300 MHz) and 600 (for 600 MHz). The chemical shifts were reported relative to solvent peaks (chloroform and water) as internal standards and reported as δ in parts per million (ppm). Multiplicities were abbreviated as s for singlet, d for doublet, t for triplet and m for multiplet.

2.2. Size Exclusion Chromatography-Multi-Angle Light Scattering (H_2O-SEC-MALS)

SEC analysis was conducted with an Agilent 1200 series HPLC system and three aqueous SEC columns provided by Polymer Standards Service (PSS). The columns were two Suprema Lux analytical columns (8 mm diameter and 5 µm particle size) and one precolumn (50 mm, 2 × 160 Å of 300 mm and 1000 Å of 300 mm). The eluent was a buffer system consisting of MilliQ water and 30% acetonitrile with 50 mM, NaH_2PO_4, 150 mM NaCl and 250 ppm NaN_3 with a pH = 7.0 (via addition of 50 mL 3 molar aqueous sodium hydroxide solution) filtered with inline 0.1 µm membrane filter and running at 0.8 mL per minute. Multi-angle light scattering was recorded via miniDAWN TREOS and differential refractive index spectra with Optilab rEX, both supplied by Wyatt Technologies EU (Dernbach, Germany). Data analysis was conducted with Astra 5 software and a dn/dc value of 0.156 for each polymer.

2.3. Dimethylacetamide-Size Exclusion Chromatography (DMAc-SEC)

SEC analysis was conducted with an SEC column provided by Polymer Standards Service (PSS). The column was a PSS GRAM linear column (8 mm diameter and 10 µm particle size), and a Jasco PU-2080 pump was used (Easton, MD, USA). The eluent was dimethylacetamide running at 1 mL per minute and the measuring temperature was 60 °C. Differential refractive index spectra were recorded with an ETA-2020 RI detector supplied by WGE BURES GmbH & Co. KG (Dallgow-Döberitz, Germany).

2.4. Freeze-Drying

Lyophilization was performed with an Alpha 1-4 LD instrument from Martin Christ Freeze Dryers GmbH. A temperature of –42 °C and a pressure of 0.1 mbar were maintained throughout the freeze-drying process.

2.5. High Pressure Liquid Chromatography (HPLC)

RP-HPLC/MS (Reversed Phase-HPLC/Mass Spectroscopy) was performed on an Agilent Technologies 1260 Infinity System using an AT 1260 G4225A degasser, G1312B binary pump, G1329B automatic liquid sampler, G1316C thermostatted column compartment, G1314F variable wavelength detector at 214 nm and an AT 6120 quadropole containing an electrospray ionisation (ESI) source. The mobile phase consisted of buffer A (water:acetonitrile 95:5 (*v*/*v*), 0.1 vol.% formic acid) and buffer B (water:acetonitrile 5:95 (*v*/*v*), 0.1 vol.% formic acid). HPLC runs were performed on a Poroshell 120 EC-C18 (3.0 × 50 mm, 2.5 µm) RP column from Agilent at a flow rate of 0.4 mL/min 95% buffer A and 5% buffer B (0–5 min), following a linear gradient to 100% buffer B (5–30 min) at 25 °C. ESI-MS for GlcNAc-oligomers and sulfates was performed using 95% buffer A and 5% buffer B without formic acid and a fragmentor voltage of 40–60 V (m/z range of 200 to 2000).

2.6. Elllipsometry

Ellipsometry was conducted with a Sentech SI-SE 800 spectroscopic ellipsometer (Sentech Instruments GmbH, Berlin, Germany) on silicon wafers (Science Services, Munich, Germany). For surface preparation, the wafers were treated in a 5:1:1 mixture of ultrapure water, hydrogen peroxide (30%) and ammonia (25%) at 70 °C for 30 min, followed by rinsing with ultrapure water. Next, the wafers were immersed in the polymer solutions containing 0.1 M NaCl for 20 min followed by immersion in 0.1 M NaCl solutions to remove unbound polymer, rinsing with pure water and drying. For ellipsometry data evaluation, the thickness of the naturally grown oxide layer was determined on uncoated wafers from the same batch (12 ± 0.3 nm) and the refractive index of the polymer layer was assumed to be 1.5 [48]. This allowed for the determination of the polymer layer thickness as the only free parameter.

2.7. Quartz Crystal Microbalance Measurements

QCM measurements were performed with a QCM-D instrument qCell T Q2 (3T analytic GmbH, Neuhausen ob Eck, Germany) with dual sensor channels equipped with quartz chips from the same company. The chips were activated by air plasma treatment for 30 s before use. A solution of 0.1 M NaCl was prepared, filtered (pore size 0.1 µm) and degassed for 20 min. The polymers were dissolved in the solution at a concentration of 0.1 mg/mL. Before the samples were injected, the chips were stabilized using a 0.1 M NaCl solution without polymer. Polymer samples were injected with a flow rate of 80 µL min^{-1} for 1000 s followed by the pumping of the pure NaCl solution for 1500 s. QCM chips were regenerated after each run by first placing them in an SDS bath for 30 min and then treating them with piranha solution (H_2SO_4:H_2O_2 30%, 3:1, *v*/*v*) for 2 min.

3. Results and Discussion

3.1. Synthesis of Monomers

The polymers to be synthetized were supposed to be varied in their overall composition of catechol, amine and amide groups, as these are thought to be the main contributors to the underwater adhesion of Mfps. Here we aimed at acrylamide-derived polymers owing to their well-established solution polymerization procedures and frequent use in functional materials. Therefore, the following four *N*-substituted acrylamide monomers were used: catechol-containing acrylamide (CAA), amide-containing acrylamide (PA), tertiary amine-containing acrylamide (TA) and hydroxy-containing acrylamide (HY) (Scheme 1).

N-(2-(2,2-dimethylbenzo-1,3-dioxol-5-yl)ethyl)acrylamide

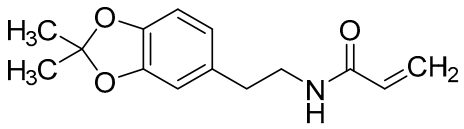

CAA (protected)

N-(2-amino-2-oxoethyl)acrylamide

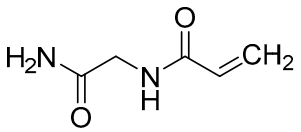

NAGA

N-(3-(dimethylamino)propyl)acrylamide

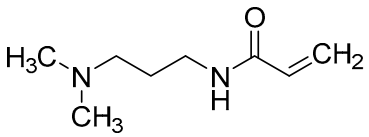

DMAPAA

N-(2-hydroxyethyl)acrylamide

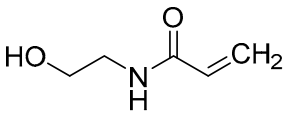

HEAA

Scheme 1. The different *N*-substituted acrylamide monomers used to build the polymers.

The CAA and PA monomers were prepared synthetically (see Supplementary Materials Chapter S1), while the TA and HY monomers were purchased commercially. Special focus was devoted to the synthesis of the protected catechol-bearing monomer CAA since catechols are prone to side reactions, which may lead to undesired crosslinking of the polymers. Here we use the acetonide-protection of the catechol monomer and make it suitable for radical polymerization and the release of the free catechol by deprotection after successful polymerization.

The synthesis of CAA was carried out in four steps (Scheme 2). The first three steps were developed according to synthesis known from the literature [49,50]. Dopamine hydrochloride was used as the starting material. Before the acetonide protecting group was attached to the catechol, the primary amine of dopamine first had to be protected with a trifluoroacetyl group using methyl trifluoroacetate. If the acetonide protecting group was introduced directly, an undesirable Pictet–Spengler condensation would otherwise occur and a tetrahydroisoquinoline species would be obtained. This reaction occurs frequently with phenylamines, such as dopamine, in the presence of aldehydes or ketones [51]. In the second step, the acetonide protecting group was attached using 2,2 dimethoxypropane, the ketal of acetone. This is an important step because catechols can be easily oxidized to quinones by atmospheric oxygen even at neutral to weakly alkaline pH [52]. Similarly, without an acetonide protecting group, undesirable crosslinking of the dopamine acrylamide monomers could occur during free radical polymerization. The introduced protecting groups are orthogonal to each other, meaning they can be cleaved off independently: The acetonide protecting group is removed under acidic conditions and the trifluoroacetyl protecting group is removed under basic conditions. After removing the trifluoroacetyl group, the resulting dopamineacetonide was reacted with acryloyl chloride to give the final monomer.

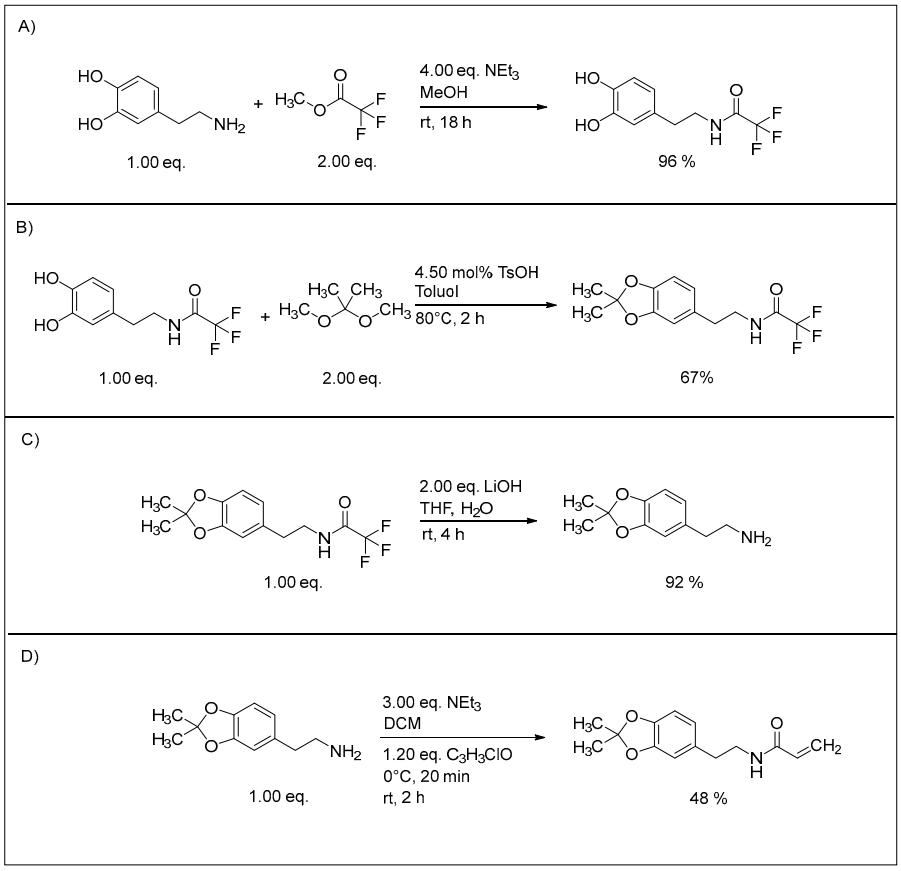

Scheme 2. Synthesis of the catechol monomer CAA. Attaching the methyltrifluoracetate protecting group to the amine (**A**), attaching the acetonide protecting group (**B**), deprotecting the methyltrifluoracetate goup (**C**), syntheses of the final CAA monomer (**D**).

The synthesis of the primary amide-bearing PA monomer (Scheme 3) was adapted from Lutz et al. with minor changes in the purification protocol (see Supplementary Information Chapter S1) [53]. The choice of using PA for the introduction of primary amide side chain residues was inspired by asparagine, as is found in some Mfps.

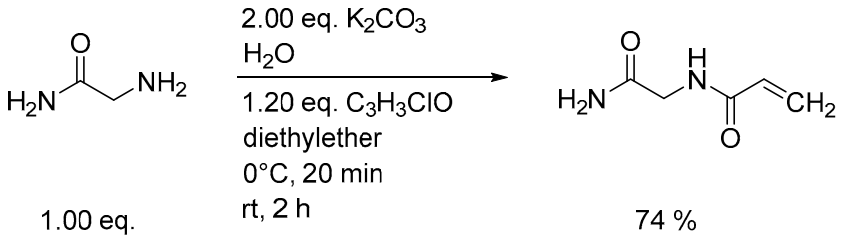

Scheme 3. Reaction conditions for the synthesis of the N-acryloylglycinamide (PA) monomer.

3.2. Polymer Synthesis

The objective was to study the polymer adsorption on silica or glass surfaces at different monomer compositions. Therefore, the monomers were copolymerized at different ratios, followed by deprotection for all CAA-containing polymers (designated CA in deprotected form). The optimal reaction conditions were determined by the variation of the polymerization parameters and analyzing the isolated polymers with regard to monomer incorporation, number-average molecular weights and dispersities (see Supplementary Materials, Section S2 for details). We focused on varying the CA and PA units which are suspected to increase adhesion via hydrogen bonding. Additionally, the amount of TA units was varied to enable the synergistic effects of the cations helping to displace the water and salt barrier. All polymers were polymerized with at least 50% of the non-adhesive "filler" monomer HY. The variation of the monomers incorporated into the target polymers and the monomer fractions selected in these allow conclusions to be drawn on the influence of the monomer interactions with each other, as well as on the influence of the monomer fractions incorporated in each case on the polymer adhesion. Overall, eight polymers with different monomer incorporation were synthesized (Table 1). In the sample code, the filler monomer HY is omitted for clarity.

Table 1. Specified ratio of theoretical monomer incorporation and target polymers obtained. The numbers in the sample code give the percentage of CAA, TA and PA units; HY is omitted.

Final Polymer (Sample Code)	Monomer Reaction Ratio [%]				Monomer Incorporation [%] [a]				$\bar{M}_n$ [kDa]	$Đ$	Yield [%]
	CAA	TA	PA	HY	CAA	TA	PA	HY			
TA52	0	50	0	50	0	52	0	48	23.5	1.97	91
PA50	0	0	50	50	0	0	50	50	50.33	1.36	39
TA15-PA13	0	15	15	70	0	15	13	72	69.9	1.74	93
CAA4-TA48	5	45	0	50	4	48	0	48	21.9	2.61	98
CAA3-PA45	5	0	45	50	3	0	45	52	23.4	1.92	45
CAA5-TA5-PA7	5	5	5	85	5	5	7	83	63.1	1.87	98
CAA4-TA22-PA17	5	22.5	22.5	50	4	22	17	57	64.4	1.73	94
CAA13-TA15-PA18	15	15	15	55	13	15	18	54	50.9	1.12	91

[a]: Determined by ^{1}H NMR-spectroscopy.

Two copolymers, TA52 and PA50, consisting of two monomers were prepared (Table 1). The main reason for their synthesis was to obtain adhesion values for polymers without catechol units for comparison. Three copolymers were synthesized with three monomers: TA15-PA13, CAA4-TA48 and CAA3-PA45. Here the intention was to be able to test the effect of the added catechol groups and to compare the potential synergy with amide and amine groups. Finally, three copolymers containing all four monomers were synthesized. The copolymers CAA4-TA22-PA17 and CAA5-TA5-PA7 were synthesized to study the effect of different TA and PA content on adhesion. The copolymer CAA13-TA15-PA18 can be used to test the extent to which adhesion changes when the catechol moiety is increased

relative to the other two comonomers. Since all monomers were incorporated in all three products, this allows interactions between all three residues and the resulting properties of the polymers to be studied. All isolated polymers were obtained as colorless or yellowish solids after purification by dialysis (MWCO 7.50 kDa) followed by lyophilization.

3.3. Acetonide Deprotection

In order to obtain catechol units for adhesion studies, the acetonide protecting group was removed from the CAA-containing copolymers right before performing the adhesion studies, so oxidation of the catechol hydroxyl groups does not occur. Successful and complete removal of the protecting groups was confirmed by ^{1}H NMR (see Supplementary Information, Figures S23–S27).

3.4. Adsorption to Quartz Surfaces

To determine the interaction of the polymers with SiO_2 surfaces, quartz crystal microbalance (QCM) and ellipsometry were used. Polymer solutions were prepared in 10 mM phosphate buffer (pH 7.0) containing 0.1 M NaCl. For QCM measurements, polymer solutions were injected at a constant rate for 1000 s followed by pumping pure, polymer-free solutions for another 1500 s to study the equilibrium polymer adsorption. The QCM-frequency traces are shown in Figure 2. To rule out variations by different chips, the measurements were performed using a single QCM chip that was regenerated by piranha solution after each run. Selected samples were analyzed by fresh chips showing similar frequency shifts. Via rinsing with pure NaCl solution after polymer adsorption, the frequency shifts decrease by roughly 5–10% for all polymer samples showing the fraction of loosely bound polymers. For determining the thickness of the polymer films as an alternative measure of polymer adsorption, ellipsometry was used. Silicon chips with naturally grown SiO_2 layers were immersed in the same polymer solutions for 20 min, followed by rinsing with pure buffer and ultra-pure water. For selected samples, the adsorption time was increased to 40 min, giving similar results compared to 20 min adsorption, confirming that the polymer layer formation was finished after 20 min.

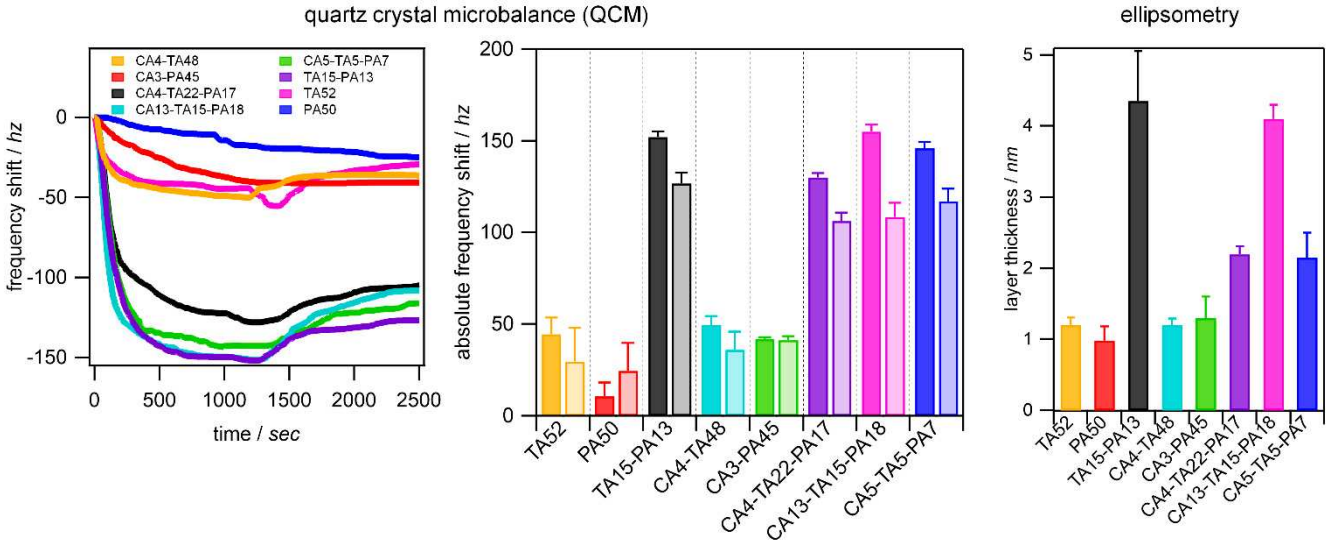

Figure 2. Polymer adsorption measured by QCM and ellipsometry on quartz surfaces. (**Left**): QCM-frequency traces for polymer samples. The dashed line at 1000 sec signifies the region of injecting polymer solutions (0–1000 s) and pumping pure buffer (1000–2500 s). (**Center**): Frequency shifts from 0 s to 1000 s (fully colored bars) and frequency shifts at 2500 s (equilibrium, light colors) after rinsing with pure NaCl solution. (**Right**): Polymer film thicknesses on quartz chips after adsorption, rinsing and drying measured by ellipsometry.

Overall, ellipsometry and QCM measurements showed similar trends: only when combing amide (PA) or catechol units (CA) with the cationic amine groups (TA) was the adsorption strong. When compared to previous results, [42] again confirms that the amine groups can synergize with catechol groups or primary amide groups to strongly bind to glass surfaces. The apparent exception was CA4-TA48 (amine and catechol), which showed low adsorption similar to TA52 (only amines), whereas TA15-PA13 (amide and amine) showed much higher adsorption. This is because TA52 and CA4-TA48 have a very high charge density due to the abundance of cationic TA units; thus, the polymers attain a stretched conformation in bulk and in the adsorbed state, leading to comparatively low film thicknesses. Therefore, highly charged polycations appear to adsorb predominantly via ionic interactions and additional hydrogen bonding via catechol had no additional effect on layer thickness. In addition, the molecular weight of CA4-TA48 was roughly three times lower compared to TA15-PA13, which may also add to the reduced layer thickness. Among the polymers that contain all four monomers, the one with the highest combined catechol and amide content (CA13-TA15-PA18) exhibits the highest film thickness and frequency shifts. Nevertheless, without catechols, but with amides and amines (TA15-PA13), adsorption was also strong. This indicates a potential synergy also between amide and amine units for adhesion to SiO_2 surfaces, which has been largely overlooked in the development of underwater adhesive polymer systems so far. Such synergy in binding to SiO_2 surfaces agrees well with earlier studies [11,12] on catechol-based mussel-inspired polymers as well as newer results where amide groups were also included. The interactions of amides and glass surfaces could be due to hydrogen bonding, where the primary amides can donate two hydrogens, similar to catechol residues. Furthermore, the zwitterionic resonance structure of the primary amide (25–30% ionic character) [54] may help to displace the salt or hydration layers on the SiO_2 surface to increase binding. Overall, we cannot conclude on the molecular details of amide vs. catechol-based adhesion, but also the natural mussel foot protein that primes the rock surface for adhesion contains many asparagine units that present primary amides close to catechol or amine units. Thus, the polymers synthesized here by standard radical polymerization present an improved mimetic of the mussel adhesives due to the added primary amides. With the established synthetic platform enabling the large-scale production of these polymers, future studies can focus on applications as well as direct mechanical adhesion tests.

4. Conclusions

In summary, we synthesized polyacrylamide-derived copolymers with catechol, amine, amide and hydroxy side chain residues via free radical polymerization and studied their adsorption on negatively charged SiO_2 surfaces from saline solutions. The developed monomers show a rather homogenous incorporation rate, suggesting the preparation of statistical copolymers. Furthermore, the obtained yields and the stability of the products suggest that well-behaved polymerization routes were established. Intriguingly, we could confirm a synergy between cationic amine groups with catechol units and the primary amide group, which led to increased adsorption on SiO_2 surfaces. Thus, the simple statistical polyacrylamide prepared mimics crucial features of natural mussel adhesion proteins even without controlling the sequence of the functional groups in detail. Further studies will explore potential applications of these polymers as adhesives and try to shed light on the molecular mechanisms behind a potential synergy of these functional groups, e.g., by mechanical tests and further varying the content of catechol amide and amine groups in the polymers.

Supplementary Materials: The following are available online at https://www.mdpi.com/article/10.3390/polym15183663/s1, Figures S1–S7: NMR data and synthesis detail for monomers, Tables S1–S3: Determination of reaction conditions for free radical polymerization, Figures S8–S22, Table S4: NMR and SEC-MALS of the final polymers, Figure S23–S27: Acetonide deprotection of final polymers. Refs. [49,53] are cited in the supplementary materials.

Author Contributions: This work was conceptualized by L.H. and S.S. The project was administrated by L.H. The methodology was designed by L.H., S.S., L.B., L.F., A.K. and M.L. The investigation was conducted by L.B. and J.M. Recourses were supplied by L.H., S.S. and A.K. The resulting data were formally analyzed by L.B., J.M., S.S. and L.H. The article was written by L.B., S.S. and L.H. All authors have read and agreed to the published version of the manuscript.

Funding: A.K. acknowledges the support of the German Research Foundation (DFG) within the Collaborative Research Center 1208 "Identity and Dynamics of Membrane Systems".

Institutional Review Board Statement: Not applicable.

Data Availability Statement: The data presented in this study are available in this article and the supplementary materials.

Conflicts of Interest: The authors declare no conflict of interest.

References

1. Israelachvili, J.; Wennerström, H. Role of hydration and water structure in biological and colloidal interactions. *Nature* **1996**, *379*, 219–225. [CrossRef]
2. Li, Y.; Liang, C.; Gao, L.; Li, S.Y.; Zhang, Y.Z.; Zhang, J.; Cao, Y. Hidden complexity of synergistic roles of Dopa and lysine for strong wet adhesion. *Mat. Chem. Front.* **2017**, *1*, 2664–2668. [CrossRef]
3. Hofman, A.H.; van Hees, I.A.; Yang, J.; Kamperman, M. Bioinspired Underwater Adhesives by Using the Supramolecular Toolbox. *Adv. Mater.* **2018**, *30*, e1704640. [CrossRef]
4. Waite, J.H. Mussel adhesion—Essential footwork. *J. Exp. Biol.* **2017**, *220*, 517–530. [CrossRef]
5. Lee, B.P.; Messersmith, P.B.; Israelachvili, J.N.; Waite, J.H. Mussel-Inspired Adhesives and Coatings. *Annu. Rev. Mater. Res.* **2011**, *41*, 99–132. [CrossRef]
6. Lee, H.; Scherer, N.F.; Messersmith, P.B. Single-molecule mechanics of mussel adhesion. *Proc. Natl. Acad. Sci. USA* **2006**, *103*, 12999–13003. [CrossRef]
7. Yu, M.; Hwang, J.; Deming, T.J. Role of l-3,4-Dihydroxyphenylalanine in Mussel Adhesive Proteins. *J. Am. Chem. Soc.* **1999**, *121*, 5825–5826. [CrossRef]
8. Lu, Q.; Danner, E.; Waite, J.H.; Israelachvili, J.N.; Zeng, H.; Hwang, D.S. Adhesion of mussel foot proteins to different substrate surfaces. *J. R. Soc. Interface* **2013**, *10*, 20120759. [CrossRef]
9. Degen, G.D.; Stow, P.R.; Lewis, R.B.; Andresen Eguiluz, R.C.; Valois, E.; Kristiansen, K.; Butler, A.; Israelachvili, J.N. Impact of Molecular Architecture and Adsorption Density on Adhesion of Mussel-Inspired Surface Primers with Catechol-Cation Synergy. *J. Am. Chem. Soc.* **2019**, *141*, 18673–18681. [CrossRef]
10. Wang, J.; Tahir, M.N.; Kappl, M.; Tremel, W.; Metz, N.; Barz, M.; Theato, P.; Butt, H.-J. Influence of Binding-Site Density in Wet Bioadhesion. *Adv. Mater.* **2008**, *20*, 3872–3876. [CrossRef]
11. Rapp, M.V.; Maier, G.P.; Dobbs, H.A.; Higdon, N.J.; Waite, J.H.; Butler, A.; Israelachvili, J.N. Defining the Catechol-Cation Synergy for Enhanced Wet Adhesion to Mineral Surfaces. *J. Am. Chem. Soc.* **2016**, *138*, 9013–9016. [CrossRef]
12. Maier, G.P.; Rapp, M.V.; Waite, J.H.; Israelachvili, J.N.; Butler, A. Adaptive synergy between catechol and lysine promotes wet adhesion by surface salt displacement. *Science* **2015**, *349*, 628–632. [CrossRef] [PubMed]
13. Li, Y.; Wang, T.; Xia, L.; Wang, L.; Qin, M.; Li, Y.; Wang, W.; Cao, Y. Single-molecule study of the synergistic effects of positive charges and Dopa for wet adhesion. *J. Mater. Chem. B* **2017**, *5*, 4416–4420. [CrossRef] [PubMed]
14. Kord Forooshani, P.; Lee, B.P. Recent approaches in designing bioadhesive materials inspired by mussel adhesive protein. *J. Polym. Sci. A Polym. Chem.* **2017**, *55*, 9–33. [CrossRef] [PubMed]
15. Quan, W.Y.; Hu, Z.; Liu, H.Z.; Ouyang, Q.Q.; Zhang, D.Y.; Li, S.D.; Li, P.W.; Yang, Z.M. Mussel-Inspired Catechol-Functionalized Hydrogels and Their Medical Applications. *Molecules* **2019**, *24*, 2586. [CrossRef]
16. Guo, Q.; Chen, J.S.; Wang, J.L.; Zeng, H.B.; Yu, J. Recent progress in synthesis and application of mussel-inspired adhesives. *Nanoscale* **2020**, *12*, 1307–1324. [CrossRef]
17. Zhang, C.; Wu, B.H.; Zhou, Y.S.; Zhou, F.; Liu, W.M.; Wang, Z.K. Mussel-inspired hydrogels: From design principles to promising applications. *Chem. Soc. Rev.* **2020**, *49*, 3605–3637. [CrossRef]
18. Zhang, W.; Wang, R.X.; Sun, Z.M.; Zhu, X.W.; Zhao, Q.; Zhang, T.F.; Cholewinski, A.; Yang, F.; Zhao, B.X.; Pinnaratip, R.; et al. Catechol-functionalized hydrogels: Biomimetic design, adhesion mechanism, and biomedical applications. *Chem. Soc. Rev.* **2020**, *49*, 433–464. [CrossRef]
19. Barros, N.R.; Chen, Y.; Hosseini, V.; Wang, W.Y.; Nasiri, R.; Mahmoodi, M.; Yalcintas, E.P.; Haghniaz, R.; Mecwan, M.M.; Karamikamkar, S.; et al. Recent developments in mussel-inspired materials for biomedical applications. *Biomater. Sci.* **2021**, *9*, 6653–6672. [CrossRef]
20. Cui, C.Y.; Liu, W.G. Recent advances in wet adhesives: Adhesion mechanism, design principle and applications. *Prog. Polym. Sci.* **2021**, *116*, 101388. [CrossRef]
21. Fan, H.L.; Gong, J.P. Bioinspired Underwater Adhesives. *Adv. Mater.* **2021**, *33*, 2102983. [CrossRef]

22. Yang, P.; Zhu, F.; Zhang, Z.B.; Cheng, Y.Y.; Wang, Z.; Li, Y.W. Stimuli-responsive polydopamine-based smart materials. *Chem. Soc. Rev.* **2021**, *50*, 8319–8343. [CrossRef] [PubMed]
23. Geng, H.; Zhang, P.; Peng, Q.; Cui, J.; Hao, J.; Zeng, H. Principles of Cation−π Interactions for Engineering Mussel-Inspired Functional Materials. *Acc. Chem. Res.* **2022**, *55*, 1171–1182. [CrossRef]
24. Narkar, A.R.; Kelley, J.D.; Pinnaratip, R.; Lee, B.P. Effect of Ionic Functional Groups on the Oxidation State and Interfacial Binding Property of Catechol-Based Adhesive. *Biomacromolecules* **2018**, *19*, 1416–1424. [CrossRef] [PubMed]
25. Zhao, Q.; Lee, D.W.; Ahn, B.K.; Seo, S.; Kaufman, Y.; Israelachvili, J.N.; Waite, J.H. Underwater contact adhesion and microarchitecture in polyelectrolyte complexes actuated by solvent exchange. *Nat. Mater.* **2016**, *15*, 407–412. [CrossRef] [PubMed]
26. Krogsgaard, M.; Behrens, M.A.; Pedersen, J.S.; Birkedal, H. Self-Healing Mussel-Inspired Multi-pH-Responsive Hydrogels. *Biomacromolecules* **2013**, *14*, 297–301. [CrossRef] [PubMed]
27. Ryu, J.H.; Lee, Y.; Kong, W.H.; Kim, T.G.; Park, T.G.; Lee, H. Catechol-Functionalized Chitosan/Pluronic Hydrogels for Tissue Adhesives and Hemostatic Materials. *Biomacromolecules* **2011**, *12*, 2653–2659. [CrossRef]
28. Saxer, S.; Portmann, C.; Tosatti, S.; Gademann, K.; Zürcher, S.; Textor, M. Surface Assembly of Catechol-Functionalized Poly(l-lysine)-graft-poly(ethylene glycol) Copolymer on Titanium Exploiting Combined Electrostatically Driven Self-Organization and Biomimetic Strong Adhesion. *Macromolecules* **2010**, *43*, 1050–1060. [CrossRef]
29. White, J.D.; Wilker, J.J. Underwater Bonding with Charged Polymer Mimics of Marine Mussel Adhesive Proteins. *Macromolecules* **2011**, *44*, 5085–5088. [CrossRef]
30. Zhai, Y.; Chen, X.; Yuan, Z.; Han, X.; Liu, H. A mussel-inspired catecholic ABA triblock copolymer exhibits better antifouling properties compared to a diblock copolymer. *Polym. Chem.* **2020**, *11*, 4622–4629. [CrossRef]
31. Ahn, B.K.; Das, S.; Linstadt, R.; Kaufman, Y.; Martinez-Rodriguez, N.R.; Mirshafian, R.; Kesselman, E.; Talmon, Y.; Lipshutz, B.H.; Israelachvili, J.N.; et al. High-performance mussel-inspired adhesives of reduced complexity. *Nat. Commun.* **2015**, *6*, 8663. [CrossRef] [PubMed]
32. Kim, B.J.; Oh, D.X.; Kim, S.; Seo, J.H.; Hwang, D.S.; Masic, A.; Han, D.K.; Cha, H.J. Mussel-Mimetic Protein-Based Adhesive Hydrogel. *Biomacromolecules* **2014**, *15*, 1579–1585. [CrossRef] [PubMed]
33. Wei, Q.; Achazi, K.; Liebe, H.; Schulz, A.; Noeske, P.L.M.; Grunwald, I.; Haag, R. Mussel-Inspired Dendritic Polymers as Universal Multifunctional Coatings. *Angew. Chem. Int. Ed.* **2014**, *53*, 11650–11655. [CrossRef] [PubMed]
34. Zhang, F.; Liu, S.W.; Zhang, Y.; Wei, Y.; Xu, J.R. Underwater bonding strength of marine mussel-inspired polymers containing DOPA-like units with amino groups. *RSC Adv.* **2012**, *2*, 8919–8921. [CrossRef]
35. Asha, A.B.; Chen, Y.J.; Zhang, H.X.; Ghaemi, S.; Ishihara, K.; Liu, Y.; Narain, R. Rapid Mussel-Inspired Surface Zwitteration for Enhanced Antifouling and Antibacterial Properties. *Langmuir* **2019**, *35*, 1621–1630. [CrossRef]
36. Deng, X.Y.; Huang, B.X.; Wang, Q.H.; Wu, W.L.; Coates, P.; Sefat, F.; Lu, C.H.; Zhang, W.; Zhang, X.M. A Mussel-Inspired Antibacterial Hydrogel with High Cell Affinity, Toughness, Self-Healing, and Recycling Properties for Wound Healing. *ACS Sustain. Chem. Eng.* **2021**, *9*, 3070–3082. [CrossRef]
37. Zhao, H.; Waite, J.H. Proteins in Load-Bearing Junctions: The Histidine-Rich Metal-Binding Protein of Mussel Byssus. *Biochemistry* **2006**, *45*, 14223–14231. [CrossRef]
38. Zhao, H.; Waite, J.H. Linking adhesive and structural proteins in the attachment plaque of Mytilus californianus. *J. Biol. Chem.* **2006**, *281*, 26150–26158. [CrossRef]
39. Rzepecki, L.M.; Hansen, K.M.; Waite, J.H. Characterization of a Cystine-Rich Polyphenolic Protein Family from the Blue Mussel *Mytilus edulis* L. *Biol. Bull.* **1992**, *183*, 123–137. [CrossRef]
40. Papov, V.V.; Diamond, T.V.; Biemann, K.; Waite, J.H. Hydroxyarginine-containing Polyphenolic Proteins in the Adhesive Plaques of the Marine Mussel *Mytilus edulis*. *J. Biol. Chem.* **1995**, *270*, 20183–20192. [CrossRef]
41. Lin, Q.; Gourdon, D.; Sun, C.; Holten-Andersen, N.; Anderson, T.H.; Waite, J.H.; Israelachvili, J.N. Adhesion mechanisms of the mussel foot proteins mfp-1 and mfp-3. *Proc. Natl. Acad. Sci. USA* **2007**, *104*, 3782–3786. [CrossRef]
42. Fischer, L.; Strzelczyk, A.K.; Wedler, N.; Kropf, C.; Schmidt, S.; Hartmann, L. Sequence-defined positioning of amine and amide residues to control catechol driven wet adhesion. *Chem. Sci.* **2020**, *11*, 9919–9924. [CrossRef]
43. Payra, D.; Naito, M.; Fujii, Y.; Yamada, N.L.; Hiromoto, S.; Singh, A. Bioinspired adhesive polymer coatings for efficient and versatile corrosion resistance. *RSC Adv.* **2015**, *5*, 15977–15984. [CrossRef]
44. Yang, J.; Keijsers, J.; van Heek, M.; Stuiver, A.; Stuart, M.A.C.; Kamperman, M. The effect of molecular composition and crosslinking on adhesion of a bio-inspired adhesive. *Polym. Chem.* **2015**, *6*, 3121–3130. [CrossRef]
45. Garcia-Penas, A.; Biswas, C.S.; Liang, W.J.; Wang, Y.; Yang, P.P.; Stadler, F.J. Effect of Hydrophobic Interactions on Lower Critical Solution Temperature for Poly(N-isopropylacrylamide-co-dopamine Methacrylamide) Copolymers. *Polymers* **2019**, *11*, 991. [CrossRef] [PubMed]
46. Yan, H.H.; Li, L.L.; Wang, Z.L.; Wang, Y.; Guo, M.; Shi, X.C.; Yeh, J.M.; Zhang, P.B. Mussel-Inspired Conducting Copolymer with Aniline Tetramer as Intelligent Biological Adhesive for Bone Tissue Engineering. *ACS Biomater. Sci. Eng.* **2020**, *6*, 634–646. [CrossRef]
47. Hennig, K.; Meyer, W. Synthesis and Characterization of Catechol-Containing Polyacrylamides with Adhesive Properties. *Molecules* **2022**, *27*, 4027. [CrossRef]
48. Hilfiker, J.N.; Stadermann, M.; Sun, J.; Tiwald, T.; Hale, J.S.; Miller, P.E.; Aracne-Ruddle, C. Determining thickness and refractive index from free-standing ultra-thin polymer films with spectroscopic ellipsometry. *Appl. Surf. Sci.* **2017**, *421*, 508–512. [CrossRef]

49. Liu, Z.; Hu, B.-H.; Messersmith, P.B. Acetonide protection of dopamine for the synthesis of highly pure N-docosahexaenoyldopamine. *Tetrahedron Lett.* **2010**, *51*, 2403–2405. [CrossRef]
50. Fischer, L.; Steffens, R.C.; Paul, T.J.; Hartmann, L. Catechol-functionalized sequence-defined glycomacromolecules as covalent inhibitors of bacterial adhesion. *Polym. Chem.* **2020**, *11*, 6091–6096. [CrossRef]
51. Stöckigt, J.; Antonchick, A.P.; Wu, F.; Waldmann, H. The Pictet–Spengler Reaction in Nature and in Organic Chemistry. *Angew. Chem. Int. Ed.* **2011**, *50*, 8538–8564. [CrossRef]
52. Yang, J.; Cohen Stuart, M.A.; Kamperman, M. Jack of all trades: Versatile catechol crosslinking mechanisms. *Chem. Soc. Rev.* **2014**, *43*, 8271–8298. [CrossRef] [PubMed]
53. Glatzel, S.; Badi, N.; Päch, M.; Laschewsky, A.; Lutz, J.-F. Well-defined synthetic polymers with a protein-like gelation behavior in water. *Chem. Commun.* **2010**, *46*, 4517–4519. [CrossRef] [PubMed]
54. Kemnitz, C.R.; Loewen, M.J. "Amide Resonance" Correlates with a Breadth of C−N Rotation Barriers. *J. Am. Chem. Soc.* **2007**, *129*, 2521–2528. [CrossRef] [PubMed]

Supporting Information

Contents

1. Monomer synthesis and characterization

***N*-(3,4-dihydroxyphenethyl)-2,2,2-trifluoroacetamide**

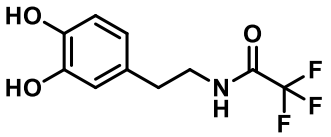

The synthesis procedure of *N*-(3,4-dihydroxyphenethyl)-2,2,2-trifluoroacetamide is known from literature[1] and was carried out according to it. In a round bottom flask, 20 g of dopamine hydrochloride 1 (105.40 mmol) was placed in methanol [2.5 mL/mmol] under an inert gas atmosphere (N_2). After the addition of 21.7 mL of methyl trifluoroacetate (210.80 mmol, 2.00 eq.) and 60 mL of triethylamine (421.60 mmol, 4.00 eq.), the apparatus was purged with nitrogen for an additional five minutes. Methanol was removed at the rotary evaporator and the pH of the crude product was adjusted to 1 by adding one milliliter of concentrated hydrochloric acid. After extraction with ethyl acetate, the organic phase was washed with water and dried with anhydrous magnesium sulfate. Ethyl acetate was removed on rotary evaporator and the product was obtained. A light brownish solid was obtained with a yield of 96%.

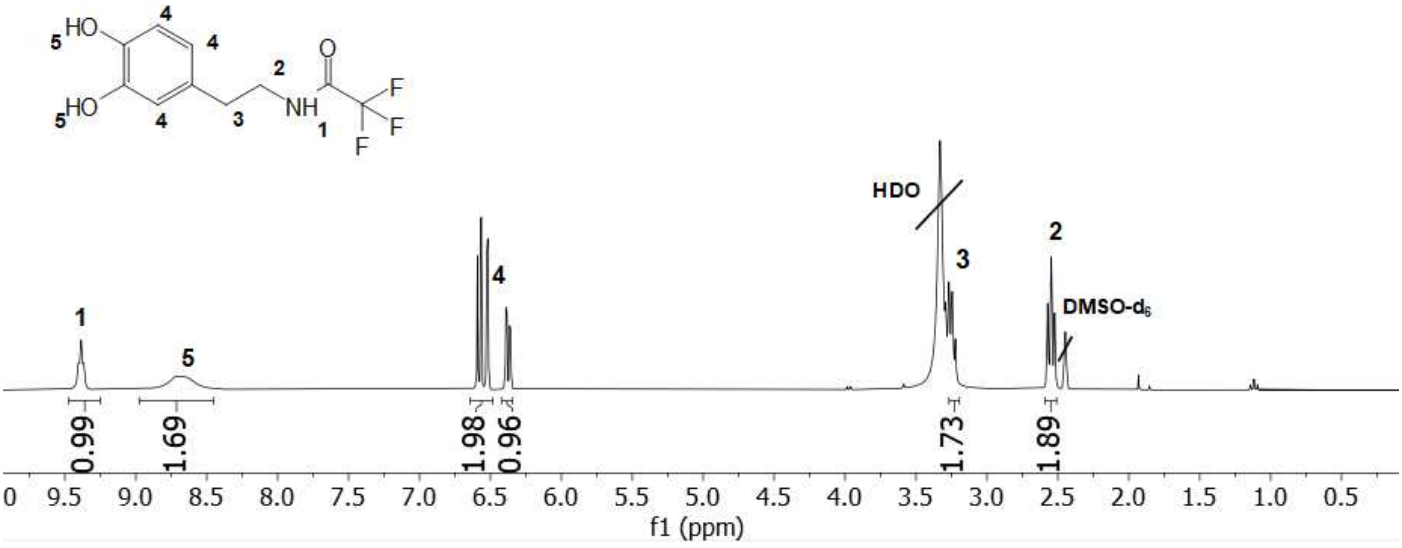

Figure S1. ^{1}H NMR-spectrum (300 MHz, DMSO-d_6) of N-(3,4-Dihydroxyphenethyl)-2,2,2-trifluoroacetamide.

^{1}H NMR (300 MHz, DMSO-*d*$_6$) δ [ppm] 9.39 (t, ^3J = 5.7 Hz, 1H, -N**H**-), 8.68 (s, 2H, -O**H**), 6.65-6.52 (m, 2H, Ar-**H**), 6.37 (dd, ^3J = 8.0, 1H, Ar-**H**), 3.29-3.16 (m, 2H, H_2O overlapping, -C**H**$_2$-NH-), 2.55 (t, ^3J = 7.4 Hz, 2H, -C**H**$_2$-Ar).

***N*-(2-(2,2-dimethylbenzo-1,3-dioxol-5-yl)ethyl)-2,2,2-trifluoroacetamide**

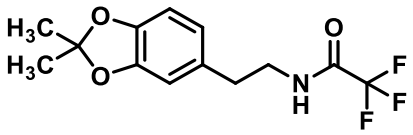

The synthesis procedure of *N*-(2-(2,2-dimethylbenzo-1,3-dioxol-5-yl)ethyl)-2,2,2-trifluoroacetamide is known from literature[1] and was carried out according to it. In a three-neck flask, 25 g of *N*-(3,4-dihydroxyphenethyl)-2,2,2-trifluoroacetamide (100.33 mmol) was placed in toluene [5 mL/mmol] under protective gas atmosphere (N_2). After addition of 24.7 mL of 2,2-dimethoxypropane (200.66 mmol, 2.00 eq.), the reaction solution was degassed for 10 min and heated at 80°C for 15 min under reflux. Then, 775 mg of *p*-toluenesulfonic acid (4.50 mol%) was added and heated at 80°C under reflux for another 2 h. The reaction solution was degassed. The cooled reaction solution was washed three times with water, dried with anhydrous magnesium sulfate, and toluene was removed on the rotary evaporator. The product was obtained as a brownish solid in 67% yield.

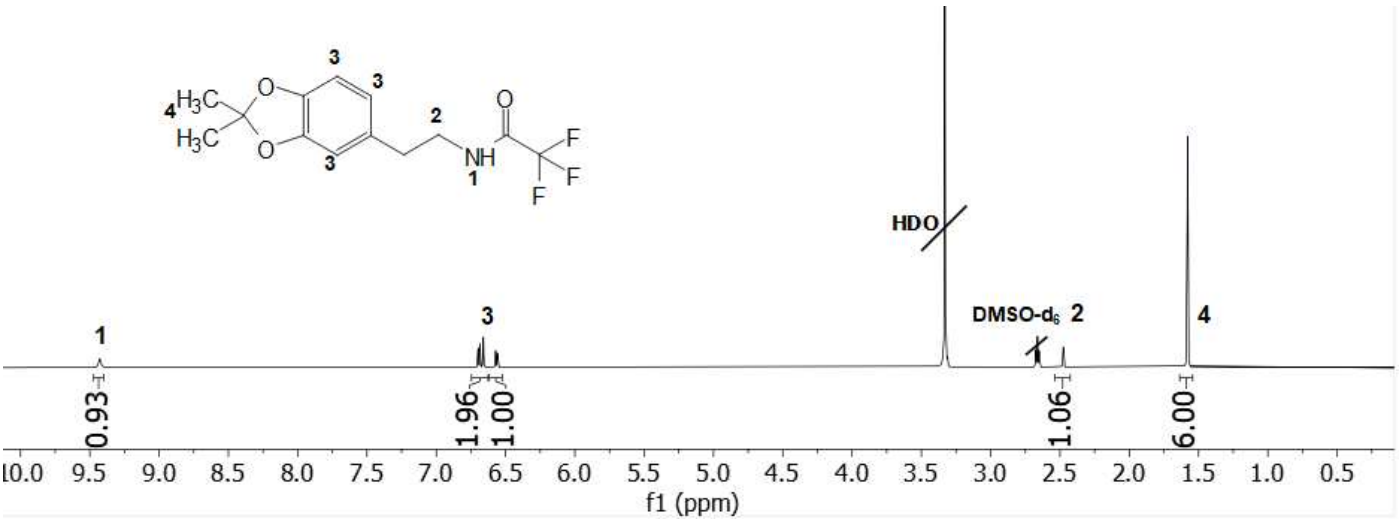

Figure S2. ^{1}H NMR spectrum (600 MHz, DMSO-d_6) of *N*-(2-(2,2-dimethylbenzo-1,3-dioxol-5-yl)ethyl)-2,2,2-trifluoroacetamide.

^{1}H NMR (600 MHz, DMSO-d_6) δ [ppm] 9.43 (t, ^3J = 5.7 Hz, 1H, -N**H**-), 6.72-6.65 (m, 2H, Ar-**H**), 6.57 (d, ^3J = 7.9, 1H, Ar-**H**), 3.30 (m, 2H, -C**H**$_2$-NH- H_2O overlapping), 2.66 (t, ^{3}J = 7.3 Hz, 2H, -C**H**$_2$-Ar-), 1.58 (s, 6H, 2 -C**H**$_3$).

2-(2,2-dimethylbenzo-1,3-dioxol-5-yl)ethan-1-amine

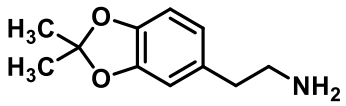

The synthesis procedure of 2-(2,2-dimethylbenzo-1,3-dioxol-5-yl)ethan-1-amine is known from literature[1] and was carried out according to this. 15 g of *N*-(2-(2,2-dimethylbenzo-1,3-dioxol-5-yl)ethyl)-2,2,2-trifluoroacetamide (51.90 mmol) was placed in THF [6 mL/mmol] and 4.32 g of LiOH (103.80 mmol, 2.00 eq.) dissolved in water [2 mL/mmol] was added. The mixture was stirred at RT for 4 h and THF was then removed on the rotary evaporator. The crude product was extracted with ethyl acetate and the organic phase was washed with water. After drying with magnesium sulfate, ethyl acetate was removed with the rotary evaporator. A brownish oil was obtained with a yield of 92%.

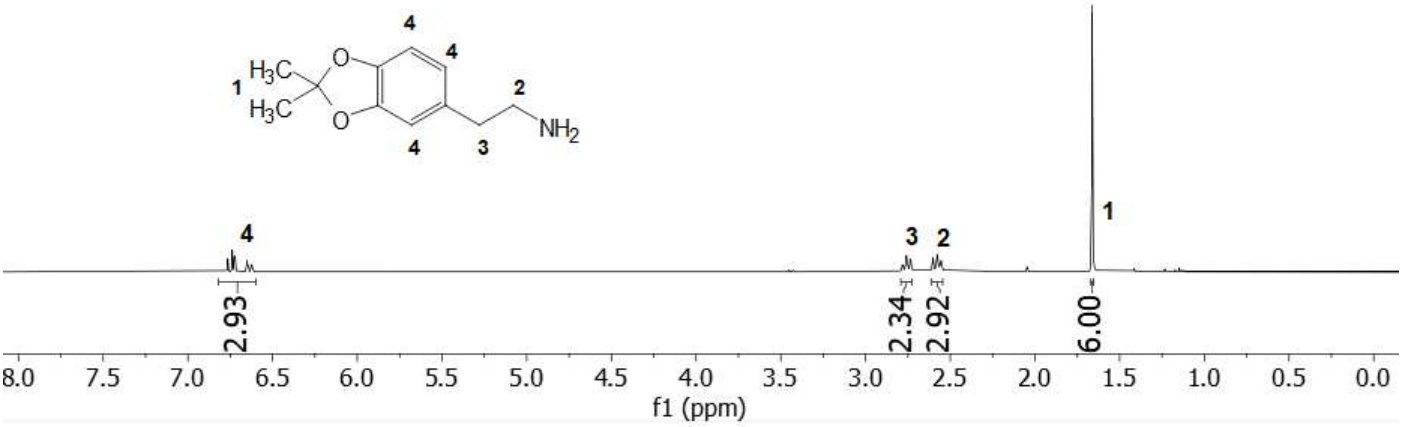

Figure S3. ^{1}H NMR-spectrum (300 MHz, DMSO-d$_6$) of 2-(2,2-dimethylbenzo-1,3-dioxol-5-yl)ethan-1-amine.

^{1}H NMR (300 MHz, DMSO-*d*$_6$) δ [ppm] 6.84-6.72 (m, 2H, Ar-**H**), 6.64 (d, ^{3}J = 7.8 Hz), 2.81-2.72 (m, 2H, -C**H**$_2$-NH-), 2.58 (t, 2H, DMSO overlapping, -C**H**$_2$-Ar), 1.66 (s, 6H, 2 -C**H**$_3$).

***N*-(2-(2,2-dimethylbenzo-1,3-dioxol-5-yl)ethyl)acrylamide (CAA monomer)**

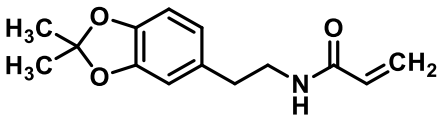

9.8 g dopamine acetonide (50.66 mmol) and 21 mL triethylamine (151.98 mmol, 3.00 eq.) were dissolved in dichloromethane [3 mL/mmol] and cooled to 0°C (ice bath). 4.95 mL of acryloyl chloride (60.79 mmol, 1.20 eq.) was added slowly (about 20 min) to the reaction solution in DCM [1 mL/mmol]. After the addition was complete, the ice bath was removed and the mixture was stirred for 2 h at RT. The reaction solution was washed three times with brine, the organic phase was dried with anhydrous magnesium sulfate, and the dichloromethane was removed on the rotary evaporator. The pressure was set no lower than 600 mBar at 40°C bath temperature so that self-initiated polymerization could not occur. After removal of the solvent, the product was purified by column chromatography. This was done on silica gel using the flash technique, with an eluent mixture consisting of ethyl acetate and *n*-hexane (EE/Hex 1/1 vol.%; Rf = 0.55). The monomer was obtained as a brown highly viscous oil with a yield of 48%.

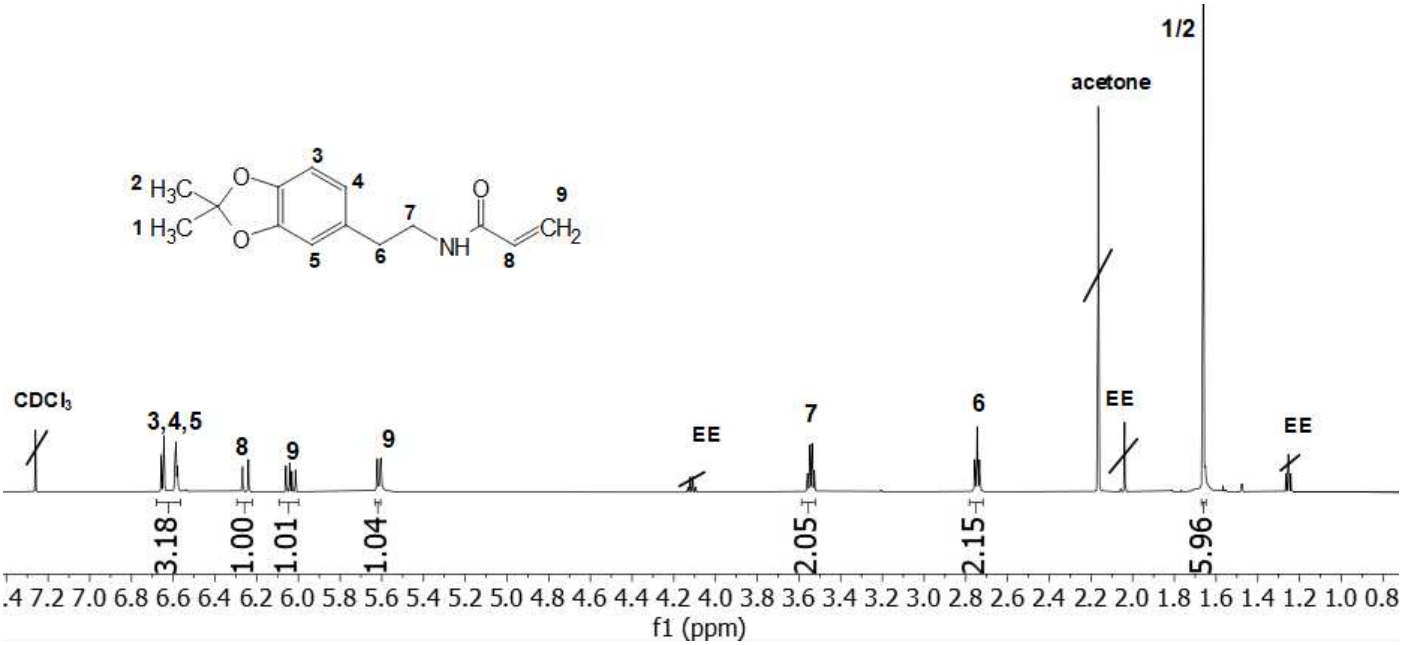

Figure S4. [1]H NMR spectrum (600 MHz, CDCl3) of the synthesized dopamineacetonide acrylamide (CAA) monomer.

[1]H NMR (600 MHz, Chloroform-*d*) δ [ppm] 6.65 (d, *J* = 8.2 Hz, 2H, Ar-**H**), 6.60-6.58(m, 1H, Ar-**H**), 6.25 (dd, *J* = 16.9, 1.4 Hz, 1H, -C**H**=CH2), 6.04 (dd, *J* = 16.9, 10.3 Hz, 1H, =C**H**2), 5.61 (dd, *J* = 10.3, 1.4 Hz, 1H, =C**H**2), 3.54 (td, [3]*J* = 6.9 Hz, 2H, -C**H**2-NH-), 2.75 (t, [3]*J* = 6.9 Hz, 2H, -C**H**2-Ar), 1.66 (s, 6H, 2 -C**H**3).

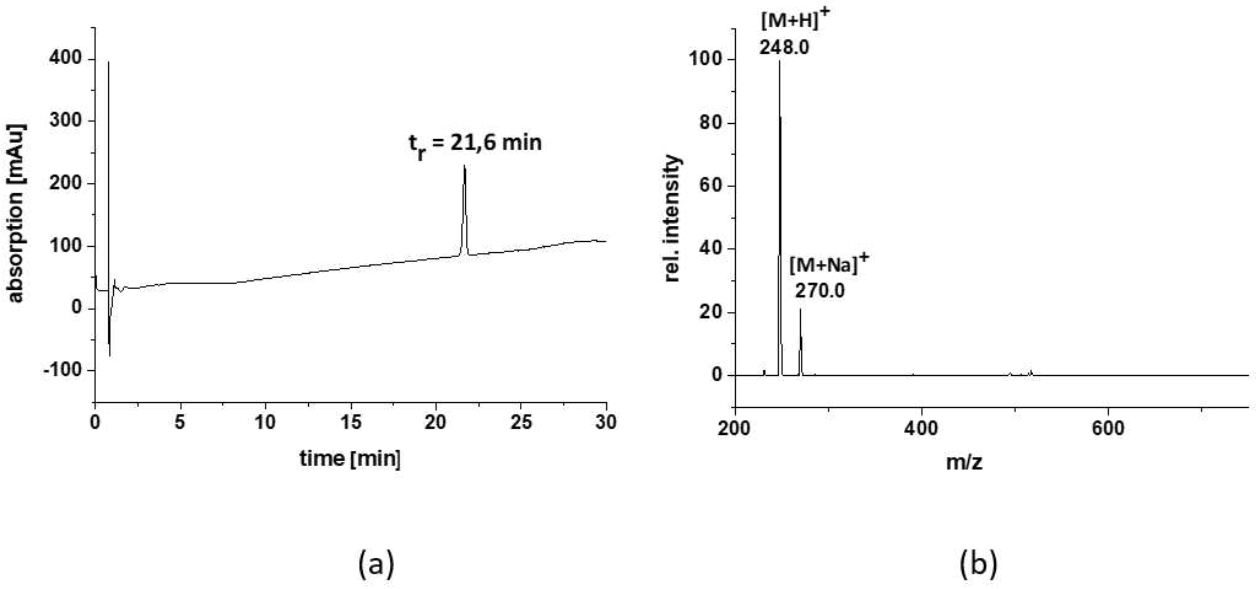

Figure S5. (a) LC-spectrum of CAA; (A: 95% H2O/ 5% MeCN/ 0.1% formic acid; 100% A -> 50% A in 30 min); (b) ESI-MS-spectrum of CAA.

ESI-MS for $C_{14}H_{17}NO_3$: $[M+H]^+$ calculated 248.29, measured 248.0.

***N*-(2-amino-2-oxoethyl)acrylamide**

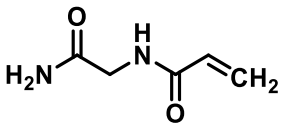

The synthesis procedure of the PA monomer *N*-(2-amino-2-oxoethyl)acrylamide is known from literature[2] and was carried out following it. 10 g glycinamide hydrochloride 2 (90.50 mmol) and 25 g potassium carbonate (181.00 mmol, 2.00 eq.) were dissolved in water [1.50 mL/mmol] and cooled to 0°C (ice bath). 8.8 mL of acryloyl chloride 5 (108.60 mmol, 1.20 eq.) in diethyl ether [2.50 mL/mmol] was added slowly (about 30 min). After addition was complete, the ice bath was removed and the reaction solution was stirred for 2 h at RT. The organic phase was removed on the rotary evaporator and the potassium carbonate was precipitated by addition of 1 L of cold acetone and filtered off. Acetone was removed on the rotary evaporator and a spatula tip of hydroquinone was added to the aqueous phase as a polymerization inhibitor. Now the aqueous phase could be removed on the rotary evaporator and the product was obtained as a colorless solid with a yield of 74 %.

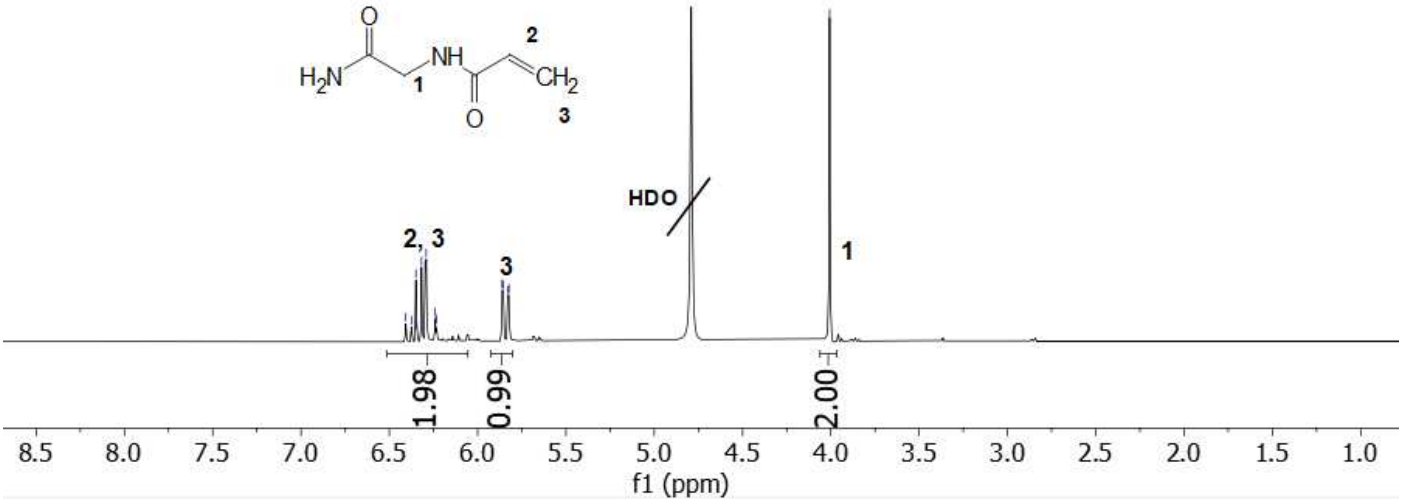

Figure S6. ^{1}H NMR spectrum (300 MHz, D_2O) of *N*-(2-amino-2-oxoethyl)acrylamide.

^{1}H NMR (300 MHz, D_2O) δ [ppm] 6.51-6.16 (m, 2H, -C**H**=C**H**$_2$), 5.84 (dd, *J* = 9.6, 2.0 Hz, 1H, =C**H**$_2$), 4.01 (s, 2H, -C**H**$_2$-)

2. Determination of reaction conditions for free radical polymerization

First, **HY** was homopolymerized to determine the basic reaction conditions for free radical polymerization of the Mfp-inspired copolymers (Scheme S1, Table S1). As expected, the average molecular weight increased by increasing the monomer concentration. Similarly, increasing the amount of initiator led to increased dispersity and lowering of the average molecular weight. Good results were obtained with an initiator amount of 1 mol% AIBN, so this was used for further copolymerizations. With 0.5 mol% initiator, no average molecular weight could be determined, since presumably the amount of initiator was too low for the reaction, or the inhibitor added to commercially purchased monomers stopped the polymerization early. With higher amounts of initiator, the measured molecular weights were too low.

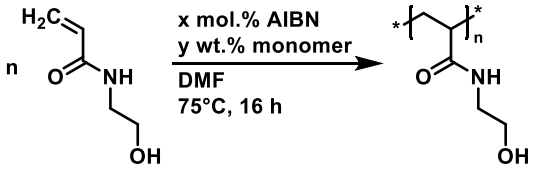

Scheme S1. Reaction scheme for the synthesis of the **HY**-homopolymer.

Table S1. Reaction conditions for homopolymerization of the HY monomer.

#	AIBN [mol%]	[Monomer] [wt.%]	$\bar{M}_n$[a] [kDa]	Đ[a]
1	0.5	5	-	-
2	1	5	6.8	1.35
3	2	5	-	-
4	3	5	4.9	1.50
5	1	10	4.1	1.40
6	1	20	14.0	1.90

[a]: determined by SEC

Subsequently, it was verified which monomer concentration leads to good results for a simplified copolymer system of **TA** and **HY** (Scheme S2, Table S2). At higher concentrations, the average molecular weight increased and at lower concentrations it decreased as expected. Since the actual incorporation of the monomers deviated only slightly from the theoretical values, and inaccuracies are to be expected in a determination by ^{1}H NMR-spectroscopy, a 1:1 incorporation of the monomers can be assumed. For the following copolymerizations, 20 wt.% monomer and 1 mol% initiator were set as reaction conditions.

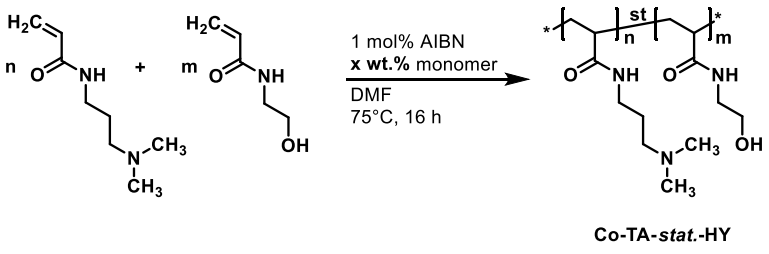

Scheme S2. Reaction scheme for the synthesis of the **TA-HY**-copolymers.

Table S2. Reaction conditions for copolymerization of **TA** and **HY**.

#	monomer ratio		monomer concentration [wt.%]	theor. TA incorporation [%]	determ. TA incorporation [%][b]	Mn[a] [kDa]	Đ[a]
	HY eq.	TA eq.					
1	1	1	5	50	58	-	-
2	3	1	5	25	28	5.6	1.30
3	6	1	5	14	15	9.0	1.60
4	1	1	20	50	53	-	-
5	3	1	20	25	28	34.0	1.23
6	6	1	20	14	17	40.0	1.80
7	6	1	10	14	-	9.4	1.45
8	6	1	30	14	-	37.0	1.65
9	6	1	50	14	-	-	-

[a]: determined by SEC, [b]: determined by ^{1}H NMR-spectroscopy

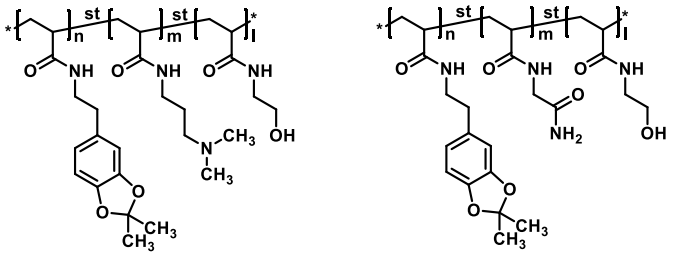

Scheme S1 Copolymers synthesized to determine optimal polymerization conditions.

The polymer composition was analyzed during the polymerization reaction to estimate the distribution of the different monomers in the final polymers. Two polymers CAA-*stat*.-TA-*stat*.-HY and CAA-*stat*.-PA-*stat*.-HY were polymerized and analyzed at different intervals during the reaction. The reactions were carried out with a theoretical monomer incorporation of 5% CAA, 45% TA and 50% HY (CAA-*stat*.-TA-*stat*.-HY) and 5% CAA, 45% PA and 50% HY (CAA-*stat*.-PA-*stat*.-HY). Monomers were placed in a microwave tube and dissolved in DMF. The reaction solution was degassed for 20 min with inert gas (N_2) and stirred for 18 h at 75°C. At the different intervals of 30 min, 1 h, 2 h, 4 h, and overnight, samples were taken from the reaction solution and the reaction was stopped by precipitation in diethyl ether. Subsequently, the obtained copolymers were dialyzed (2 kDa exclusion size) and lyophilized. ^{1}H NMR-spectroscopy was used to determine the monomer composition (Table S3).

Table S3. Obtained monomer incorporation in the copolymer CAA-TA-HY.

	monomer incorporation [%][a]					
	CAA-*stat.*-TA-*stat.*-HY			**CAA-*stat.*-PA-*stat.*-HY**		
	CAA	**TA**	**HY**	**CAA**	**PA**	**HY**
30 min	6	51	43	4.5	43	52.5
60 min	4	53	43	5.5	38	56.5
120 min	3	56	41	6.5	39	54.5
240 min	3	54	43	-	-	-
over night	2.5	53.5	44	-	-	-

[a]: determined by ^{1}H NMR-spectroscopy

3. Synthesis and characterization of final polymers

PA50-*stat.*-HY50

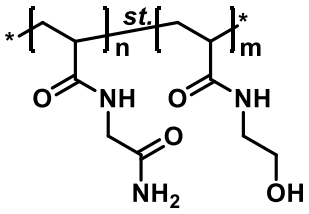

1.54 g of *N*-acryloylglycinamide (12.00 mmol), 1.38 g of *N*-hydroxyethylacrylamide (12.00 mmol, 1.00 eq.), and 39.41 mg of AIBN (1 mol%) were placed in a microwave tube and dissolved in DMF. The reaction solution was degassed for 20 min with inert gas (N_2) and stirred for 18 h at 75°C. The mixture was then poured onto diethyl ether to precipitate the polymer. After centrifugation for 5 min and decantation of the ether, the polymer was dried under a nitrogen atmosphere. It was then dissolved in water and dialyzed with a dialysis tube with a MWCO of 7.50 kDa for five cycles. After subsequent lyophilization, the polymer PA50-*stat.*-HY50 was obtained as a colorless solid with a yield of 39%.

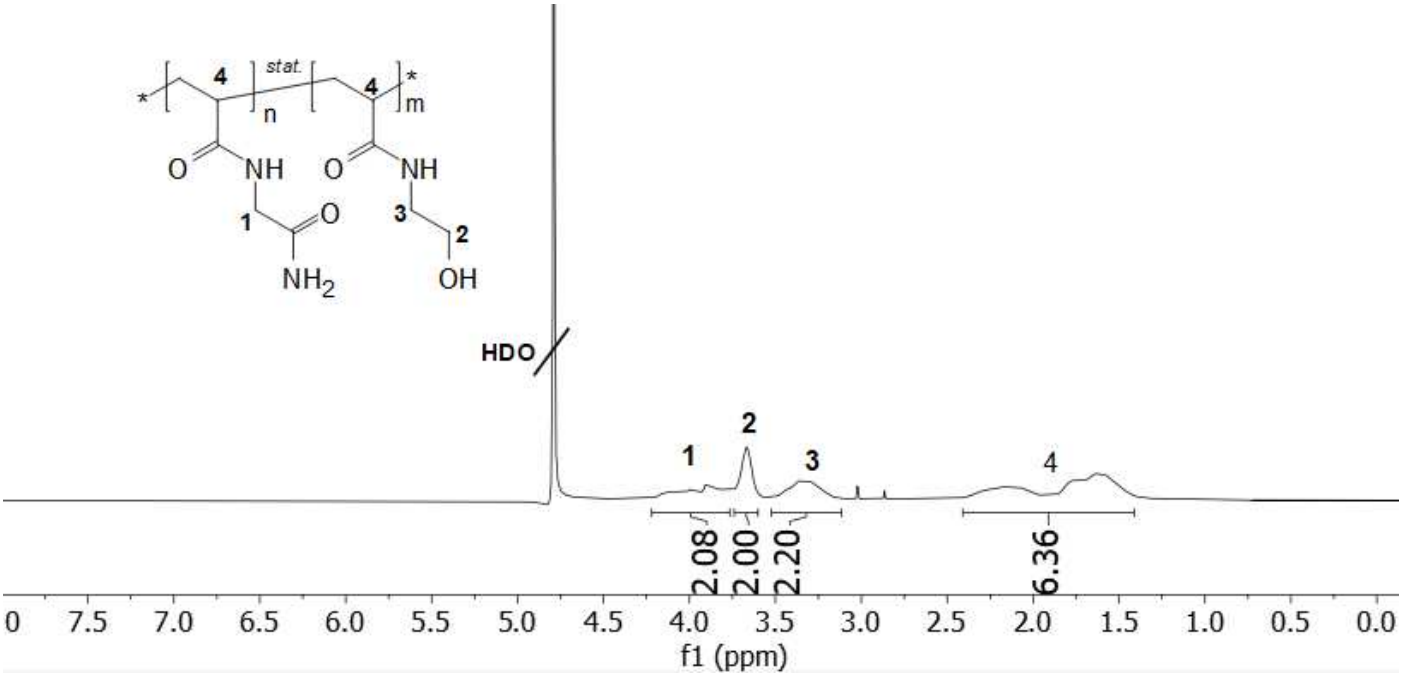

Figure S7. ^{1}H NMR spectrum (300 MHz, D_2O) of **PA50-*stat.*-HY50**.

^{1}H NMR (300 MHz, D_2O) δ [ppm] 3.94 (m, **1**), 3.67 (s, **2**), 3.34 (s, **3**), 2.47-1.36 (m, **4**).

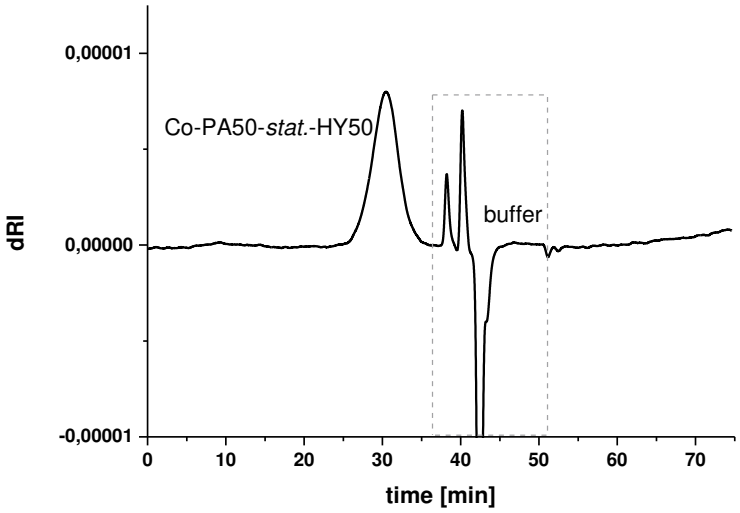

Figure S8. H_2O SEC-MALS spectrum of **PA50-*stat.*-HY50**.

SEC-MALS: $\overline{M}_n$ = 50.33 kDa; Đ = 1.36

TA52-*stat.*-HY48

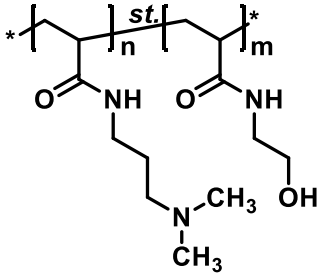

1.64 mL of dimethylaminopropylacrylamide (10.00 mmol), 1.151 g of *N*-hydroxyethylacrylamide (10.00 mmol, 1.00 eq.), and 32.84 mg of AIBN (1 mol%) were placed in a microwave tube and dissolved in 14.3 mL of DMF. The reaction solution was degassed for 20 min with inert gas (N_2) and stirred for 18 h at 75°C. The solution was then poured onto diethyl ether, which was acidified with 0.5 mL trifluoroacetic acid, to precipitate the polymer. After centrifugation for 5 min and decantation of the ether, the polymer was dried under a nitrogen atmosphere. It was then dissolved in a little water and dialyzed with a dialysis tube with a MWCO of 7.50 kDa for five cycles. After subsequent lyophilization, the polymer TA52-*stat.*-HY48 was obtained as a colorless solid with a yield of 91%.

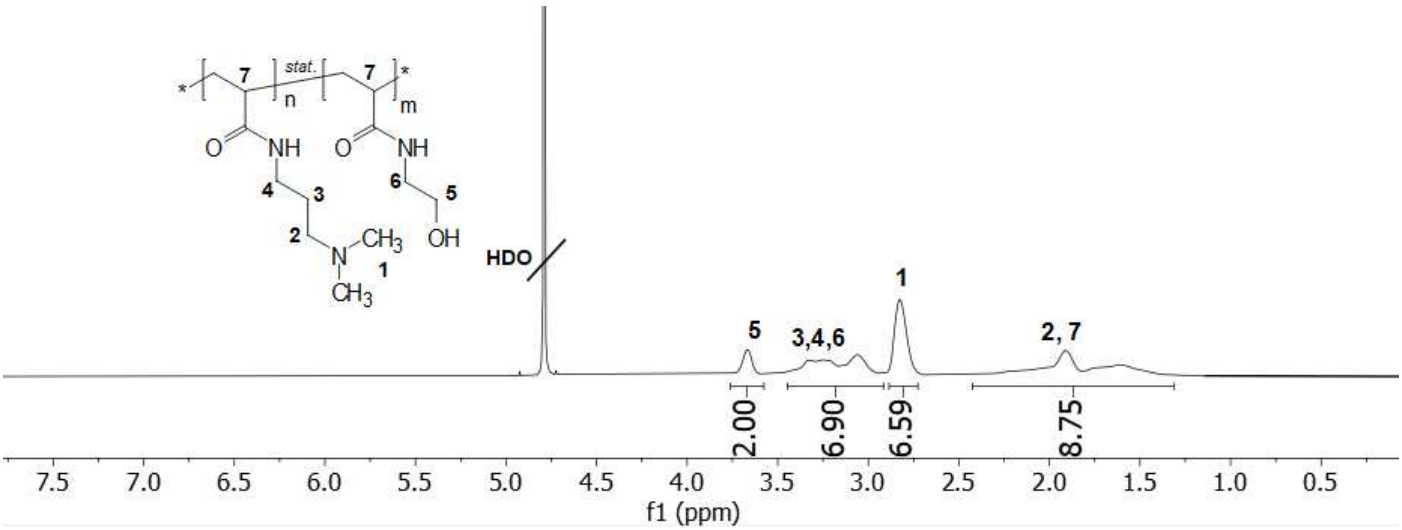

Figure S9. ^{1}H NMR spectrum (300 MHz, D_2O) of **TA52-*stat.*-HY48**.

^{1}H NMR (300 MHz, D_2O) δ [ppm] 3.67 (s, **5**), 3.53-2.94 (m, **3**, **4**, **6**), 2.82 (s, **1**), 2.41-1.28 (m, **7**, **2**).

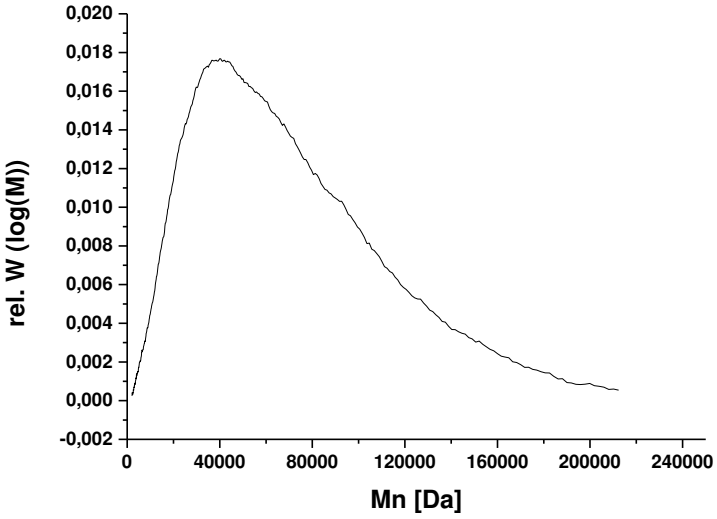

Figure S10. DMAC-SEC spectrum of **TA52-*stat.*-HY48**.

SEC: $\overline{M}_n$ = 23.5 kDa; Đ = 1.97

CAA4-*stat.*-TA48-*stat.*-HY48

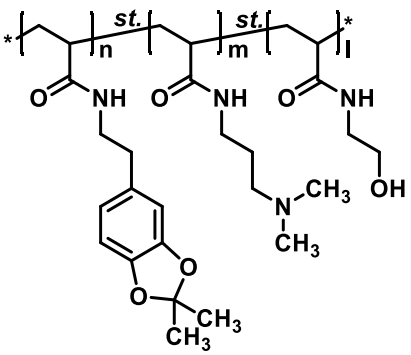

0.247 g CAA monomer (1.00 mmol), 1.48 mL dimethylaminopropylacrylamide (9.00 mmol, 9.00 eq.), 1.15 g *N*-hydroxyethylacrylamide (10.00 mmol, 10.00 eq.), and 32.84 mg AIBN (1 mol%) were placed in a microwave tube and dissolved in DMF. The reaction solution was degassed for 20 min with inert gas (N_2) and stirred for 18 h at 75°C. Then, the solution was poured onto diethyl ether, which was acidified with 0.5 mL of trifluoroacetic acid, thus precipitating the polymer. After centrifugation for 5 min and decantation of the ether, the polymer was dried under a nitrogen atmosphere. It was then dissolved in water and dialyzed with a dialysis tube with a MWCO of 7.50 kDa for five cycles. After subsequent lyophilization, the polymer CAA4-*stat.*-TA48-*stat.*-HY48 was obtained as a yellowish solid with a yield of 98%. The monomer incorporation was verified by ^{1}H NMR spectroscopy.

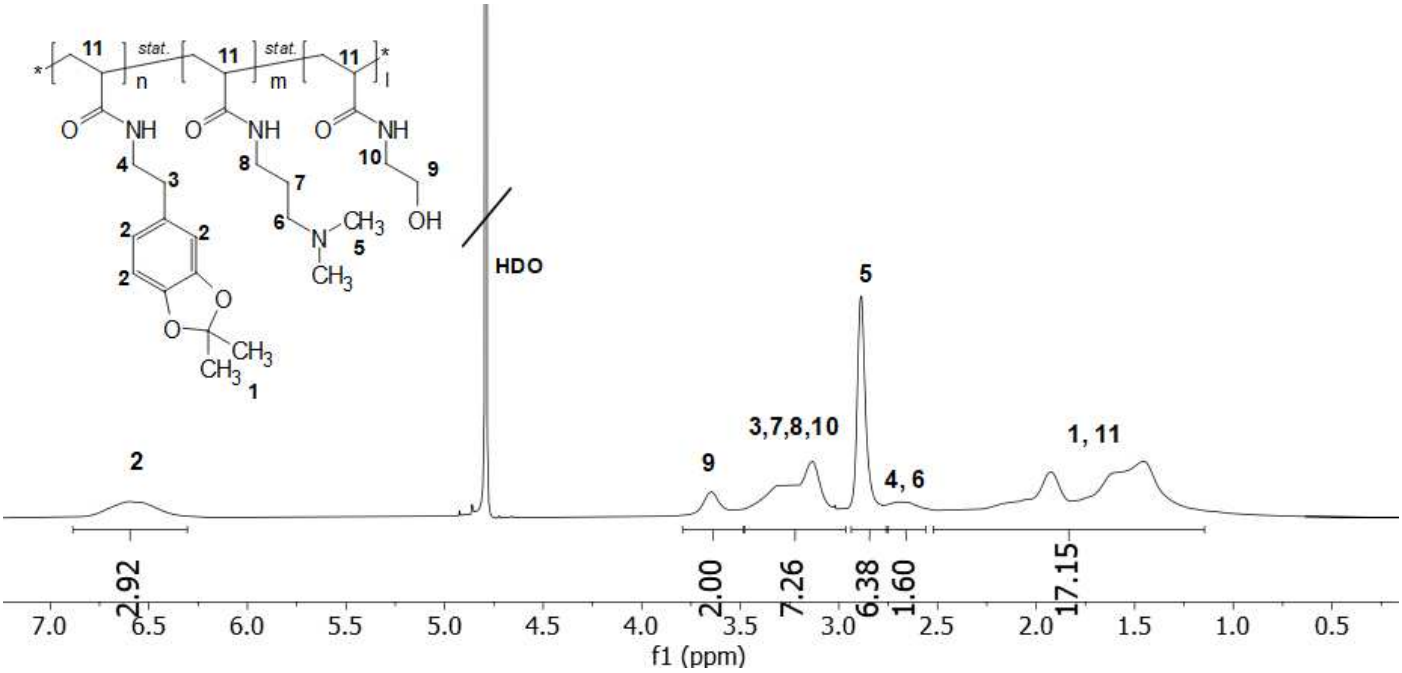

Figure S1. ^{1}H NMR spectrum (300 MHz, D_2O) of **CAA4-*stat.*-TA48-*stat.*-HY48**.

^{1}H NMR (300 MHz, D_2O) δ [ppm] 6.79 (s, **2**), 3.67 (s, **9**), 3.52-3.05 (m, **3**, **7** ,**8**, **10**), 2.89 (s, **5**), 2.76-2.54 (s, **6**, **4**), 2.45-1.29(m, **1**, **11**).

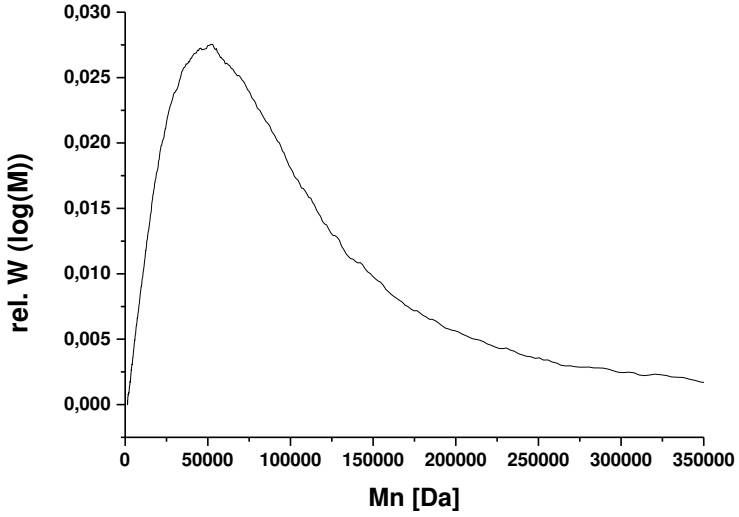

Figure S2. DMAC-SEC spectrum of **CAA4-*stat.*-TA48-*stat.*-HY48.**

SEC: $\overline{M}_n$ = 21.9 kDa; Đ = 2.61

CAA3-*stat.*-PA45-*stat.*-HY52

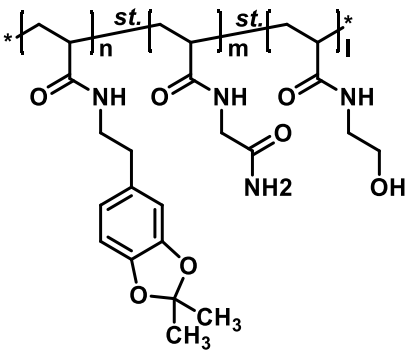

0.247 g CAA monomer (1.00 mmol), 1.15 g *N*-acryloylglycinamide (9.00 mmol, 9.00 eq.), 1.15 g *N*-hydroxyethylacrylamide (10.00 mmol, 10.00 eq.), and 32.84 mg AIBN (1 mol%) were placed in a microwave tube and dissolved in DMF (20 wt.%). The reaction solution was degassed for 20 min with inert gas (N_2) and stirred for 18 h at 75°C. Then, the solution was poured onto diethyl ether, thus precipitating the polymer. After centrifugation for 5 min and decantation of the ether, the polymer was dried under a nitrogen atmosphere. It was then dissolved in water and dialyzed with a dialysis tube with a MWCO of 7.50 kDa for five cycles. After subsequent lyophilization, the polymer CAA4-*stat.*-PA45-*stat.*-HY52 was obtained as a yellowish solid with a yield of 45%. The monomer incorporation was verified by ^{1}H NMR spectroscopy.

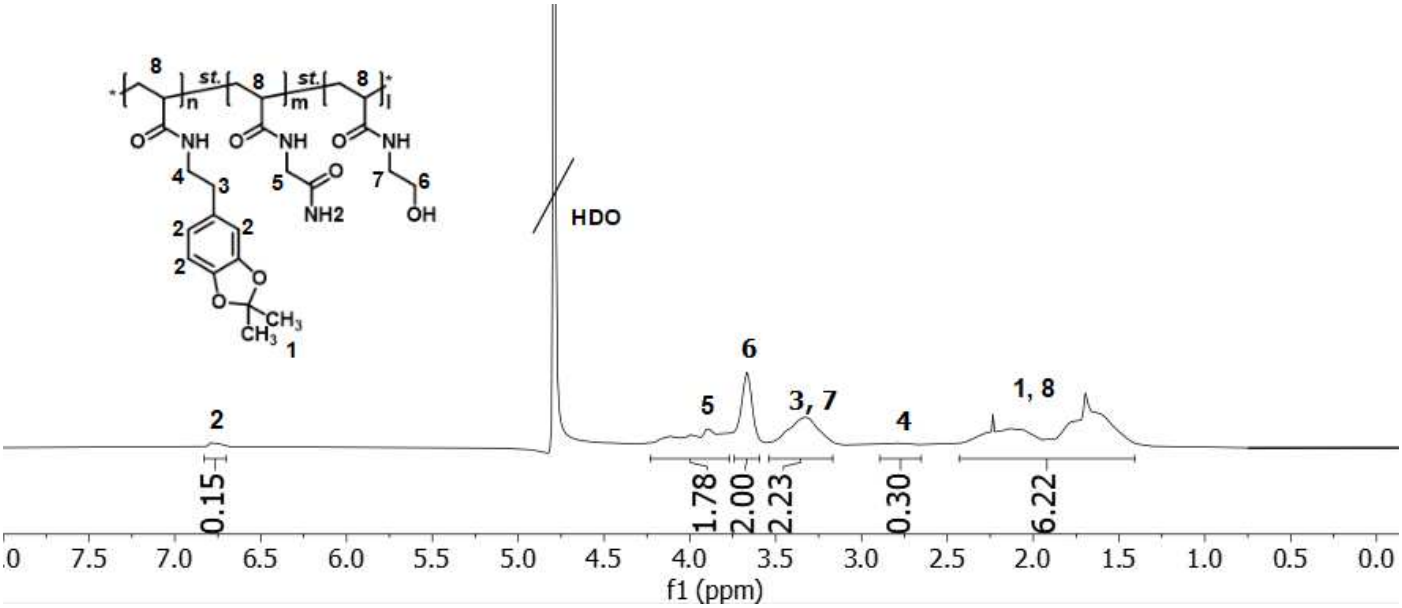

Figure S3. ^{1}H NMR spectrum (300 MHz, D_2O) of **CAA3-*stat.*-PA42-*stat.*-HY52**.

^{1}H NMR (300 MHz, D_2O) δ [ppm] δ [ppm] 6.77 (s, **2**), 4.32-3.76 (m, **5**), 3.67 (s, **6**), 3.51-3.15 (m, **3**, **7**), 2.75 (s, **4**), 2.60-1.36(m, **1, 8**).

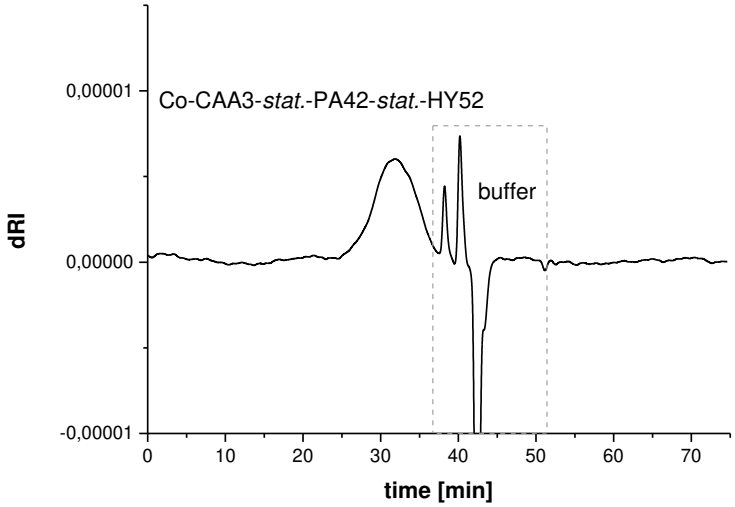

Figure S4. H_2O-SEC-MALS spectrum of **CAA3-*stat.*-PA42-*stat.*-HY52.**

SEC-MALS: $\overline{M}_n$ = 23.4 kDa; Đ = 1.92

TA15-*stat.*-PA13-*stat.*-HY72

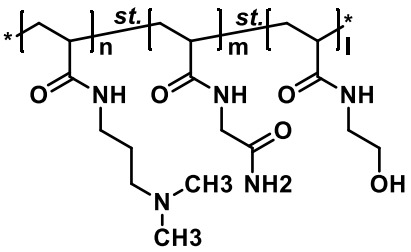

0.493 mL dimethylaminopropylacrylamide (3.00 mmol), 0.384 g *N*-acryloylglycinamide (3.00 mmol, 1.00 eq.), 1.612 g *N*-hydroxyethylacrylamide (14.00 mmol, 4.70 eq.), and 32.84 mg AIBN (1 mol%) were placed in a microwave tube and dissolved in DMF (20 wt.%). The reaction solution was degassed for 20 min with inert gas (N_2) and stirred for 18 h at 75°C. Then, the solution was poured onto diethyl ether, which was acidified with 0.5 mL of trifluoroacetic acid, thus precipitating the polymer. After centrifugation for 5 min and decantation of the ether, the polymer was dried under a nitrogen atmosphere. It was then dissolved in water and dialyzed with a dialysis tube with a MWCO of 7.50 kDa for five cycles. After subsequent lyophilization, the polymer TA15-*stat.*-PA13-*stat.*-HY72 was obtained as a colorless solid with a yield of 93%. The monomer incorporation was verified by ^{1}H NMR spectroscopy.

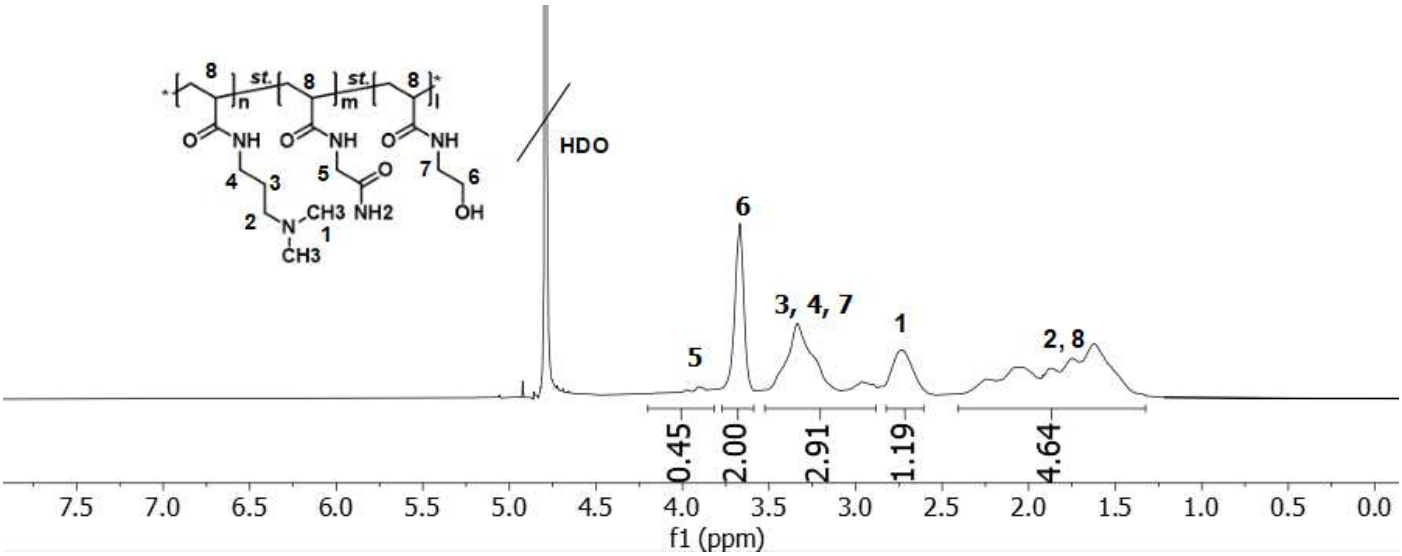

Figure S5. ^{1}H NMR spectrum (300 MHz, D_2O) of **TA15-*stat.*-PA13-*stat.*-HY72**.

^{1}H NMR (300 MHz, D_2O) δ [ppm] δ [ppm] 4.32-3.84(m, **5**), 3.67 (s, **6**), 3.33 (m, **3**, **4**, **7**), 2.73 (s, **1**), 2.41-1.37 (m, **2**, **8**).

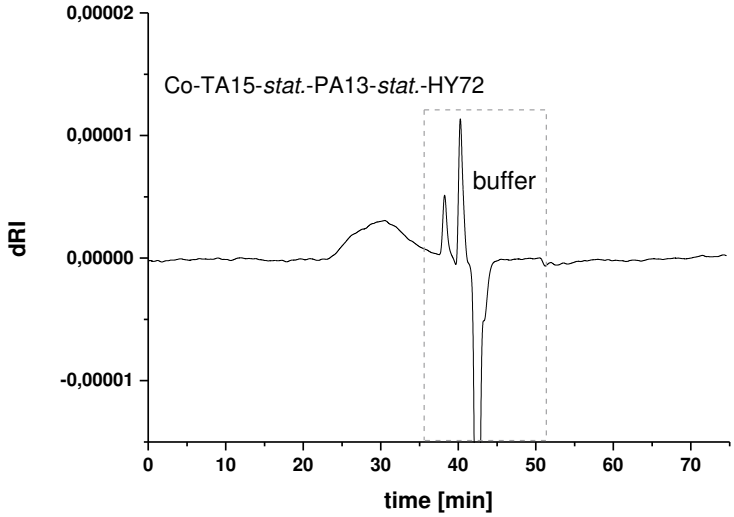

Figure S6. H_2O-SEC-MALS spectrum of **TA15-*stat.*-PA13-*stat.*-HY72.**

SEC-MALS: $\overline{M}_n$ = 69.93 kDa; Đ = 1.74

CAA-*stat.*-TA-*stat.*-PA-*stat.*-HY

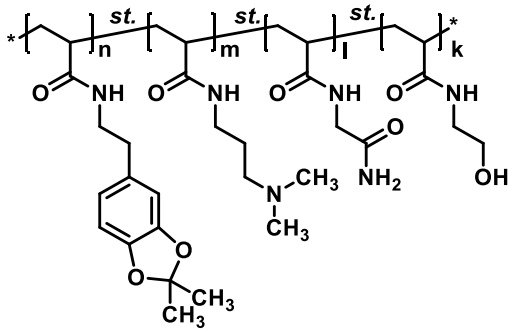

CAA monomer (1.0 eq.), dimethylaminopropylacrylamide (TA monomer, **x** eq., see Table S4), *N*-acryloylglycinamide (PA monomer, **y** eq., see Table S4), *N*-hydroxyethylacrylamide (HY monomer, **z** eq., see Table S4), and AIBN (1 mol%) were placed in a microwave tube and dissolved in DMF (20 wt.%). The reaction solution was degassed for 20 min with inert gas (N_2) and stirred for 18 h at 75°C. Then, the solution was poured onto diethyl ether, which was acidified with 0.5 mL of trifluoroacetic acid, thus precipitating the polymer. After centrifugation for 5 min and decantation of the ether, the polymer was dried under a nitrogen atmosphere. It was then dissolved in water and dialyzed with a dialysis tube with a MWCO of 7.50 kDa for five cycles. After subsequent lyophilization, the polymer TA15-*stat.*-PA13-*stat.*-HY72 was obtained as a colorless solid with a yield of 93%. The monomer incorporation was verified by ^{1}H NMR spectroscopy.

Table S4. Used quantities and equivalents build the final polymers by incorporation of all four monomers.

polymer	Used equivalents				yield [%]
	CAA	**TA**	**PA**	**HY**	
CAA4-*stat.*-TA22-*stat.*-PA17-*stat.*-HY57	1.00 (0.247 g)	4.50 (0.740 mL)	4.50 (0.576 g)	10.00 (1.151 g)	85
CAA13-*stat.*-TA15-*stat.*-PA18-*stat.*-HY54	1.00 (0.742 g)	1.00 (0.493 mL)	1.00 (0.384 g)	3.70 (1.266 g)	91
CAA5-*stat.*-TA5-*stat.*-PA7-*stat.*-HY83	1.00 (0.247 g)	1.00 (0.164 mL)	1.00 (0.128 g)	17.00 (1.957 g)	94

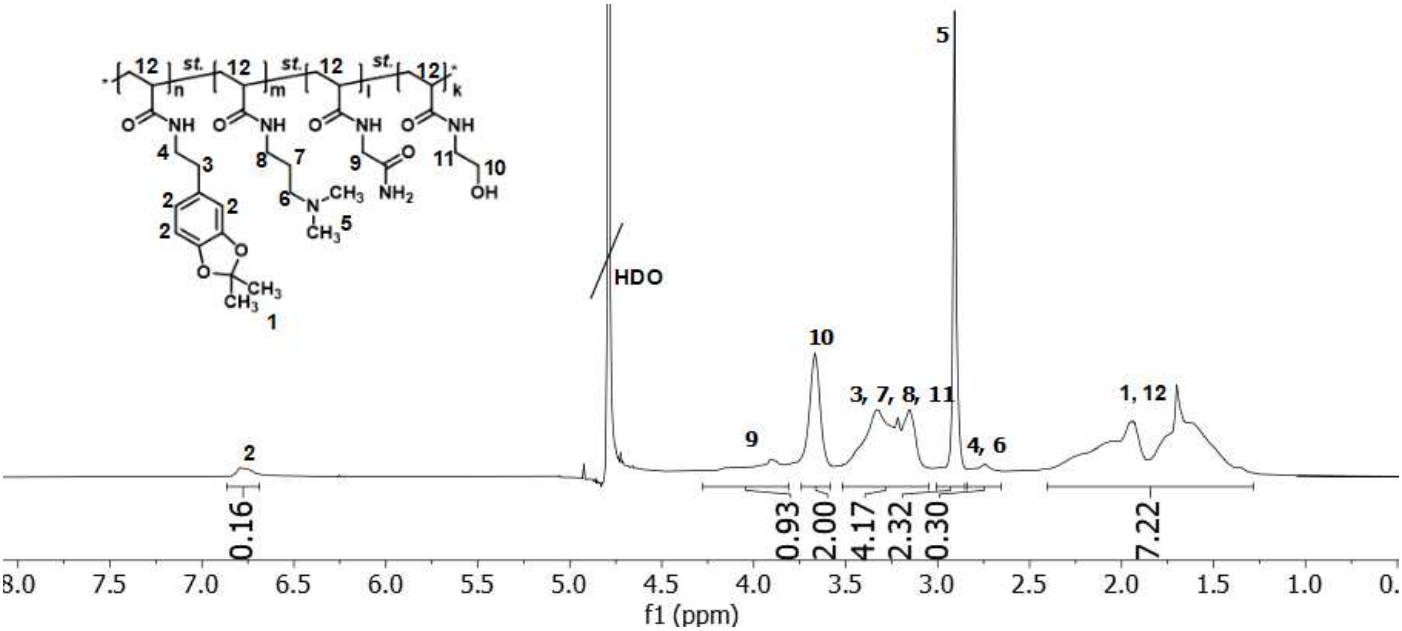

Figure S7. ^{1}H NMR spectrum (300 MHz, D_2O) of **CAA4-*stat.*-TA22-*stat.*-PA17-*stat.*-HY57**.

^{1}H NMR (300 MHz, D_2O) δ [ppm] δ [ppm] 6.77 (s, **2**), 4.35-3.80 (m, **9**), 3.67 (s, **10**), 3.48-3.06(m, **3**, **7**, **8**, **11**), 2.91 (s, **5**), 2.70 (s, **4**, **6**), 2.51-1.24 (m, **1**, **12**).

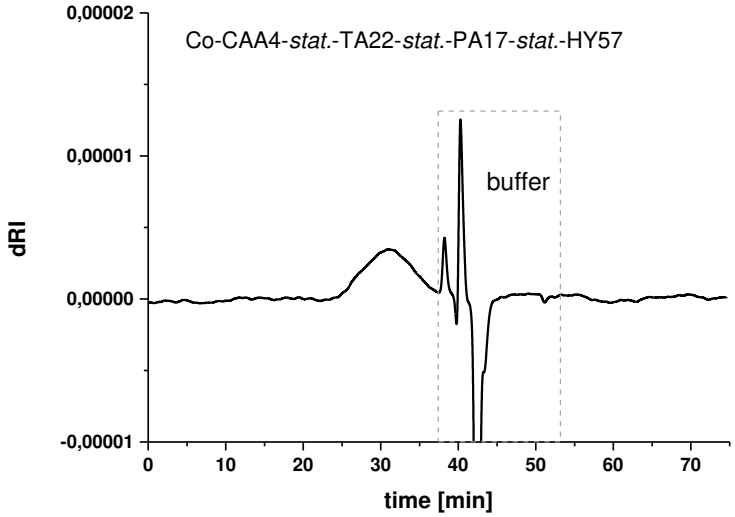

Figure S8. H_2O-SEC-MALS spectrum of **CAA4-*stat.*-TA22-*stat.*-PA17-*stat.*-HY57.**

SEC-MALS: $\overline{M}_n$ = 64.43 kDa; Đ = 1.73

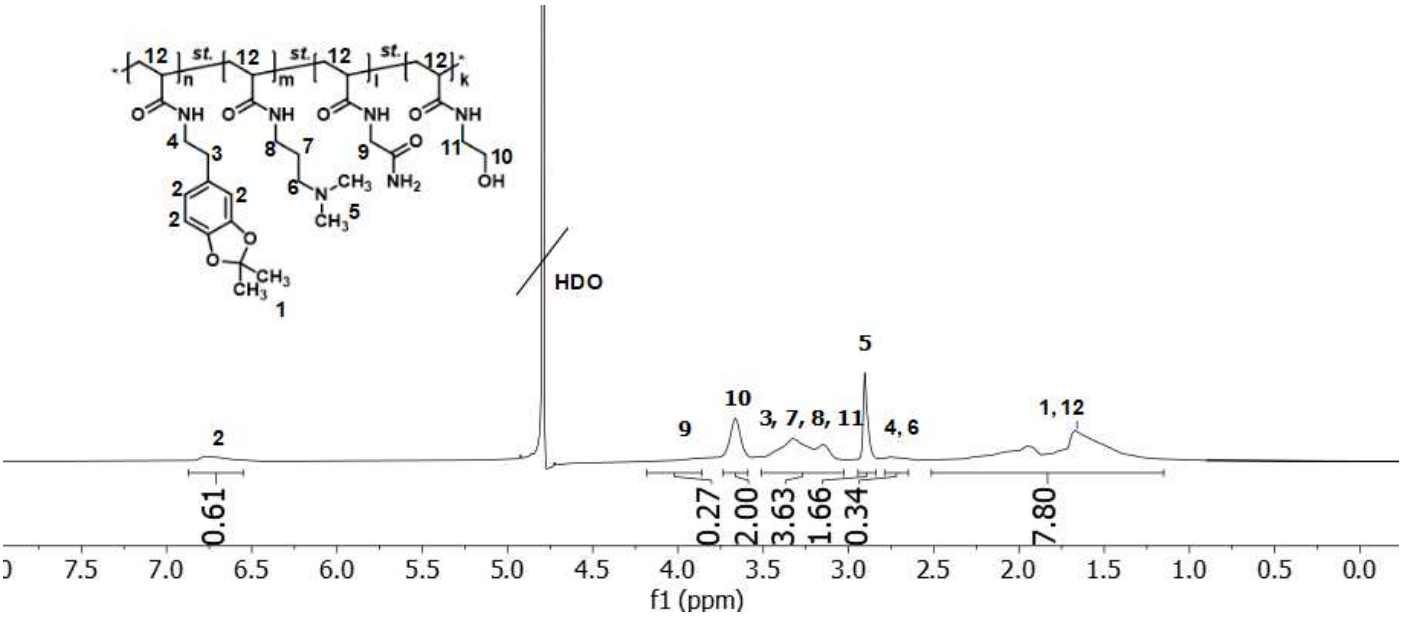

Figure S9. ^1H NMR spectrum (300 MHz, D_2O) of **CAA13-*stat.*-TA15-*stat.*-PA18-*stat.*-HY54**.

^1H NMR (300 MHz, D_2O) δ [ppm] δ [ppm] 6.75 (s, **2**), 4.20-3.82 (m, **9**), 3.66 (s, **10**), 3.52-3.04 (m, **3**, **7**, **8**, **11**), 2.90 (s, **5**), 2.73 (s, **4**, **6**), 2.48-1.31 (m, **1**, **12**).

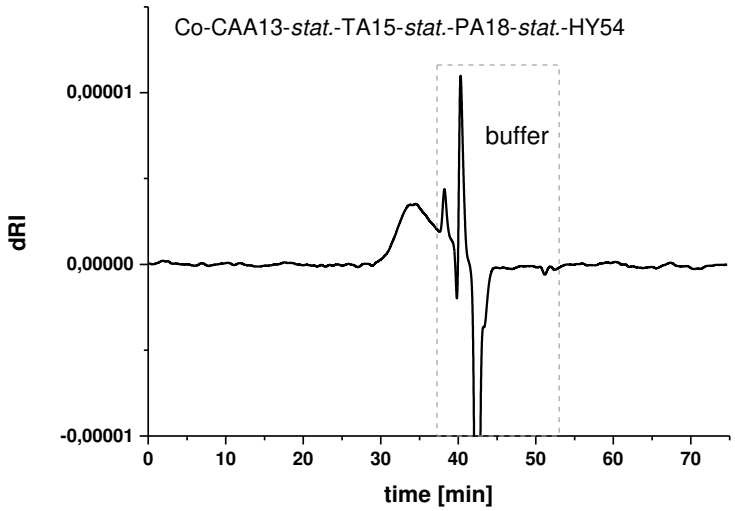

Figure S20. H_2O-SEC-MALS spectrum of **CAA13-*stat.*-TA15-*stat.*-PA18-*stat.*-HY54.**

SEC-MALS: $\overline{M}_n$ = 50.90 kDa; Đ = 1.12

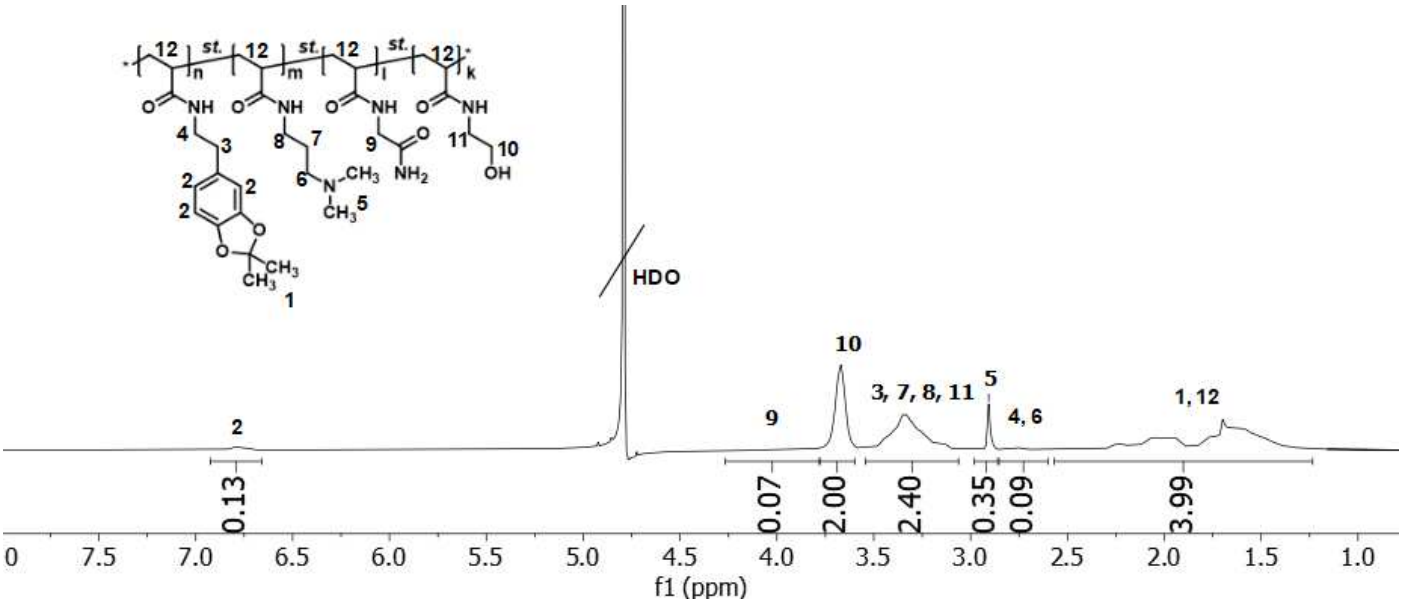

Figure S10. ^{1}H NMR spectrum (300 MHz, D_2O) of **CAA5-*stat.*-TA5-*stat.*-PA7-*stat.*-HY83**.

^{1}H NMR (300 MHz, D_2O) δ [ppm] δ [ppm] 6.77 (s, **2**), 4.23-3.83 (m, **9**), 3.67 (s, **10**), 3.52-3.06 (s, **3**, **7**, **8**, **11**), 2.91 (s, **5**), 2.74 (s, **4**, **6**), 2.47-1.26 (m, **1**, **12**).

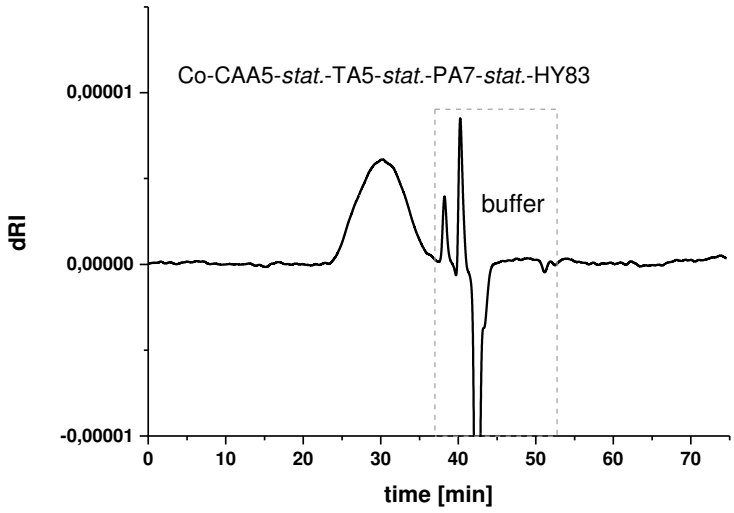

Figure S11. H_2O-SEC-MALS spectrum of **CAA5-*stat.*-TA5-*stat.*-PA7-*stat.*-HY83.**

SEC-MALS: $\overline{M}_n$ = 63.10 kDa; Đ = 1.87

4. Acetonide deprotection of final polymers

In order to obtain catechol units for adhesion studies, the acetonide protecting group was removed from the CAA monomers. The reaction was carried out in a mixture of TFA/H_2O (95:5) and the solution was stirred for 3 h at room temperature. After work-up by precipitation in diethyl ether followed by lyophilization, the polymers were stored under an inert gas atmosphere.

CAA4-*stat.*-TA48-*stat.*-HY48

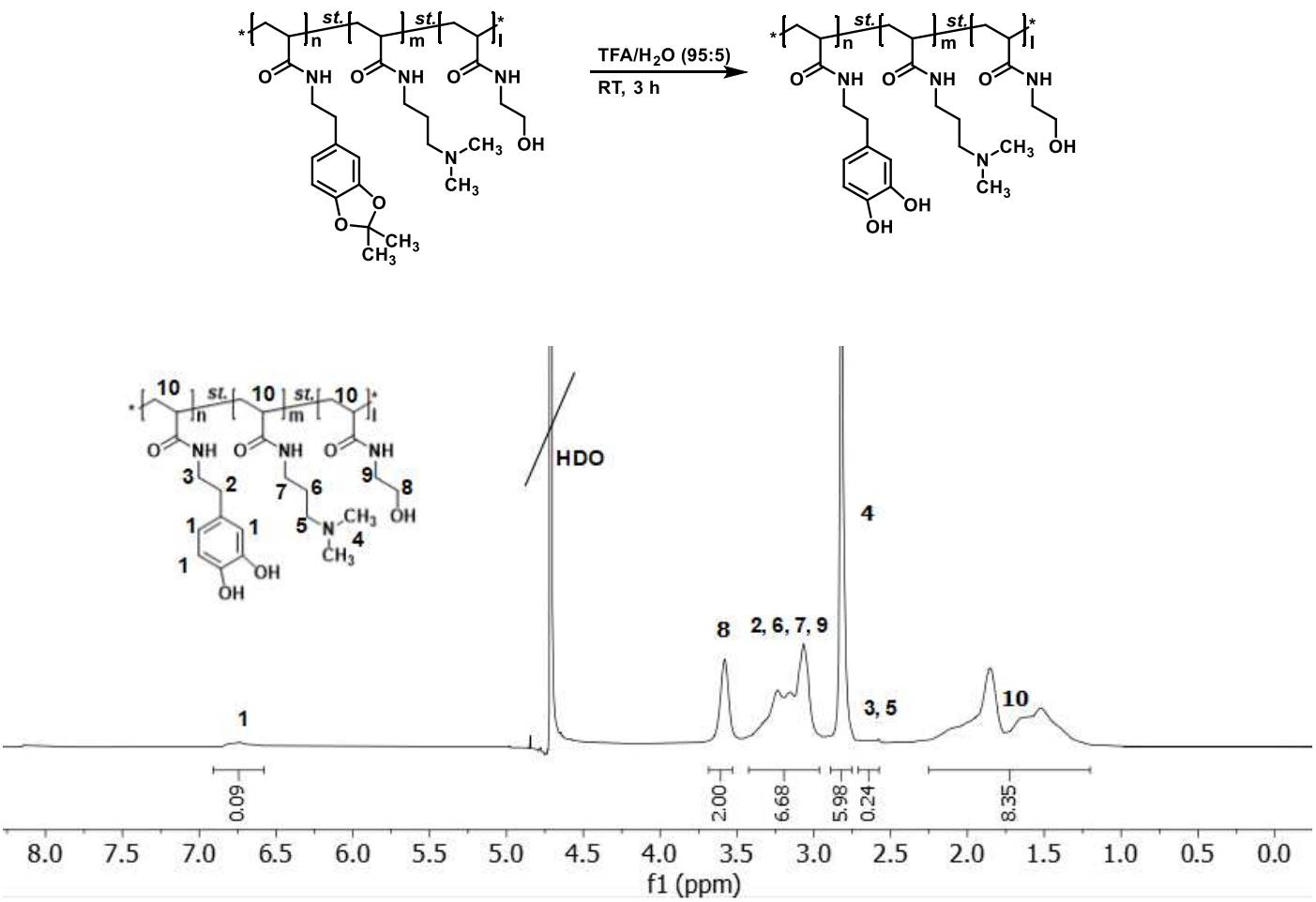

Figure S12. ^{1}H NMR spectrum (300 MHz, D_2O) of **Co-CA4-*stat.*-TA48-*stat.*-HY48**.

CAA3-*stat.*-PA45-*stat.*-HY52

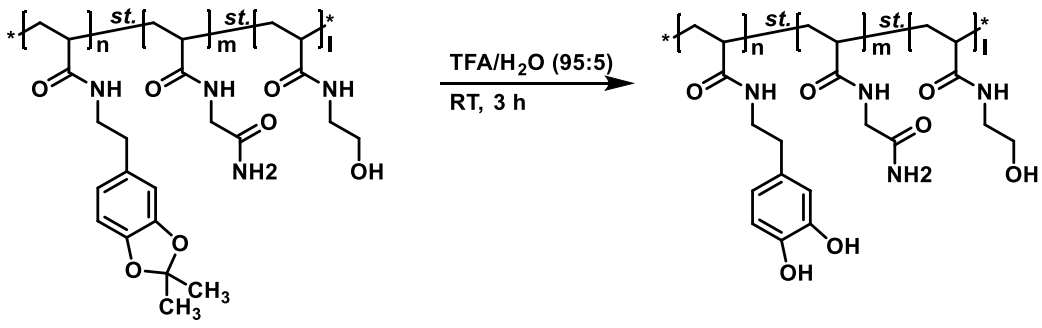

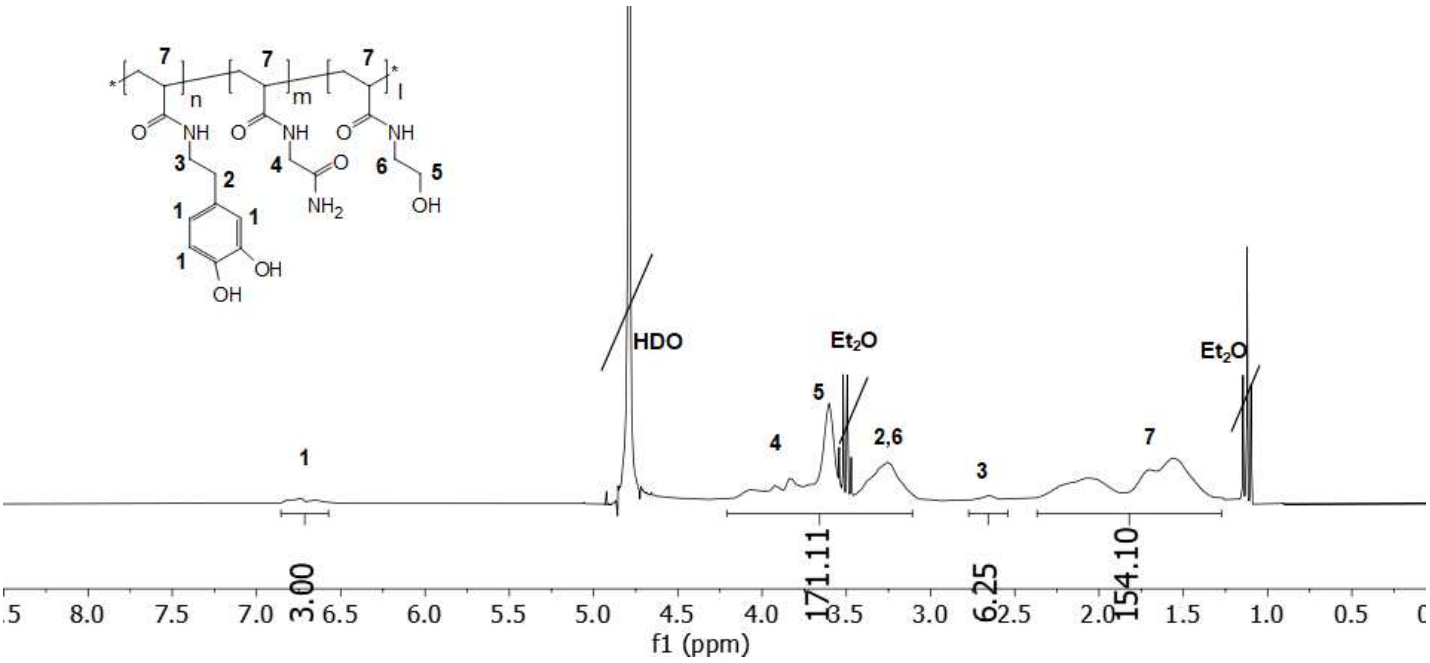

Figure S13. ^{1}H NMR spectrum (300 MHz, D_2O) of **Co-CA3-*stat.*-TA45-*stat.*-HY52**.

CAA4-*stat.*-TA22-*stat.*-PA17-*stat.*-HY57

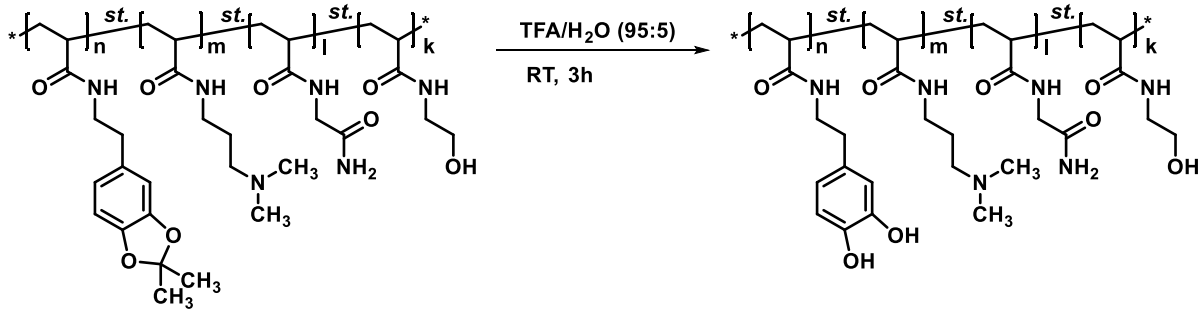

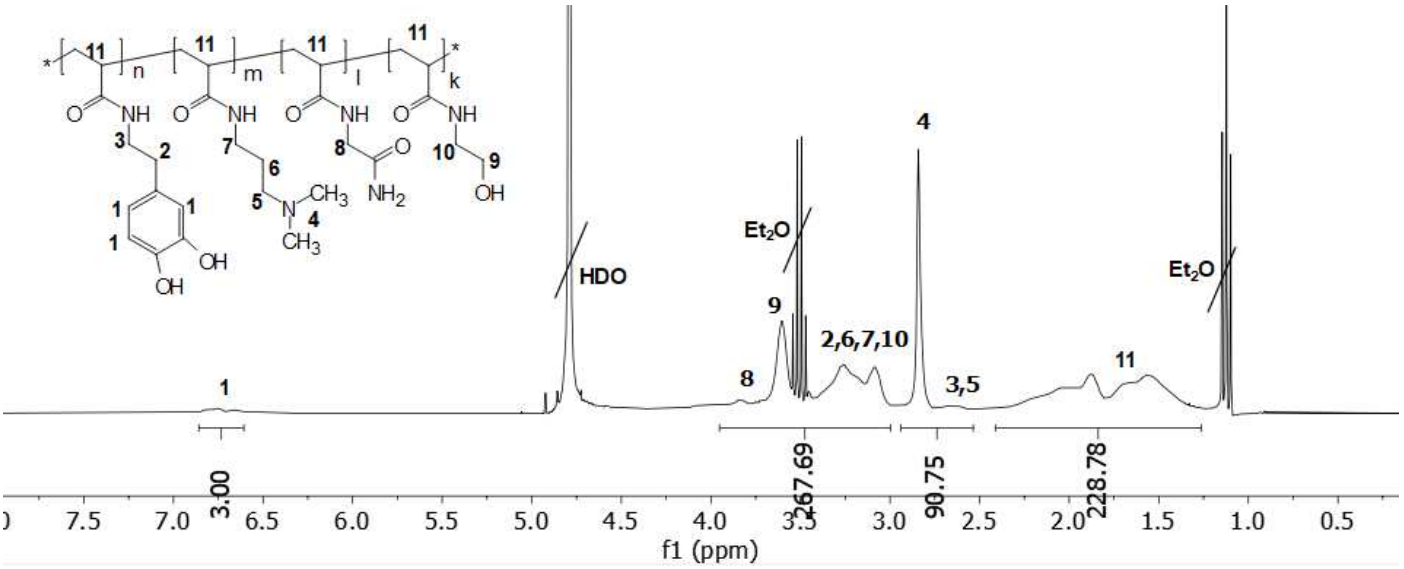

Figure S14. ^{1}H NMR spectrum (300 MHz, D_2O) of **CAA4-*stat.*-TA22-*stat.*-PA17-*stat.*-HY57.**

CAA13-*stat.*-TA15-*stat.*-PA18-*stat.*-HY54

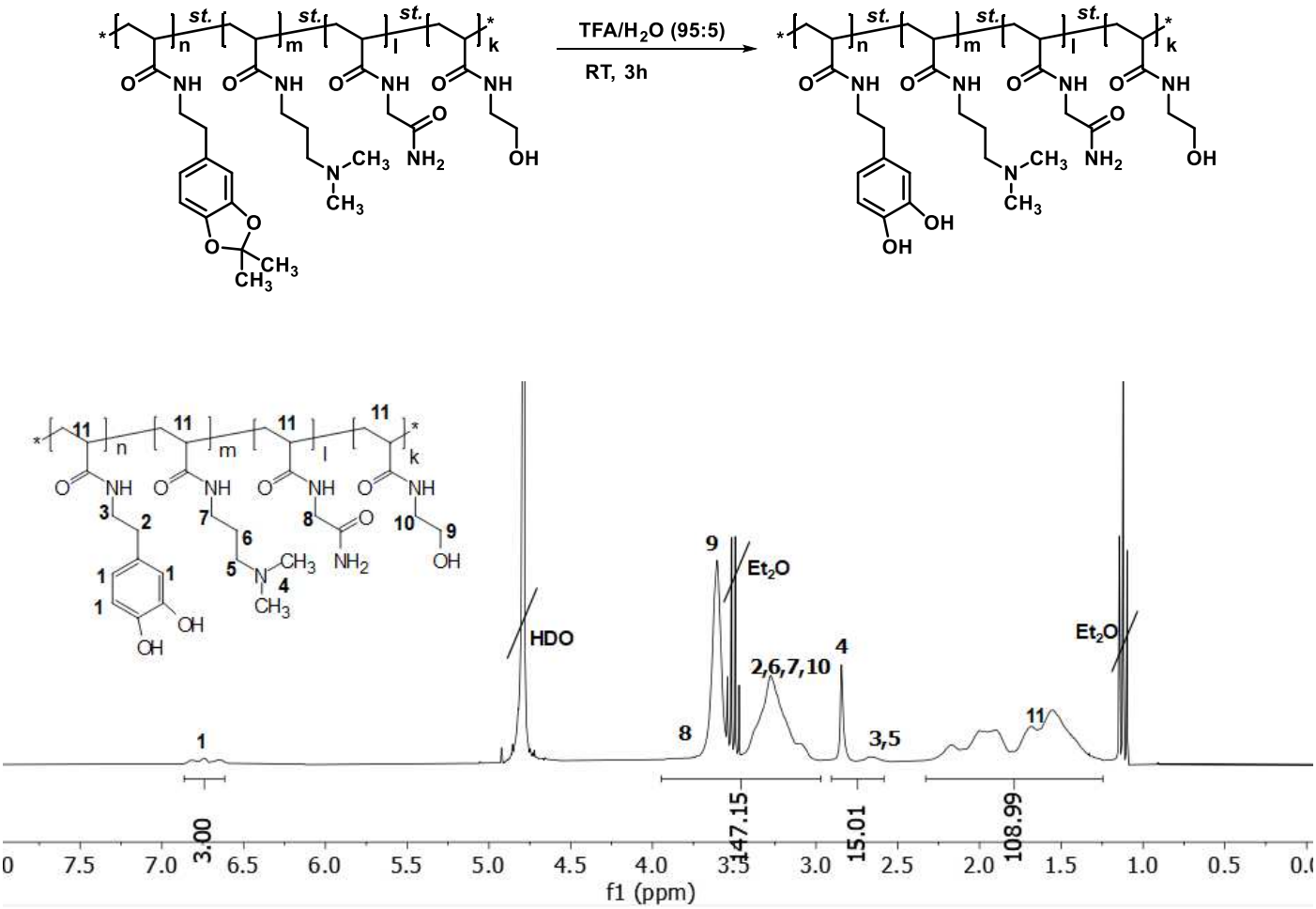

Figure S15. ^{1}H NMR spectrum (300 MHz, D_2O) of **CAA13-*stat.*-TA15-*stat.*-PA18-*stat.*-HY54.**

CAA5-*stat.*-TA5-*stat.*-PA7-*stat.*-HY83

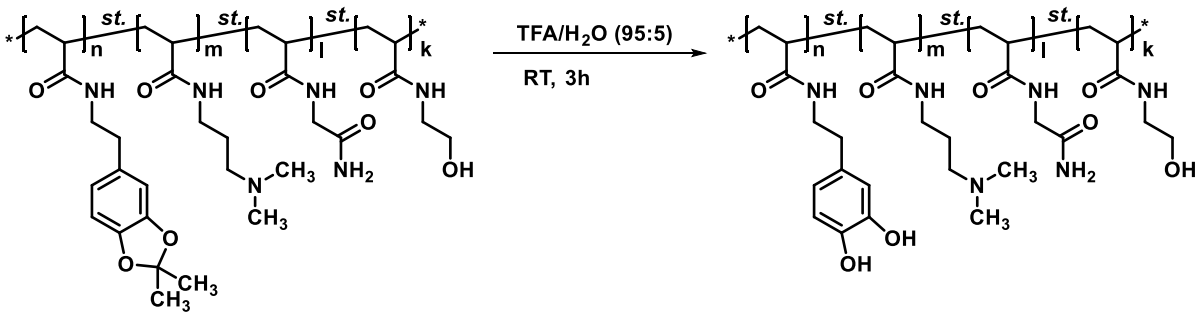

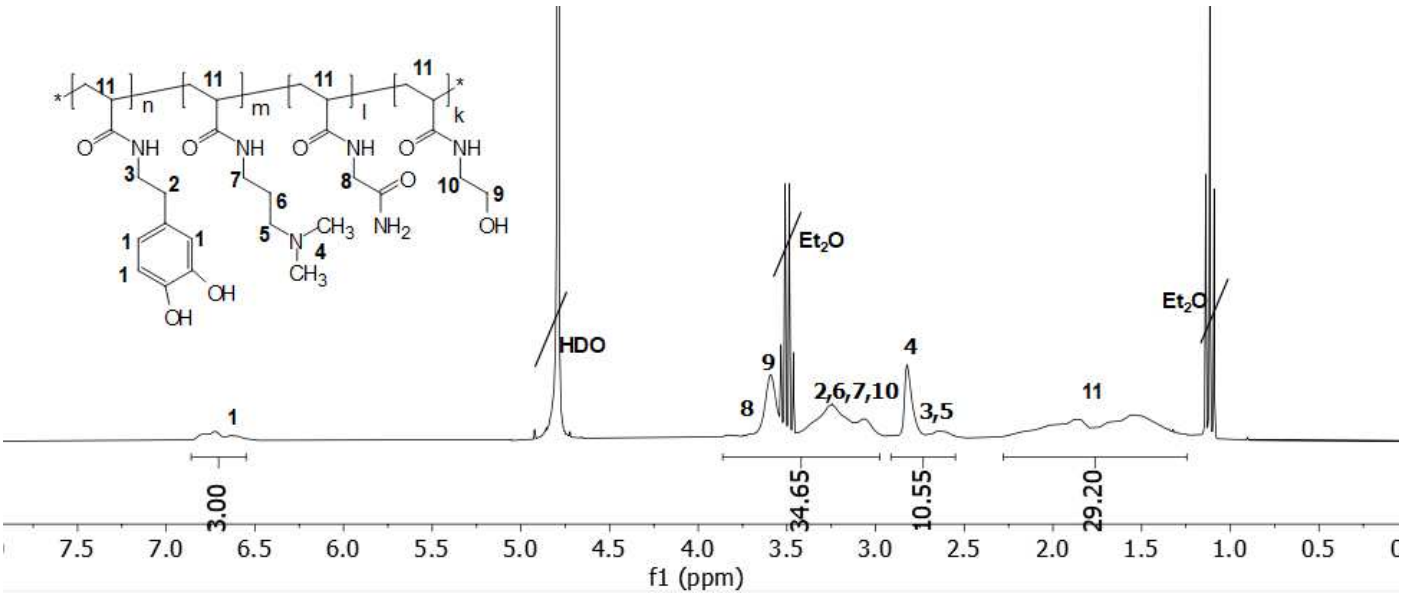

Figure S16. ^{1}H NMR spectrum (300 MHz, D_2O) of **CAA5-*stat.*-TA5-*stat.*-PA7-*stat.*-HY83.**

References

1. Liu, Z.; Hu, B.-H.; Messersmith, P.B. Acetonide protection of dopamine for the synthesis of highly pure N-docosahexaenoyldopamine. *Tetrahedron Lett.* **2010**, *51*, 2403-2405, doi:https://doi.org/10.1016/j.tetlet.2010.02.089.
2. Glatzel, S.; Badi, N.; Päch, M.; Laschewsky, A.; Lutz, J.-F. Well-defined synthetic polymers with a protein-like gelation behavior in water. *Chem. Commun.* **2010**, *46*, 4517-4519, doi:10.1039/C0CC00038H.

4. Conclusion and Outlook

The aim of this work was the investigation and development of a new type of thiol-initiated controlled radical photopolymerization in solution, based on the polymerization on thiol-functionalized surfaces introduced by Braunschweig *et al.*[55], and to optimize it by specifically changing the monomers, initiators used and varying the polymerization parameters. In addition, free radical polymerization was used to derive two classes of biomimetic polymers to mimic and tune bioadhesion – GAG mimetic glycopolymers and catechol-containing polymers mimicking adhesive mussel foot proteins.

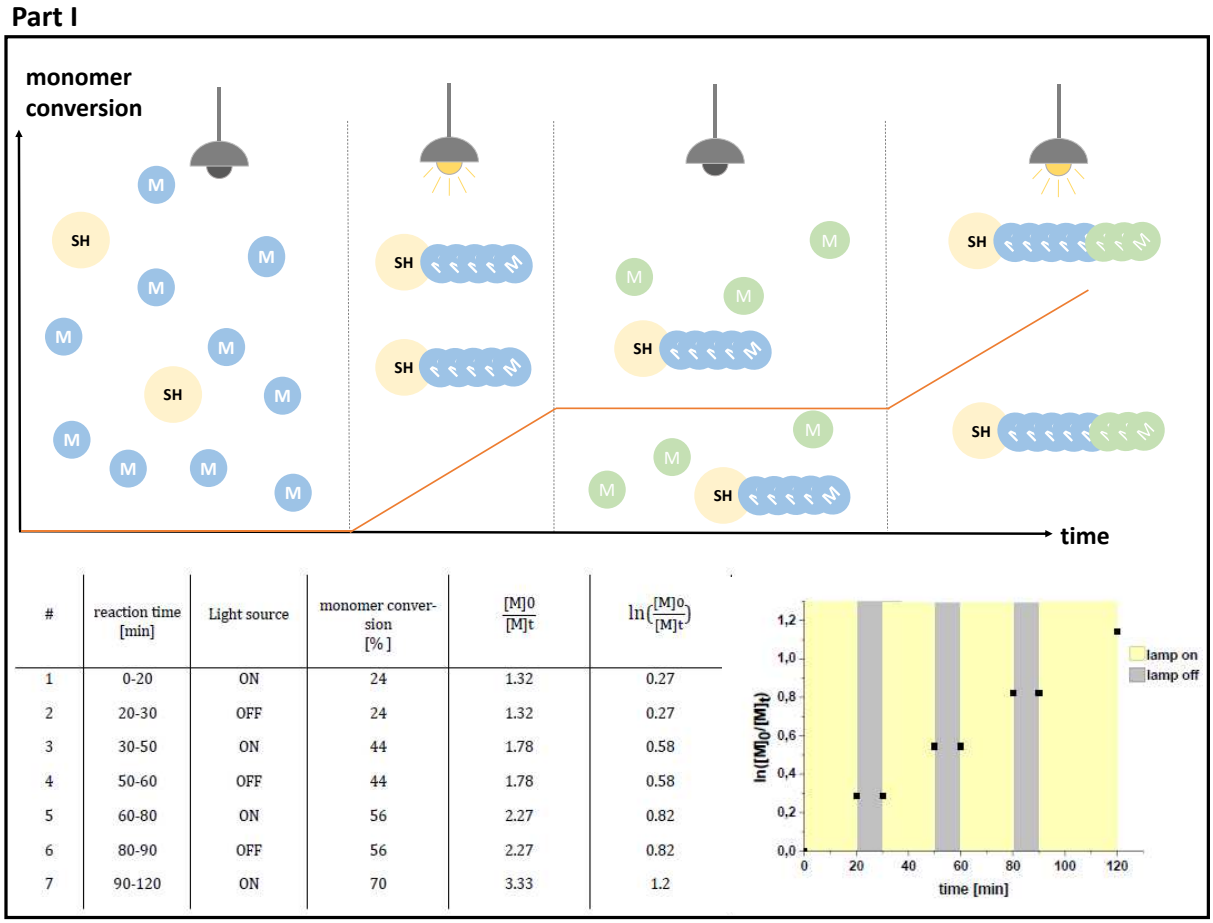

#	reaction time [min]	Light source	monomer conversion [%]	$\frac{[M]0}{[M]t}$	$\ln(\frac{[M]0}{[M]t})$
1	0-20	ON	24	1.32	0.27
2	20-30	OFF	24	1.32	0.27
3	30-50	ON	44	1.78	0.58
4	50-60	OFF	44	1.78	0.58
5	60-80	ON	56	2.27	0.82
6	80-90	OFF	56	2.27	0.82
7	90-120	ON	70	3.33	1.2

Figure 22. Schematic representation of TIRP with its characteristic growth behavior during light on an off phases including experimentally measured data, with SH = thiol source and M = (meht)acrylate / acrylamide monomer.[1]

In the first part of the thesis, the successful transfer of the surface-initiated polymerization method by Braunschweig into solution was realized. This new photopolymerization method is called TIRP - thiol-induced, light-activated controlled radical polymerization. For TIRP, a photoinitiator/photocatalyst system consisting of TPO/$Ir(ppy)_3$ was used and the polymerization was carried out at 405 nm wavelength. Four optimized polymerization conditions are presented to demonstrate control of the polymerization. In all four routes, tritylthiol serves as the thiol source, as it is easy to handle and the thiol contains the desired reactivity due its stabilizing phenyl groups. *N*-hydroxyethylacrylamide (HEAA) and *tert*-butyl

methacrylate served as monomers for the optimized systems. For both monomers, polymers with 20 and 100 repeating units each and dispersities in the controlled range (1.0-1.3) were successfully synthesized. Characterization via H NMR and SEC was performed to demonstrate the control over the chain lengths and dispersities of the optimized polymers.

An important factor for the desired control over the polymer properties, was the choice of the ideal irradiation intensity. For HEAA, as an acrylamide, an intensity of 2.61 mW/cm^2 was sufficient, while this was too high for the more reactive *tert*-butyl methacrylate, which showed free radical polymerization characteristics at 2.61 mW/cm^2. By lowering the intensity to 1.15 mW/cm^2, the optimum intensity was also found for the methacrylate monomer, resulting again in controlled polymers. Furthermore, the control of TIRP was demonstrated by kinetic studies. Here, by taking reaction samples at defined reaction times and measuring them immediately by ^{1}H NMR, it was possible to determine the monomer conversion during polymerization.

A characteristic of controlled polymerization methods is a linear relationship of the monomer conversion to the chain length formed during the reaction. This linear relationship was confirmed by the ^{1}H NMR experiments. Another aspect of controlled reactions is the possibility to stop and reinitiate polymer growth. Thus, irradiation was interrupted and resumed three times during polymerization. Before and after each interruption, ^{1}H NMR spectra of the reaction mixture was recorded and the conversion of the reaction at each point was determined. As expected, it was successfully shown that as soon as the light was turned off, conversion stopped. However, when irradiation continued, the reaction also continued and the conversion increased again. This could be repeated several times, which is a clear indication of a controlled radical polymerization.

Another characteristic of controlled polymerization methods is the possibility of producing block copolymers by reinitiating already isolated polymers. It was possible to show that already isolated HEAA polymers could be reinitiated to extend the polymer with further HEAA monomer as well as to synthesize a block copolymer using a mannose acrylamide monomer. Both block copolymers exhibited dispersities in the controlled range after isolation. In order to optimize the applied polymerization parameters, the ratio of TPO to thiol, the concentration of Ir(ppy)$_3$, the irradiation intensity as well as the choice of thiol and monomer were varied in several experiments. The optimum TPO:thiol ratio was determined to be 1:1. Controlled properties were demonstrated at this ratio and undesired by-products leading to the increase of dispersity could be excluded.

This finding led to the postulation of a reaction mechanism for TIRP, which was supported by further analysis. In detail, the reaction was carried out both, without monomer and with only one repeating unit. Thereby, the products that were postulated from the mechanism could be detected via ESI-MS-

analysis and MALDI-ToF analysis. Moreover, additional support for the mechanism was provided by cooperation partners Meisner *et al.* who calculated energy barriers of the individual mechanistic steps.

The optimal $Ir(ppy)_3$ concentration was determined to be 0.05 mol% (based on the monomer). With higher or lower concentrations, either polymers with features of free radical polymerizations or no polymerization at all was observed. Another important parameter in TIRP is the choice of thiol and respectively the choice of the correct irradiation intensity depending on the type of thiol used. For thiols that form a stabilized thiyl radical after the start reaction due to their substituents, such as thiophenol, the irradiation intensity had to be increased to obtain a controlled character. When a less stabilized thiol, such as benzyl mercaptane or trimethylsilyl ethane thiol, was chosen, the previous irradiance for tritylthiol (2.61 mW/cm^2) was too high and had to be lowered to retain CRP characteristics.

Overall, this work systematically evaluated and optimized the key reaction parameters of TIRP as CRP which now also allows other researcher to apply this method and adapt it to various other monomer and polymer systems. A main advantage of TIRP over other CRPs is the readily available thiols that are used as initiators, in comparison to ATRP and RAFT initiators that often have to be prepared specifically for the targeted polymer. In the working group of Prof. Hartmann, experiments are performed also using free thiols on enzymes or proteins as initiators, for example, to modify or extend their properties with specially selected monomers. This also demonstrates that TIRP can be performed under mild conditions and in the future might even be compatible with polymerizations under physiological conditions.

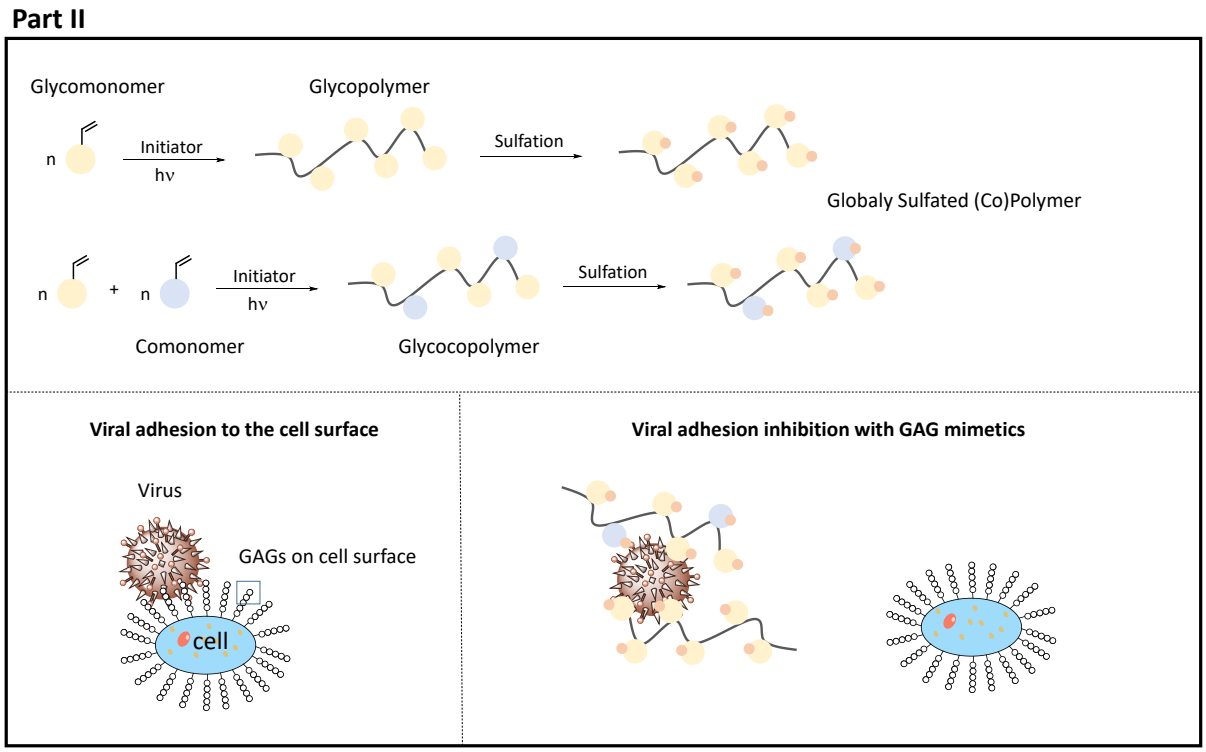

Figure 23. Synthesis of GAG mimetic glyco(co)polymers and their application in viral adhesion inhibition.

In the second part of this thesis, eleven different GAG mimetics were successfully synthesized for testing in viral inhibition adhesion studies against SARS-CoV-2. For this purpose, a mannose acrylamide monomer was synthesized by the reaction of acetyl protected mannose with HEAA following the synthesis protocol of Wilkins *et al*.[163] To investigate the effect of a linker between mannose and the polymer backbone on viral adhesion, a mannose monomer without HEAA linker was also prepared with mannose directly attached to the acrylic moiety. Mannose homopolymers with repeat units of 10, 30, 70, 200, 300, and 800 from monomers with linker and one monomer with a repeating unit of 60 without linker were successfully prepared and characterized. Copolymers were synthesized from the mannose monomer with linker and HEAA. Three copolymers with repeating units of 70 each were successfully synthesized, with a mannose ratio of 30%, 50% and 70% incorporated per copolymer. For comparison, a copolymer with a repeating unit of 300 and a mannose content of 50% was also prepared. The hydroxy groups of all polymers were sulfated to obtain the final GAG mimetics. With the aim of complete sulfation, it was possible to achieve about 90% sulfation in all polymers, leading to highly negatively charged GAG mimetics. The degrees of sulfation were determined via elemental analysis. It was hypothesized that besides the length of the polymers, the charge density is also of importance. Therefore, DLS measurements of the polymers were carried out to determine the hydrodynamic radii of the charged GAG mimetics. The results of the DLS measurements showed that the hydrodynamic radii increased with increasing sulfated mannose number. The copolymers that contained lower amounts of mannose had lower hydrodynamic radii than those with higher amounts of mannose. After

successful synthesis, sulfation and characterization, all polymers were sent to cooperation partners Schelhaas *et al.* to be investigated in viral inhibition adhesion studies against SARS-CoV-2. The samples were also examined in anticoagulation studies, since GAGs such as heparin are used as anticoagulants to inhibit blood clotting. In short, all GAG mimetics showed inhibitory potential in blocking virus adhesion and infection (data not shown in this thesis). Interestingly, GAG mimetics with lower sulfated mannose density showed similar inhibition effects but clearly decreased anticoagulant properties (data not shown in this thesis) which makes them highly relevant for future biomedical applications. Current work in the Hartmann lab explores GAG mimetics of different architecture, e.g., branched and hyperbranched polymers, to further test for the effects of ligand density. Here, also TIRP as CRP is now used to derive controlled GAG mimetic polymers.

Part III

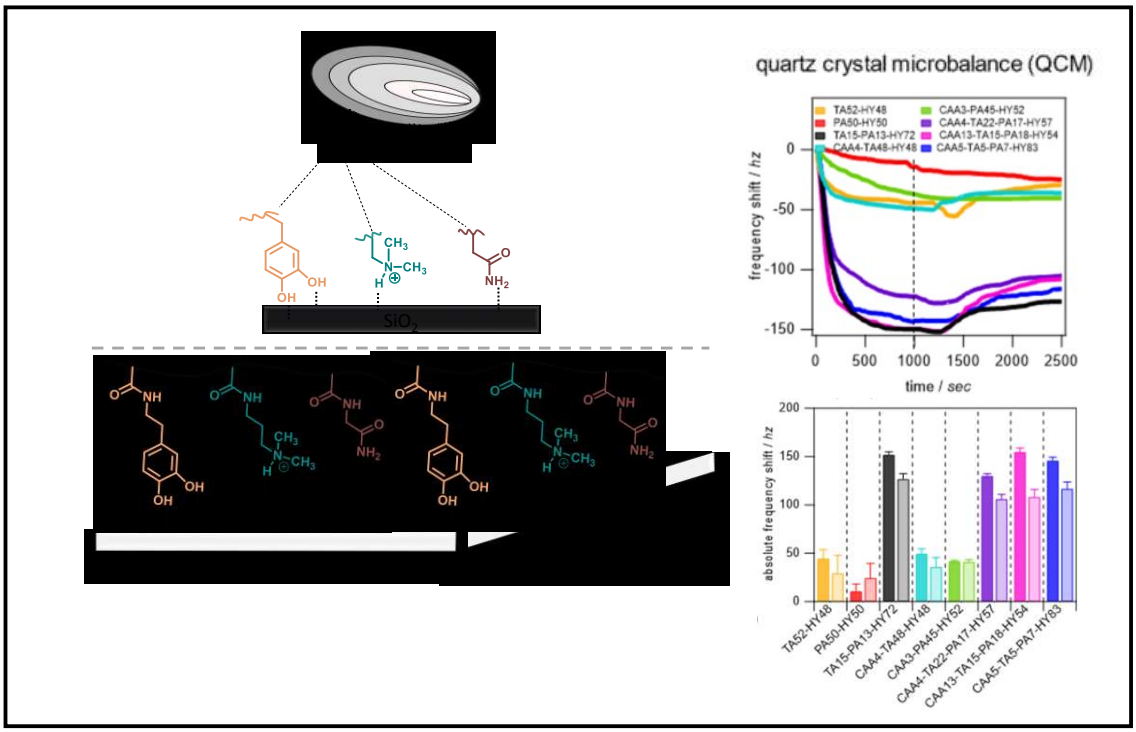

Figure 24. Schematic representation of mussel adhesion to glass surface and glass adhesion of mussel inspired catechol containing copolymers as well as the results of the quarz crystal microbalance measurements. Upper right graph: The dashed line at 1000 sec signifies the region of injecting polymer solutions (0-1000 sec) and pumping pure buffer (1000-2500 sec). Bottom right graph: Frequency shifts from 0 sec to 1000 sec (fully colored bars) and frequency shifts at 2500 sec (equilibrium, light colors).[164]

In the third part of this work, eight previously synthesized mussel-inspired polymers, were investigated for their property of adsorption on glass in aqueous medium. The polymers were synthesized from four defined monomers via free radical polymerization: the catechol-containing *N*-(3,4-dihydroxyphenethyl)acrylamide (CA), *N*-(3-(dimethylamino)propyl)acrylamide (TA), containing a tertiary amine, *N*-(2-amino-2-oxoethyl)acrylamide (PA), bearing a primary amide, and *N*-hydroxyethylacrylamide (HY). Eight polymers with different monomer combinations and incorporation ratios were prepared prior to

this thesis. Here the catechol moieties were still acetonide functionalized. However, in this work the acetonide protecting groups were cleaved to receive eight final polymers. The monomer combinations used for the final polymers were TA-HY, PA-HY, CA-TA-HY, CA-PA-HY, TA-PA-HY and three times CA-TA-PA-HY with different monomer incorporation. These eight final polymers were characterized via H NMR and SEC to determine the incorporation ratios and molecular weights. It was successfully shown that in free radical synthesized polymers a synergy between catechol, primary amide and cationic amine affects the adhesion of polymers to a SiO_2 surface, as in their natural model. Previous work in the Hartmann Lab also showed this synergy for catechol, amine and amide functionalized oligomers. However, the confirmation of those synergies in long chain polymers could be essential for further applications, e.g. for the development of catechol based adhesives. For this purpose, the adsorption of the final polymers was investigated using both quartz crystal microbalance (QCM) and ellipsometry on quartz glass in aqueous medium. It was successfully shown that polymers that contained the tertiary amine, showed significantly higher adsorptions than those without cationic group. A synergy of the amine with both the catechol monomer and the primary amide, that positively influenced adsorption, was thus confirmed for long chain polymers. At high amine contents adsorption decreased again, which can be explained by the more stretched conformation of the polymer resulting from a high repulsive charge density within the polymer coil. The highest adsorption was detected for the polymer with all four monomers incorporated while having the highest catechol content. Thus, the synergy of catechol, amine and amide, and also a synergy between amine and amide for enhancing adsorption was successfully confirmed for long chain polymers. In future research, these findings may help to specifically enhance the adhesive properties of artificial adhesives that are mussel-inspired. To better understand the mechanism of the demonstrated synergy, further analysis of the polymer properties could be undertaken, or additional polymers with different incorporation ratios could be synthesized. Another possibility for future studies is to synthesize polymers by using the same monomers, but via controlled radical polymerization techniques to specifically influence the monomer sequence of the polymers.

5. Appendix

5.1. List of Abbreviations

AIBN	Azobis(isobutyronitrile)
eq.	Equivalents
ATRP	Atom transfer radical polymerization
BSA	Bovine serum albumin
c	Concentration
CRP	Controlled radical polymerization
CSIRO	Commonwealth Scientific and Industrial Research Organisation
Đ	dispersity
DA	Dopamine acrylamide
DAAA	Dopamine acetonide acrylamide
DBPO	dibenzoyl peroxide
DCM	Dichlormethane
DMAPAA	Dimethylaminopropyl acrylamide
DMF	*N,N*-Dimethylformamide
EE	Ethyl acetate
ESI	Electrospray-Ionisation
et al.	(lat.) Et alii (m.) or et aliae (f.)
FRP	Free radical polymerization
GAG	Glycosaminoglycan
GalNAc	*N*-Acetyl galactosamine
GlcA	Glucuronic Acid
GlcNAc	*N*-Acetyl glucosamine
h	(lat.) Hora, hour
hν	photon energy (h: Planck constant; ν: frequency)
HEAA	*N*-Hydroxyethyl acrylamide
HP	Heparin
HPLC	High performance liquid chromatography
HPV	Human Papillomavius
HR-MS	High resolution mass spectrometry

HS	Heparan sulfate
HSV	Herpes Simplex Virus
IdoA	Iduronic Acid
$Ir(ppy)_3$	Tris(2-phenylpyridine)iridium(III)
kDa	Kilodalton
L-DOPA	*L*-3,4-Dihydroxyphenylalanine
LED	Light emitting diode
M	[mol/L]
M_n	Number-average molecular weight
M_w	Weight-average molecular weight
MeOH	Methanol
Mfp	Musselfootprotein
min	Minute
Mol.%	Molpercent
MS	Mass spectrometry
n	Number of repeating units
NAGA	*N*-Acryloyl glycinamide
NMP	Nitroxide mediated polymerization
NMR	Nuclear magnetic resonance
ppm	Parts per million
QCM	Quartz crystal microbalance
quat.	Quaternary
RAFT	Reversible addition-fragmentation chain transfer
RDRP	Reversible-deactivation radical polymerizations
Rf	Retarding-front
RT	Room temperature
SEC-MALS	Size exclusion chromatography-multi angle light scattering
SPPoS	Solid phase polymer synthesis
t	Time
T	Temperature
TIRP	Thiol-induced, Light-Activated Controlled Radical Polymerization

TFA	Trifluoro acetic acid
THF	Tetrahydrofuran
TLC	thin layer chromatography
TMS	Trimethylsilyl
TPO	Diphenyl-(2,4,6-trimethylbenzoyl)-phosphine oxide
UV	Ultraviolet
Wt.%	Weight percent
X	Heteroatom
λ	Wavelength in nm

5.2. List of Figures

6. Acknowledgments

First of all, I would like to thank Prof. Dr. Laura Hartmann in particular for the opportunity to write my doctoral thesis in her working group. Also for the exciting projects I was allowed to work on, as well as any help with questions, problems and new ideas, which made the projects so diverse.

I would like to thank PD Dr. Klaus Schaper for taking on the role of the second supervisor and also for being my mentor during my doctoral studies at HHU.

Special thanks go to Prof. Dr. Adam B. Braunschweig and Daniel Valles for their significant contribution to the idea generation and our regular discussions about TIRP.

I would also like to thank Prof. Dr. Stephan Schmidt, Jun.-Prof. Dr. Jan Meisner, Prof. Dr. Mario Schelhaas, Dr. Susanne Boye and Tillmann Wigger for the close cooperations in the different projects.

At the institute of macromolecular chemistry, I would especially like to thank Dr. Monir Tabatabai for her corrections of the experimental parts of my publications and the discussions about those, Stephanie Scheelen for measurements on the THF and DMF-GPC, as well as for her care that we do not run out of laboratory equipment and Michaela Kitza, who was always a help with all organizational questions.

I would like to thank Mohanad Aian, Dr. Peter Tommes and Ralf Bügel for the NMR measurements, Maldi-ToFs and ESI-MS analytics. Also many thanks go to Gaby Zerta for the elemental analytical measurements.

Many thanks also to the students whose theses I was allowed to supervise, Rene Kleiner, Thorben Schwedhelm and Simon Walber. It was a pleasure to work with you.

A huge thank you to the whole working group for several unforgettable evenings and nights in- and outside of the university and also the great working atmosphere.

Thanks to the coincidence that gifted me a Bubbele for the time of my thesis and further.

A big thank you to my former colleagues Luca-Cesare Blawitzki and Dr. Lukas Fischer for our “special” and sometimes inappropriate triangular relationship and also that their names start with the same letter as mine, which is a strong pillar of this relationship. L^3.

My very special thanks go to my family and my wife Sarah, without whose support of any kind this work would not have been possible.

Thank you Fabi for the coffee.

7. References

1. Bonda, L.; Valles, D. J.; Wigger, T. L.; Meisner, J.; Braunschweig, A. B.; Hartmann, L., TIRP– Thiol-Induced, Light-Activated Controlled Radical Polymerization. *Macromolecules* **2023,** *56* (14), 5512-5523.
2. Mülhaupt, R., Hermann Staudinger and the origin of macromolecular chemistry. *Angewandte Chemie International Edition* **2004,** *43* (9), 1054-1063.
3. Wang, X.; An, Z., Enzyme-initiated reversible addition− fragmentation chain transfer (RAFT) polymerization: Precision polymer synthesis via enzymatic catalysis. In *Methods in Enzymology*, Elsevier: 2019; Vol. 627, pp 291-319.
4. Chen, C., Redox-controlled polymerization and copolymerization. *ACS Catalysis* **2018,** *8* (6), 5506-5514.
5. Magenau, A. J.; Strandwitz, N. C.; Gennaro, A.; Matyjaszewski, K., Electrochemically mediated atom transfer radical polymerization. *Science* **2011,** *332* (6025), 81-84.
6. Andrzejewska, E., Free radical photopolymerization of multifunctional monomers. In *Three-Dimensional Microfabrication Using Two-Photon Polymerization*, Elsevier: 2016; pp 62-81.
7. Braun, D., Origins and development of initiation of free radical polymerization processes. *International Journal of Polymer Science* **2009,** *2009*.
8. Norrish, R. G. W.; Brookman, E., The mechanism of polymerization reactions. I. The polymerization of styrene and methyl methacrylate. *Proceedings of the Royal Society of London. Series A. Mathematical and Physical Sciences* **1939,** *171* (945), 147-171.
9. Staudinger, H.; Kohlschütter, H., Über hochpolymere Verbindungen, 55. Mitteil.: Über Poly-acrylsäure. *Berichte der deutschen chemischen Gesellschaft (A and B Series)* **1931,** *64* (8), 2091-2098.
10. Mayo, F. R.; Lewis, F. M., Copolymerization. I. A basis for comparing the behavior of monomers in copolymerization; the copolymerization of styrene and methyl methacrylate. *Journal of the American Chemical Society* **1944,** *66* (9), 1594-1601.
11. Mayo, F. R.; Lewis, F. M.; Walling, C., (b) Propagation. Copolymerisation: the effects of structure on the reactions of ethylenic bonds with free radicals. *Discussions of the Faraday Society* **1947,** *2*, 285-295.
12. Moad, G.; Chiefari, J.; Mayadunne, R. T.; Moad, C. L.; Postma, A.; Rizzardo, E.; Thang, S. H. In *Initiating free radical polymerization*, Macromolecular Symposia, Wiley Online Library: 2002; pp 65-80.
13. Matyjaszewski, K.; Davis, T. P., Handbook of radical polymerization. **2002**.
14. Ballard, N.; Asua, J. M., Radical polymerization of acrylic monomers: An overview. *Progress in Polymer Science* **2018,** *79*, 40-60.
15. Barthet, C.; Hickey, A. J.; Cairns, D. B.; Armes, S. P., Synthesis of novel polymer–silica colloidal nanocomposites via free-radical polymerization of vinyl monomers. *Advanced Materials* **1999,** *11* (5), 408-410.
16. Dworakowska, S.; Lorandi, F.; Gorczyński, A.; Matyjaszewski, K., Toward green atom transfer radical polymerization: Current status and future challenges. *Advanced Science* **2022,** *9* (19), 2106076.
17. Parkatzidis, K.; Rolland, M.; Truong, N. P.; Anastasaki, A., Tailoring polymer dispersity by mixing ATRP initiators. *Polymer Chemistry* **2021,** *12* (39), 5583-5588.
18. Destarac, M., Controlled radical polymerization: industrial stakes, obstacles and achievements. *Macromolecular Reaction Engineering* **2010,** *4* (3-4), 165-179.
19. Zhong, M.; Matyjaszewski, K., How fast can a CRP be conducted with preserved chain end functionality? *Macromolecules* **2011,** *44* (8), 2668-2677.
20. Pan, X.; Tasdelen, M. A.; Laun, J.; Junkers, T.; Yagci, Y.; Matyjaszewski, K., Photomediated controlled radical polymerization. *Progress in Polymer Science* **2016,** *62*, 73-125.
21. Chen, M.; Zhong, M.; Johnson, J. A., Light-controlled radical polymerization: mechanisms, methods, and applications. *Chemical reviews* **2016,** *116* (17), 10167-10211.
22. Otsu, T.; Yoshida, M., Role of initiator-transfer agent-terminator (iniferter) in radical polymerizations: Polymer design by organic disulfides as iniferters. *Die Makromolekulare Chemie, Rapid Communications* **1982,** *3* (2), 127-132.

23. Solomon, D. H.; Rizzardo, E.; Cacioli, P., Polymerization process and polymers produced thereby. Google Patents: 1986.
24. Georges, M. K.; Veregin, R. P.; Kazmaier, P. M.; Hamer, G. K., Narrow molecular weight resins by a free-radical polymerization process. *Macromolecules* **1993,** *26* (11), 2987-2988.
25. Nicolas, J.; Guillaneuf, Y.; Lefay, C.; Bertin, D.; Gigmes, D.; Charleux, B., Nitroxide-mediated polymerization. *Progress in Polymer Science* **2013,** *38* (1), 63-235.
26. Hawker, C. J., Molecular weight control by a" living" free-radical polymerization process. *Journal of the American Chemical Society* **1994,** *116* (24), 11185-11186.
27. Hawker, C. J.; Barclay, G. G.; Orellana, A.; Dao, J.; Devonport, W., Initiating systems for nitroxide-mediated "living" free radical polymerizations: synthesis and evaluation. *Macromolecules* **1996,** *29* (16), 5245-5254.
28. Wang, J.-S.; Matyjaszewski, K., Controlled/" living" radical polymerization. atom transfer radical polymerization in the presence of transition-metal complexes. *Journal of the American Chemical Society* **1995,** *117* (20), 5614-5615.
29. Matyjaszewski, K., Atom transfer radical polymerization: from mechanisms to applications. *Israel Journal of Chemistry* **2012,** *52* (3-4), 206-220.
30. Krys, P.; Matyjaszewski, K., Kinetics of atom transfer radical polymerization. *European Polymer Journal* **2017,** *89*, 482-523.
31. Ribelli, T. G.; Augustine, K. F.; Fantin, M.; Krys, P.; Poli, R.; Matyjaszewski, K., Disproportionation or combination? The termination of acrylate radicals in ATRP. *Macromolecules* **2017,** *50* (20), 7920-7929.
32. Matyjaszewski, K.; Xia, J., Atom transfer radical polymerization. *Chemical reviews* **2001,** *101* (9), 2921-2990.
33. Gromada, J.; Matyjaszewski, K., Simultaneous reverse and normal initiation in atom transfer radical polymerization. *Macromolecules* **2001,** *34* (22), 7664-7671.
34. Jakubowski, W.; Matyjaszewski, K., Activator generated by electron transfer for atom transfer radical polymerization. *Macromolecules* **2005,** *38* (10), 4139-4146.
35. Konkolewicz, D.; Krys, P.; Gois, J. R.; Mendonca, P. V.; Zhong, M.; Wang, Y.; Gennaro, A.; Isse, A. A.; Fantin, M.; Matyjaszewski, K., Aqueous RDRP in the presence of Cu0: The exceptional activity of CuI confirms the SARA ATRP mechanism. *Macromolecules* **2014,** *47* (2), 560-570.
36. Harrisson, S.; Nicolas, J., In the (very) long run we are all dead: Activation and termination in SET-LRP/SARA-ATRP. *ACS Macro Letters* **2014,** *3* (7), 643-647.
37. Tasdelen, M. A.; Uygun, M.; Yagci, Y., Photoinduced controlled radical polymerization. *Macromolecular rapid communications* **2011,** *32* (1), 58-62.
38. Boyer, C.; Corrigan, N. A.; Jung, K.; Nguyen, D.; Nguyen, T.-K.; Adnan, N. N. M.; Oliver, S.; Shanmugam, S.; Yeow, J., Copper-mediated living radical polymerization (atom transfer radical polymerization and copper (0) mediated polymerization): from fundamentals to bioapplications. *Chemical reviews* **2016,** *116* (4), 1803-1949.
39. Pintauer, T.; Matyjaszewski, K., Atom transfer radical addition and polymerization reactions catalyzed by ppm amounts of copper complexes. *Chemical Society Reviews* **2008,** *37* (6), 1087-1097.
40. Corpart, P.; Charmot, D.; Biadatti, T.; Zard, S.; Michelet, D. In *WO 9858974 [(1999*, Chem Abstracts, 1998; p 82018.
41. Chiefari, J.; Chong, Y.; Ercole, F.; Krstina, J.; Jeffery, J.; Le, T. P.; Mayadunne, R. T.; Meijs, G. F.; Moad, C. L.; Moad, G., Living free-radical polymerization by reversible addition-fragmentation chain transfer: the RAFT process. *Macromolecules* **1998,** *31* (16), 5559.
42. Rizzardo, E.; Chen, M.; Chong, B.; Moad, G.; Skidmore, M.; Thang, S. H. In *RAFT polymerization: Adding to the picture*, Macromolecular symposia, Wiley Online Library: 2007; pp 104-116.
43. Barner-Kowollik, C., *Handbook of RAFT polymerization*. John Wiley & Sons: 2008.
44. Moad, G.; Rizzardo, E.; Thang, S. H., RAFT polymerization and some of its applications. *Chemistry–An Asian Journal* **2013,** *8* (8), 1634-1644.
45. Moad, G., An industrial history of RAFT polymerization. *RAFT Polymerization: Methods, Synthesis and Applications* **2021,** *2*, 1077-1169.

46. Blyth, J.; Hofmann, A. W., Ueber das Styrol und einige seiner Zersetzungsproducte. *Justus Liebigs Annalen der Chemie* **1845,** *53* (3), 289-329.
47. Ciamician, G., The photochemistry of the future. *Science* **1912,** *36* (926), 385-394.
48. Gibson, I.; Rosen, D. W.; Stucker, B.; Gibson, I.; Rosen, D. W.; Stucker, B., Photopolymerization processes. *Additive Manufacturing Technologies: Rapid Prototyping to Direct Digital Manufacturing* **2010**, 78-119.
49. LEVINOS, S.; ANILINE, G.; DIV, F. C. B. N. A. *INVESTIGATION OF THE PHOTOPOLYMERIZATION PROCESS*; 1961.
50. Tasdelen, M. A.; Yagci, Y., Light-induced click reactions. *Angewandte Chemie International Edition* **2013,** *52* (23), 5930-5938.
51. Corrigan, N.; Yeow, J.; Judzewitsch, P.; Xu, J.; Boyer, C., Seeing the Light: Advancing Materials Chemistry through Photopolymerization. *Angewandte Chemie International Edition* **2019,** *58* (16), 5170-5189.
52. Corrigan, N.; Xu, J.; Boyer, C., A photoinitiation system for conventional and controlled radical polymerization at visible and NIR wavelengths. *Macromolecules* **2016,** *49* (9), 3274-3285.
53. Ohtsuki, A.; Lei, L.; Tanishima, M.; Goto, A.; Kaji, H., Photocontrolled organocatalyzed living radical polymerization feasible over a wide range of wavelengths. *Journal of the American Chemical Society* **2015,** *137* (16), 5610-5617.
54. Tian, C.; Wang, P.; Ni, Y.; Zhang, L.; Cheng, Z.; Zhu, X., Photocontrolled Iodine-Mediated Reversible-Deactivation Radical Polymerization: Solution Polymerization of Methacrylates by Irradiation with NIR LED Light. *Angewandte Chemie International Edition* **2020,** *59* (10), 3910-3916.
55. Wong, A. M.; Valles, D. J.; Carbonell, C.; Chambers, C. L.; Rozenfeld, A. Y.; Aldasooky, R. W.; Braunschweig, A. B., Controlled-height brush polymer patterns via surface-initiated thiol-methacrylate photopolymerizations. *ACS Macro Letters* **2019,** *8* (11), 1474-1478.
56. Bagheri, A.; Jin, J., Photopolymerization in 3D printing. *ACS Applied Polymer Materials* **2019,** *1* (4), 593-611.
57. Allen, N. S.; Marin, M. C.; Edge, M.; Davies, D. W.; Garrett, J.; Jones, F.; Navaratnam, S.; Parsons, B. J., Photochemistry and photoinduced chemical crosslinking activity of type I & II co-reactive photoinitiators in acrylated prepolymers. *Journal of Photochemistry and Photobiology A: Chemistry* **1999,** *126* (1-3), 135-149.
58. Ribas-Massonis, A.; Cicujano, M.; Duran, J.; Besalú, E.; Poater, A., Free-Radical Photopolymerization for Curing Products for Refinish Coatings Market. *Polymers* **2022,** *14* (14), 2856.
59. Wu, J.; Zhao, Z.; Hamel, C. M.; Mu, X.; Kuang, X.; Guo, Z.; Qi, H. J., Evolution of material properties during free radical photopolymerization. *Journal of the Mechanics and Physics of Solids* **2018,** *112*, 25-49.
60. Andrzejewska, E., Photopolymerization kinetics of multifunctional monomers. *Progress in polymer science* **2001,** *26* (4), 605-665.
61. Atai, M.; Watts, D. C., A new kinetic model for the photopolymerization shrinkage-strain of dental composites and resin-monomers. *Dental Materials* **2006,** *22* (8), 785-791.
62. Check, C.; Chartoff, R.; Chang, S., Inkjet printing of 3D nano-composites formed by photopolymerization of an acrylate monomer. *Reactive and Functional Polymers* **2015,** *97*, 116-122.
63. Yoshida, E., Nitroxide-mediated photo-controlled/living radical dispersion polymerization of methyl methacrylate. *Colloid and Polymer Science* **2011,** *289*, 1625-1630.
64. Fors, B. P.; Hawker, C. J., Control of a living radical polymerization of methacrylates by light. *Angewandte Chemie International Edition* **2012,** *51* (35), 8850-8853.
65. Phommalysack-Lovan, J.; Chu, Y.; Boyer, C.; Xu, J., PET-RAFT polymerisation: towards green and precision polymer manufacturing. *Chemical communications* **2018,** *54* (50), 6591-6606.
66. Posner, T., Beiträge zur Kenntniss der ungesättigten Verbindungen. II. Ueber die Addition von Mercaptanen an ungesättigte Kohlenwasserstoffe. *Berichte der deutschen chemischen Gesellschaft* **1905,** *38* (1), 646-657.
67. Hoyle, C. E.; Lee, T. Y.; Roper, T., Thiol–enes: Chemistry of the past with promise for the future. *Journal of Polymer Science Part A: Polymer Chemistry* **2004,** *42* (21), 5301-5338.

68. Machado, T. O.; Sayer, C.; Araujo, P. H., Thiol-ene polymerisation: A promising technique to obtain novel biomaterials. *European Polymer Journal* **2017,** *86*, 200-215.
69. Marvel, C.; Chambers, R., Polyalkylene sulfides from diolefins and dimercaptans. *Journal of the American Chemical Society* **1948,** *70* (3), 993-998.
70. Hoyle, C. E.; Bowman, C. N., Thiol–ene click chemistry. *Angewandte Chemie International Edition* **2010,** *49* (9), 1540-1573.
71. Morgan, C.; Magnotta, F.; Ketley, A., Thiol/ene photocurable polymers. *Journal of Polymer Science: Polymer Chemistry Edition* **1977,** *15* (3), 627-645.
72. Nair, D. P.; Podgorski, M.; Chatani, S.; Gong, T.; Xi, W.; Fenoli, C. R.; Bowman, C. N., The thiol-Michael addition click reaction: a powerful and widely used tool in materials chemistry. *Chemistry of Materials* **2014,** *26* (1), 724-744.
73. Carlson, D. D.; Knight, A. R., Reactions of thiyl radicals. XI. Further investigations of thiol–disulfide photolyses in the liquid phase. *Canadian Journal of Chemistry* **1973,** *51* (9), 1410-1415.
74. Cramer, N. B.; Davies, T.; O'Brien, A. K.; Bowman, C. N., Mechanism and modeling of a thiol–ene photopolymerization. *Macromolecules* **2003,** *36* (12), 4631-4636.
75. Kade, M. J.; Burke, D. J.; Hawker, C. J., The power of thiol-ene chemistry. *Journal of Polymer Science Part A: Polymer Chemistry* **2010,** *48* (4), 743-750.
76. Wang, Y.; Bruno, B. J.; Cornillie, S.; Nogieira, J. M.; Chen, D.; Cheatham III, T. E.; Lim, C. S.; Chou, D. H. C., Application of Thiol–yne/Thiol–ene reactions for peptide and protein macrocyclizations. *Chemistry–A European Journal* **2017,** *23* (29), 7087-7092.
77. Li, M.; De, P.; Li, H.; Sumerlin, B. S., Conjugation of RAFT-generated polymers to proteins by two consecutive thiol–ene reactions. *Polymer Chemistry* **2010,** *1* (6), 854-859.
78. Nolan, M. D.; Scanlan, E. M., Applications of thiol-ene chemistry for peptide science. *Frontiers in chemistry* **2020,** *8*, 583272.
79. Valdebenito, A.; Espinoza, P.; Lissi, E.; Encinas, M., Bovine serum albumin as chain transfer agent in the acrylamide polymerization. Protein-polymer conjugates. *Polymer* **2010,** *51* (12), 2503-2507.
80. Bontempo, D.; Heredia, K. L.; Fish, B. A.; Maynard, H. D., Cysteine-reactive polymers synthesized by atom transfer radical polymerization for conjugation to proteins. *Journal of the American Chemical Society* **2004,** *126* (47), 15372-15373.
81. Boyer, C.; Bulmus, V.; Liu, J.; Davis, T. P.; Stenzel, M. H.; Barner-Kowollik, C., Well-defined protein− polymer conjugates via in situ RAFT polymerization. *Journal of the American Chemical Society* **2007,** *129* (22), 7145-7154.
82. Nakamura, K.; Era, S.; Ozaki, Y.; Sogami, M.; Hayashi, T.; Murakami, M., Conformational changes in seventeen cystine disulfide bridges of bovine serum albumin proved by Raman spectroscopy. *Febs Letters* **1997,** *417* (3), 375-378.
83. Gilbert, H. F., [2] Thiol/disulfide exchange equilibria and disulfidebond stability. *Methods in enzymology* **1995,** *251*, 8-28.
84. Ko, J. H.; Maynard, H. D., A guide to maximizing the therapeutic potential of protein–polymer conjugates by rational design. *Chemical Society Reviews* **2018,** *47* (24), 8998-9014.
85. Spears, R. J.; McMahon, C.; Chudasama, V., Cysteine protecting groups: Applications in peptide and protein science. *Chemical Society Reviews* **2021,** *50* (19), 11098-11155.
86. Drotleff, S.; Lungwitz, U.; Breunig, M.; Dennis, A.; Blunk, T.; Teßmar, J.; Göpferich, A., Biomimetic polymers in pharmaceutical and biomedical sciences. *European Journal of Pharmaceutics and Biopharmaceutics* **2004,** *58* (2), 385-407.
87. Canalle, L. A.; Löwik, D. W.; van Hest, J. C., Polypeptide–polymer bioconjugates. *Chemical Society Reviews* **2010,** *39* (1), 329-353.
88. Otero, T. F., Biomimetic conducting polymers: synthesis, materials, properties, functions, and devices. *Polymer Reviews* **2013,** *53* (3), 311-351.
89. Vázquez-Dorbatt, V.; Lee, J.; Lin, E. W.; Maynard, H. D., Synthesis of glycopolymers by controlled radical polymerization techniques and their applications. *ChemBioChem* **2012,** *13* (17), 2478-2487.

90. Ladmiral, V.; Melia, E.; Haddleton, D. M., Synthetic glycopolymers: an overview. *European Polymer Journal* **2004,** *40* (3), 431-449.
91. Ohno, K.; Tsujii, Y.; Fukuda, T., Synthesis of a well-defined glycopolymer by atom transfer radical polymerization. *Journal of Polymer Science Part A: Polymer Chemistry* **1998,** *36* (14), 2473-2481.
92. Muthukrishnan, S.; Mori, H.; Müller, A. H., Synthesis and characterization of methacrylate-type hyperbranched glycopolymers via self-condensing atom transfer radical copolymerization. *Macromolecules* **2005,** *38* (8), 3108-3119.
93. Muthukrishnan, S.; Plamper, F.; Mori, H.; Müller, A. H., Synthesis and characterization of glycomethacrylate hybrid stars from silsesquioxane nanoparticles. *Macromolecules* **2005,** *38* (26), 10631-10642.
94. Vázquez-Dorbatt, V.; Maynard, H. D., Biotinylated glycopolymers synthesized by atom transfer radical polymerization. *Biomacromolecules* **2006,** *7* (8), 2297-2302.
95. Lowe, A. B.; Sumerlin, B. S.; McCormick, C. L., The direct polymerization of 2-methacryloxyethyl glucoside via aqueous reversible addition-fragmentation chain transfer (RAFT) polymerization. *Polymer* **2003,** *44* (22), 6761-6765.
96. Narain, R.; Housni, A.; Gody, G.; Boullanger, P.; Charreyre, M.-T.; Delair, T., Preparation of biotinylated glyconanoparticles via a photochemical process and study of their bioconjugation to streptavidin. *Langmuir* **2007,** *23* (26), 12835-12841.
97. Pearson, S.; Scarano, W.; Stenzel, M. H., Micelles based on gold-glycopolymer complexes as new chemotherapy drug delivery agents. *Chemical Communications* **2012,** *48* (39), 4695-4697.
98. Song, E.-H.; Manganiello, M. J.; Chow, Y.-H.; Ghosn, B.; Convertine, A. J.; Stayton, P. S.; Schnapp, L. M.; Ratner, D. M., In vivo targeting of alveolar macrophages via RAFT-based glycopolymers. *Biomaterials* **2012,** *33* (28), 6889-6897.
99. Stepuk, A.; Halter, J. G.; Schaetz, A.; Grass, R. N.; Stark, W. J., Mussel-inspired load bearing metal–polymer glues. *Chemical Communications* **2012,** *48* (50), 6238-6240.
100. Chung, H.; Glass, P.; Pothen, J. M.; Sitti, M.; Washburn, N. R., Enhanced adhesion of dopamine methacrylamide elastomers via viscoelasticity tuning. *Biomacromolecules* **2011,** *12* (2), 342-347.
101. Chen, X.; Lee, G. S.; Zettl, A.; Bertozzi, C. R., Biomimetic engineering of carbon nanotubes by using cell surface mucin mimics. *Angewandte Chemie* **2004,** *116* (45), 6237-6242.
102. Mulchandani, N.; Narayan, R., Redesigning Carbon–Carbon Backbone Polymers for Biodegradability–Compostability at the End-of-Life Stage. *Molecules* **2023,** *28* (9), 3832.
103. Geng, J.; Mantovani, G.; Tao, L.; Nicolas, J.; Chen, G.; Wallis, R.; Mitchell, D. A.; Johnson, B. R.; Evans, S. D.; Haddleton, D. M., Site-directed conjugation of "clicked" glycopolymers to form glycoprotein mimics: binding to mammalian lectin and induction of immunological function. *Journal of the American Chemical Society* **2007,** *129* (49), 15156-15163.
104. Hu, Z.; Liu, Y.; Hong, C.; Pan, C., Synthesis of well-defined glycoconjugate polyacrylamides via preactivated polymers prepared by ATRP. *Journal of applied polymer science* **2005,** *98* (1), 189-194.
105. Kjellén, L.; Lindahl, U., Proteoglycans: structures and interactions. *Annual review of biochemistry* **1991,** *60* (1), 443-475.
106. Gray, E.; Mulloy, B.; Barrowcliffe, T. W., Heparin and low-molecular-weight heparin. *Thrombosis and haemostasis* **2008,** *99* (11), 807-818.
107. Florian, J. A.; Kosky, J. R.; Ainslie, K.; Pang, Z.; Dull, R. O.; Tarbell, J. M., Heparan sulfate proteoglycan is a mechanosensor on endothelial cells. *Circulation research* **2003,** *93* (10), e136-e142.
108. Kreuger, J.; Spillmann, D.; Li, J.-p.; Lindahl, U., Interactions between heparan sulfate and proteins: the concept of specificity. *The Journal of cell biology* **2006,** *174* (3), 323.
109. Kreuger, J.; Kjellén, L., Heparan sulfate biosynthesis: regulation and variability. *Journal of Histochemistry & Cytochemistry* **2012,** *60* (12), 898-907.
110. Hoffmann, M.; Snyder, N. L.; Hartmann, L., Polymers inspired by heparin and heparan sulfate for viral targeting. *Macromolecules* **2022,** *55* (18), 7957-7973.
111. Sasisekharan, R.; Venkataraman, G., Heparin and heparan sulfate: biosynthesis, structure and function. *Current opinion in chemical biology* **2000,** *4* (6), 626-631.

112. Meneghetti, M. C.; Hughes, A. J.; Rudd, T. R.; Nader, H. B.; Powell, A. K.; Yates, E. A.; Lima, M. A., Heparan sulfate and heparin interactions with proteins. *Journal of the Royal Society Interface* **2015,** *12* (110), 20150589.
113. Pongener, I.; O'Shea, C.; Wootton, H.; Watkinson, M.; Miller, G. J., Developments in the chemical synthesis of heparin and heparan sulfate. *The Chemical Record* **2021,** *21* (11), 3238-3255.
114. Shieh, M.-T.; WuDunn, D.; Montgomery, R. I.; Esko, J. D.; Spear, P. G., Cell surface receptors for herpes simplex virus are heparan sulfate proteoglycans. *The Journal of cell biology* **1992,** *116* (5), 1273-1281.
115. Shukla, D.; Liu, J.; Blaiklock, P.; Shworak, N. W.; Bai, X.; Esko, J. D.; Cohen, G. H.; Eisenberg, R. J.; Rosenberg, R. D.; Spear, P. G., A novel role for 3-O-sulfated heparan sulfate in herpes simplex virus 1 entry. *Cell* **1999,** *99* (1), 13-22.
116. WuDUNN, D.; Spear, P. G., Initial interaction of herpes simplex virus with cells is binding to heparan sulfate. *Journal of virology* **1989,** *63* (1), 52-58.
117. Koganti, R.; Memon, A.; Shukla, D. In *Emerging roles of heparan sulfate proteoglycans in viral pathogenesis*, Seminars in Thrombosis and Hemostasis, Thieme Medical Publishers, Inc. 333 Seventh Avenue, 18th Floor, New York, NY …: 2021; pp 283-294.
118. Clausen, T. M.; Sandoval, D. R.; Spliid, C. B.; Pihl, J.; Perrett, H. R.; Painter, C. D.; Narayanan, A.; Majowicz, S. A.; Kwong, E. M.; McVicar, R. N., SARS-CoV-2 infection depends on cellular heparan sulfate and ACE2. *Cell* **2020,** *183* (4), 1043-1057. e15.
119. De Pasquale, V.; Quiccione, M. S.; Tafuri, S.; Avallone, L.; Pavone, L. M., Heparan sulfate proteoglycans in viral infection and treatment: A special focus on SARS-CoV-2. *International Journal of Molecular Sciences* **2021,** *22* (12), 6574.
120. Kim, S. Y.; Li, B.; Linhardt, R. J., Pathogenesis and inhibition of flaviviruses from a carbohydrate perspective. *Pharmaceuticals* **2017,** *10* (2), 44.
121. Bernard, K. A.; Klimstra, W. B.; Johnston, R. E., Mutations in the E2 glycoprotein of Venezuelan equine encephalitis virus confer heparan sulfate interaction, low morbidity, and rapid clearance from blood of mice. *Virology* **2000,** *276* (1), 93-103.
122. Mycroft-West, C. J.; Su, D.; Pagani, I.; Rudd, T. R.; Elli, S.; Gandhi, N. S.; Guimond, S. E.; Miller, G. J.; Meneghetti, M. C.; Nader, H. B., Heparin inhibits cellular invasion by SARS-CoV-2: structural dependence of the interaction of the spike S1 receptor-binding domain with heparin. *Thrombosis and haemostasis* **2020,** *120* (12), 1700-1715.
123. Kwon, P. S.; Oh, H.; Kwon, S.-J.; Jin, W.; Zhang, F.; Fraser, K.; Hong, J. J.; Linhardt, R. J.; Dordick, J. S., Sulfated polysaccharides effectively inhibit SARS-CoV-2 in vitro. *Cell discovery* **2020,** *6* (1), 50.
124. Gangji, R. N.; Sankaranarayanan, N. V.; Elste, J.; Al-Horani, R. A.; Afosah, D. K.; Joshi, R.; Tiwari, V.; Desai, U. R., Inhibition of herpes simplex virus-1 entry into human cells by nonsaccharide glycosaminoglycan mimetics. *ACS Medicinal Chemistry Letters* **2018,** *9* (8), 797-802.
125. Morla, S., Glycosaminoglycans and glycosaminoglycan mimetics in cancer and inflammation. *International journal of molecular sciences* **2019,** *20* (8), 1963.
126. Schandock, F.; Riber, C. F.; Röcker, A.; Müller, J. A.; Harms, M.; Gajda, P.; Zuwala, K.; Andersen, A. H.; Løvschall, K. B.; Tolstrup, M., Macromolecular antiviral agents against Zika, Ebola, SARS, and other pathogenic viruses. *Advanced Healthcare Materials* **2017,** *6* (23), 1700748.
127. Soria-Martinez, L.; Bauer, S.; Giesler, M.; Schelhaas, S.; Materlik, J.; Janus, K.; Pierzyna, P.; Becker, M.; Snyder, N. L.; Hartmann, L., Prophylactic antiviral activity of sulfated glycomimetic oligomers and polymers. *Journal of the American Chemical Society* **2020,** *142* (11), 5252-5265.
128. Oh, Y. I.; Sheng, G. J.; Chang, S. K.; Hsieh-Wilson, L. C., Tailored glycopolymers as anticoagulant heparin mimetics. *Angewandte Chemie* **2013,** *125* (45), 12012-12015.
129. Rapp, M. V.; Maier, G. P.; Dobbs, H. A.; Higdon, N. J.; Waite, J. H.; Butler, A.; Israelachvili, J. N., Defining the catechol–cation synergy for enhanced wet adhesion to mineral surfaces. *Journal of the American Chemical Society* **2016,** *138* (29), 9013-9016.
130. Qin, Z.; Buehler, M. J., Impact tolerance in mussel thread networks by heterogeneous material distribution. *Nature communications* **2013,** *4* (1), 2187.

131. Israelachvili, J.; Wennerström, H., Role of hydration and water structure in biological and colloidal interactions. *Nature* **1996,** *379* (6562), 219-225.
132. Maier, G. P.; Rapp, M. V.; Waite, J. H.; Israelachvili, J. N.; Butler, A., Adaptive synergy between catechol and lysine promotes wet adhesion by surface salt displacement. *Science* **2015,** *349* (6248), 628-632.
133. Hwang, D. S.; Zeng, H.; Masic, A.; Harrington, M. J.; Israelachvili, J. N.; Waite, J. H., Protein-and metal-dependent interactions of a prominent protein in mussel adhesive plaques. *Journal of biological chemistry* **2010,** *285* (33), 25850-25858.
134. Kord Forooshani, P.; Lee, B. P., Recent approaches in designing bioadhesive materials inspired by mussel adhesive protein. *Journal of Polymer Science Part A: Polymer Chemistry* **2017,** *55* (1), 9-33.
135. Papov, V. V.; Diamond, T. V.; Biemann, K.; Waite, J. H., Hydroxyarginine-containing Polyphenolic Proteins in the Adhesive Plaques of the Marine Mussel Mytilus edulis (∗). *Journal of Biological Chemistry* **1995,** *270* (34), 20183-20192.
136. Zhao, H.; Robertson, N. B.; Jewhurst, S. A.; Waite, J. H., Probing the adhesive footprints of Mytilus californianus byssus. *Journal of Biological Chemistry* **2006,** *281* (16), 11090-11096.
137. Lee, B. P.; Messersmith, P. B.; Israelachvili, J. N.; Waite, J. H., Mussel-inspired adhesives and coatings. *Annual review of materials research* **2011,** *41*, 99-132.
138. Fischer, L.; Strzelczyk, A. K.; Wedler, N.; Kropf, C.; Schmidt, S.; Hartmann, L., Sequence-defined positioning of amine and amide residues to control catechol driven wet adhesion. *Chemical science* **2020,** *11* (36), 9919-9924.
139. Waite, J. H.; Qin, X., Polyphosphoprotein from the adhesive pads of Mytilus edulis. *Biochemistry* **2001,** *40* (9), 2887-2893.
140. Long, J. R.; Dindot, J. L.; Zebroski, H.; Kiihne, S.; Clark, R. H.; Campbell, A. A.; Stayton, P. S.; Drobny, G. P., A peptide that inhibits hydroxyapatite growth is in an extended conformation on the crystal surface. *Proceedings of the National Academy of Sciences* **1998,** *95* (21), 12083-12087.
141. Xu, H.; Nishida, J.; Ma, W.; Wu, H.; Kobayashi, M.; Otsuka, H.; Takahara, A., Competition between oxidation and coordination in cross-linking of polystyrene copolymer containing catechol groups. *ACS Macro Letters* **2012,** *1* (4), 457-460.
142. Yu, J.; Yu, J., Effects of interfacial redox in mussel adhesive protein films on mica. *Adhesive Interactions of Mussel Foot Proteins* **2014**, 21-30.
143. Hofman, A. H.; van Hees, I. A.; Yang, J.; Kamperman, M., Bioinspired underwater adhesives by using the supramolecular toolbox. *Advanced materials* **2018,** *30* (19), 1704640.
144. Waite, J. H., Mussel adhesion–essential footwork. *Journal of Experimental Biology* **2017,** *220* (4), 517-530.
145. Lee, H.; Dellatore, S. M.; Miller, W. M.; Messersmith, P. B., Mussel-inspired surface chemistry for multifunctional coatings. *science* **2007,** *318* (5849), 426-430.
146. Dubey, S.; Singh, D.; Misra, R., Enzymatic synthesis and various properties of poly (catechol). *Enzyme and microbial technology* **1998,** *23* (7-8), 432-437.
147. Fan, X.; Lin, L.; Dalsin, J. L.; Messersmith, P. B., Biomimetic anchor for surface-initiated polymerization from metal substrates. *Journal of the American Chemical Society* **2005,** *127* (45), 15843-15847.
148. Liu, J.; Yang, W.; Zareie, H. M.; Gooding, J. J.; Davis, T. P., pH-Detachable polymer brushes formed using titanium− diol coordination chemistry and living radical polymerization (RAFT). *Macromolecules* **2009,** *42* (8), 2931-2939.
149. Liu, Z.; Hu, B.-H.; Messersmith, P. B., Acetonide protection of dopamine for the synthesis of highly pure N-docosahexaenoyldopamine. *Tetrahedron letters* **2010,** *51* (18), 2403-2405.
150. Punna, S.; Meunier, S.; Finn, M., A hierarchy of aryloxide deprotection by boron tribromide. *Organic Letters* **2004,** *6* (16), 2777-2779.
151. Matos-Pérez, C. R.; White, J. D.; Wilker, J. J., Polymer composition and substrate influences on the adhesive bonding of a biomimetic, cross-linking polymer. *Journal of the American Chemical Society* **2012,** *134* (22), 9498-9505.

152. White, J. D.; Wilker, J. J., Underwater bonding with charged polymer mimics of marine mussel adhesive proteins. *Macromolecules* **2011,** *44* (13), 5085-5088.
153. Wang, J.; Tahir, M.; Kappl, M.; Tremel, W.; Metz, N.; Barz, M.; Theato, P.; Butt, H. J., Influence of binding-site density in wet bioadhesion. *Advanced Materials* **2008,** *20* (20), 3872-3876.
154. Yu, M.; Deming, T. J., Synthetic polypeptide mimics of marine adhesives. *Macromolecules* **1998,** *31* (15), 4739-4745.
155. Li, L.; Li, Y.; Luo, X.; Deng, J.; Yang, W., Helical poly (N-propargylamide) s with functional catechol groups: Synthesis and adsorption of metal ions in aqueous solution. *Reactive and Functional Polymers* **2010,** *70* (12), 938-943.
156. Malisova, B.; Tosatti, S.; Textor, M.; Gademann, K.; Zürcher, S., Poly (ethylene glycol) adlayers immobilized to metal oxide substrates through catechol derivatives: influence of assembly conditions on formation and stability. *Langmuir* **2010,** *26* (6), 4018-4026.
157. Westwood, G.; Horton, T. N.; Wilker, J. J., Simplified polymer mimics of cross-linking adhesive proteins. *Macromolecules* **2007,** *40* (11), 3960-3964.
158. Bae, K. H.; Kim, Y. B.; Lee, Y.; Hwang, J.; Park, H.; Park, T. G., Bioinspired synthesis and characterization of gadolinium-labeled magnetite nanoparticles for dual contrast T 1-and T 2-weighted magnetic resonance imaging. *Bioconjugate chemistry* **2010,** *21* (3), 505-512.
159. Black, K. C.; Liu, Z.; Messersmith, P. B., Catechol redox induced formation of metal core–polymer shell nanoparticles. *Chemistry of Materials* **2011,** *23* (5), 1130-1135.
160. Bernard, J.; Branger, C.; Beurroies, I.; Denoyel, R.; Margaillan, A., Catechol immobilized on crosslinked polystyrene resins by grafting or copolymerization: Incidence on metal ions adsorption. *Reactive and Functional Polymers* **2012,** *72* (1), 98-106.
161. Hu, B. H.; Messersmith, P., Enzymatically cross-linked hydrogels and their adhesive strength to biosurfaces. *Orthodontics & craniofacial research* **2005,** *8* (3), 145-149.
162. Murphy, J. L.; Vollenweider, L.; Xu, F.; Lee, B. P., Adhesive performance of biomimetic adhesive-coated biologic scaffolds. *Biomacromolecules* **2010,** *11* (11), 2976-2984.
163. Wilkins, L. E.; Phillips, D. J.; Deller, R. C.; Davies, G.-L.; Gibson, M. I., Synthesis and characterisation of glucose-functional glycopolymers and gold nanoparticles: study of their potential interactions with ovine red blood cells. *Carbohydrate research* **2015,** *405*, 47-54.
164. Bonda, L.; Müller, J.; Fischer, L.; Löwe, M.; Kedrov, A.; Schmidt, S.; Hartmann, L., Facile Synthesis of Catechol-Containing Polyacrylamide Copolymers: Synergistic Effects of Amine, Amide and Catechol Residues in Mussel-Inspired Adhesives. *Polymers* **2023,** *15* (18), 3663.